Gopal B. Saha

Physics and Radiobiology of Nuclear Medicine

Fourth Edition

Springer

Physics and Radiobiology of Nuclear Medicine

Gopal B. Saha, Ph.D.

Physics and Radiobiology of Nuclear Medicine

Fourth Edition

Springer

Gopal B. Saha, Ph.D.
Emeritus Staff
Cleveland Clinic
Cleveland, OH 44195
USA

ISBN 978-1-4614-4011-6 ISBN 978-1-4614-4012-3 (eBook)
DOI 10.1007/978-1-4614-4012-3
Springer New York Dordrecht Heidelberg London

Library of Congress Control Number: 2012948009

Printed on acid-free paper

Springer is part of Springer Science+Business Media (www.springer.com)

To
All my benefactors

Preface

The fourth edition of this book has been prompted by a need to provide up-to-date information in keeping up with perpetual growth and improvement in instrumentation and techniques employed in nuclear medicine since its last edition in 2006. Like the past editions, the book is intended for the radiology and nuclear medicine residents to prepare for the American Board of Nuclear Medicine, American Board of Radiology and American Board of Science in Nuclear Medicine examinations, all of which require strong physics background. Also, it will serve as a textbook on nuclear medicine physics and instrumentation for nuclear medicine technologists taking the Nuclear Medicine Technology Certification Board examination.

The organization of the book has been kept the same as in the previous editions consisting of 16 chapters—starting with basics in initial chapters and then progressing into more developed techniques in later chapters. Chapters 1–4, 6, 8 and 11 have no major changes. An expanded description of a cyclotron and two examples of calculation of yield of activity produced are added to Chapter 5 along with the updating of Table 5.1. Chapter 7 includes additional information on the ion chamber survey meter, proportional counter, and G-M counter. The section on solid state digital cameras has been revised in Chapter 9. In Chapter 10, several changes have been made, namely, an expanded collimator section, a detailed description of "contrast", and a more detailed quality control section. Changes in Chapter 12 include: detailed iterative reconstruction method, description of CT scanners in SPECT/CT, detailed description of attenuation correction in SPECT/CT, and expanded sections on partial volume effects and quality control of CT scanners. Included in Chapter 13 are: upgraded information on detectors and PET scanners; a new section on PET/MR including the attenuation correction method and its quality control tests; the time of flight technique; several scatter correction techniques; and a section on accreditation of nuclear medicine and PET facilities. Doses in Table 14.4 have been updated, and new tables with revised pediatric dosages have been included in Chapter 14. For consistency, the section, "Sources of Radiation exposure in USA" has been removed from Chapter 16 and added to Chapter 15 with revised data, while the sections "Dirty Bombs", "Verification Card for Radioactive Patients" and "Radiation Phobia" have been moved from

Chapter 15 and added to Chapter 16. “European Regulations Governing Radiations” in Chapter 16 has been revised. A number of figures and tables have been added for better explanation of the text contents throughout the book.

It has been a great pleasure to work with, for which I am ever grateful to, Andrew Moyer, Senior Editor of Clinical Medicine at Springer, for his sincere support during the publication of several of my books by Springer including this one. I would like to thank Ian Hayes, Editorial Assistant, and Joseph Quatela, Senior Production Editor of Springer for their support in the production of this book.

Gopal B. Saha, Ph.D.

Contents

1
Structure of Matter

Matter and Energy

The existence of the universe is explained by two entities: matter and energy. These two entities are interchangeable and exist in different forms to make up all things visible or invisible in the universe. Whereas matter has a definite size, shape, and form, energy has different forms but no size and shape.

Matter is characterized by its quantity, called the *mass*, and is composed of the smallest unit, the atom. In atomic physics, the unit of mass is the atomic mass unit (amu), which is equal to 1.66×10^{-27} kg.

Energy is the capacity to do work and can exist in several forms: kinetic energy (which is due to the motion of matter); potential energy (which is due to the position and configuration of matter); thermal energy (which is due to the motion of atoms or molecules in matter); electrical energy (which is due to the flow of electrons across an electric potential); chemical energy (which is due to chemical reaction); and radiation (energy in motion). Energy can change from one form to another. Of all these forms, radiation is of great importance in nuclear medicine and, therefore, will be discussed in detail.

Mass and energy are interchangeable, and one is created at the expense of the other. This is predicted by the Einstein's mass–energy relationship:

$$E = mc^2 \tag{1.1}$$

where E is energy in ergs, m is the mass in grams, and c is the velocity of light in a vacuum given as 3×10^{10} cm/s. This relationship states that everything around us can be classified as matter or energy.

G. B. Saha, *Physics and Radiobiology of Nuclear Medicine,*
DOI 10.1007/978-1-4614-4012-3_1,

Radiation

Radiation is a form of energy in motion through space. It is emitted by one object and absorbed or scattered by another. Radiations are of two types:

1. *Particulate radiations:* Examples of these radiations are energetic electrons, protons, neutrons, α-particles, and so forth. They have mass and charge, except neutrons, which are neutral particles. The velocity of their motion depends on their kinetic energy. The particulate radiations originate from radioactive decay, cosmic rays, nuclear reactions, and so forth.
2. *Electromagnetic radiations:* These radiations are a form of energy in motion that does not have mass and charge and can propagate as either waves or discrete packets of energy, called the *photons* or *quanta*. These radiations travel with the velocity of light. Various examples of electromagnetic radiations include radio waves, visible light, heat waves, γ-radiations, and so forth, and they differ from each other in wavelength and hence in energy. Note that the sound waves are not electromagnetic radiations.

The energy E of an electromagnetic radiation is given by

$$E = hv = \frac{hc}{\lambda} \tag{1.2}$$

where h is the Planck constant given as 6.625×10^{-27} erg · s/cycle, v is the frequency in hertz (Hz), defined as 1 cycle per second, λ is the wavelength in centimeters, and c is the velocity of light in vacuum, which is equal to nearly 3×10^{10} cm/s.

The energy of an electromagnetic radiation is given in electron volts (eV), which is defined as the energy acquired by an electron when accelerated through a potential difference of 1 V. Using 1 eV = 1.602×10^{-12} erg, Eq. (1.2) becomes

$$E(\text{eV}) = \frac{1.24 \times 10^{-4}}{\lambda} \tag{1.3}$$

where λ is given in centimeters. Table 1.1 lists the different electromagnetic radiations along with their frequencies and wavelengths.

TABLE 1.1. Characteristics of different electromagnetic radiations.

Type	Energy (eV)	Frequency (Hz)	Wavelength (cm)
Radio, TV	10^{-10}–10^{-6}	10^{4}–10^{8}	10^{2}–10^{6}
Microwave	10^{-6}–10^{-2}	10^{8}–10^{12}	10^{-2}–10^{2}
Infrared	10^{-2}–1	10^{12}–10^{14}	10^{-4}–10^{-2}
Visible	1–2	10^{14}–10^{15}	10^{-5}–10^{-4}
Ultraviolet	2–100	10^{15}–10^{16}	10^{-6}–0^{-5}
x-Rays and γ-rays	100–10^{7}	10^{16}–10^{21}	10^{-11}–10^{-6}

Table 1.2. Characteristics of electrons and nucleons.

Particle	Charge	Mass (amu)[a]	Mass (kg)	Mass (MeV)[b]
Electron	−1	0.000549	0.9108×10^{-30}	0.511
Proton	+1	1.00728	1.6721×10^{-27}	938.78
Neutron	0	1.00867	1.6744×10^{-27}	939.07

[a] amu = 1 atomic mass unit = 1.66×10^{-27} kg = 1/12 of the mass of ^{12}C.
[b] 1 atomic mass unit = 931 MeV.

The Atom

For the purpose of this book, the atom can be considered as the smallest unit in the composition of matter. The atom is composed of a nucleus at the center and one or more electrons orbiting around the nucleus. The nucleus consists of protons and neutrons, collectively called *nucleons*. The protons are positively charged particles with a mass of 1.00728 amu, and the neutrons are electrically neutral particles with a mass of 1.00867 amu. The electrons are negatively charged particles with a mass of 0.000549 amu. The protons and neutrons are about 1836 times heavier than the electrons but the neutron is heavier than the proton by one electron mass (i.e., by 0.511 MeV). The number of electrons is equal to the number of protons, thus resulting in a neutral atom of an element. The characteristics of these particles are given in Table 1.2. The size of the atom is about 10^{-8} cm (called the angstrom, Å), whereas the nucleus has the size of 10^{-13} cm (termed the Fermi, F). The density of the nucleus is of the order of 10^{14} g/cm^3. The electronic arrangement determines the chemical properties of an element, whereas the nuclear structure dictates the stability and radioactive transformation of the atom.

Electronic Structure of the Atom

Several theories have been put forward to describe the electronic structure of the atom, among which the theory of Niels Bohr, proposed in 1913, is the most plausible one and still holds today. The Bohr's atomic theory states that electrons rotate around the nucleus in discrete energy shells that are stationary and arranged in increasing order of energy. These shells are designated as the *K* shell, *L* shell, *M* shell, *N* shell, and so forth. When an electron jumps from the upper shell to the lower shell, the difference in energy between the two shells appears as electromagnetic radiations or photons. When an electron is raised from the lower shell to the upper shell, the energy difference is absorbed and must be supplied for the process to occur.

The detailed description of the Bohr's atomic structure is provided by the quantum theory in physics. According to this theory, each shell is designated by a quantum number *n*, called the *principal quantum number*, and denoted by integers, for example, 1 for the *K* shell, 2 for the *L* shell, 3 for the *M* shell, 4 for the *N* shell, and 5 for the *O* shell. Each energy shell is subdivided into subshells or orbit-

als, which are designated as s, p, d, f, and so on. For a principal quantum number n, there are n orbitals in a given shell. These orbitals are assigned the *azimuthal quantum numbers*, l, which represent the electron's angular momentum and can assume numerical values of $l = 0, 1, 2\ldots n-1$. Thus for the s orbital, $l = 0$; the p orbital, $l = 1$; the d orbital, $l = 2$; the f orbital, $l = 3$; and so forth. According to this description, the K shell has one orbital, designated as $1s$, the L shell has two orbitals, designated as $2s$ and $2p$, and so forth. The orientation of the electron's magnetic moment in a magnetic field is described by the *magnetic quantum number*, m. The values of m can be $m = -l, -(l-1),\ldots, 0,\ldots (l-1), l$. Each electron rotates about its own axis clockwise or anticlockwise, and the *spin quantum number*, s ($s = -1/2$ or $+1/2$) is assigned to each electron to specify this rotation.

The electron configuration of the atoms of different elements is governed by the following rules:

1. No two electrons can have the same values for all four quantum numbers in a given atom.
2. The orbital of the lowest energy will be filled in first, followed by the next higher energy orbital. The relative energies of the orbitals are $1s < 2s < 2p < 3s < 3p < 4s < 3d < 4p < 5s < 4d < 5p < 6s < 4f < 5d < 6p < 7s$. This order of energy is valid for lighter elements and is somewhat different in heavier elements.
3. There can be a maximum of $2(2l + 1)$ electrons in each orbital.
4. For given values of n and l, each of the available orbitals is first singly occupied such that no electron pairing occurs. Only when all orbitals are singly occupied does electron pairing take place.
5. Each energy shell contains a maximum of $2n^2$ electrons.

The hydrogen atom has one proton in the nucleus and one electron in the orbit. Its electronic structure is represented as $1s^1$. The helium atom has two electrons, which are accommodated in the $1s$ orbital, and thus has the structure of $1s^2$. Now let us consider the structure of ${}^{16}_{8}\mathrm{O}$, which has eight electrons. The first two electrons will fill the $1s$ orbital. The next two electrons will go to the $2s$ orbital. There are three p orbitals, designated as p_x, p_y, p_z, which will be occupied by three electrons individually. The eighth electron will occupy the p_x orbital pairing with the electron already in it. Thus, the electronic configuration of ${}^{16}_{8}\mathrm{O}$ is given by $1s^2 2s^2 2p^4$.

The electron configurations in different orbitals and shells are illustrated in Table 1.3, and the structure of ${}_{28}\mathrm{Ni}$ is shown in Fig. 1.1.

The electronic structure of the atom characterizes the chemical properties of elements. The outermost shell in the most stable and chemically inert elements such as neon, argon, krypton, and xenon has the electronic structure of ns^2np^6. Helium, although a noble gas, has the $1s^2$ configuration.

Elements having electronic configurations different from that of the noble gases either lose or gain electrons to achieve the structure ns^2np^6 of the nearest noble gas atom. The electrons in these shells are called the *valence electrons* and are primarily responsible for the chemical bond formation.

TABLE 1.3. Electron configurations in different energy shells.

Principal shell	Principal quantum number (n)	Orbital (l)	No. of electrons $= 2(2l+1)$ in each orbital	$2n^2$
K	1	*s*(0)	2	2
L	2	*s*(0)	2	
		p(1)	6	8
M	3	*s*(0)	2	
		p(1)	6	
		d(2)	10	18
N	4	*s*(0)	2	
		p(1)	6	
		d(2)	10	
		f(3)	14	32
O	5	*s*(0)	2	
		p(1)	6	
		d(2)	10	
		f(3)	14	
		g(4)	18	50

Electrons in different shells are held by *binding energy* in different shells of the atom. The binding energy of an electron is defined as the energy that is required to be supplied to remove it completely from a shell. The binding energy of the electron is the greatest in the *K* shell and decreases with higher shells such as *L*, *M*, and so on. The binding energy also increases with increasing atomic number of the elements. Thus, the *K*-shell binding energy (21.05 keV) of technetium, with atomic number 43, is higher than the *K*-shell binding energy (1.08 keV) of sodium, with atomic number 11. The *K*-shell binding energy of electrons in several elements are: carbon, 0.28 keV, gallium, 10.37 keV, technetium, 21.05 keV; indium, 27.93 keV; iodine, 33.16 keV; lead, 88.00 keV.

When an electron is removed completely from an atom, the process is called *ionization*. The atom is said to be ionized and becomes an ion. On the other hand, when the electron is raised from a lower energy shell to an upper energy shell, the process is called *excitation*. Both ionization and excitation processes require a supply of energy from outside the atom such as heating, applying an electric field, and so forth. In the excited atoms, electrons jump from the upper energy shell to

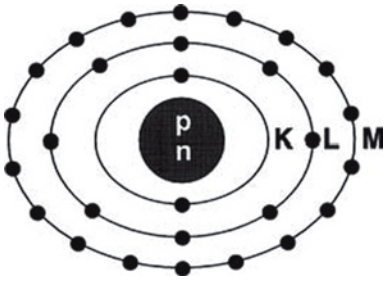

FIG. 1.1. The electronic configuration of $_{28}$Ni. The *K* shell has 2 electrons, the *L* shell has 8 electrons, and the *M* shell has 18 electrons.

the lower energy shell to achieve stability. The difference in energy appears as electromagnetic radiations or photons. Thus, if the binding energy of *K*-shell electrons in, say, bromine is 13.5 keV and the *L*-shell binding energy is 1.8 keV, the transition of electrons from the *L* shell to the *K* shell will occur with the emission of 11.7 keV (13.5 − 1.8 = 11.7 keV) photons. As we shall see later, these radiations are called the *characteristic x-rays* of the product atom.

Structure of the Nucleus

As already stated, the nucleus of an atom is composed of protons and neutrons. The number of protons is called the *atomic number* of the element and denoted by *Z*. The number of neutrons is denoted by *N*, and the sum of the protons and neutrons, $Z + N$, is called the *mass number*, denoted by *A*. The symbolic representation of an element, *X*, is given by ${}^{A}_{Z}X_{N}$. For example, sodium has 11 protons and 12 neutrons with a total of 23 nucleons. Thus, it is represented as ${}^{23}_{11}\mathrm{Na}_{12}$. However, the atomic number *Z* of an element is known, and *N* can be calculated as *A*–*Z*; therefore, it suffices to simply write ^{23}Na (or Na-23).

To explain the various physical observations related to the nucleus of an atom, two models for the nuclear structure have been proposed: the liquid drop model and the shell model. The liquid drop model was introduced by Niels Bohr and assumes a spherical nucleus composed of closely packed nucleons. This model explains various phenomena, such as nuclear density, energetics of particle emission in nuclear reactions, and fission of heavy nuclei.

In the shell models, both protons and neutrons are arranged in discrete energy shells in a manner similar to the electron shells of the atom in the Bohr atomic theory. Similar to the electronic configuration of the noble gas atoms, nuclei with 2, 8, 20, 28, 50, 82, or 126 protons or neutrons are found to be very stable. These nucleon numbers are called the *magic numbers*.

It is observed that atomic nuclei containing an odd number of protons or neutrons are normally less stable than those with an even number of protons or neutrons. Thus, nuclei with even numbers of protons and neutrons are more stable, whereas those with odd numbers of protons and neutrons are less stable. For example, ^{12}C with six protons and six neutrons is more stable than ^{13}C containing six protons and seven neutrons. There are 280 naturally-occurring stable nuclides of which 166 are even *N*–even *Z*, 57 are even–odd, 53 are odd–even, and only 4 are odd–odd.

The stability of these elements is dictated by the configuration of protons and neutrons in the nucleus. The ratio of the number of neutrons to the number of protons (*N*/*Z*) is an approximate indicator of the stability of a nucleus. The *N*/*Z* ratio is 1 in low-*Z* elements such as ${}^{12}_{6}\mathrm{C}$, ${}^{14}_{7}\mathrm{N}$, and ${}^{16}_{8}\mathrm{O}$, but it increases with increasing atomic number of elements. For example, it is 1.40 for ${}^{127}_{53}\mathrm{I}$ and 1.54 for ${}^{208}_{82}\mathrm{Pb}$. The plot of the atomic number versus the neutron number of all nuclides is shown in Fig. 1.2. All stable nuclear species fall on or around what is called the *line of stability*. The nuclear species on the left side of the line have fewer neutrons and more protons; that is, they are proton-rich. On the other hand, those on the right

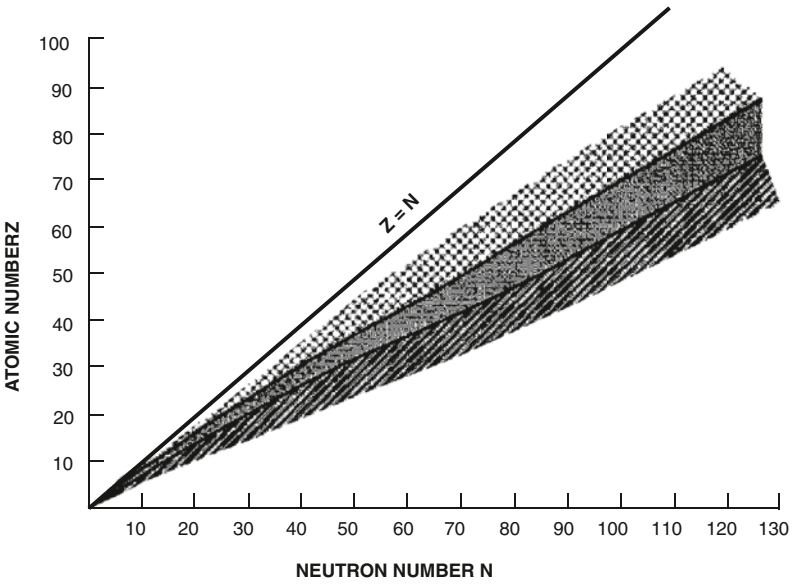

FIG. 1.2. The plot of atomic number (Z) versus the number of neutrons (N) for allnuclides. The proton-rich nuclides fall on the left (dotted) and the neutron-rich nuclides fall on the right (cross-hatched) of the line of stability, indicated by the dark-shaded area. The solid line represents nuclides with $Z=N$.

side of the line have fewer protons and more neutrons; that is, they are neutron-rich. The nuclides away from the line of stability are unstable and disintegrate to achieve stability.

Nuclear Binding Energy

According to the classical electrostatic theory, the nucleus of an atom cannot exist as a single entity, because of the electrostatic repulsive force among the protons in the nucleus. The stability of the nucleus is explained by the existence of a strong binding force called the *nuclear force*, which overcomes the repulsive force of the protons. The nuclear force is effective equally among all nucleons and exists only in the nucleus, having no influence outside the nucleus. The short range of the nuclear force leads to a very small size ($\sim 10^{-13}$ cm) and very high density ($\sim 10^{14}$ g/cm^3) of the nucleus.

The mass M of a nucleus is always less than the combined masses of the nucleons A in the nucleus. The difference in mass ($M–A$) is termed the *mass defect*, which has been used as binding energy for all nucleons in the nucleus. The average binding energy of a nucleon is equal to the total binding energy (calculated from the mass defect) divided by the number of nucleons. It is of the order of 6–9 MeV, although the binding energy of an individual nucleon has a definite

value, depending on the shell it occupies. The binding energy of a nucleon must be supplied to completely remove it from the nucleus. Note that whereas the binding energy of the nucleons is in the megaelectron volt (MeV) range, the electron binding energy in the atomic orbital is of the order of kiloelectron volts (keV), a factor of 1000 lower.

Nuclear Nomenclature

A *nuclide* is an atomic species with a definite number of protons and neutrons arranged in a definite order in the nucleus.

Radionuclides are those nuclides that are unstable and thus decay by emission of particles or electromagnetic radiations or by spontaneous fission.

Isotopes are the nuclides having the same atomic number Z but different mass number A. Isotopes exhibit the same chemical properties. Examples of carbon isotopes are $^{11}_{6}C$, $^{12}_{6}C$, and $^{13}_{6}C$.

Isotones are the nuclides having the same number of neutrons N but different numbers of protons. Examples of isotones are: $^{134}_{55}Cs$, $^{133}_{54}Xe$, and $^{132}_{53}I$, each having 79 neutrons.

Isobars are the nuclides with the same number of nucleons, that is, the same mass number A, but a different combination of protons and neutrons. For example: ^{82}Y, ^{82}Sr, ^{82}Rb, and ^{82}Kr are all isobars having the mass number 82.

Isomers are the nuclides with the same number of protons and neutrons, but having different energy states and spins. ^{99}Tc and ^{99m}Tc are isomers of the same nuclide. Individual nuclides can exist in different energy states above the ground state due to excitation. These excited states are called the *isomeric states*, which can have a lifetime varying from picoseconds to years. When the isomeric states are long-lived, they are referred to as *metastable states*. These states are denoted by "m" as in ^{99m}Tc.

Chart of the Nuclides

Nearly 3700 nuclides, both stable and unstable, are arranged in the form of a chart, called the *chart of the nuclides*, a section of which is presented in Fig. 1.3. Each square in the chart represents a specific nuclide, containing various information such as the half-life, type and energy of radiations, and so forth of the nuclide, and neutron capture cross section of the stable nuclide. The nuclides are arranged in increasing neutron number N horizontally and in increasing proton number Z vertically. Each horizontal group of squares contains all isotopes of the same element, whereas the vertical group contains all isotones with the same number of neutrons. For isomers, the square is subdivided into sections representing each isomer.

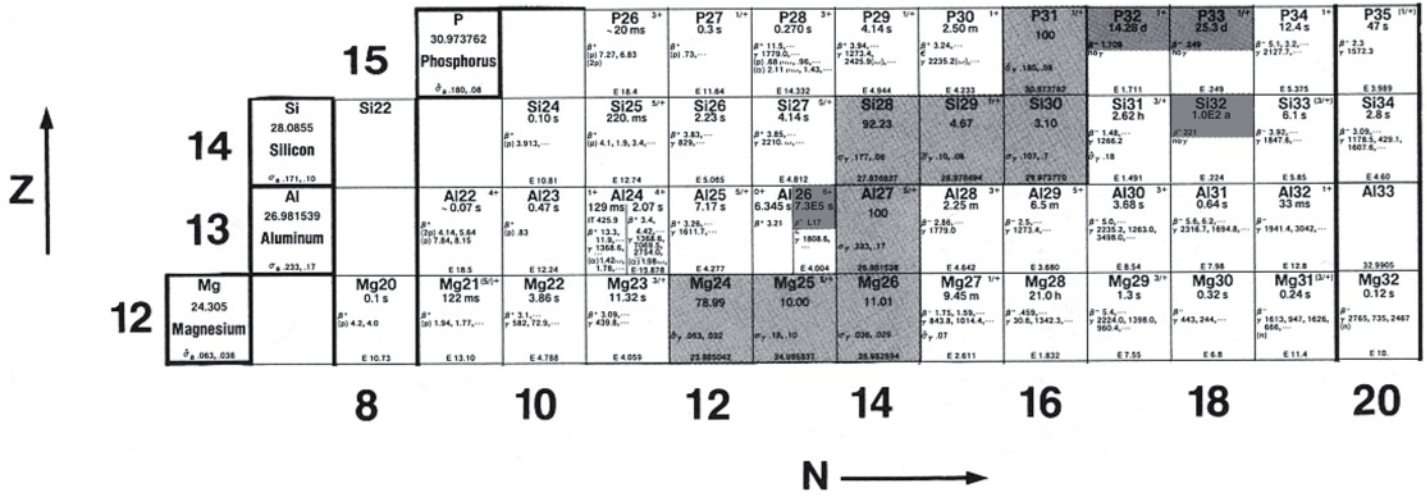

FIG. 1.3. A section of the chart of nuclides. (Courtesy of Knolls Atomic Power Laboratory, Schenectady, New York, operated by the General Electric Company for Naval Reactors, the U.S. Department of Energy.)

Questions

1. If a mass of matter (m) is converted to electromagnetic radiation, what should be the energy of this radiation?
2. Describe the Bohr's atomic theory in terms of the electronic configuration of the atom.
3. What is the difference between the orbital electron binding energy and the nuclear binding energy of an atom?
4. Define the mass defect and mass number of an atom. What does the mass defect account for?
5. Write the electronic configuration of ^{99m}Tc and ^{131}I.
6. How many electrons can the 3*d* orbital contain?
7. The electron binding energy of the *K* shell in an atom is higher than that of the *L* shell. True or false?
8. What is the difference between ionization and excitation of an atom?
9. What is a metastable state of a nuclide? How is it designated?

Suggested Readings

Evans RD. *The Atomic Nucleus*. Malabar, FL: Kreiger; 1982.

Friedlander G, Kennedy TW, Miller JM. *Nuclear and Radiochemistry*. 3rd ed. New York: Wiley; 1981.

Turner JE. *Atoms, Radiation, and Radiation Protection*. 2nd ed. New York: Wiley; 1995.

2
Radioactive Decay

In 1896, Henri Becquerel first discovered natural radioactivity in potassium uranyl sulfate. Artificial radioactivity was not produced until 1934, when I. Curie and F. Joliot made boron, aluminum, and magnesium radioactive by bombarding them with α-particles from polonium. This introduction of artificial radioactivity prompted the invention of cyclotrons and reactors in which many radionuclides are now produced. So far, more than 3400 radionuclides have been artificially produced and characterized in terms of their physical properties.

Radionuclides are unstable and decay by emission of particle or γ-radiation to achieve stable configuration of protons and neutrons in the nucleus. As already mentioned, the stability of a nuclide in most cases is determined by the N/Z ratio of the nucleus. Thus, as will be seen later, whether a nuclide will decay by a particular particle emission or γ-ray emission is determined by the N/Z and/or excitation energy of the nucleus. Radionuclides can decay by one or more of the six modes: *spontaneous fission, isomeric transition (IT), alpha (α) decay, beta (β^-) decay, positron (β^+) decay, and electron capture (EC) decay*. In all decay modes, energy, charge, and mass are conserved. Different decay modes of radionuclides are described later in detail.

Spontaneous Fission

Fission is a process in which a heavy nucleus breaks into two fragments accompanied by the emission of two or three neutrons. The neutrons carry a mean energy of 1.5 MeV and the process releases about 200 MeV energy that appears mostly as heat.

Spontaneous fission occurs in heavy nuclei, but its probability is low and increases with mass number of the nuclei. The half-life for spontaneous fission is 2×10^{17} years for ^{235}U and only 55 days for ^{254}Cf. As an alternative to the spontaneous fission, the heavy nuclei can decay by α-particle or γ-ray emission.

G. B. Saha, *Physics and Radiobiology of Nuclear Medicine,*
DOI 10.1007/978-1-4614-4012-3_2,

Isomeric Transition

As previously mentioned, a nucleus can exist in different energy or excited states above the ground state, which is considered as the state involving the arrangement of protons and neutrons with the least amount of energy. These excited states are called the *isomeric states* and have lifetimes of fractions of picoseconds to many years. When isomeric states are long-lived, they are referred to as *metastable states* and denoted by "m" as in ^{99m}Tc. An excited nucleus decays to a lower energy state by giving off its energy, and such transitions are called isomeric transitions (ITs). Several isomeric transitions may occur from intermediate excited states prior to reaching the ground state. As will be seen later, a parent radionuclide may decay to an upper isomeric state of the product nucleus by α-particle or β-particle emission, in which case the isomeric state returns to the ground state by one or more isomeric transitions. A typical isomeric transition of ^{99m}Tc is illustrated in Fig. 2.1. Isomeric transitions can occur in two ways: gamma (γ)-ray emission and internal conversion.

Gamma (γ)-Ray Emission

The common mode of an isomeric transition from an upper energy state of a nucleus to a lower energy state is by emission of an electromagnetic radiation, called the γ-ray. The energy of the γ-ray emitted is the difference between the two isomeric states. For example, a decay of a 525-keV isomeric state to a 210-keV isomeric state will result in the emission of a 315-keV γ-ray.

Internal Conversion

An alternative to the γ-ray emission is the *internal conversion* process. The excited nucleus transfers the excitation energy to an orbital electron—preferably

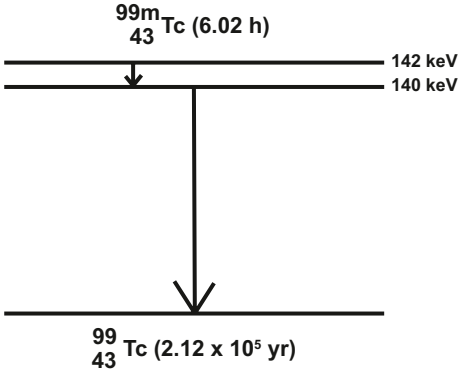

FIG. 2.1. Isometric transition of ^{99m}Tc. Ten percent of the decay follows internal conversion.

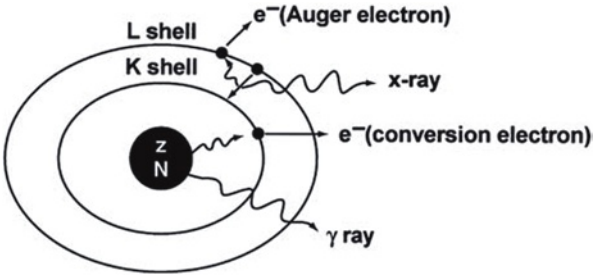

FIG. 2.2. Internal conversion process. The excitation energy of the nucleus is transferred to a *K*-shell electron, which is then ejected with kinetic energy equal to E_γ–E_B, and the *K*-shell vacancy is filled by an electron from the *L* shell. The energy difference between the *L* shell and *K* shell appears as the characteristic *K* x-ray. Alternatively, the characteristic *K* x-ray may transfer its energy to an *L*-shell electron, called the Auger electron, which is then ejected.

the *K*-shell electron—of its own atom, which is then ejected from the shell, provided the excitation energy is greater than the binding energy of the electron (Fig. 2.2). The ejected electron is called the *conversion electron* and carries the kinetic energy equal to $E_\gamma - E_B$, where E_γ is the excitation energy and E_B is the binding energy of the electron. Even though the *K*-shell electrons are more likely to be ejected because of the proximity to the nucleus, the electrons from the *L* shell, *M* shell, and so forth also may be ejected by the internal conversion process. The ratio of the number of conversion electrons (N_e) to the number of observed γ-radiations (N_γ) is referred to as the *conversion coefficient*, given as $\alpha = N_e/N_\gamma$. The conversion coefficients are subscripted as α_K, α_L, α_M… depending on which shell the electron is ejected from. The total conversion coefficient α_T is then given by

$$\alpha_T = \alpha_K + \alpha_L + \alpha_M + \cdots$$

Problem 2.1
If the total conversion coefficient (α_T) is 0.11 for the 140-keV γ-rays of ^{99m}Tc, calculate the percentage of 140-keV γ-radiations available for imaging.

Answer

$$\alpha_T = \frac{N_e}{N_\gamma} = 0.11$$

$$N_e = 0.11 N_\gamma$$

Total number of disintegrations

$$\begin{aligned} &= N_e + N_\gamma \\ &= 0.11N_\gamma + N_\gamma \\ &= 1.11N_\gamma \end{aligned}$$

Thus, the percentage of γ-radiations

$$\begin{aligned} &= \frac{N_\gamma}{1.11N_\gamma} \times 100 \\ &= \frac{1}{1.11} \times 100 \\ &= 90\ \% \end{aligned}$$

An internal conversion process leaves an atom with a vacancy in one of its shells, which is filled by an electron from the next higher shell. Such situations may also occur in nuclides decaying by electron capture (see later). When an L electron fills in a K-shell vacancy, the energy difference between the K shell and the L shell appears as a *characteristic K x-ray*. Alternatively, this transition energy may be transferred to an orbital electron, which is emitted with a kinetic energy equal to the characteristic x-ray energy minus its binding energy. These electrons are called *Auger electrons*, and the process is termed the *Auger process*, analogous to internal conversion. The Auger electrons are monoenergetic. Because the characteristic x-ray energy (energy difference between the two shells) is always less than the binding energy of the K-shell electron, the latter cannot undergo the Auger process and cannot be emitted as an Auger electron.

The vacancy in the shell resulting from an Auger process is filled by the transition of an electron from the next upper shell, followed by emission of similar characteristic x-rays and/or Auger electrons. The fraction of vacancies in a given shell that are filled by emitting characteristic x-ray emissions is called the *fluorescence yield*, and the fraction that is filled by the Auger processes is the *Auger yield*. The Auger process increases with the increasing atomic number of the atom.

Alpha (α)-Decay

The α-decay occurs mostly in heavy nuclides such as uranium, radon, plutonium, and so forth. Beryllium-8 is the only lightest nuclide that decays by breaking up into two α-particles. The α-particles are basically helium ions with two protons and two neutrons in the nucleus and two electrons removed from the orbital of the helium atom. After α-decay, the atomic number of the nucleus is reduced by 2 and the mass number by 4.

$$^{222}_{86}\text{Rn} \rightarrow {}^{218}_{84}\text{Po} + \alpha$$

The α-particles from a given radionuclide all have discrete energies corresponding to the decay of the initial nuclide to a particular energy level of the product (including, of course, its ground state). The energy of the α-particles is, as a rule, equal to the energy difference between the two levels and ranges from 1 to 10 MeV. The high-energy α-particles normally originate from the short-lived heavy radionuclides and vice versa. The range of the α-particles is very short in matter and is approximately 0.03 mm in body tissue. The α-particles can be stopped by a piece of paper, a few centimeters of air, and gloves.

Beta (β^-)-Decay

When a radionuclide is neutron rich—that is, the N/Z ratio is greater than that of the nearest stable nuclide—it decays by the emission of a β^--particle (note that it is an electron[1]) and an antineutrino, $\bar{\nu}$. In the β^--decay process, a neutron is converted to a proton, thus raising the atomic number Z of the product by 1. Thus:

$$n \rightarrow p + \beta^- + \bar{\nu}$$

The difference in rest masses between the parent nuclide and the daughter nuclide plus β^--particle appears as the kinetic energy, which is called the *transition or decay energy*, denoted by E_{max}. The β^--particles carry E_{max} or part of it, exhibiting a spectrum of energy as shown in Fig. 2.3. The average energy of the β^--particles is about one-third of E_{max}. This observation indicates that β^--particles often carry only a part of the transition energy, and energy is not apparently conserved in β^--decay. To satisfy the law of energy conservation, a particle called the *antineutrino*, $\bar{\nu}$, with no charge and a negligible mass has been postulated, which carries the remainder of E_{max} in each β^--decay. The existence of antineutrinos has been proven experimentally.

In β^--decay, the parent nuclide may decay to the ground state or an excited state of the daughter nuclide and also, if energetically permitted, may emit several β^--particles. The excited states then decay to the ground state by γ-ray emission or internal conversion (Fig. 2.4).

The decay process of a radionuclide is normally represented by what is called the *decay scheme*. Typical decay schemes of ^{131}I and ^{99}Mo are shown in Figs. 2.4 and 2.5, respectively. The β^--decay is shown by a left-to-right arrow from the parent nuclide to the daughter nuclide, whereas the isomeric transition is displayed by a vertical arrow between the two states. (Note: The β^+-decay is shown by a two-step right-to-left arrow between the two states, the electron capture decay by a right-to-left arrow, and the α-decay by a down arrow). Although it is often said that ^{131}I emits 364-keV γ-rays, it should be understood that the 364-keV γ-ray

[1] The difference between a β^--particle and an electron is that a β^--particle originates from the nucleus, and an electron originates from the extranuclear electron orbitals.

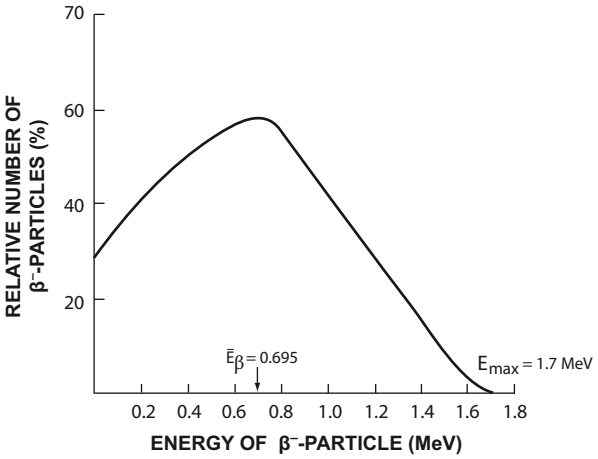

FIG. 2.3. A typical energy spectrum of the β^--particles of ^{32}P.

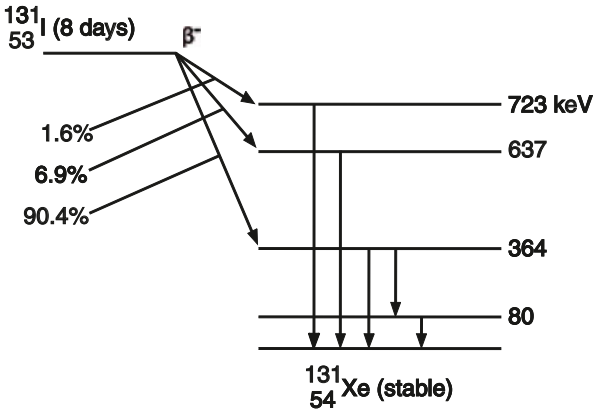

FIG. 2.4. Decay scheme of ^{131}I. Eighty-one percent of the total ^{131}I radionuclides decay by 364-keV γ-ray emission. The 8.0-day half-life of ^{131}I is shown in parentheses.

belongs to ^{131}Xe as an isomeric state. This is true for all β^--, β^+-, or electron capture decays that are followed by γ-ray emission.

Some examples of β^--decay follow:

$$^{99}_{42}\mathrm{Mo} \rightarrow {}^{99\mathrm{m}}_{43}\mathrm{Tc} + \beta^- + \bar{\nu}$$

$$^{131}_{53}\mathrm{I} \rightarrow {}^{131}_{54}\mathrm{Xe} + \beta^- + \bar{\nu}$$

$$^{67}_{29}\mathrm{Cu} \rightarrow {}^{67}_{30}\mathrm{Zn} + \beta^- + \bar{\nu}$$

$$^{90}_{38}\mathrm{Sr} \rightarrow {}^{90}_{39}\mathrm{Y} + \beta^- + \bar{\nu}$$

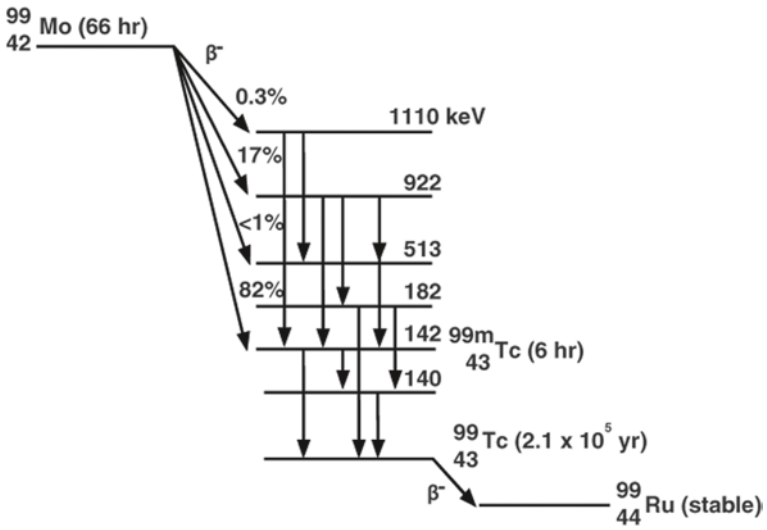

FIG. 2.5. Decay scheme of ^{99}Mo. Approximately 87 % of the total ^{99}Mo ultimately decays to ^{99m}Tc, and the remaining 13 % decays to ^{99}Tc. A 2-keV transition occurs from the 142-keV level to the 140-keV level. All the 2-keV γ-rays are internally converted. (The energy levels are not shown in scale.)

It should be noted that in β^--decay, the atomic number of the daughter nuclide is increased by 1 and the mass number remains the same.

Positron (β^+)-Decay

When a radionuclide is proton rich—that is, the N/Z ratio is low relative to that of the nearest stable nuclide—it can decay by positron (β^+) emission accompanied by the emission of a neutrino (ν), which is an opposite entity of the antineutrino. In β^+-decay, essentially a proton is converted to a neutron plus a positron, thus, decreasing the atomic number Z of the daughter nuclide by 1. Thus,

$$p \rightarrow n + \beta^+ + \nu$$

Positron emission takes place when the parent nuclide has a minimum of mass-energy equivalent of 1.022 MeV more than the daughter nuclide. The requirement of 1.022 MeV for β^+-decay arises from the fact that one electron mass has to be added to a proton to produce a neutron and one positron is created. Since each electron or positron mass is equal to 0.511 MeV, one electron and one positron are equal to 1.022 MeV, which is required as a minimum for β^+-decay. Energy in excess of 1.022 MeV (E_{max}–1.022) is shared as kinetic energy between

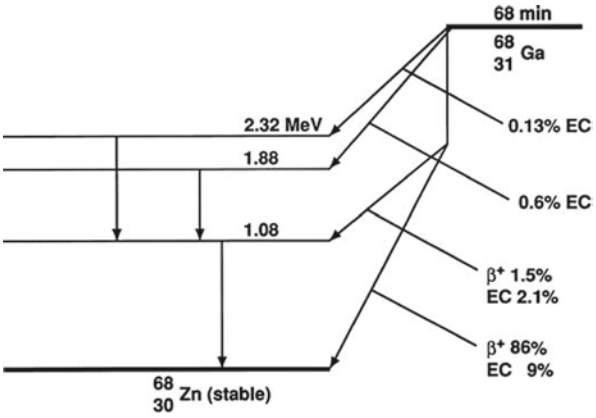

FIG. 2.6. Decay scheme of ^{68}Ga. The positrons are annihilated in medium to give rise to two 511-keV γ-rays emitted in opposite directions.

the β^+particle and v. This results in an energy spectrum of β^+ particles similar to the β^--particles. The parent nuclide may decay by one or more ground states of the daughter nuclide, followed by γ-ray emission or internal conversion.

Some examples of β^+-decay follow:

$$
\begin{aligned}
{}^{18}_{9}\mathrm{F} &\rightarrow {}^{18}_{8}\mathrm{O} + \beta^+ + v \\
{}^{68}_{31}\mathrm{Ga} &\rightarrow {}^{68}_{30}\mathrm{Zn} + \beta^+ + v \\
{}^{13}_{7}\mathrm{N} &\rightarrow {}^{13}_{6}\mathrm{C} + \beta^+ + v \\
{}^{15}_{8}\mathrm{O} &\rightarrow {}^{15}_{7}\mathrm{N} + \beta^+ + v
\end{aligned}
$$

The energetic β^+-particle loses energy while passing through matter. The range of positrons is short in matter. When it loses almost all of its energy, it combines with an atomic electron of the medium and is annihilated, giving rise to two photons of 511 keV emitted in opposite directions. These photons are called *annihilation radiations*.

The decay scheme of ^{68}Ga is presented in Fig. 2.6. Note that the β^+-decay is represented by a two-step right-to-left arrow.

Electron Capture

Decay by electron capture (EC) is an alternative to the β^+-decay for proton-rich radionuclides with N/Z lower than that of the stable nuclide. In EC decay, an electron from an extranuclear shell, particularly the K shell because of its proximity,

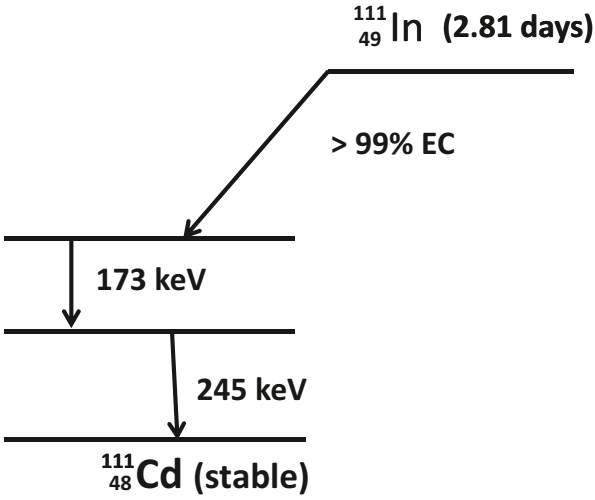

FIG. 2.7. Decay scheme of ^{111}In illustrating the electron capture process. The abundances of 171 and 245-keV γ-rays are 90 and 94 %, respectively.

is captured by a proton in the nucleus, forming a neutron accompanied by the emission of a neutrino for conservation of energy. Thus,

$$p + e^- \rightarrow n + \nu$$

In this process, the atomic number of the daughter nuclide is lowered by 1. The EC process occurs usually in nuclides having mass-energy equivalent less than 1.022 MeV. In nuclides having energy greater than 1.022 MeV, both EC and β^+-decay can occur, although the probability of β^+-decay increases with higher energy. The decay scheme of ^{111}In is shown in Fig. 2.7. The EC decay is indicated by a right-to-left arrow. Some examples of EC decay follow:

$$\begin{aligned}
^{111}_{49}\mathrm{In} + e^- &\rightarrow {}^{111}_{48}\mathrm{Cd} + \nu \\
^{67}_{31}\mathrm{Ga} + e^- &\rightarrow {}^{67}_{30}\mathrm{Zn} + \nu \\
^{125}_{53}\mathrm{I} + e^- &\rightarrow {}^{125}_{52}\mathrm{Te} + \nu \\
^{57}_{27}\mathrm{Co} + e^- &\rightarrow {}^{57}_{26}\mathrm{Fe} + \nu \\
^{123}_{53}\mathrm{I} + e^- &\rightarrow {}^{123}_{52}\mathrm{Te} + \nu
\end{aligned}$$

In EC decay, analogous to the situation in internal conversion, a vacancy is created in the shell from which the electron is captured. It is filled in by the transition of an electron from the next upper shell, in which case the difference in energy between the two shells appears as a characteristic x-ray of the daughter nuclide. Also, as described earlier, instead of characteristic x-ray emission, the Auger process can occur, whereby an Auger electron is emitted.

Questions

1. What are the primary criteria for β^+ and β^--decay?
2. If the mass-energy difference between the proton-rich parent nuclide and the daughter nuclide is 1.2 MeV, could the parent radionuclide decay by β^+ decay and/or electron capture? If the energy difference is 0.8 MeV, what should be the mode of decay?
3. If the total conversion coefficient (α_T) of 195-keV γ-rays of a radionuclide is 0.23, calculate the percentage of 195-keV photons available for imaging.
4. Can a *K*-shell electron be emitted as an Auger electron? Explain.
5. Explain how characteristic x-rays and Auger electrons are emitted.
6. Why is an antineutrino emitted in β^--decay?
7. A *K*-shell electron is ejected by the internal conversion of a 155-keV γ-ray photon. If the binding energy of the *K*-shell electron is 25 keV, what is the kinetic energy of the electron?
8. What is the average energy of the β^--particles emitted from a radionuclide?
9. Explain the production of annihilation radiations.

Suggested Readings

Evans RD. *The Atomic Nucleus*. Malabar, FL: Kreiger; 1982.

Friedlander G, Kennedy JW, Miller JM. *Nuclear and Radiochemistry*. 3rd ed. New York: Wiley; 1981.

Turner JE. *Atoms, Radiation, and Radiation Protection*. 2nd ed. New York: Wiley; 1995.

3
Kinetics of Radioactive Decay

Radioactive Decay Equations

General Equation

As mentioned in Chapter 2, radionuclides decay by spontaneous fission, α-, β^--, and β^+-particle emissions, electron capture, or isomeric transition. The radioactive decay is a random process, and it is not possible to tell which atom from a group of atoms disintegrates at a specific time. Thus, one can only talk about the average number of radionuclides disintegrating during a period of time. This gives the disintegration rate of a particular radionuclide.

The disintegration rate of a radionuclide, that is, the number of disintegrations per unit time, given as $-dN/dt$, is proportional to the total number of radioactive atoms present at that time. Mathematically,

$$\frac{-dN}{dt} = \lambda N \tag{3.1}$$

where N is the number of radioactive atoms present, and λ is referred to as the *decay constant* of the radionuclide. As can be seen from Eq. (3.1), it is a small fraction of the radioactive atoms that decays in a very short period of time. The unit of λ is $(\text{time})^{-1}$. Thus, if λ is 0.2 s^{-1} for a radionuclide, then 20 % of the radioactive atoms present will disappear per second.

The disintegration rate $-dN/dt$ is referred to as the *radioactivity* or simply the *activity* of the radionuclide and denoted by A. It should be understood from Eq. (3.1) that the same amount of radioactivity means the same disintegration rate for any radionuclide, but the total number of atoms present and the decay constants differ for different radionuclides. For example, a radioactive sample A containing 10^6 atoms and with $\lambda = 0.01$ min^{-1} would give the same disintegration rate (10,000 disintegrations per minute) as that by a radioactive sample B containing 2×10^6 atoms and with a decay constant 0.005 min^{-1}.

G. B. Saha, *Physics and Radiobiology of Nuclear Medicine,*
DOI 10.1007/978-1-4614-4012-3_3,

Now from the preceding discussion, the following equation can be written:

$$A = \lambda N \tag{3.2}$$

From a knowledge of the decay constant and radioactivity of a radionuclide, one can calculate the total number of atoms or mass of the radionuclides present (using Avogadro's number 1 g · atom = 6.02×10^{23} atoms).

Because Eq. (3.1) is a first-order differential equation, the solution of this equation by integration leads to

$$N_t = N_0 e^{-\lambda t} \tag{3.3}$$

where N_0 and N_t are the number of radioactive atoms at $t = 0$ and time t, respectively. Equation (3.3) is an exponential equation indicating that the radioactivity decays exponentially. By multiplying both sides of Eq. (3.3) by λ, one obtains

$$A_t = A_0 e^{-\lambda t} \tag{3.4}$$

The factor $e^{-\lambda t}$ is called the *decay factor*. The decay factor becomes $e^{+\lambda t}$ if the activity at time t before $t = 0$ is to be determined. The plot of activity versus time on a linear graph gives an exponential curve, as shown in Fig. 3.1. However, if the activity is plotted against time on semilogarithmic paper, a straight line results, as shown in Fig. 3.2.

Half-Life

Every radionuclide is characterized by a *half-life*, which is defined as the time required to reduce its initial activity to one half. It is usually denoted by $t_{1/2}$ and is unique for a radionuclide. It is related to the decay constant λ of a radionuclide by

$$\lambda = \frac{0.693}{t_{1/2}} \tag{3.5}$$

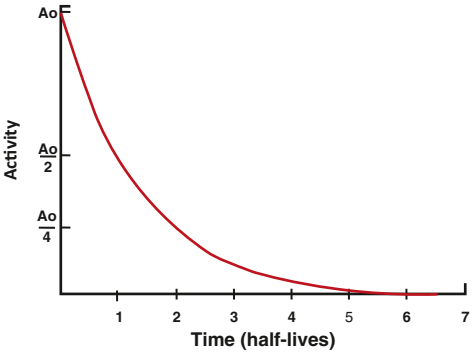

FIG. 3.1. Plot of radioactivity versus-time on a linear graph indicating an exponential curve.

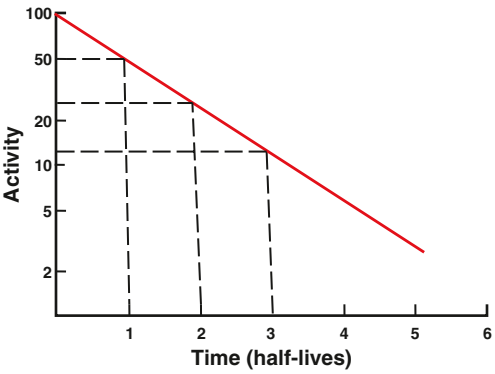

FIG. 3.2. Plot of radioactivity against time on a semilogarithmic graph indicating a straight line. The half-life of the radionuclide can be determined from the slope of the line, which is given as the decay constant λ. Alternatively, an activity and half its value and their corresponding times are read from the plot. The difference in the two time readings gives the half-life.

From the definition of half-life, it is understood that A_0 is reduced to $A_0/2$ in one half-life; to $A_0/4$, that is, to $A_0/2^2$ in two half-lives; to $A_0/8$, that is, to $A_0/2^3$ in three half-lives; and so forth. In n half-lives of decay, it is reduced to $A_0/2^n$. Thus, the radioactivity A_t at time t can be calculated from the initial radioactivity A_0 by

$$A_t = \frac{A_0}{2^n} = \frac{A_0}{2^{(t/t_{1/2})}} = A_0(0.5)^{t/t_{1/2}} \tag{3.6}$$

where t is the time of decay. Here, $t/t_{1/2}$ can be an integer or a fraction depending on t and $t_{1/2}$. For example, a radioactive sample with $t_{1/2} = 3.2$ days decaying at a rate of 10,000 disintegrations per minute would give, after seven days of decay, $10{,}000/2^{(7/3.2)} = 10{,}000/2^{2.2} = 10{,}000/4.59 = 2178$ disintegrations per minute.

It should be noted that ten half-lives of decay reduce the radioactivity by a factor of about $1000(2^{10} = 1024)$, or to 0.1 % of the initial activity.

The half-life of a radionuclide is determined by measuring the radioactivity at different time intervals and plotting them on semilogarithmic paper, as shown in Fig. 3.2. An initial activity and half its value are read from the line, and the corresponding times are noted. The difference in time between the two readings gives the half-life of the radionuclide. For a very long-lived radionuclide, the half-life is determined by Eq. (3.2) from a knowledge of its activity and the number of atoms present. The number of atoms N can be calculated from the weight W of the radionuclide with atomic weight A and Avogadro's number 6.02×10^{23} atoms per g · atom as follows:

$$N = \frac{W}{A} \times 6.02 \times 10^{23} \tag{3.7}$$

When two or more radionuclides are present in a sample, the measured count of such a sample comprises counts of all individual radionuclides. A semilogarithmic plot of the activity of a two-component sample versus time is shown in

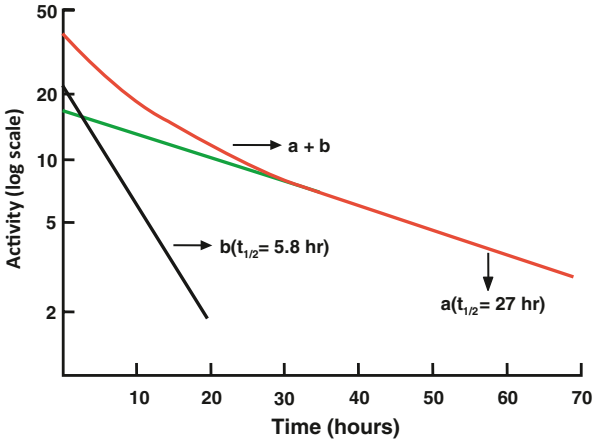

FIG. 3.3. A composite radioactive decay curve for a sample containing two radionuclides of different half-lives. The long-lived component (*a*) has a half-life of 27 h and the short-lived component (*b*) has a half-life of 5.8 h.

Fig. 3.3. The half-life of each of the two radionuclides can be determined by what is called the *peeling or stripping method*. In this method, first, the tail part (second component) of the curve is extrapolated as a straight line up to the ordinate, and its half-life can be determined as mentioned previously (e.g., 27 h). Second, the activity values on this line are subtracted from those on the composite line to obtain the activity values for the first component. A straight line is drawn through these points, and the half-life of the first component is determined (e.g., 5.8 h). The stripping method can be applied to more than two components in the similar manner.

Mean Life

Another relevant quantity of a radionuclide is its *mean life*, which is the average lifetime of a group of radionuclides. It is denoted by τ and is related to the decay constant λ and half-life $t_{1/2}$ as follows:

$$\tau = \frac{1}{\lambda} \tag{3.8}$$

$$\tau = \frac{t_{1/2}}{0.693} = 1.44\, t_{1/2} \tag{3.9}$$

In one mean life, the activity of a radionuclide is reduced to 37 % of its initial value.

Effective Half-Life

As already mentioned, a radionuclide decays exponentially with a definite half-life, which is called the *physical half-life*, denoted by T_p (or $t_{1/2}$). The physical half-life of a radionuclide is independent of its physicochemical conditions. Analogous to physical decay, radiopharmaceuticals administered to humans disappear exponentially from the biological system through fecal excretion, urinary excretion, perspiration, or other routes. Thus, after in vivo administration every radiopharmaceutical has a *biological half-life* (T_b), which is defined as the time needed for half of the radiopharmaceutical to disappear from the biologic system. It is related to decay constant λ_b by $\lambda_b = 0.693/T_b$.

Obviously, in any biologic system, the loss of a radiopharmaceutical is due to both the physical decay of the radionuclide and the biologic elimination of the radiopharmaceutical. The net or effective rate (λ_e) of loss of radioactivity is then related to λ_p and λ_b by

$$\lambda_e = \lambda_p + \lambda_b \tag{3.10}$$

Because $\lambda = 0.693/t_{1/2}$, it follows that

$$\frac{1}{T_e} = \frac{1}{T_p} + \frac{1}{T_b} \tag{3.11}$$

or,

$$T_e = \frac{T_p \times T_b}{T_p + T_b} \tag{3.12}$$

The effective half-life, T_e, is always less than the shorter of T_p or T_b. For a very long T_p and a short T_b, T_e is almost equal to T_b. Similarly, for a very long T_b and short T_p, T_e is almost equal to T_p.

Units of Radioactivity

The unit of radioactivity is a curie. It is defined as

$$\begin{aligned} 1\text{curie (Ci)} &= 3.7 \times 10^{10} \text{ disintegrations per second (dps)} \\ &= 2.22 \times 10^{12} \text{ disintegrations per minute (dpm)} \end{aligned}$$

$$\begin{aligned} 1 \text{ millicurie (mCi)} &= 3.7 \times 10^{7} \text{ dps} \\ &= 2.22 \times 10^{9} \text{ dpm} \end{aligned}$$

$$1 \text{ microcurie } (\mu\text{Ci}) = 3.7 \times 10^4 \text{ dps}$$
$$= 2.22 \times 10^6 \text{ dpm}$$

The System Internationale (SI) unit for radioactivity is the becquerel (Bq), which is defined as 1 dps. Thus,

$$1 \text{ becquerel (Bq)} = 1 \text{ dps} = 2.7 \times 10^{-11} \text{ Ci}$$

$$1 \text{ kilobecquerel (kBq)} = 10^3 \text{ dps} = 2.7 \times 10^{-8} \text{ Ci}$$

$$1 \text{ megabecquerel (MBq)} = 10^6 \text{ dps} = 2.7 \times 10^{-5} \text{ Ci}$$

$$1 \text{ gigabecquerel (GBq)} = 10^9 \text{ dps} = 2.7 \times 10^{-2} \text{ Ci}$$

$$1 \text{ terabecquerel (TBq)} = 10^{12} \text{ dps} = 27 \text{ Ci}$$

Similarly,

$$1 \text{ Ci} = 3.7 \times 10^{10} \text{ Bq} = 37 \text{ GBq}$$

$$1 \text{ mCi} = 3.7 \times 10^7 \text{ Bq} = 37 \text{ MBq}$$

$$1 \mu\text{Ci} = 3.7 \times 10^4 \text{ Bq} = 37 \text{ kBq}$$

Specific Activity

The presence of "cold," or nonradioactive, atoms in a radioactive sample always induces competition between them in their chemical reactions or localization in a body organ, thereby compromising the concentration of the radioactive atoms in the organs. Thus, each radionuclide or radioactive sample is characterized by *specific activity*, which is defined as the radioactivity per unit mass of a radionuclide or a radioactive sample. For example, suppose that a 200-mg ^{123}I-labeled monoclonal antibody sample contains 350-mCi (12.95-GBq) ^{123}I radioactivity. Its specific activity would be 350/200 = 1.75 mCi/mg or 64.75 MBq/mg. Sometimes, it is confused with concentration, which is defined as the radioactivity per unit volume of a sample. If a 10-ml radioactive sample contains 50 mCi (1.85 GBq), it will have a concentration of 50/10 = 5 mCi/ml or 185 MBq/ml.

Specific activity is at times expressed as radioactivity per mole of a labeled compound, for example, mCi/mole (MBq/mole) or mCi/μmole (MBq/μmole) for ^{3}H-, ^{14}C-, and ^{35}S-labeled compounds.

The specific activity of a carrier-free (see Chapter 5) radionuclide sample is related to its half-life and mass number A: the shorter the half-life and the lower the A, the higher the specific activity. The specific activity of a carrier-free

radionuclide with mass number A and half-life $t_{1/2}$ in hours can be calculated as follows:

Suppose 1 mg of a carrier-free radionuclide is present in the sample.

$$\text{Number of atoms in the sample} = \frac{1 \times 10^{-3}}{A} \times 6.02 \times 10^{23} = \frac{6.02 \times 10^{20}}{A}$$

$$\text{Decay constant } \lambda = \frac{0.693}{t_{1/2} \times 60 \times 60} \text{sec}^{-1}$$

$$\begin{aligned} \text{Thus, disintegration rate } D &= \lambda N \\ &= \frac{0.693 \times 6.02 \times 10^{20}}{t_{1/2} \times A \times 60 \times 60} \\ &= \frac{1.1589 \times 10^{17}}{A \times t_{1/2}} \text{ dps} \end{aligned}$$

$$\begin{aligned} \text{Thus, specific activity (mCi/mg)} &= \frac{1.1589 \times 10^{17}}{A \times t_{1/2} \times 3.7 \times 10^{7}} \\ &= \frac{3.13 \times 10^{9}}{A \times t_{1/2}} \end{aligned} \quad (3.13)$$

where A is the mass number of the radionuclide, and $t_{1/2}$ is the half-life of the radionuclide in hours.

From Eq. (3.13), specific activities of carrier-free ^{99m}Tc and ^{131}I can be calculated as 5.27×10^6 mCi/mg (1.95×10^5 GBq/mg) and 1.25×10^5 mCi/mg (4.6×10^3 GBq/mg), respectively.

Calculation

Some examples related to the calculation of radioactivity and its decay follow:

Problem 3.1
Calculate the total number of atoms and total mass of ^{201}Tl present in 10 mCi (370 MBq) of ^{201}Tl ($t_{1/2} = 3.04$d).

Answer
For ^{201}Tl,

$$\lambda = \frac{0.693}{3.04 \times 24 \times 60 \times 60} = 2.638 \times 10^{-6} \text{ sec}^{-1}$$

$$A = 10 \times 3.7 \times 10^7 = 3.7 \times 10^8 \text{ dps}$$

Using Eq. (3.2),

$$N = \frac{A}{\lambda} = \frac{3.7 \times 10^8}{2.638 \times 10^{-6}} = 1.40 \times 10^{14} \text{ atoms}$$

Because 1 g · atom ^{201}Tl = 201 g ^{201}Tl = 6.02×10^{23} atoms of ^{201}Tl (Avogadro's number),

$$\begin{aligned}\text{Mass of } ^{201}\text{Tl in 10 mCi(370 MBq)} &= \frac{1.40 \times 10^{14} \times 201}{6.02 \times 10^{23}} \\ &= 46.7 \times 10^{-9} \text{ g} \\ &= 46.7 \text{ ng}\end{aligned}$$

Therefore, 10 mCi of ^{201}Tl contains 1.4×10^{14} atoms and 46.7 ng.

Problem 3.2
At 10:00 a.m., the ^{99m}Tc radioactivity was measured as 150 mCi (5.55 GBq) on Wednesday. What was the activity at 6 a.m. and 3 p.m. on the same day ($t_{1/2}$of ^{99m}Tc = 6 h)?

Answer
Time from 6 a.m. to 10 a.m. is 4 h:

$$\lambda \text{ for } ^{99m}\text{Tc} = \frac{0.693}{6} = 0.1155\,\text{h}^{-1}$$

$$\begin{aligned}A_t &= 150 \text{ mCi (5.55 GBq)} \\ A_0 &= ?\end{aligned}$$

Using Eq. (3.4)

$$\begin{aligned}150 &= A_0 e^{+0.1155 \times 4} \\ A_0 &= 150 \times e^{0.462} \\ &= 150 \times 1.5872 \\ &= 238.1\text{mCi (8.81 GBq)at 6 a.m.}\end{aligned}$$

Time from 10 a.m. to 3 p.m. is 5 h:

$$\begin{aligned}A_0 &= 150 \text{ mCi} \\ A_t &= ?\end{aligned}$$

Using Eq. (3.4)

$$\begin{aligned} A_t &= 150 \times e^{-0.1155 \times 5} \\ &= 150 \times e^{-0.5775} \\ &= 150 \times 0.5613 \\ &= 84.2\,\text{mCi (3.1 GBq) at 3 p.m.} \end{aligned}$$

Problem 3.3
If a radionuclide decays at a rate of 30 %/h, what is its half-life?

Answer

$$\lambda = 0.3\,\text{h}^{-1}$$

$$\lambda = \frac{0.693}{t_{1/2}}$$

$$t_{1/2} = \frac{0.693}{\lambda} = \frac{0.693}{0.3}\,\text{h} = 2.31\,\text{h}$$

Problem 3.4
If 11 % of ^{99m}Tc-labeled diisopropyliminodiacetic acid (DISIDA) is eliminated via renal excretion, 35 % by fecal excretion, and 3.5 % by perspiration in 5 h from the human body, what is the effective half-life of the radiopharmaceutical ($T_p = 6$ h for ^{99m}Tc)?

Answer

$$\begin{aligned} \text{Total biological elimination} &= 11\,\% + 35\,\% + 3.5\,\% \\ &= 49.5\,\%\ \text{in 5 h} \end{aligned}$$

$$\begin{aligned} \text{Therefore},\ T_b &\approx 5\ \text{h} \\ T_p &= 6\ \text{h} \end{aligned}$$

$$T_e = \frac{T_b \times T_p}{T_b + T_p} = \frac{5 \times 6}{5 + 6} = \frac{30}{11} = 2.7\ \text{h}$$

Successive Decay Equations

General Equation

In the preceding section, we derived equations for the activity of any radionuclide that is decaying. Here we shall derive equations for the activity of a radionuclide that is growing from another radionuclide and at the same time is itself decaying.

If a parent radionuclide p decays to a daughter radionuclide d, which in turn decays to another radionuclide (i.e., $p \rightarrow d \rightarrow$), then the rate of growth of d becomes

$$\frac{dN_d}{dt} = \lambda_p N_p - \lambda_d N_d \tag{3.14}$$

By integration, Eq. (3.14) becomes

$$(A_d)_t = \lambda_d N_d = \frac{\lambda_d (A_p)_0}{\lambda_d - \lambda_p}(e^{-\lambda_p t} - e^{-\lambda_d t}) \tag{3.15}$$

Equation (3.15) gives the activity of the daughter nuclide d at time t as a result of growth from the parent nuclide p and also due to the decay of the daughter itself.

Transient Equilibrium

If $\lambda_d > \lambda_p$, that is, $(t_{1/2})_d < (t_{1/2})_p$, then $e^{-\lambda_d t}$ in Eq. (3.15) is negligible compared to $e^{-\lambda_p t}$ when t is sufficiently long. Then Eq. (3.15) becomes

$$(A_d)_t = \frac{\lambda_d (A_p)_0}{\lambda_d - \lambda_p} e^{-\lambda_p t} = \frac{\lambda_d (A_p)_t}{\lambda_d - \lambda_p} \tag{3.16}$$

$$= \frac{(t_{1/2})_p (A_p)_t}{(t_{1/2})_p - (t_{1/2})_d} \tag{3.17}$$

This relationship is called the *transient equilibrium*. This equilibrium holds good when $(t_{1/2})_p$ and $(t_{1/2})_d$ differ by a factor of about 10–50. The semilogarithmic plot of this equilibrium equation is shown in Fig. 3.4. The daughter nuclide initially builds up as a result of the decay of the parent nuclide, reaches a maximum, and then achieves the transient equilibrium decaying with an apparent half-life of the parent nuclide. In equilibrium, the ratio of the daughter to parent activity is constant. It can be seen from Eq. (3.17) that the daughter activity is always greater than the parent activity, because $(t_{1/2})_p/((t_{1/2})_p - (t_{1/2})_d)$ is always greater than 1. The time to reach maximum daughter activity is given by the formula:

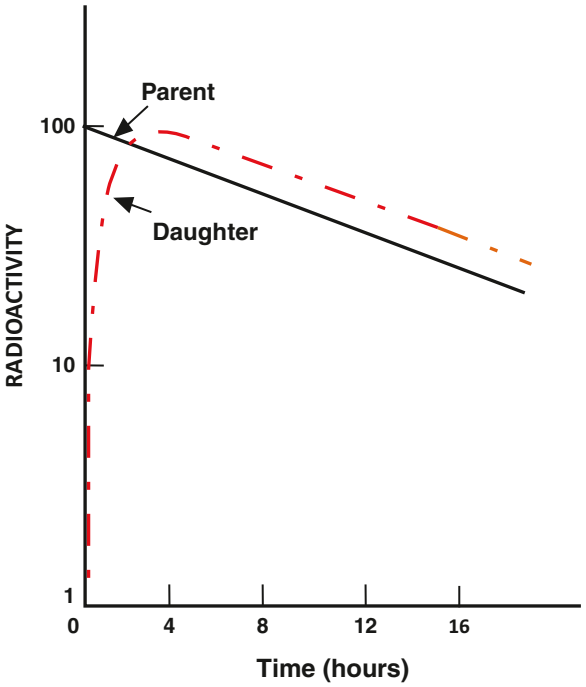

FIG. 3.4. Plot of activity versus time on a semilogarithmic graph illustrating the transient equilibrium. Note that the daughter activity reaches a maximum, then transient equilibrium, and follows an apparent half-life of the parent. The daughter activity is higher than the parent activity at equilibrium.

$$t_{\max} = \frac{1.44 \times (t_{1/2})_p \times (t_{1/2})_d \times \ln((t_{1/2})_p/(t_{1/2})_d)}{((t_{1/2})_p - (t_{1/2})_d)} \tag{3.18}$$

A typical example of transient equilibrium is ^{99}Mo ($t_{1/2}$ = 66 h) decaying to ^{99m}Tc ($t_{1/2}$ = 6 h). Because 87 % of ^{99}Mo decays to ^{99m}Tc, and the remaining 13 % to the ground state, Eqs. (3.15), (3.16), and (3.17) must be multiplied by a factor of 0.87. Therefore, in the time–activity plot, the ^{99m}Tc daughter activity will be lower than the ^{99}Mo parent activity (Fig. 3.5). Also, the ^{99m}Tc activity reaches maximum in about 23 h, i.e., $4(t_{1/2})_d$ (Eq. (3.18)).

Secular Equilibrium

When $\lambda_d \gg \lambda_p$, that is, when the parent half-life is much longer than that of the daughter nuclide, in Eq. (3.16), we can neglect λ_p compared to λ_d. Then Eq. (3.16) becomes

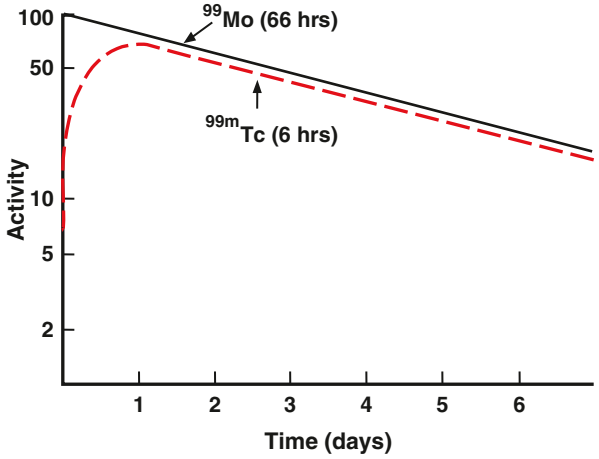

FIG. 3.5. Plot of logarithm of ^{99} Mo and ^{99m}Tc activities versus time showing transient equilibrium. The activity of the daughter ^{99m}Tc is less than that of the parent ^{99} Mo, because only 87 % of ^{99}Mo decays to ^{99m}Tc. If 100 % of the parent were to decay to the daughter, then the daughter activity would be higher than the parent activity after reaching equilibrium, as recognized from Eq. (3.17), and Fig. 3.4.

$$(A_d)_t = (A_p)_t \tag{3.19}$$

Equation (3.19) represents the *secular equilibrium*. This equilibrium holds when the half-life of the parent is much longer than that of the daughter nuclide by more than a factor of 100 or so. In secular equilibrium, both parent and daughter activities are equal, and both decay with the half-life of the parent nuclide. A semilogarithmic plot of activity versus time representing secular equilibrium is shown in Fig. 3.6. Typical examples of secular equilibrium are ^{113}Sn ($t_{1/2}$ = 117 days) decaying to ^{113m}In ($t_{1/2}$ = 100 min), and ^{68}Ge ($t_{1/2}$ = 280 days) decaying to ^{68} Ga ($t_{1/2}$ = 68 min).

Questions

1. Calculate (a) the total number of atoms and (b) the total mass of ^{131}I present in a 30-mCi (1.11-GBq) ^{131}I sample ($t_{1/2}$ = 8.0 days).
2. Calculate (a) the disintegration rate per minute and (b) the activity in curies and becquerels present in 1 mg of ^{201}Tl ($t_{1/2}$ = 73 h).
3. A radiopharmaceutical has a biologic half-life of 10 h in humans and a physical half-life of 23 h. What is the effective half-life of the radiopharmaceutical?
4. If the radioactivity of ^{111}In ($t_{1/2}$ = 2.8 days) is 200 mCi (7.4 GBq) on Monday noon, what is the activity (a) at 10:00 a.m. the Friday before and (b) at 1:00 p.m. the Wednesday after?

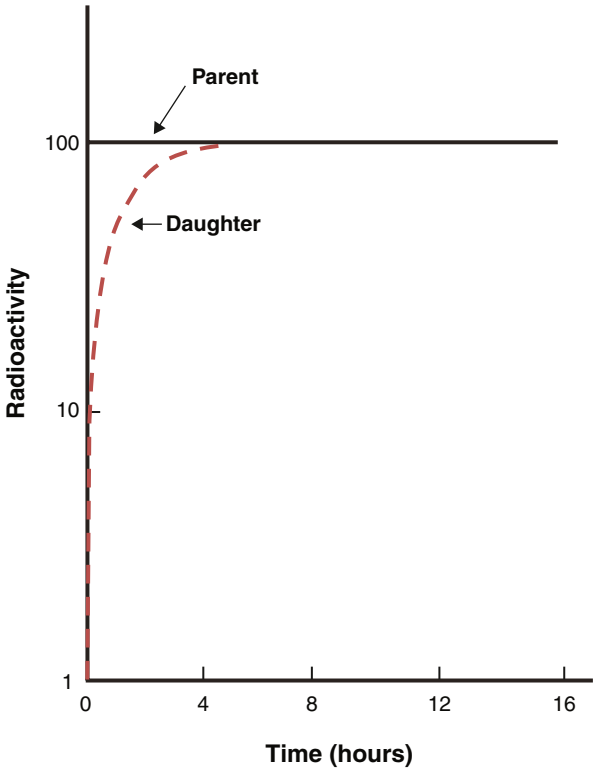

FIG. 3.6. Plot of activity versus time illustrating secular equilibrium. In equilibrium, the daughter activity becomes equal to that of the parent.

5. How long will it take for a 10-mCi (370-MBq) sample of ^{123}I ($t_{1/2}$ = 13.2 h) and a 50-mCi (1.85-MBq) sample of ^{99m}Tc ($t_{1/2}$ = 6 h) to possess the same activity?
6. What is the time interval during which ^{111}In ($t_{1/2}$ = 2.8 days) decays to 37 % of the original activity?
7. For antibody labeling, 5 mCi of $^{111}InCl_3$ is required. What amount of $^{111}InCl_3$ should be shipped if transportation takes one day?
8. What are the specific conditions of transient equilibrium and secular equilibrium?
9. How long will it take for the decay of 7/8 of an ^{18}F ($t_{1/2}$ = 110 min) sample?
10. What fraction of the original activity of a radionuclide has decayed in a period equal to the mean life of the radionuclide?
11. A radioactive sample initially gives 8564 cpm and 2 h later gives 3000 cpm. Calculate the half-life of the radionuclide.
12. If N atoms of a sample decay in one half-life, how many atoms would decay in the next half-life?

13. The ^{99}Mo ($t_{1/2}$ = 66 h) and ^{99m}Tc ($t_{1/2}$ = 6 h) are in transient equilibrium in a Moly generator. If 600 mCi (22.2 GBq) of ^{99}Mo is present in the generator, what would be the activity of ^{99m}Tc 132 h later, assuming that 87 % of ^{99}Mo decays to ^{99m}Tc?
14. A radionuclide decays with a half-life of 10 days to a radionuclide whose half-life is 1.5 h. Approximately how long will it take for the daughter activity to reach a maximum?

Suggested Readings

Cherry SR, Sorensen JA, Phelps ME. *Physics in Nuclear Medicine*. 3rd ed. Philadelphia: W. B Saunders; 2003.

Friedlander G, Kennedy JW, Miller JM. *Nuclear Chemistry and Radiochemistry*. 3rd ed. New York: Wiley; 1981.

Saha GB. *Fundamentals of Nuclear Pharmacy*. 6th ed. New York: Springer; 2010.

4
Statistics of Radiation Counting

As mentioned in previous chapters, radioactive decay is a random process, and therefore one can expect fluctuations in the measurement of radioactivity. The detailed discussion of the statistical treatment of radioactive measurements is beyond the scope of this book. Only the salient points of statistics related to radiation counting are given here.

Error, Accuracy, and Precision

In the measurement of any quantity, an error in or deviation from the true value is likely to occur. Errors can be two types: *systematic* and *random*. Systematic errors appear as constant deviations and arise from malfunctioning instruments and inappropriate experimental conditions. These errors can be eliminated by rectifying the incorrect situations. Random errors are variable deviations and arise from the fluctuations in experimental conditions such as high-voltage fluctuations or statistical fluctuations in a quantity such as radioactive decay.

The *accuracy* of a measurement of a quantity indicates how closely it agrees with the "true" value. The *precision* of a series of measurements describes the reproducibility of the measurement, although the measurements may differ from the "average" or "mean" value. The closer the measurement is to the average value, the higher the precision, whereas the closer the measurement is to the true value, the more accurate the measurement. Remember that a series of measurements may be quite precise, but their average value may be far from the true value (i.e., less accurate). Precision can be improved by eliminating the random errors, whereas better accuracy is obtained by removing both the random and systematic errors.

G. B. Saha, *Physics and Radiobiology of Nuclear Medicine,*
DOI 10.1007/978-1-4614-4012-3_4,

Mean and Standard Deviation

When a series of measurements is made on a radioactive sample, the most likely value of these measurements is the *average*, or *mean* value, which is obtained by adding the values of all measurements divided by the number of measurements. The mean value is denoted by $\overline{n}$.

The standard deviation of a series of measurements indicates the deviation from the mean value and is a measure of the precision of the measurements. Radioactive decay follows the Poisson distribution law, from which one can show that if a radioactive sample gives an average count of $\overline{n}$, then its standard deviation σ is given by

$$\sigma = \sqrt{\overline{n}} \tag{4.1}$$

The mean of measurements is then expressed as

$$\overline{n} \pm \sigma$$

Gaussian Distribution

If a series of measurements are made repeatedly on a radioactive sample giving a mean count $\overline{n}$, then the distribution of counts would normally follow a Poisson distribution. If the number of measurements is large, the distribution can be approximated by a Gaussian distribution, illustrated in Fig. 4.1. It can be seen that

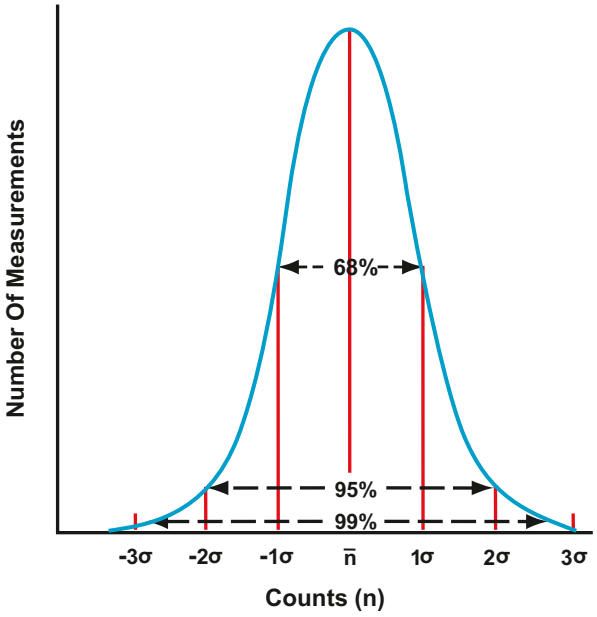

FIG. 4.1. A Gaussian distribution of radioactive measurements. Note the 68 % confidence level at $\pm 1\sigma$, 95 % confidence level at $\pm 2\sigma$, and 99 % confidence level at $\pm 3\sigma$.

68 % of all measurements fall within one standard deviation on either side of the mean, that is, within the range $\overline{n} \pm \sigma$; 95 % of all measurements fall within the range $\overline{n} \pm 2\sigma$; and 99 % fall within the range $\overline{n} \pm 3\sigma$. Also the Gaussian curve shows that half of the measurements are below the mean value, and the other half are above it.

The standard deviations in radioactive measurements indicate the statistical fluctuations of radioactive decay. For practical reasons, only single counts are obtained on radioactive samples instead of multiple repeat counts to determine the mean value. In this situation, if a single count n of a radioactive sample is large, then n can be estimated as close to $\overline{n}$; that is, $\overline{n} = n$ and $\sigma = \sqrt{n}$. It can then be said that there is a 68 % chance that the true value of the count falls within $n \pm \sigma$ or that the count n falls within one standard deviation of the true value (Fig. 4.1). This is called the 68 % *confidence level*. That is, one is 68 % confident that the count n is within one standard deviation of the true value. Similarly, 95 % and 99 % *confidence levels* can be set at two standard deviations (2σ) and three standard deviations (3σ), respectively, of any single radioactive count.

Another useful quantity in the statistical analysis of the counting data is the percent standard deviation, which is given as

$$\%\,\sigma = \frac{\sigma}{n} \times 100 = \frac{100\sqrt{n}}{n} = \frac{100}{\sqrt{n}} \tag{4.2}$$

Equation (4.2) indicates that as n increases, the % σ decreases, and hence, precision of the measurement increases. Thus, the precision of a count of a radioactive sample can be increased by accumulating a large number of counts in a single measurement. For example, for a count of 10,000, % σ is 1 %, whereas for 1,000,000, % σ is 0.1 %.

Problem 4.1
How many counts should be collected for a radioactive sample to have a 2 % error at a 95 % comfidence level?

Answer
95 % comfidence level is 2σ, that is, $2\sqrt{n}$

$$2\ \% = \frac{2\sigma \times 100}{n} = \frac{2\sqrt{n} \times 100}{n}$$

Therefore,

$$2 = \frac{200}{\sqrt{n}}$$

$$\sqrt{n} = 100$$

$$n = 10{,}000 \text{ counts}$$

Standard Deviation of Count Rates

The standard deviation of a count rate is

$$\sigma_c = \frac{\sigma}{t}$$

where σ is the standard deviation of the total count n of a radioactive sample obtained in time t. Because n is equal to the count rate c times the counting time t,

$$\sigma_c = \sqrt{n}/t = \sqrt{ct}/t = \sqrt{\frac{c}{t}} \tag{4.3}$$

Problem 4.2
A radioactive sample is counted for 12 min and gives 8640 counts. Calculate the count rate and its standard deviation for the sample.

Answer

$$\text{Count rate } c = \frac{8640}{12} = 720 \text{ counts per minute (cpm)}$$

Standard deviation,

$$\sigma_c = \sqrt{c/t} = \sqrt{720/12} \approx 8$$

Therefore, the count rate is 720 ± 8 cpm.

Propagation of Errors

Situations arise in which two quantities, say x and y, with their respective standard deviations, σ_x and σ_y, are either added, subtracted, multiplied, or divided. The standard deviations of the results of these arithmetic operations are given by the following expressions:

Addition:

$$\sigma_{x+y} = \sqrt{\sigma_x^2 + \sigma_y^2} \tag{4.4}$$

Subtraction:

$$\sigma_{x-y} = \sqrt{\sigma_x^2 + \sigma_y^2} \tag{4.5}$$

Multiplication:

$$\sigma_{(x\times y)} = (x \times y)\sqrt{(\sigma_x/x)^2 + (\sigma_y/y)^2} \tag{4.6}$$

Division:

$$\sigma_{(x/y)} = (x/y)\sqrt{(\sigma_x/x)^2 + (\sigma_y/y)^2} \tag{4.7}$$

Problem 4.3
A radioactive sample and the background were counted each for 5 min and found to give 8000 counts and 3000 counts, respectively. Calculate the net count rate, its standard deviation, and percent standard deviation.

Answer

$$\text{Gross sample count rate} = \frac{8000}{5} = 1600 \text{ cpm}$$

$$\text{Background count rate} = \frac{3000}{5} = 600 \text{ cpm}$$

$$\text{Net count rate} = 1600 - 600 = 1000 \text{ cpm}$$

Using Eqs. (4.3) and (4.5)

$$\sigma_c = \sqrt{\left(\sqrt{\frac{1600}{5}}\right)^2 + \left(\sqrt{\frac{600}{5}}\right)^2}$$

$$= \sqrt{\frac{1600}{5} + \frac{600}{5}}$$

$$= \frac{1}{\sqrt{5}}\sqrt{1600 + 600}$$

$$= \frac{1}{2.24}\sqrt{2200}$$

$$= \frac{46.9}{2.24}$$

$$\approx 21 \text{ cpm}$$

Thus, the count rate of the sample is 1000 ± 21 cpm

$$\% \text{ standard deviation of the count rate} = \frac{21}{1000} \times 100 = 2.1\ \%$$

Problem 4.4
A thyroid patient is given a ^{131}I–NaI capsule to measure the 24-h thyroid uptake. The 2-min counts are: standard, 90,000; room background, 1000; thyroid, 40,000; and thigh, 2000. Calculate the thyroid uptake and its percent standard deviation.

Answer

Net standard count = 90,000 − 1000 = 89,000

$$\sigma_s = \sqrt{90{,}000 + 1000} = 302$$

Net thyroid count = 40,000 − 2000 = 38,000

$$\sigma_t = \sqrt{40{,}000 + 2000} = 205$$

Percent thyroid uptake

$$= \frac{38{,}000}{89{,}000} \times 100 = 42.7\ \%$$

Standard deviation in uptake (using Eq. (4.7))

$$= \frac{38{,}000}{89{,}000} \times \sqrt{\left(\frac{302}{89{,}000}\right)^2 + \left(\frac{205}{38{,}000}\right)^2}$$

$$= 0.427 \times \sqrt{0.000011514 + 0.000029103}$$
$$= 0.427 \times 0.006373$$
$$= 0.0027$$

$$\% \text{ standard deviation in uptake} = \frac{0.0027}{0.427} \times 100 = 0.63\ \%$$

Thus, the thyroid uptake = 42.7 ± 0.63 %.

It should be noted that although all counts were taken for 2 min, count rates (cpm) were not used in the calculations. One can do similar calculations using count rates and obtain the same results.

Chi-Square Test

The chi-square (χ^2) test is a useful test for verifying if the variations in a set of measurements are due to statistical randomness of the data or due to variations in entities, such as equipment, patients, and the like, used in the measurements. The latter variations may be systematic, such as a fixed voltage drop throughout the measurement or random, such as fluctuations in voltage supply to the equipment. If there are N measurements made of a parameter, then for Gaussian distribution of the data, which is true in radioactive measurement, the χ^2 is given by

$$\chi^2 = \sum_{i}^{N} \frac{\left(X_i - \overline{X}\right)^2}{\overline{X}} \tag{4.8}$$

where X_i is the value of the ith measurement and $\overline{X}$ is the average of N measurements. The value of N should be 10 or larger. The χ^2 values are given in Table 4.1 for various probability (p) values as a function of degree of freedom, which is equal to the number of measurements minus one, N–1.

In Table 4.1, for a series of eight measurements, (degrees of freedom 7), there is a 50 % chance of the value of chi-square being greater than 6.35 and equal probability of its being smaller. Similarly, the probability of chi-square being as large as 12.02 is only 10 %, and being as large as 18.48 is only 1 %. Typically, χ^2 values that fall within 0.1–0.95 are acceptable. If the observed χ^2 value falls outside this range, it is an indication that the variation is beyond the statistical randomness of the data and something is wrong with the experimental set-up, for example, measuring equipment, measurement technique, and so on.

In performing the χ^2 test, a number of measurements (a minimum of ten) are made of the quantity, and the mean and χ^2 of the measured values are calculated by Eq. (4.8). The χ^2 value is then compared with the value in Table 4.1 corresponding to the actual degree of freedom and for a particular p value.

TABLE 4.1. Critical chi-square values.

Degree of Freedom ($N-1$)	Probability						
	0.99	0.95	0.90	0.50	0.10	0.05	0.01
	That the calculated chi-square value will be equal to or greater than						
2	0.02	0.10	0.21	1.39	4.61	5.99	9.21
3	0.13	0.35	0.58	2.37	6.25	7.82	11.35
4	0.30	0.71	1.06	3.36	7.78	9.49	13.28
5	0.55	1.15	1.61	4.35	9.24	11.07	15.09
6	0.87	1.64	2.20	5.35	10.65	12.59	16.81
7	1.24	2.17	2.83	6.35	12.02	14.07	18.48
8	1.65	2.73	3.49	7.34	13.36	15.51	20.09
9	2.09	3.33	4.17	8.34	14.68	16.92	21.67
10	2.56	3.94	4.87	9.34	15.99	18.31	23.21
11	3.05	4.58	5.58	10.34	17.28	19.68	24.73
12	3.57	5.23	6.30	11.34	18.55	21.03	26.22
13	4.11	5.89	7.04	12.34	19.81	22.36	27.69
14	4.66	6.57	7.79	13.34	21.06	23.69	29.14
15	5.23	7.26	8.55	14.34	22.31	25.00	30.58
16	5.81	7.96	9.31	15.34	23.54	26.30	32.00
17	6.41	8.67	10.09	16.34	24.77	27.59	33.41
18	7.02	9.39	10.87	17.34	25.99	28.87	34.81
19	7.63	10.12	11.65	18.34	27.20	30.14	36.19
20	8.26	10.85	12.44	19.34	28.41	31.41	37.57
21	8.90	11.59	13.24	20.34	29.62	32.67	38.93
22	9.54	12.34	14.04	21.34	30.81	33.92	40.29
23	10.20	13.09	14.85	22.34	32.01	35.17	41.64
24	10.86	13.85	15.66	23.34	33.20	36.42	42.98
25	11.53	14.61	16.47	24.34	34.38	37.38	44.31
26	12.20	15.38	17.29	25.34	35.56	38.89	45.64
27	12.88	16.15	18.11	26.34	36.74	40.11	46.96
28	13.57	16.93	18.94	27.34	37.92	41.34	48.28
29	14.26	17.71	19.77	28.34	39.09	42.56	49.59

Problem 4.5

The following repeat counts of a radioactive sample were obtained in a well-counter. Use the χ^2 test to see if the variations in counts are due to statistical variations of radioactivity or the counter is not working properly.

4580	4263
4635	4481
4625	4356
4578	4699
4525	4344
4668	4483
4391	4529

Answer

The average value of 14 measurements is $\overline{N} = 4511$.

Using Eq. (4.8),

$$\chi^2 = \frac{227637}{4511} = 50.5$$

From Table 4.1, for degree of freedom 13 and the p-value of 0.01, $\chi^2 = 27.69$. The computed χ^2 far exceeds the theoretical value, so something in addition to the statistical fluctuations of the counts is operating. Most likely, the well-counter is not functioning properly.

Minimum Detectable Activity

The efficiency of different detectors is limited by the dead time at high count rates and by statistical fluctuations at low count rates of the backgrounds. In the latter situation, the minimum detectable activity (MDA) that gives a statistically significant count is given by

$$MDA = 3\sigma_R = 3\sqrt{R_B/t} \tag{4.9}$$

where σ_R is the standard deviation of the background count rate R_B obtained by counting over a period of time t. Equation (4.9) requires that the sample count rate must be at least three standard deviations of the background to be significant.

Evaluation of Diagnostic Tests

It is often required to evaluate the usefulness of a new diagnostic test to determine the presence or absence of a particular disease. This aspect of the test is commonly described by two entities: sensitivity and specificity. The sensitivity of a test is the probability of being able to identify correctly those having the disease in a diseased population (true positive, TP). The specificity of the test is the probability of being able to identify correctly those who do not have the disease in a healthy population (true negative, TN). By these definitions, it is obvious that a given test may not identify all patients correctly whether or not they have the disease. This results in false-positives (FP) in the healthy group and false-negatives (FN) in the diseased group.

It should be noted that when sensitivity is assessed for a diseased population or specificity for a healthy group, the disease or healthy status of the group must be assessed by an established standard diagnostic test. This test is called the "gold standard" and is considered the best method available for comparison. As determined by the gold standard in a group of N patients, if N_P is the total number of persons with disease, and N_A is the total number of persons without disease, then the results of the new test can be summarized in Table 4.2. The following parameters can be obtained from data in Table 4.2.

$$Sensitivity = \frac{TP}{TP + FN} = \frac{TP}{N_P} \tag{4.10}$$

TABLE 4.2. Distribution of data obtained by a new diagnostic test.

Test result	Disease present	Disease absent	Totals
+	TP	FP	N^+
–	FN	TN	N^-
Total	N_p	N_A	N

$$Specificity = \frac{TN}{TN + FP} = \frac{TN}{N_A} \tag{4.11}$$

$$Accuracy = \frac{TP + TN}{TP + TN + FP + FN} \tag{4.12}$$

$$Positive\ predictive\ value = \frac{TP}{TP + FP} \tag{4.13}$$

$$Negative\ predictive\ value = \frac{TN}{TN + FN} \tag{4.14}$$

Problem 4.6
In a group of 1000 patients, 840 patients (Group A) had brain tumor and 160 patients (Group B) did not have tumor by biopsies. The SPECT study diagnosed 780 patients having tumor in Group A and 15 patients having tumor in Group B. Calculate the sensitivity, specificity, accuracy, positive predictive value, and negative predictive value of the SPECT study.

Answer
True positive = 780
True negative = 160 – 15 = 145
False negative = 840 – 780 = 60
False positive = 15

$$Sensitivity = \frac{780}{780 + 60} = \frac{780}{840} \times 100 = 92.6\ \%$$

$$Specificity = \frac{145}{145 + 15} = \frac{145}{160} \times 100 = 90.6\ \%$$

$$Accuracy = \frac{780 + 145}{780 + 145 + 60 + 15} = \frac{925}{1000} \times 100 = 92.5\ \%$$

$$Positive\ predictive\ value = \frac{780}{780 + 15} = \frac{780}{795} \times 100 = 98.1\ \%$$

$$Negative\ predictive\ value = \frac{145}{145 + 60} = \frac{145}{205} \times 100 = 70.7\ \%$$

Questions

1. Define accuracy and precision.
2. Do systematic errors give an accurate measurement? Can systematic errors give a precise measurement?
3. A radioactive sample gives 15,360 counts in 9 min:
   (a) What are the count rate of the sample and its standard deviation?
   (b) If the sample contained a background count rate of 60 cpm obtained from a 2-min count, what would be the net count rate of the sample and its standard deviation?
4. How many counts of a sample are to be collected to have a 1 % error at the 95 % confidence level?
5. Within how many standard deviations of a mean count of 62,001 is 730?
6. To achieve an estimated percent standard error of 3 %, how many counts must be collected?
7. The χ^2 value of 11 measurements of a quantity is 4.2. What is the probability that the variations of measurements are due to statistical variations of the quantity?

Suggested Readings

Bahn AK. *Basic Medical Statistics*. New York: Grune & Stratton; 1972.

Martin PM. Nuclear medicine statistics. In: Rollo FD, ed. *Nuclear Medicine Physics, Instrumentation and Agents*. St. Louis: Mosby; 1977:479–512.

5
Production of Radionuclides

Currently more than 3700 nuclides are known, of which nearly 3420 are radioactive, and the rest are stable. The majority of radionuclides are artificially produced in the cyclotron and reactor. Some short-lived radionuclides are available from the so-called radionuclide generators in which a long-lived parent radionuclide are loaded and decay to a short-lived daughter radionuclide. The following is a brief description of the sources of different radionuclides.

Cyclotron-Produced Radionuclides

Charged particles can be accelerated under an electromagnetic field in cyclotrons or linear accelerators to have high kinetic energy, which are then allowed to react with stable nuclides to cause nuclear reactions producing different radionuclides. For radionuclide production in nuclear medicine, cyclotrons are commonly used. Both positively charged (protons, α-particles) or negatively charged (H^-) particles can be accelerated in cyclotrons, and their construction and specific use are discussed below.

A typical cyclotron consists of two hollow D-like copper structures called "dee" separated by a small gap (Fig. 5.1). The dees (A & B) are kept in a high vacuum tank, and an electromagnetic field is applied between them. Positive or negative ions are produced in an arc ion source at the gap, which are then attracted toward the oppositely charged dee. The magnetic field then bends them in a circular path instead of letting them in a straight path. When the charged particles arrive at the gap, the electrical polarity is changed, by which the particles are repelled by the like charges and attracted by the opposite charges, thereby gaining further acceleration. This scenario happens every time the particles cross the gap between the two dees and approach toward the periphery with increasing energy. Ultimately the particles are deflected outside in the form of a beam by a deflector D through a window W. The kinetic energy of the particles depends on the charge (e) and mass (m) of the particle, the magnetic field (H) in Gauss, and the radius (r) of the cyclotron, as given below:

G. B. Saha, *Physics and Radiobiology of Nuclear Medicine,*
DOI 10.1007/978-1-4614-4012-3_5,

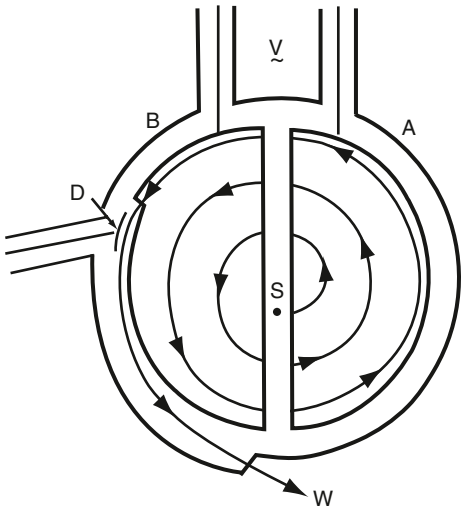

FIG. 5.1. Schematics of a cyclotron. *A* and *B* dees with vacuum, *D* deflector, *S* ion source, *V* alternating voltage, *W* window.

$$K.E. = \frac{H^2 e^2 r^2}{2m} \tag{5.1}$$

The beam energy may range from a few keV to several billion electron volts (BeV or GeV) depending on the design of the cyclotron. Charged particles such as protons, deuterons, α-particles, H^- etc. can be accelerated in a cyclotron. In some special cyclotrons, heavy ions like ^{32}S are also accelerated.

There are several features that distinctively characterize positive ion or negative ion cyclotrons. Negative ion cyclotrons need to be run under relatively higher vacuum than positive ion cyclotrons (~10^{-7} Torr vs 10^{-5} Torr), because H^- can lose electrons by encounters with any molecule during acceleration. The beam extraction efficiency in positive ion cyclotrons is ~ 80 % and the remaining 20 % is lost by interaction with the cyclotron housing inducing radioactivity. This warrants more shielding around these cyclotrons. In contrast, since negative ions are extracted with ~ 100 % efficiency and do not interact with the nucleus of any nuclide, the cyclotron housing is not activated, thus requiring less shielding. Targets can be bombarded internally at any radius of the positive ion cyclotrons for radionuclide production, whereas this is not possible in negative ion cyclotrons for lack of nuclear interaction of negative ions with target nuclei. In latter cyclotrons, the particle beam is intercepted with a thin carbon foil (~ 5 μm) toward the exit of the beam to strip two electrons from H^- forming an external proton (positive) beam to cause nuclear reactions in target nuclei. In positive ion cyclotrons, a deflector routes the particle beam outside for external irradiation of targets. A unique advantage of negative cyclotrons is that the particle beam can be split into two beams by placing one carbon stripping foil to cover only a part of the beam area and another foil at some distance away covering the remaining area. Thus, two same targets or two different targets can be irradiated simultaneously with the two beams to produce radionuclides.

Medical cyclotrons are compact negative ion cyclotrons that are commonly used for production of short-lived radionuclides such as ^{18}F, ^{11}C, ^{13}N, ^{15}O, and so on used in positron emission tomography (PET) imaging. These nuclides are produced with low energy particles and hence the small size of the cyclotron that can be installed in a small room. In contrast, several medically-useful radionuclides such as ^{111}In, ^{67}Ga, etc. require high energy particles and so large cyclotrons, normally positive ion cyclotrons, are used for their production. The typical energy of the medical cyclotrons ranges between 3–18 MeV.

Some medical cyclotrons have provisions for acceleration of deuteron and H^- interchangeably. Whereas high energy cyclotrons are shielded mostly by thick concrete walls, medical cyclotrons are self-shielded with lead blocks for reasons of compact nature. Four lead block quadrants are mounted on casters that wheel them in and out for closing and opening for easy access to service the cyclotron. Siemens, GE Healthcare, IBA, Best Cyclotrons, and Advanced Cyclotron Systems are the major manufacturers of medical cyclotrons in the USA.

When targets of stable elements are irradiated by placing them in the external beam of the accelerated particles or in the internal beam at a given radius inside a cyclotron, the accelerated particles interact with the target nuclei, and nuclear reactions take place. In a nuclear reaction, the incident particle may leave the nucleus after interaction with a nucleon, leaving some of its energy in it, or it may be completely absorbed by the nucleus, depending on the energy of the incident particle. In either case, a nucleus with excitation energy is formed and the excitation energy is disposed of by the emission of nucleons (i.e., protons and neutrons). Particle emission is followed by γ-ray emission when the former is no longer energetically feasible. Depending on the energy deposited by the incident particle, several nucleons are emitted randomly from the irradiated target nucleus, leading to the formation of different nuclides. As the energy of the irradiating particle is increased, more nucleons are emitted, and therefore a wider variety of nuclides is produced.

An example of a typical cyclotron-produced radionuclide is ^{111}In, which is produced by irradiating ^{111}Cd with 12-MeV protons in a cyclotron. The nuclear reaction is written as follows:

$$^{111}Cd(p,\ n)^{111}In$$

where ^{111}Cd is the target nuclide, the proton p is the irradiating particle, the neutron n is the emitted particle, and ^{111}In is the product radionuclide. In this case, a second nucleon may not be emitted, because there is not enough energy left after the emission of the first neutron. The excitation energy that is not sufficient to emit any more nucleons will be dissipated by γ-ray emission.

As can be understood, radionuclides produced with atomic numbers different from those of the target isotopes do not contain any stable ("cold," or "carrier") isotope detectable by ordinary analytical methods, and such preparations are called *carrier-free*. In practice, however, it is impossible to have these preparations without the presence of any stable isotopes. Another term for these preparations is *no-carrier-added* (NCA), meaning that no stable isotope has been added purposely to the preparations.

The target material for irradiation must be pure and preferably monoisotopic or at least enriched isotopically to avoid the production of extraneous radionuclides. Because various isotopes of different elements may be produced in a target, it is necessary to isolate isotopes of a single element; this can be accomplished by appropriate chemical methods such as solvent extraction, precipitation, ion exchange, and distillation. Cyclotron-produced radionuclides are usually proton-rich and therefore decay by β^+-emission or electron capture.

Reactor-Produced Radionuclides

A variety of radionuclides is produced in nuclear reactors. A nuclear reactor is constructed with fuel rods made of fissile materials such as enriched ^{235}U and ^{239}Pu. These fuel nuclei undergo spontaneous fission with extremely low probability. *Fission* is defined as the breakup of a heavy nucleus into two fragments of approximately equal mass, accompanied by the emission of two to three neutrons with mean energies of about 1.5 MeV. In each fission, there is a concomitant energy release of ~200 MeV that appears as heat and is usually removed by heat exchangers to produce electricity in the nuclear power plant.

Neutrons emitted in each fission can cause further fission of other fissionable nuclei in the fuel rod, provided the right conditions exist. This obviously will initiate a chain reaction, ultimately leading to a possible meltdown of the reactor core. This chain reaction must be controlled, which is in part accomplished by the proper size, shape, and mass of the fuel material and other complicated and ingenious engineering techniques. To maintain a self-sustained chain reaction, only one fission neutron is needed and excess neutrons (more than one) are removed by cadmium rods, called *control rods*, which are positioned in the reactor core (cadmium has a high probability of absorbing a thermal neutron). Babcox & Wilcox and Westinghouse are the major manufacturers of nuclear reactors in the USA.

The fuel rods of fissile materials are interspersed in the reactor core with spaces in between. Neutrons emitted with a mean energy of 1.5 MeV from the surface of the fuel rod have a low probability of interacting with other nuclei and therefore do not serve any useful purpose. It has been found, however, that neutrons with thermal energy (0.025 eV) interact with many other stable nuclei efficiently, producing various radionuclides. To make the high-energy neutrons, or so-called fast neutrons, more useful, they are thermalized or slowed down by interaction with low molecular weight materials, such as water, heavy water (D_2O), beryllium, and graphite (C), which are distributed in the spaces between the fuel rods. These materials are called *moderators*. The flux, or intensity, of the thermal neutrons so obtained ranges from 10^{11} to 10^{14} neutrons/cm^2 · s, and they are useful in the production of many radionuclides. When a target element is inserted in the reactor core, a thermal neutron will interact with the target nucleus, with a definite probability of producing another nuclide. The probability of formation of a radionuclide by thermal neutrons varies from element to element.

In the reactor, two types of interaction with thermal neutrons occur to produce various radionuclides: fission of heavy elements and neutron capture or (n, γ) reaction. These two nuclear reactions are described next.

Fission or (n, f) Reaction

When a target of heavy elements is inserted in the reactor core, heavy nuclei absorb thermal neutrons and undergo fission. Fissionable heavy elements are ^{235}U, ^{239}Pu, ^{237}Np, ^{233}U, ^{232}Th, and many others having atomic numbers greater than 92. Fission of heavy elements may also be induced in a cyclotron by irradiation with high-energy charged particles, but fission probability depends on the type and energy of the irradiating particle. Nuclides produced by fission may range in atomic number from about 28 to nearly 65. These isotopes of different elements are separated by appropriate chemical procedures that involve precipitation, solvent extraction, ion exchange, chromatography, and distillation. The fission radionuclides are normally carrier-free or NCA, and therefore radionuclides of high specific activity are available from fission. The fission products are usually neutron-rich and decay by β^--emission.

Many clinically useful radionuclides such as ^{131}I, ^{99}Mo, ^{133}Xe, and ^{137}Cs are produced by fission of ^{235}U. An example of thermal fission of ^{235}U follows, showing a few representative radionuclides:

$$
\begin{aligned}
{}^{235}_{92}\mathrm{U} + {}^{1}_{0}\mathrm{n} &\rightarrow {}^{236}_{92}\mathrm{U} \rightarrow {}^{131}_{53}\mathrm{I} + {}^{102}_{39}\mathrm{Y} + 3{}^{1}_{0}\mathrm{n} \\
&\rightarrow {}^{99}_{42}\mathrm{Mo} + {}^{135}_{50}\mathrm{Sn} + 2{}^{1}_{0}\mathrm{n} \\
&\rightarrow {}^{117}_{46}\mathrm{Pd} + {}^{117}_{46}\mathrm{Pd} + 2{}^{1}_{0}\mathrm{n} \\
&\rightarrow {}^{133}_{54}\mathrm{Xe} + {}^{101}_{38}\mathrm{Sr} + 2{}^{1}_{0}\mathrm{n} \\
&\rightarrow {}^{137}_{55}\mathrm{Cs} + {}^{97}_{37}\mathrm{Rb} + 2{}^{1}_{0}\mathrm{n} \\
&\rightarrow {}^{155}_{62}\mathrm{Sm} + {}^{78}_{30}\mathrm{Zn} + 3{}^{1}_{0}\mathrm{n} \\
&\rightarrow {}^{156}_{62}\mathrm{Sm} + {}^{77}_{30}\mathrm{Zn} + 3{}^{1}_{0}\mathrm{n}
\end{aligned}
$$

Many other nuclides besides those mentioned in the example are also produced. For ^{99}Mo production, high enriched uranium (HEU) is commonly used for irradiation, which contains more than 90 % ^{235}U in the target. The irradiation is carried out for 5–10 days. Now investigators are attempting to use low enriched uranium (LEU) target that contains less than 20 % ^{235}U. This technique requires a longer irradiation for production of sufficient ^{99}Mo and is less expensive. However in view of the current problem in sufficient supply of ^{99}Mo, this technique has drawn considerable interest in nuclear medicine community.

Neutron Capture or (n,γ) Reaction

In neutron capture reaction, the target nucleus captures one thermal neutron and emits γ-rays to produce an isotope of the same element. The radionuclide so produced is therefore not carrier-free, and its specific activity is relatively low. This reaction takes place in almost all elements with varying probability. Some examples of neutron capture reactions are $^{98}Mo(n, \gamma)^{99}Mo$, $^{196}Hg(n, \gamma)^{197}Hg$, and $^{50}Cr(n, \gamma)^{51}Cr$. Molybdenum-99 so produced is called the *irradiated molybdenum* as opposed to the *fission molybdenum* described earlier. This method is commonly used in the analysis of trace elements in various samples.

The method of production and various characteristics of radionuclides commonly used in nuclear medicine are presented in Table 5.1.

Target and Its Processing

Various types of targets have been designed and used for both reactor and cyclotron irradiation. In the design of targets, primary consideration is given to heat deposition in the target by irradiation with neutrons in the reactor or charged particles in the cyclotron. In both cases, the temperature can rise to 1000 °C, and if proper material is not used or a method of heat dissipation is not properly designed, the target is likely to be burned or melted. For this reason, water cooling of the cyclotron probe to which the target is attached is commonly adopted. In the case of the reactor, the core cooling with heavy water is sufficient to cool the target. Most often, the targets are designed in the form of a foil to maximize heat dissipation.

The common form of the target is metallic foil, for example, copper, aluminum, uranium, vanadium, and so on. Other forms of targets are oxides, carbonates, nitrates, and chlorides contained in an aluminum tubing, which is then flattened to maximize the heat loss. Aluminum tubing is used because of its high melting point. In some cases, compounds are deposited on the appropriate metallic foil by vacuum distillation or by electrodeposition, and the plated foils are then used as targets. In specific cases, high-pressure gases (e.g., ^{124}Xe for ^{123}I production) and liquid targets (e.g., $H_2{}^{18}O$ for ^{18}F production) are also used.

Equation for Production of Radionuclides

While irradiating a target for the production of a radionuclide, it is essential to know various parameters affecting its production, preferably in a mathematical form, to estimate how much of it would be produced for a given set of parameters. These parameters are therefore discussed below.

The activity of a radionuclide produced by irradiation of a target material with charged particles in a cyclotron or with neutrons in a nuclear reactor is given by

TABLE 5.1. Characteristics of commonly used radionuclides.

Nuclide	Physical half-life	Mode of delay (%)	γ-ray energy* (MeV)	γ-ray abundance (%)	Common production method
$^{3}_{1}H$	12.3 year	β^- (100)	–	–	$^{6}Li(n, \alpha)^{3}H$
$^{11}_{6}C$	20.4 min	β^+ (100)	0.511 (Annihilation)	200	$^{10}B(d, n)^{11}C$ $^{14}N(p, \alpha)^{11}C$
$^{13}_{7}N$	10 min	β^+ (100)	0.511 (Annihilation)	200	$^{12}C(d, n)^{13}N$ $^{16}O(p, \alpha)^{13}N$ $^{13}C(p, n)^{13}N$
$^{14}_{6}C$	5730 year	β^- (100)	–	–	$^{14}N(n, p)^{14}C$
$^{15}_{8}O$	2 min	β^+ (100)	0.511 (Annihilation)	200	$^{14}N(d, n)^{15}O$ $^{15}N(p, n)^{15}O$
$^{18}_{9}F$	110 min	β^+ (97) EC (3)	0.511 (Annihilation)	194	$^{18}O(p, n)^{18}F$
$^{32}_{15}P$	14.3 days	β^- (100)	–	–	$^{32}S(n, p)^{32}P$
$^{57}_{27}Co$	271 days	EC (100)	0.014 0.122 0.136	9 86 11	$^{56}Fe(d, n)^{57}Co$
$^{58}_{27}Co$	71 days	β^+ (14.9) EC (85.1)	0.811	99.5	$^{55}Mn(\alpha, n)^{58}Co$
$^{59}_{26}Fe$	45 days	β^- (100)	1.099 1.292	56 43	$^{58}Fe(n, \gamma)^{59}Fe$
$^{60}_{27}Co$	5.2 year	β^- (100)	1.173 1.332	100 100	$^{59}Co(n, \gamma)^{60}Co$
$^{62}_{28}Zn$	9.3 h	β^+ (8) EC (92)	0.420 0.511 0.548 0.597	25 31 15 26	$^{63}Cu(p, 2n)^{62}Zn$
$^{62}_{29}Cu$	9.7 min	β^+ (97) EC (3)	0.511 (Annihilation)	194	$^{62}Ni(p, n)^{62}Cu$ $^{62}Zn \xrightarrow[9.3\,h]{\beta^+,\,EC} {}^{62}Cu$
$^{67}_{29}Cu$	2.6 days	β^- (100)	0.185 0.92	49 23	$^{67}Zn(n, p)^{67}Cu$
$^{67}_{31}Ga$	78 h	EC (100)	0.093 0.184 0.300 0.393	40 20 17 5	$^{68}Zn(p, 2n)^{67}Ga$
$^{68}_{31}Ga$	68 min	β^+ (89) EC (11)	0.511 (Annihilation)	178	$^{68}Zn(p, n)^{68}Ga$
$^{68}_{32}Ge$	270.8 days	β^+ (100)	–	–	$^{66}Zn(\alpha, 2n)^{68}Ge$
$^{82}_{37}Rb$	75 s	β^+ (95) EC (5)	0.511 0.777	190 13.4	$^{98}Mo \xrightarrow{spallation} {}^{82}Sr$ $\downarrow 25.6\ d$ ^{82}Rb
$^{82}_{38}Sr$	25.6 days	EC (100)	–	–	$^{98}Mo \xrightarrow{spallation} {}^{82}Sr$
$^{89}_{38}Sr$	50.6 days	β^- (100)	–	–	$^{88}Sr(n, \gamma)^{89}Sr$
$^{90}_{38}Sr$	28.6 year	β^- (100)	–	–	$^{235}U(n, f)^{90}Sr$

TABLE 5.1. (continued)

Nuclide	Physical half-life	Mode of delay (%)	γ-ray energy* (MeV)	γ-ray abundance (%)	Common production method
$^{90}_{39}$Y	2.7 days	β^- (100)	–	–	^{89}Y(n, γ)^{90}Y
$^{99}_{42}$Mo	66 h	β^- (100)	0.181	6	^{90}Sr $\xrightarrow[\beta^-]{28.6\text{year}}$ ^{90}Y
			0.740	12	^{98}Mo(n, γ)^{99}Mo
			0.780	4	^{235}U(n, f)^{99}Mo
$^{99m}_{43}$Tc	6.0 h	IT (100)	0.140	90	^{100}Mo(p, 2n)^{99m}Tc
					^{99}Mo $\xrightarrow[66\text{ h}]{\beta^-}$ ^{99m}Tc
$^{111}_{49}$In	2.8 days	EC (100)	0.171	90	^{111}Cd(p, n)^{111}In
			0.245	94	
$^{123}_{53}$I	13.2 h	EC (100)	0.159	83	^{121}Sb(α, 2n)^{123}I
					^{127}I(p, 5n)^{123}Xe ↓2.1 h ^{123}I
					^{124}Xe(p, 2n)^{123}Cs ↓5.9 min ^{123}Xe ↓2.1 h ^{123}I
$^{124}_{53}$I	4.2 days	β^+ (23)	511	46	^{124}Te(p, n)^{124}I
		EC (77)	603	61	
$^{125}_{53}$I	60 days	EC (100)	0.035	7	^{124}Xe(n, γ)^{125}Xe
			X-ray (0.027–0.032)	140	^{125}Xe $\xrightarrow[17\text{ h}]{\text{EC}}$ ^{125}I
$^{131}_{53}$I	8.0 days	β^- (100)	0.284	6	^{130}Te(n, γ)^{131}Te
			0.364	81	^{235}U(n, f)^{131}Te
			0.637	7	^{131}Te $\xrightarrow[25\text{min}]{\beta^-}$ ^{131}I
					^{235}U(n, f)^{131}I
$^{133}_{54}$Xe	5.3 days	β^- (100)	0.081	37	^{235}U(n, f)^{133}Xe
$^{137}_{55}$Cs	30.0 year	β^- (100)	0.662	85	^{235}U(n, f)^{137}Cs
$^{153}_{62}$Sm	1.9 days	β^- (100)	70	5	^{152}Sm(n, γ)^{153}Sm
			103	28	
$^{186}_{75}$ Re	3.8 days	β^- (92)	137	9	^{185}Re(n, γ)^{186}Re
		EC (8)			
$^{201}_{81}$TI	73 h	EC (100)	0.167	9.4	^{203}TI(p, 3n)^{201}Pb
			X-ray (0.069–0.083)	93	^{201}Pb $\xrightarrow[9.3\text{ h}]{\text{EC}}$ ^{201}TI

*γ-rays with abundance less than 4 % have not been cited
d, deuteron; EC, electron capture; f, fission; IT, isomeric transition; n, neutron; p, proton
Data from Browne E, Finestone RB. *Table of Radioactive Isotopes*. New York: Wiley; 1986

$$A = IN\sigma(1 - e^{-\lambda t}) \tag{5.1}$$

where

A = activity in disintegrations per second of the radionuclide produced

I = intensity or flux of the irradiating particles (number of particles/(cm^2 · s))

N = number of target atoms

σ = formation cross section (probability) of the radionuclide (cm^2); it is given in units of "barn," which is equal to 10^{-24} cm^2

λ = decay constant given by $0.693/t_{1/2}$ (s^{-1})

t = duration of irradiation (s).

Equation (5.1) indicates that the amount of radioactivity produced depends on the intensity and energy (related to the cross-section σ) of the incident particles, the amount of the target material, the half-life of the radionuclide produced, and the duration of irradiation. The term $(1 - e^{-\lambda t})$ is called the *saturation factor* and approaches unity when t is approximately 5–6 half-lives of the radionuclide in question. At that time, the yield of the product nuclide becomes maximum, and its rates of production and decay become equal. For a period of irradiation of 5–6 half-lives, Eq. (5.1) becomes

$$A = IN\sigma. \tag{5.2}$$

A graphic representation of Eqs. (5.1) and (5.2) is given in Fig. 5.2.

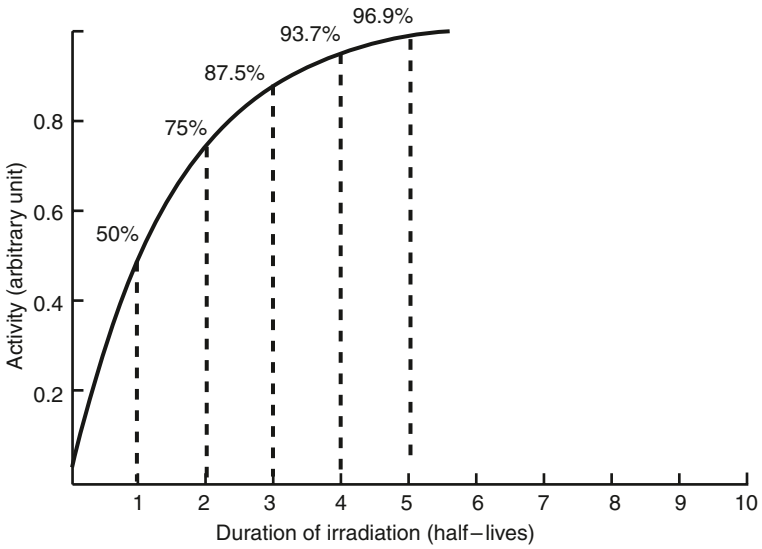

FIG. 5.2. Production of radionuclides in a reactor or a cyclotron. The activity produced reaches a maximum (saturation) in 5–6 half-lives of the radionuclide.

The intensity of the irradiating particles is measured by various physical techniques, the description of which is beyond the scope of this book; however, the values are available from the operator of the cyclotron or the reactor. Normally, the neutron flux is of the order of 10^{14} neutrons/s · cm^2 and the proton beam runs around the orders of 10^{12} protons/s · cm^2. The formation cross sections of various nuclides are determined by experimental methods using Eq. (5.1), and they have been compiled and published by many investigators. The number of atoms N of the target is calculated from the weight W of the material irradiated, the atomic weight A_w and natural abundance K of the target isotope, and Avogadro's number (6.02×10^{23}) as follows:

$$N = \frac{W \times K}{A_w} \times 6.02 \times 10^{23} \tag{5.3}$$

After irradiation, isotopes of different elements may be produced and therefore should be separated by the appropriate chemical methods. These radionuclides are identified and quantitated by detecting their radiations and measuring their half-lives by the use of the NaI(Tl) or Ge(Li) detectors coupled to a multichannel pulse height analyzer. They may also be assayed in an ionization chamber if the amount of radioactivity is high.

Problem 5.1
Calculate the activity of ^{99}Mo produced when 3 g of ^{235}U is bombarded for 3 days in a nuclear reactor, given that neutron flux is 10^{14} neutron/(s · cm^2), $t_{1/2}$ of ^{99}Mo is 66 h and the formation cross-section for ^{99}Mo is 30 barn.

Answer

$$\text{Neutron flux (I)} = 10^{14}\text{n/(s} \cdot \text{cm}^2\text{)}$$

$$\text{No of } ^{235}\text{U atoms (N)} = (3/235) \times 6.02 \times 10^{23} = 7.69 \times 10^{21}$$

$$\text{Formation cross-section } (\sigma) \text{ for } ^{99}\text{Mo} = 30 \text{ barn} = 30 \times 10^{-24} \text{ cm}^2 = 3 \times 10^{-23} \text{ cm}^2$$

$$\text{Time of bombardment (t)} = 3 \times 24 \times 60 \times 60 = 2.592 \times 10^5 \text{ s}$$

$$\text{Decay constant } (\lambda) \text{ for } ^{99}\text{Mo} = 0.693/(66 \times 60 \times 60) = 2.92 \times 10^{-6} \text{ s}^{-1}$$

$$\text{Activity of } ^{99}\text{Mo} = 10^{14} \times 7.69 \times 10^{21} \times 3 \times 10^{-23} \times \left(1 - e^{-2.92 \times 10^{-6} \times 2.592 \times 10^5}\right)$$

$$= 1.22 \times 10^{13} = 12.2 \text{ TBq}$$

$$= 329.7 \text{ Ci}$$

Problem 5.2
How long a target of 2 g of ^{18}O-water needs to be bombarded to produce 10 curies of ^{18}F by the ^{18}O(p, n)^{18}F reaction, given that the proton beam intensity is 50 μA/cm^2, ^{18}O enrichment is 75 %, the formation cross-section is 200 mbarn and $t_{1/2}$ of ^{18}F is 110 min.

Answer
Since 1 ampere (A) is equal to 1 coulomb (C)/sec and 1 C equals to 6.25×10^{18} protons, the number of protons in 50 μA/cm^2 is

$$I = 50 \times 10^{-6} \times 6.25 \times 10^{18} = 3.125 \times 10^{14} \text{ proton/s} \cdot \text{cm}^2$$

Effective molecular weight of enriched water is $0.25 \times 18 + 0.75 \times 20 = 19.5$

$$\text{No of target atoms (N)} = ((0.75 \times 2)/19.5) \times 6.02 \times 10^{23}$$
$$= 4.63 \times 10^{22} \text{ atoms of } ^{18}\text{O}$$

$$\text{Cross section } (\sigma) = 200 \times 10^{-27} \text{ cm}^2 = 2 \times 10^{-25} \text{ cm}^2$$

$$\text{Decay constant } (\lambda) = 0.693/(110 \times 60) = 1.05 \times 10^{-4} \text{ s}^{-1} = 0.000105 \text{ s}^{-1}$$

$$\text{Activity (A)} = 10 \times 3.7 \times 10^{10} \text{ dps} = 3.7 \times 10^{11} \text{ dps}$$

Now,

$$3.7 \times 10^{11} = 3.125 \times 10^{14} \times 4.63 \times 10^{22} \times 2 \times 10^{-25} \times \left(1 - e^{-0.000105 \times t}\right)$$
$$= 2.89 \times 10^{12} \left(1 - e^{-0.000105 \times t}\right)$$

$$1 - e^{-0.000105 \times t} = 0.128$$
$$e^{-0.000105 \times t} = 0.8720$$

$$t = \frac{0.1370}{0.000105}$$
$$= 1304 \text{ s}$$
$$= 21.7 \text{ min}$$

Radionuclide Generators

Radionuclide generators provide the convenient sources of short-lived radionuclides that are very useful clinically. The basic requirements for a generator are that *a parent radionuclide has a longer half-life than that of the daughter* radionuclide,

and the daughter can be easily separated from the parent. In a generator, a long-lived parent radionuclide is allowed to decay to its short-lived daughter radionuclide, and the latter is then chemically separated. The importance of radionuclide generators lies in the fact that they are easily transportable and serve as sources of short-lived radionuclides in institutions without cyclotron or reactor facilities.

A radionuclide generator consists of a glass or plastic column fitted at the bottom with a fretted disk. The column is filled with adsorbent material such as ion exchange resin, alumina, and so forth, on which the parent nuclide is adsorbed. The parent decays to the daughter until transient or secular equilibrium is established (Eqs. (3.17) and (3.18)) in several half-lives of the daughter. After equilibrium, the daughter appears to decay with the same half-life as the parent. Because of the differences in chemical properties, the daughter activity is eluted with an appropriate solvent, leaving the parent on the column. After elution, the daughter activity builds up again and can be eluted repeatedly.

A schematic diagram of a radionuclide generator is shown in Fig. 5.3. The vial containing the eluant is first inverted onto needle A, and an evacuated vial is then inverted on the other needle B. The vacuum in the vial on needle B draws the eluant from the vial A through the column and elutes the daughter nuclide, leaving the parent nuclide on the column. In some commercial generators, a bottle of eluant is placed inside the housing, and aliquots of eluant are used up in each elution by the evacuated vial.

An ideal radionuclide generator should be simple and sturdy for transportation. The generator eluate should be free of the parent nuclide and the adsorbent material.

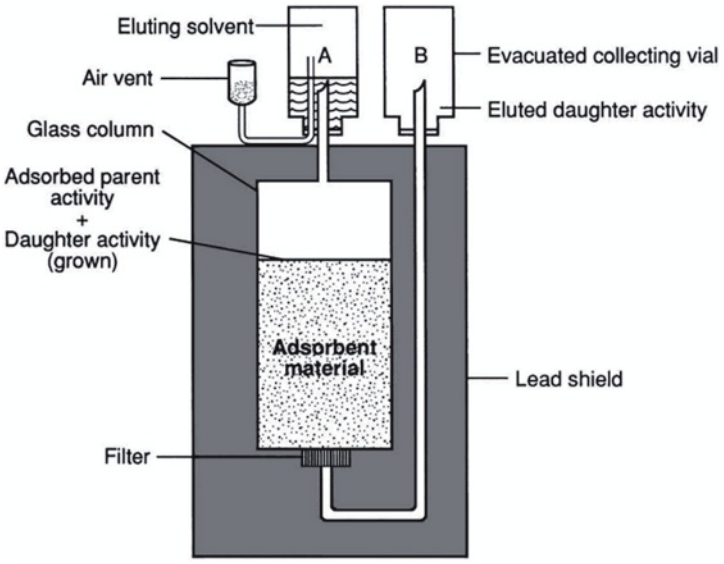

FIG. 5.3. Typical radionuclide generator system. Vacuum in vial *B* draws the eluant from vial *A* through adsorbent material, and the daughter is collected in vial *B*.

Several radionuclide generators are available for ready supply of short-lived radionuclides: ^{99}Mo(66 h)–^{99m}Tc(6 h); ^{113}Sn(117 days)–^{113m}In(100 min); ^{68}Ge(271 days)–^{68}Ga(68 min); ^{82}Sr(25.6 days)–^{82}Rb(75 s); ^{81}Rb(4.6 h)–^{81m}Kr(13 s). Of these, the ^{99}Mo–^{99m}Tc generator is the workhorse of nuclear pharmacy in nuclear medicine.

^{99}Mo–^{99m}Tc *Generator*

The ^{99}Mo–^{99m}Tc generator is constructed with alumina (Al_2O_3) loaded in a plastic or glass column. The ^{99}Mo activity is adsorbed on alumina in the chemical form MoO_4^{2-} (molybdate) and in various amounts. The amount of alumina used is about 5–10 g depending on the ^{99}Mo activity. Currently, all generators use fission-produced ^{99}Mo. The growth and decay of ^{99m}Tc along with the decay of ^{99}Mo is shown in Fig. 3.5 in Chapter 3. The ^{99m}Tc activity is eluted with 0.9 % NaCl solution (isotonic saline) and obtained in the chemical form of $Na^{99m}TcO_4$.

Considering that only 87 % of ^{99}Mo decays to ^{99m}Tc, the ^{99m}Tc activity A_{Tc} can be calculated from Eq. (3.15) as follows:

$$A_{Tc} = 0.957(A_{Mo})_0\left(e^{-0.0105t} - e^{-0.1155t}\right) \tag{5.4}$$

where $(A_{Mo})_0$ is the ^{99}Mo activity at $t = 0$, $\lambda_{Mo} = 0.0105\ h^{-1}$, and $\lambda_{Tc} = 0.1155\ h^{-1}$. The time t has the unit of hour. At transient equilibrium (from Eq. (3.16)),

$$\begin{aligned} A_{Tc} &= 0.957(A_{Mo})_0 e^{-0.0105t}. \\ &= 0.957(A_{Mo})_t \end{aligned} \tag{5.5}$$

Upon elution with saline, approximately 75–85 % of the total activity is eluted from the column. After about 4 half-lives, the ^{99m}Tc activity again reaches maximum.

Problem 5.3
A 2.5-Ci ^{99}Mo–^{99m}Tc generator calibrated for Thursday noon was received on Wednesday afternoon. What would be the ^{99m}Tc activity, eluted at 8:00 a.m. on Friday, assuming a transient equilibrium between ^{99}Mo and ^{99m}Tc at the time of elution, and 85 % elution yield?

Answer
^{99}Mo activity on Thursday noon = 2500 mCi
The time from Thursday noon to 8:00 a.m. on Friday = 20 h

$$\text{Therefore, } {}^{99}\text{Mo activity at } 8{:}00 \text{ a.m. Friday} = 2500 \times \exp(-0.0105 \times 20) = 2026 \text{ mCi}$$

Using Eq. (5.5) at transient equilibrium,

$$^{99m}\text{Tc activity} = 0.957 \times 2026 \times 0.85 = 1648 \text{ mCi}$$

The ^{99}Mo activity is likely to be eluted in trace quantities along with ^{99m}Tc activity. This is called the ^{99}Mo or *Moly breakthrough*. The presence of ^{99}Mo gives unnecessary radiation dose to the patient. According to the Nuclear Regulatory Commission (NRC) regulations, *the permissible limit for* ^{99}Mo *breakthrough is* 0.15 μCi (5.5 kBq) *per millicurie* (37 MBq) *of* ^{99m}Tc *at the time of injection*. The ^{99}Mo breakthrough is determined by the detection of high-energy photons (740 keV and 780 keV) of ^{99}Mo in a dose calibrator after stopping 140-keV photons of ^{99m}Tc in a lead container (6 mm thick).

Aluminum also is likely to be eluted along with ^{99m}Tc activity and must be checked. The presence of aluminum interferes with the preparation of ^{99m}Tc-labeled sulfur colloid by forming larger particles, which are trapped in the lungs. It also agglutinates the red blood cells during labeling. Its acceptable limit is 10 μg/ml of ^{99m}Tc solution. Aluminum ion (Al^{3+}) is checked by the colorometric test using a paper strip impregnated with a coloring agent and comparing the intensity of the color developed by the sample solution with that by a standard test solution (10 μg/ml). If the sample color is more intense than the standard color, the ^{99m}Tc sample is not acceptable for use.

Cyclotron production of ^{99m}Tc

In recent years, there was a severe shortage of fission-produced ^{99}Mo due to the closing of major reactors – some for ageing and some for maintenance – in several countries. This led to an acute shortage of ^{99m}Tc in nuclear medicine communities throughout the world causing great difficulty in patient care. Investigators have been looking for alternative sources of ^{99m}Tc and suggested that ^{99m}Tc can be produced in a medium-energy cyclotron by the ^{100}Mo(p, 2n)^{99m}Tc reaction in quantities sufficient to supply daily to several hospitals for all necessary nuclear imaging studies. It has been shown that at 24 MeV proton energy and a beam current of 500 μA, nearly 74.3 Ci (2.75 TBq) of ^{99m}Tc can be produced for two 6-hr bombardments (Scholten et al., 1999). Considering a 10 hr decay and 15 % loss during processing and an average patient dosage of 25 mCi (0.93 GBq), almost 800 dosages of ^{99m}Tc products can be prepared – sufficient enough to serve a large metropolitan of ~ 5–7 million people. Because of the lack of generator possibility, many cyclotrons have to be installed throughout individual countries for ^{99m}Tc production by this method.

Questions

1. Describe the different methods of production of radionuclides. Which method gives relatively more proton-rich and neutron-rich radionuclides?
2. What are the differences between a positive ion and a negative ion cyclotron?
3. What is the average number of neutrons emitted in fission?

4. What is the difference between carrier-free and no-carrier-added radionuclides?
5. Why are cadmium rods and graphite used in the reactor?
6. If ^{68}Zn is bombarded with protons in a cyclotron and three neutrons are emitted from the nucleus, what is the product of the nuclear reaction? Write the nuclear reaction.
7. (a) What are the primary requirements for a radionuclide generator?
   (b) How long does it take to reach transient equilibrium in a ^{99}Mo–^{99m}Tc generator?
   (c) What is the permissible limit of ^{99}Mo breakthrough in the ^{99m}Tc eluate?
   (d) A 20-mCi (740-MBq) ^{99m}Tceluate is found to contain 10 μCi (0.37 MBq) of ^{99}Mo. Can this preparation be injected into a patient?
8. Why is Al^{3+} undesirable in the ^{99m}Tceluate? What is the permissible limit of Al^{3+} in the ^{99m}Tc eluate?
9. A 2-Ci (74-GBq) ^{99}Mo–^{99m}Tc generator calibrated for Thursday noon was eluted at 10 a.m. on the following Monday. Calculate the ^{99m}Tc activity assuming 80 % yield and 87 % of ^{99}Mo decays to ^{99m}Tc.
10. Calculate the activity in millicuries (MBq) of ^{111}In produced by irradiation of 1 g of pure ^{111}Cd for 3 h with 12-MeV protons having a beam intensity of 10^{13} particles/(cm^2 sec). The cross section for formation of ^{111}In($t_{1/2}$ = 2.8 days) is 200 millibarns (1 millibarn = 10^{-27} cm^2).

References and Suggested Readings

Colombetti LG. Radionuclide generators. In: Rayudu GVS, ed. *Radiotracers for Medical Applications.* Boca Raton, Fla: CRC Press; 1983;II:133–168.

Friedlander G, Kennedy JW, Macias ES, Miller JM. *Nuclear and Radiochemistry.* 3rd ed. New York: Wiley; 1981.

Gelbard AS, Hara T, Tilbury RS, Laughlin JS. Recent aspects of cyclotron production of medically useful radionuclides. In: *Radiopharmaceuticals and Labelled Compounds.* Vienna: IAEA; 1973:239–247.

Mirzadeh S, Mausner LF, Garland MA. Reactor-produced medical radionuclides. In: Vértes A, Nagy S, Klencsár Z, eds. *Handbook of Nuclear Chemistry.* Vol 4, Dordrecht: Kluwer; 2003.

Noronha OPD, Sewatkar AB, Ganatra RD, et al. Fission-produced ^{99}Mo–^{99m}Tc generator system for medical use. *J Nucl Med Biol.* 1976;20:32–36.

Poggenburg JK. The nuclear reactor and its products. *SeminNucl Med.* 1974;4:229–243.

Quaim SM. Cyclotron production of medical radionuclides. In: Vértes A, Nagy S, Klencsár Z, eds. *Handbook of Nuclear Chemistry.* Vol 4, Dordrecht: Kluwer; 2003.

Saha GB. Miscellaneous tracers for imaging. In: Rayudu GVS, ed. *Radiotracers for Medical Applications.* Boca Raton, Fla: CRC Press; 1983; II:119–132.

Saha GB. *Fundamentals of Nuclear Pharmacy.* 6th ed. New York: Springer; 2010.

Saha GB. *Basics of PET Imaging.* 2nd ed. New York: Springer; 2010.

Saha GB, MacIntyre WJ, Go RT. Cyclotron and positron emission tomography radiopharmaceuticals for clinical imaging. *Semin Nucl Med.* 1992;22:150–161.

Scholten B, Lambrecht RM, Cogneau et al. Excitation functions for the cyclotron production of ^{99m}Tc and ^{99}Mo. *Appl Radiat* Isotopes 1999;51:69.

6
Interaction of Radiation with Matter

All particulate and electromagnetic radiations can interact with the atoms of an absorber during their passage through it, producing ionization and excitation of the absorber atoms. These radiations are called *ionizing radiations*. Because particulate radiations have mass and electromagnetic radiations do not, the latter travel through matter longer distance before losing all energy than the former of the same energy. Electromagnetic radiations are therefore called *penetrating* radiations and particulate radiations *non-penetrating* radiations. The mechanisms of interaction with matter, however, differ for the two types of radiation, and therefore they are discussed separately.

Interaction of Charged Particles with Matter

The energetic charged particles such as α-particles, protons, deuterons, and β-particles (electrons) interact with the absorber atoms, while passing through it. The interaction occurs primarily with the orbital electrons of the atoms and rarely with the nucleus. During the interaction, both *ionization* and *excitation* as well as the breakdown of the molecule may occur. In excitation, the charged particle transfers all or part of its energy to the orbital electrons, raising them to higher energy shells. In ionization, the energy transfer may be sufficient to overcome the binding energy of the orbital electrons, ultimately ejecting them from the atom. Electrons ejected from the atoms by the incident charged particles are called *primary electrons*, which may have sufficient kinetic energy to produce further excitation or ionization in the absorber. The high-energy secondary electrons from secondary ionizations are referred to as *delta* (δ-) rays. The process of excitation and ionization will continue until the incident particle and all electrons come to rest. Both these processes may rupture chemical bonds in the molecules of the absorber, forming various chemical entities.

When charged particles travel through a medium at a speed greater than the speed of light, they polarize the molecules of the medium, which then turn back rapidly to their ground state, emitting radiation in the process. The emitted radiation is

G. B. Saha, *Physics and Radiobiology of Nuclear Medicine,*
DOI 10.1007/978-1-4614-4012-3_6,

bluish in color, which is called *Cerenkov* radiation. The charged particles traveling at more than the light speed creates a photonic shock wave in the medium, similar to a situation when a supersonic body traveling at more than the speed of sound creates sound shock wave. This effect can be observed with electrons of a few hundred keV energy, whereas α- particles and protons require several thousands of MeV to exceed the velocity of light and so to produce Cerenkov effect. Since its probability is low, it is of no practical importance in nuclear medicine.

In ionization, an average energy of W is required to produce an ion pair in the absorber and varies somewhat with the type of absorber. The value of W is about 35 eV in air and less in oxygen and xenon gases but falls in the range of 25–45 eV for most gases. The process of ionization, that is, the formation of ion pairs, is often used as a means of the detection of charged particles in ion chambers and Geiger–Müller counters described in Chapter 7.

Three important quantities associated with the passage of charged particles through matter are specific ionization, linear energy transfer, and range of the particle in the absorber, and these are described next.

Specific Ionization

Specific ionization (SI) is the total number of ion pairs produced per unit length of the path of the incident radiation. The SI values of α-particles are slightly greater than those of protons and deuterons, which in turn are larger than those of electrons.

Specific ionization increases with decreasing energy of the charged particle because of the increased probability of interaction at low energies. Therefore, toward the end of the travel, the charged particle shows a sharp increase in ionization (Fig. 6.1). This peak ionization is called *Bragg ionization*. This phenomenon is predominant for heavy charged particles and is negligible for electrons.

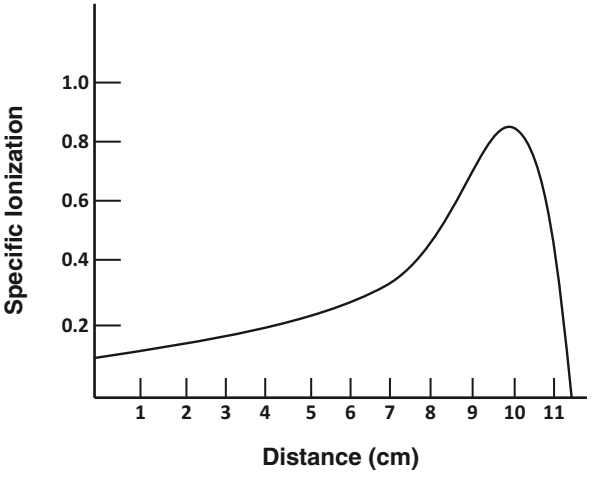

FIG. 6.1. Illustration of Bragg ionization showing a peak near the end of the travel of the charged particle.

Table 6.1. LET values of some radiations in tissue.

Radiation	LET (keV/μm)
3 MV x-rays	0.5
250 KV x-rays	3.0
5-MeV α-particles	100.0
1-MeV electrons	0.25
14-MeV neutrons	20.0

Linear Energy Transfer

The linear energy transfer (LET) is the amount of energy deposited per unit length of the path by the radiation. From the preceding, it is clear that

$$\text{LET} = \text{SI} \times W \tag{6.1}$$

The LET is expressed in units of keV/μm and is very useful in concepts of radiation protection. Electromagnetic radiations and β-particles interact with matter, losing only little energy per interaction and therefore have low LETs. In contrast, heavy particles (α-particles, neutrons, and protons) lose energy very rapidly, producing many ionizations in a short distance, and thus have high LETs. Some comparative approximate LET values in keV/mm in tissue are given in Table 6.1.

Problem 6.1
If a particulate radiation produces 45,000 ion pairs per centimeter in air, calculate the LET of the radiation.

Answer

$$\text{W} = 35 \text{ eV per ion pair}$$

Using Eq. (6.1),

$$\begin{aligned}\text{LET} &= \text{SI} \times W \\ &= 45,000 \times 35 \\ &= 1,575,000 \text{ eV/cm} \\ &= 157.5 \text{ eV/}\mu\text{m} \\ &= 0.1575 \text{ keV/}\mu\text{m}.\end{aligned}$$

Range

The *range* (R) of a charged particle in an absorber is the straight-line distance traversed by the particle in the direction of the particle. The range of a particle depends on the mass, charge, and kinetic energy of the particle and also on the density of the absorber. The heavier and more highly charged particles have shorter

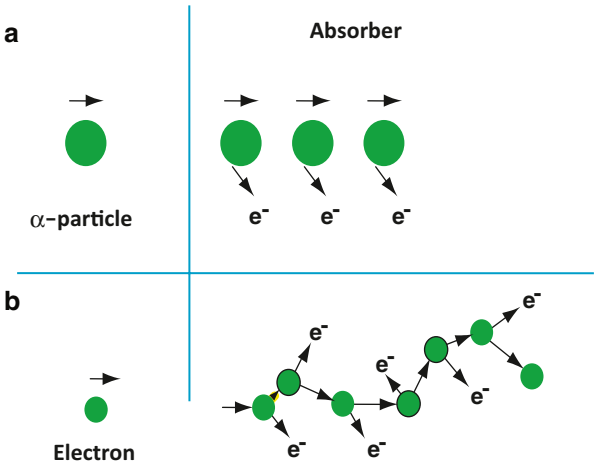

FIG. 6.2. Concept of passage of α particles and electrons through an absorber: **a** heavy α particles move in almost a *straight line*, **b** light electrons move in *zigzag paths*.

ranges than lighter and lower charged particles. The range of charged particles increases with the energy of the particle. Thus, a 10-MeV particle will have a longer range than a 1-MeV particle. The range of the particle depends on the density of the absorber, in that the denser the absorber, the shorter the range. The unit of range is given in mg/cm^2 of the absorber.

Depending on the type of the charged particle, the entire path of travel may be unidirectional along the initial direction of motion, or tortuous (Fig. 6.2). Because the α-particle loses only a small fraction of energy in a single collision with an electron because of its heavier mass and is not appreciably deflected in the collision, the α-particle path is nearly a straight line along its initial direction (Fig. 6.2a). Many collisions in a short distance create many ion pairs in a small volume. In contrast, β-particles or electrons interact with extra nuclear orbital electrons of the same mass and are deflected considerably. This leads to tortuous paths of these particles (Fig. 6.2b). In this situation, the true range is less than the total path traveled by the particle.

It is seen that the ranges of all identical particles in a given absorber are not exactly the same but show a spread of 3–4 % near the end of their path (Fig. 6.3). This phenomenon, referred to as the *straggling of the ranges*, results from the statistical fluctuations in the number of collisions and in the energy loss per collision. The range straggling is less prominent with α-particles but is severe with electrons because it is mostly related to the mass of the particle. The light mass electrons are considerably deflected during collisions and hence exhibit more straggling. If the transmission of a beam of charged particles through absorbers of different thicknesses is measured, the beam intensity will remain constant until the region of range straggling is encountered, where the beam intensity falls sharply from its initial value to zero. The absorber thickness that reduces the beam intensity by one half is called the *mean range*. The mean range of heavier particles such as α-particles is more well defined than that of electrons. Because

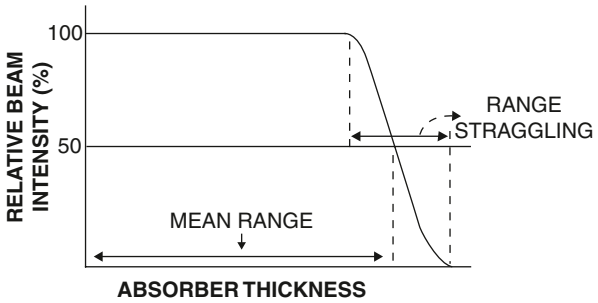

FIG. 6.3. Mean range and straggling of charged particles in an absorber.

β^--particles are emitted with a continuous energy spectrum, their absorption, and hence their ranges, become quite complicated.

Bremsstrahlung

When energetic charged particles, particularly electrons, pass through matter and come close to the nucleus of the atom, they lose energy as a result of deceleration in the Coulomb field of atomic nuclei. The loss in energy appears as an x-ray that is called *bremsstrahlung* (German for "braking" or "slowing down" radiation). These bremsstrahlung radiations are commonly used in radiographic procedures and are generated by striking a tungsten target with a highly accelerated electron beam.

Bremsstrahlung production increases with the kinetic energy of the particle and the atomic number (Z) of the absorber. For example, a 10-MeV electron loses about 50 % of its energy by bremsstrahlung, whereas a 90-MeV electron loses almost 90 % of its energy by this process. The bremsstrahlung production is proportional to Z^2 of the absorber atom. Therefore, bremsstrahlung is unimportant in lighter metals such as air, aluminum, and so forth, whereas it is very significant in heavy metals such as lead and tungsten. High-energy β^--particles from radionuclides such as ^{32}P can produce bremsstrahlung in heavy metals such as lead and tungsten. For this reason, these radionuclides are stored in low-Z materials such as plastic containers rather than in lead containers.

Bremsstrahlung is inversely proportional to the mass of the charged particles and therefore is insignificant for heavy particles, namely α-particles and protons, because the probability of penetrating close to the nuclei is relatively low due to their heavier masses.

Annihilation

When energetic β^+-particles pass through an absorber, they lose energy via interaction with orbital electrons of the atoms of the absorber. When the β^+-particle comes to almost rest after losing all energy, it combines with an orbital electron of the absorber atom and produces two 511-keV annihilation radiations that are emitted in opposite directions (180°). These annihilation radiations are the basis

of positron emission tomography (PET) in which two photons are detected in coincidence, which is discussed in Chapter 13.

Interaction of γ-Radiations with Matter

Mechanism of Interaction of γ-Radiations

When penetrating γ-rays pass through matter, they lose energy by interaction with the orbital electrons or the nucleus of the absorber atom. The γ-ray photons may lose all of their energy, or a fraction of it, in a single encounter. The specific ionization of γ-rays is one-tenth to one-hundredth of that caused by a non-penetrating electron of the same energy. There is no quantity equivalent to a range of particles for γ-rays, but they travel a long path in the absorber before losing all energy. The average energy loss per ion pair produced by the photons is the same as for electrons, that is, 35 keV in air.

There are several mechanisms by which γ-rays interact with absorber atoms during their passage through matter, and they are described below.

Photoelectric Effect

In the photoelectric effect, the incident γ-ray transfers all its energy to an orbital electron of the absorber atom whereby the electron, called the *photoelectron*, is ejected with kinetic energy equal to $E_\gamma - E_B$, where E_γ and E_B are the energy of the γ-ray and the binding energy of the electron, respectively (Fig. 6.4). The photoelectron loses its energy by ionization and excitation in the absorber, as discussed previously. The photoelectric effect occurs primarily in the low-energy range and decreases sharply with increasing photon energy. It also increases very rapidly with increasing atomic number Z of the absorber atom. Roughly, the pho-

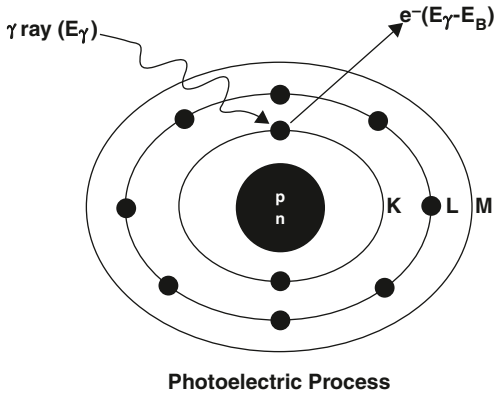

FIG. 6.4. The photoelectric effect in which a γ-ray with energy E_γ transfers all its energy to a K-shell electron, and the electron is ejected with $E_\gamma - E_B$, where E_B is the binding energy of the K-shell electron.

toelectric effect is proportional to Z^3/E_γ^3. The photoelectric contribution from the 0.15-MeV γ-rays in aluminum ($Z = 13$) is about the same (~ 5 %) as that from the 4.7-MeV γ-rays in lead ($Z = 82$).

The photoelectric effect occurs primarily with the *K*-shell electrons, with about 20 % contribution from the *L*-shell electrons and even less from higher shells. There are sharp increases (discontinuities) in photoelectric effects at energies exactly equal to binding energies of *K*-, *L*- (etc.) shell electrons. These are called *K*-, *L*- (etc.) absorption edges. The vacancy created by the ejection of an orbital electron is filled in by the transition of an electron from the upper energy shell. It is then followed by emission of a characteristic x-ray or Auger electron, analogous to the situations in internal conversion or electron capture decay.

Compton Scattering

In Compton scattering, the γ-ray photon transfers only a part of its energy to an electron in the outer shell of the absorber atom, and the electron is ejected. The photon, itself with reduced energy, is deflected from its original direction (Fig. 6.5). This process is called the *Compton scattering*. The scattered photon of lower energy may then undergo further photoelectric or Compton interaction, and the Compton electron may cause ionization or excitation, as discussed previously.

At low energies, only a small fraction of the photon energy is transferred to the Compton electron, and the photon and the Compton electron are scattered at an angle θ. Using the law of conservation of momentum and energy, the scattered photon energy is given by

$$E_{sc} = E_\gamma/[1 + (E_\gamma/0.511)(1 - \cos\theta)] \tag{6.2}$$

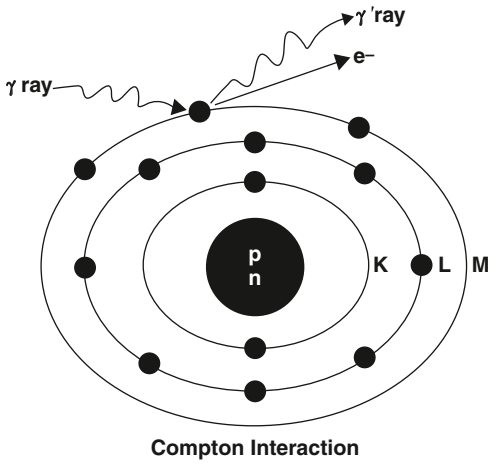

Fig. 6.5. The Compton scattering, in which a γ-ray interacts with an outer orbital electron of an absorber atom. Only a part of the photon energy is transferred to the electron, and the photon itself is scattered at an angle. The scattered photon may undergo subsequent photoelectric effect or Compton scattering in the absorber or may escape the absorber.

where E_γ and E_{sc} are the energies in MeV of the initial and scattered photons. The scattered photon energy varies from a maximum in a collision at 0° (forward) to a minimum at θ = 180° in a backscattering collision. Conversely, the Compton electron carries a minimum energy in the forward collision to a maximum energy in the backscattering collision. At higher energies, both the scattered photon and the Compton electron are predominantly scattered in the forward direction.

If the photon is backscattered, that is, scattered at 180°, then the backscattered photon has the energy E_{sc} given by the expression (cos180° = −1):

$$E_{sc} = E_\gamma/(1 + E_\gamma/0.256) \tag{6.3}$$

In backscattering of a 140-keV photon, the scattered photon and the Compton electron would have 91 and 49 keV, respectively, whereas for a 1330-keV photon these values are 215 and 1115 keV, respectively. It can be seen that as the photon energy increases, the scattered photon energy approaches the minimum limit of 256 keV, and the Compton electron receives the maximum energy.

Compton scattering is almost independent of the atomic number Z of the absorber. Compton scattering contributes primarily in the energy range of 0.1–10 MeV, depending on the type of absorber.

Pair Production

When the γ-ray photon energy is greater than 1.02 MeV, the photon can interact with the nucleus of the absorber atom during its passage through it, and a positive electron and a negative electron are produced at the expense of the photon (Fig. 6.6). The energy in excess of 1.02 MeV appears as the kinetic energy of the two particles. This process is called *pair production*. It varies almost linearly with Z^2 of the absorber and increases slowly with the energy of the photon. In soft tissue,

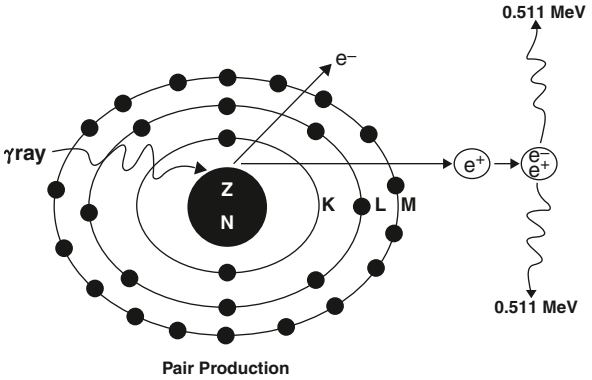

FIG. 6.6. Illustration of the pair production process. An energetic γ-ray with energy greater than 1.02 MeV interacts with the nucleus, and one positive electron (e^+) and one negative electron (e^-) are produced at the expense of the photon. The photon energy in excess of 1.02 MeV appears as the kinetic energy of the two particles. The positive electron eventually undergoes annihilation to produce two 511-keV photons emitted in opposite directions.

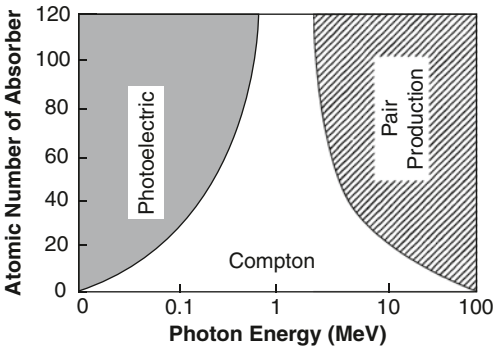

Fig. 6.7. Relative contributions of the photoelectric effect, Compton scattering, and pair production as a function of photon energy in absorbers of different atomic numbers. (Adapted with permission from Hendee WR. *Medical Radiation Physics*.1st ed. Chicago: Year Book Medical Publishers, Inc; 1970: 141).

pair production is insignificant at energies up to 10 MeV above 1.02 MeV. Positive electrons created by pair production are annihilated to produce two 0.511-MeV photons identical to those produced by positrons from radioactive decay.

The relative importance of photoelectric, Compton, and pair production interactions with absorbers of different atomic numbers is shown in Fig. 6.7, as a function of the energy of the incident photons. It is seen that the photoelectric effect is predominant in high Z absorbers at lower energies (<0.1 MeV), whereas the Compton scattering is predominant in intermediate Z absorbers at medium energies (~1 MeV). At higher energies (>10 MeV), pair production predominates in all Z absorbers.

Raleigh Scattering

In Raleigh scattering, a γ-ray can interact with the atom as a whole atom instead of individual orbital electrons, whereby the photon energy is spent for the atom to oscillate in phase. The atom then releases the energy in the form of a γ-ray with almost the same energy as the initial γ-ray, which is emitted at a slightly different angle than the original γ-ray. This scattering is also termed coherent or classical scattering. Since it occurs only with low energy photons (<40 keV) and also its overall probability of occurrence is low, it is of little significance in nuclear medicine.

Photodisintegration

When the γ-ray photon energy is very high (>10 MeV), the photon may interact with the nucleus of the absorber atom and transfer sufficient energy to the nucleus such that one or more nucleons may be emitted. This process is called the *photodisintegration reaction*, or *photonuclear reaction* and produces new nuclides. The (γ, n) reactions on targets such as ^{12}C and ^{14}N have been used to produce ^{11}C and ^{13}N radionuclides but now are rarely used to produce radionuclides.

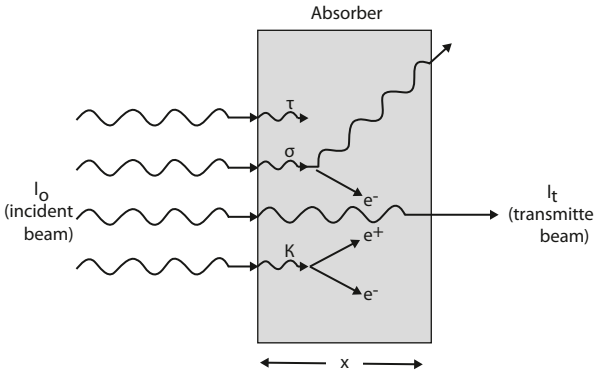

FIG. 6.8. Illustration of attenuation of a photon beam (I_0) in an absorber of thickness x. Attenuation comprises a photoelectric effect (τ), Compton scattering (σ), and pair production (κ). Photons passing through the absorber without interaction constitute the transmitted beam (I_t).

Attenuation of γ-Radiations

Linear and Mass Attenuation Coefficients

γ-ray and x-ray photons are either attenuated or transmitted as they travel through an absorber. Attenuation results from absorption by the photoelectric effect, Compton scattering, and pair production at higher energies. Depending on the photon energy and the density and thickness of the absorber, some of the photons may pass through the absorber without any interaction leading to the transmission of the photons (Fig. 6.8). Attenuation of γ-radiations is an important factor in radiation protection.

As shown in Fig. 6.8, if a photon beam of initial intensity I_0 passes through an absorber of thickness x, then the transmitted beam I_t is given by the exponential equation

$$I_t = I_0 e^{-\mu x}. \tag{6.4}$$

where μ is the *linear attenuation coefficient* of the absorber for the photons of interest and has the unit of cm^{-1}. The factor $e^{-\mu x}$ represents the fraction of the photons transmitted. Because attenuation is primarily due to photoelectric, Compton, and pair production interactions, the linear attenuation coefficient μ is the sum of photoelectric coefficient (τ), Compton coefficient (σ), and pair production coefficient (κ). Thus,

$$\mu = \tau + \sigma + \kappa. \tag{6.5}$$

Linear attenuation coefficients normally decrease with the energy of the γ-ray or x-ray photons and increase with the atomic number and density of the absorber. The relative contributions of photoelectric effect, Compton scattering, and pair production in water (equivalent to body tissue) at different energies are illustrated in Fig. 6.9.

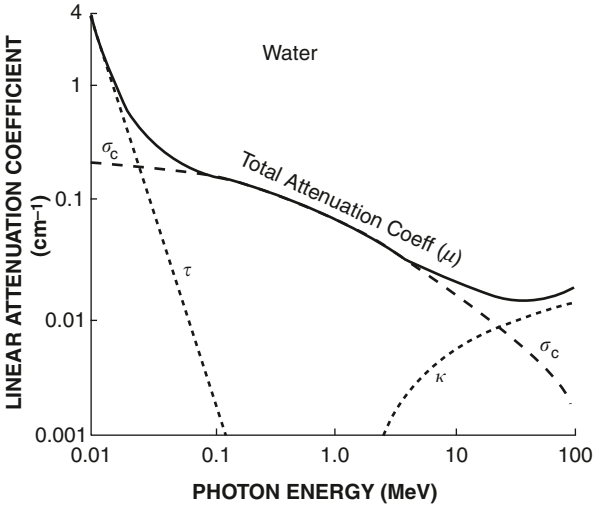

FIG. 6.9. Plot of linear attenuation coefficient of γ-ray interaction in water (equivalent to body tissue) as a function of photon energy. The relative contributions of photoelectric, Compton, and pair production processes are illustrated.

An important quantity, μ_m, called the *mass attenuation coefficient*, is given by the linear attenuation coefficient divided by the density ρ of the absorber

$$\mu_m = \frac{\mu}{\rho} \tag{6.6}$$

The mass attenuation coefficient μ_m has the unit of cm^2/g or cm^2/mg. The mass attenuation coefficients for fat, bone, muscle, iodine, and lead are given in Fig. 6.10.

Half-Value Layer

The concept of *half-value layer* (HVL) of an absorbing material for γ- or x-radiations is important in the design of shielding for radiation protection. It is defined as the thickness of the absorber that reduces the intensity of a photon beam by one-half. Thus, an HVL of an absorber around a source of γ-radiations with an exposure rate of 150 mR/ h will reduce the exposure rate to 75 mR/ h. The HVL depends on the energy of the radiation and the atomic number of the absorber. It is greater for high-energy photons and smaller for high-*Z* materials.

For monoenergetic photons, the HVL of an absorber is related to its linear attenuation coefficient as follows:

$$\text{HVL} = \frac{0.693}{\mu}. \tag{6.7}$$

Because μ has the unit of cm^{-1}, the HVL has the unit of cm. The HVLs of lead for different radionuclides are given in Table 6.2.

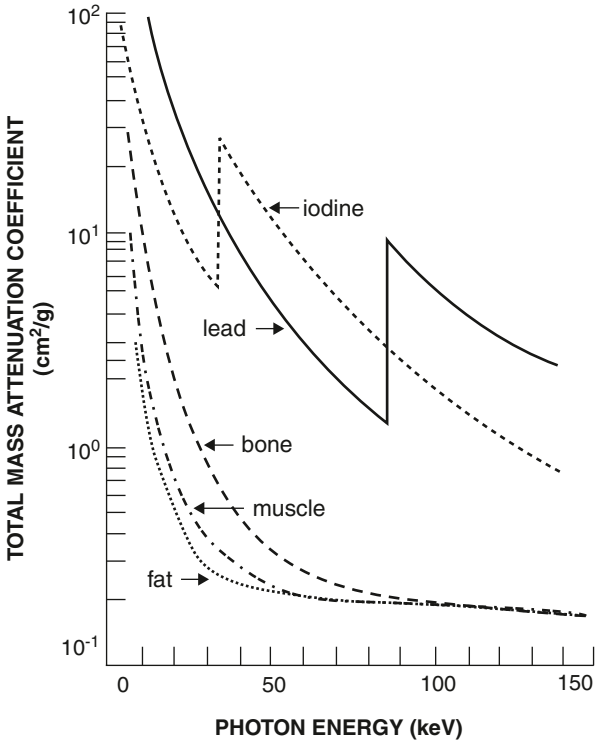

FIG. 6.10. Attenuation coefficients for fat, muscle, bone, iodine, and lead as a function of photon energy. (Adapted with permission from Hendee WR. *Medical Radiation Physics*. 1st ed. Chicago: Year Book Medical Publishers, Inc; 1970: 221).

TABLE 6.2. Half-value layer values (HVLs) of lead for commonly used radionuclides.

Radionuclides	HVL, Lead (cm)[a]	HVL, Water (cm)[b]
^{137}Cs	0.65	–
^{99m}Tc	0.03	4.6
^{201}Tl	0.02	–
^{99}Mo	0.70	–
^{67}Ga	0.10	–
^{123}I	0.04	–
^{111}In	0.10	–
^{125}I	0.003	1.7
^{57}Co	0.02	–
^{131}I	0.30	6.3
^{18}F	0.39	11.2

[a] Adapted from Goodwin PN. Radiation safety for patients and personnel. In: Freeman LM, editors. *Freeman and Johnson's Clinical Radionuclide Imaging*. 3rd ed. Philadelphia: WB Saunders; 1984: 320.

[b] HVL in water is considered equivalent to HVL in tissue.

Another important quantity, tenth-value layer (TVL), is the thickness of an absorber that reduces the initial beam by a factor of ten. It is given by

$$\text{TVL} = -\frac{\ln(0.1)}{\mu}$$

$$= \frac{2.30}{\mu} \tag{6.8}$$

$$= 3.32 \ \text{HVL} \tag{6.9}$$

Problem 6.2
If the HVL of lead for the 140-keV photons of ^{99m}Tc is 0.03 cm of lead, calculate the linear attenuation coefficient of lead for the 140-keV photons and the amount of lead needed to reduce the exposure of a point source of radiation by 70 %.

Answer

$$\mu = \frac{0.693}{\text{HVL}} = \frac{0.693}{0.03} = 23.1 \ \text{cm}^{-1}$$

Because the initial beam is reduced by 70 %, the remaining beam is 30 %.

$$0.3 = 1 \times e^{-23.1 \times x}$$

$$\ln(0.3) = -23.1 \times x$$

$$1.20 = 23.1 \times x$$

$$x = 0.052 \ \text{cm}$$

$$= 0.52 \ \text{mm}$$

Thus, 0.52 mm of lead will reduce a beam of 140-keV photons by 70 %.

Interaction of Neutrons with Matter

Because neutrons are neutral particles, their interactions in the absorber differ from those of the charged particles. They interact primarily with the nucleus of the absorber atom and very little with the orbital electrons. The neutrons can interact with the atomic nuclei in three ways: elastic scattering, inelastic scattering, and neutron capture. If the sum of the kinetic energies of the neutron and the nucleus before collision is equal to the sum of these quantities after collision, then

the interaction is called *elastic*. If a part of the initial energy is used for the excitation of the struck nucleus, the collision is termed *inelastic*. In neutron capture, a neutron is captured by the absorber nucleus, and a new excited nuclide is formed. Depending on the energy deposited, an α-particle, a proton, a neutron, or γ-rays can be emitted from the excited nucleus, and a new product nuclide (usually radioactive) is produced.

Questions

1. (a) What is the difference between excitation and ionization?
   (b) How are δ-rays produced?
   (c) How much energy is required on the average to produce an ion pair in air by charged particles?
2. Define specific ionization (SI), linear energy transfer (LET), and range (R).
3. Electromagnetic radiations and electrons have low LETs compared to heavy particles (e.g., α-particles), which have high LETs. Explain.
4. The range of an α-particle is almost equal to the total path traveled, whereas the range of an electron is less than the total path traveled by the particle. Explain.
5. Indicate how the range of a charged particle is affected by the following conditions:
   (a) As the mass increases, the range increases or decreases.
   (b) As the energy of the particle increases, the range increases or decreases.
   (c) As the charge of the particle increases, the range increases or decreases.
6. Define Bragg ionization and straggling of ranges. Which has more straggling, an α-particle or an electron? Explain.
7. How is bremsstrahlung produced? Does its production increase or decrease with increasing kinetic energy of the electron and the atomic number of the absorber? Explain why ^{32}P is stored in plastic containers.
8. Discuss the mechanism of the photoelectric effect. Does this process increase or decrease with increasing energy of the γ-ray and with increasing atomic number of the absorber?
9. A 0.495-MeV γ-ray interacts with a *K*-shell electron by the photoelectric process. If the binding energy of the *K*-shell electron is 28 keV, what happens to the rest of the photon energy?
10. (a) Explain the Compton scattering of electromagnetic radiations in the absorber.
    (b) Does it depend on the atomic number of the absorber?
    (c) How is it affected by the γ-ray energy?
11. If a relatively high-energy γ-ray is scattered at 180° (backscattered) by the Compton scattering, what is the maximum energy of the scattered photon?
12. (a) How does pair production occur?
    (b) Why does pair production require a minimum of 1.02 MeV for γ-ray energy?
    (c) Is this process affected by the atomic number of the absorber and the photon energy?

13. Which electrons of the absorber atom are involved in the photoelectric and Compton interactions of electromagnetic radiations?
14. (a) Discuss the attenuation of a photon beam passing through an absorber.
    (b) Does it depend on the density and the atomic number of the absorber?
    (c) Define the half-value layer (HVL) of an absorbing material for a γ-ray energy.
15. If 1 mCi of a radionuclide is adequately shielded by 5 HVLs of a shielding material, how many HVLs are needed to provide equal shielding for (a) 5 mCi and (b) 8mCi?
16. A 1-mm lead apron will afford approximately twice as much protection as a 0.5-mm apron, or does this shielding depend on the energy of the radiation?
17. How many HVLs are approximately equivalent to three tenth-value layers?
18. Suppose 5 % of the 364-keV photons of ^{131}I are transmitted after passing through a lead brick of 10-cm thickness. Calculate the HVL of lead for ^{131}I.
19. There is a 75 % chance that a monoenergetic photon beam will be attenuated by 4 mm of lead. What is the HVL of lead for the photon?
20. Which of the following radiations has the highest LET?
    (a) 120-keV x-ray
    (b) 100-keV electron
    (c) 5-MeV α-particle
    (d) 10-MeV proton
    (e) 14-MeV neutron
21. Define Cerenkov radiation and Raleigh scattering.

Suggested Readings

Cherry SR, Sorensen JA, Philips ME. *Physics in Nuclear Medicine*. 3rd ed. Philadelphia: W.B. Saunders; 2003.

Friedlander G, Kennedy JW, Miller JM. *Nuclear and Radiochemistry*. 3rd ed. New York: Wiley; 1981.

Johns HE, Cunningham JR. *The Physics of Radiology*. 4th ed. Springfield, Ill: Charles C Thomas; 1983.

Knoll GF. *Radiation Protection and Measurement*. 4th ed. New York: Wiley; 2010.

Lapp RE, Andrews HL. *Nuclear Radiation Physics*. 4th ed. Englewood Cliffs, NJ: Prentice-Hall; 1972.

7
Gas-Filled Detectors

Principles of Gas-Filled Detectors

The operation of a gas-filled detector is based on the ionization of gas molecules by radiation, followed by collection of the ion pairs as charge or current with the application of a voltage between two electrodes. The measured charge or current is proportional to the applied voltage and the amount and energy of radiation, and depends on the type and pressure of the gas.

A schematic diagram of a gas-filled detector is shown in Fig. 7.1. When an ionizing radiation beam passes through the gas, it causes ionization of the gas molecules and ion pairs are produced depending on the type and pressure of the gas. When a voltage is applied between the two electrodes, the negative electrons will move to the anode and the positive ions to the cathode, thus producing a current that can be measured on a meter.

At very low voltages, the ion pairs do not receive enough acceleration to reach the electrodes and therefore may combine together to form the original molecule instead of being collected by the electrodes. This region is called the *region of recombination* (Fig. 7.2). As the applied voltage is gradually increased, a *region of saturation* is encountered, where the current measured remains almost the same over the range of applied voltages. In this region, only the primary ion pairs formed by the initial radiations are collected. Individual events cannot be detected; only the total current passing through the chamber is measured. Because specific ionization differs for α-, β-, and γ-radiations, the amount of current produced by these radiations differs in this region. The voltage in this region is of the order of 50–300 V. Ionization chambers such as dose calibrators are operated in this region.

When the applied voltage is further increased, the electrons and positive ions gain such high velocities and energies during their acceleration toward the electrodes that they cause secondary ionization. The latter will increase the measured current. This process is referred to as the *gas amplification*. This factor can be as high as 10^6 per individual primary event depending on the design of the gas detector and the applied voltage. In this region, the total current measured is equal to the number of ionizations caused by the primary radiation multiplied by the gas amplification factor. In this region, the current increases with the applied voltage

G. B. Saha, *Physics and Radiobiology of Nuclear Medicine,*
DOI 10.1007/978-1-4614-4012-3_7,

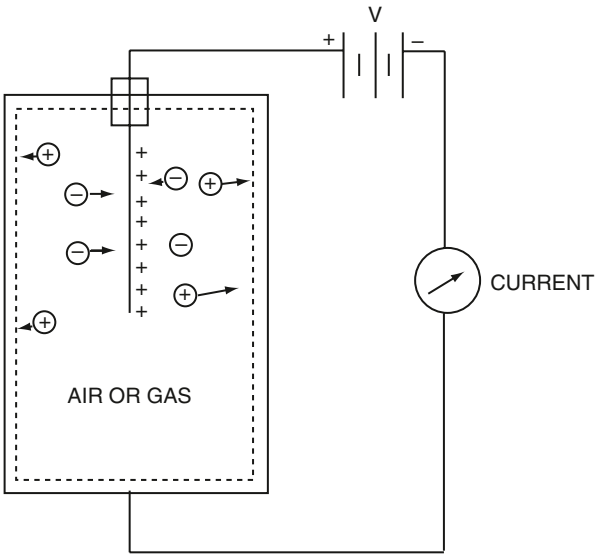

FIG. 7.1. A schematic diagram of a gas-filled detector illustrating the principles of operation.

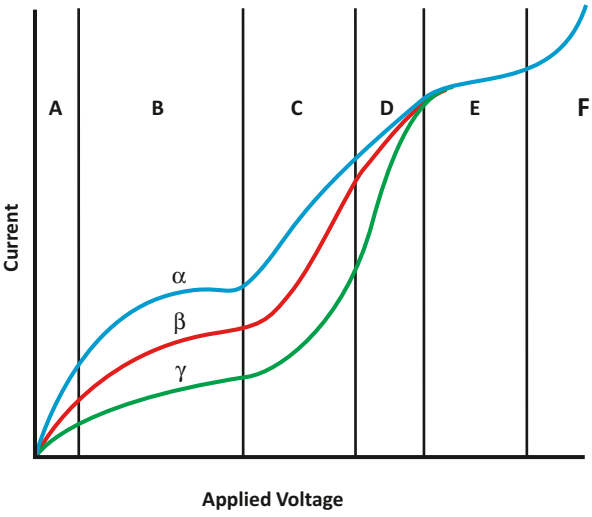

FIG. 7.2. A composite curve illustrating the current output as a result of increasing voltages for different radiations. **a** Region of recombination, **b** region of saturation, **c** proportional region, **d** region of limited proportionality, **e** Geiger region, and **f** continuous discharge.

in proportion to the initial number of ion pairs produced by the incident radiation. Therefore, as in the case of the region of saturation, the current amplification is relatively proportional to the types of radiations, e.g., α-, β-, and γ-radiations. This region is referred to as the *proportional region* (see Fig. 7.2). Proportional coun-

ters are usually filled with 90 % argon and 10 % methane (P-10) at atmospheric pressure. These counters can be used to count individual counts and to discriminate radiations of different energies, but are not commonly used for γ- and x-ray counting because of poor counting efficiency (<1 %).

As the applied voltage is increased further, the current produced by different types of radiation tends to become identical. The voltage range over which the current tends to converge is referred to as the *region of limited proportionality*. This region is not practically used for detecting any radiation in nuclear medicine.

With additional increase in voltage beyond the region of limited proportionality, the current becomes identical for all radiations, regardless of how many ion pairs are produced by the incident radiations. This region is referred to as the *Geiger region* (see Fig. 7.2). In the Geiger voltage region, the current is produced by an avalanche of interactions. When highly accelerated electrons strike the anode with a great force, ultraviolet (UV) light is emitted, which causes further emission of photoelectrons by gas ionization and from the chamber walls. The photoelectrons will again strike the anode to produce more UV, and hence an avalanche spreads along the entire length of the anode. The amplification factor can be as high as 10^{10}. During the avalanche, however, the lightweight electrons are quickly attracted to the anode, whereas a sheath of slow-moving heavy positive ions builds up around the anode. As a result, the voltage gradient falls below the value necessary for ion multiplication, and therefore the avalanche is terminated. All this occurs in less than 0.5 μs, and the counter is left insensitive and must recover before another event can be counted.

Recovery begins with the migration of the positive ions toward the cathode (i.e., chamber wall) and takes about 200 μs at a gas pressure of 0.1 atmosphere, which is equal to the dead time of the counter that varies with gas pressure. As the positive ions approach the cathode, secondary electrons may be emitted from the surface of the cathode, which then set another discharge just about 200 μs after the previous one. Such repetitive discharges that are due to secondary electrons are independent of the types and energy of radiation that the counter is intended to measure. The emission of secondary electrons is suppressed by a technique known as *quenching* to eliminate repetitive counter discharges (see later).

As the applied voltage is increased beyond the Geiger region, a single ionizing event produces a series of repetitive discharges leading to what is called *spontaneous discharge*. This region is called the *region of continuous discharge* because the gas may be ionized in the absence of radiation at this high voltage (see Fig. 7.2). Operation of a detector in this region may cause damage to the detector.

Ionization Chambers

Ionization chambers are operated at voltages in the saturation region that spans 50–300 V. The detector is a cylindrical or rectangular chamber filled with air or a gas, sometimes at high pressure. A central wire and the chamber act as the electrodes and the current is measured by an electrometer. The detection efficiency of

the ionization chambers for x-rays and γ-rays is very low (<1 %) and depends on the energy of these radiations. Ionization chambers are primarily used for measuring high-intensity radiation such as x-ray beams and high activity of radiopharmaceuticals. Ion chamber survey meters, dose calibrators, and pocket dosimeters are the common ionization chambers used in nuclear medicine.

Ion Chamber Survey Meter

An ion chamber survey meter consists of a metallic box fitted with a voltage circuitry operated by batteries to measure the ionization current or ion-pairs produced by interaction of radiations with the gas molecules in the chamber. The readings are displayed in analog or digital mode on scales over four or five decades (background to 50 R/h). They can be used to measure α, β and γ-ray exposure rates; however, for measurement of γ-ray exposure alone, a retractable beta shield (1000 mg/cm^2) is placed beside a thin window (7 mg/cm^2) of the chamber. The shield is removed when measuring α and β particle exposures. However, in the case of α particle exposure, the pulse mode counting is applied due to large voltage pulses produced, whereas in the case of β and γ rays, the current mode is employed. Most meters are operated at ambient atmospheric pressure, whereas in some, high pressure is employed using argon or similar gas. In the latter, the probability of photon interaction increases and hence the sensitivity. However, the operation of the meter at atmospheric pressure is affected by variations in temperature and atmospheric pressure at different geographical locations causing a change in gas density, and so readings will differ from the calibration value. Correction circuits are installed in current ion chambers to correct for the temperature and pressure changes. A typical ion chamber is shown in Fig. 7.3.

According to NRC regulations, the ion chambers must be calibrated annually with a calibration source. ^{137}Cs ($t_{1/2}$ = 30 year) with 662 keV photons is commonly

FIG. 7.3. An ion chamber survey meter (Courtesy of Ludlum Instruments, Inc. Sweetwater, TX).

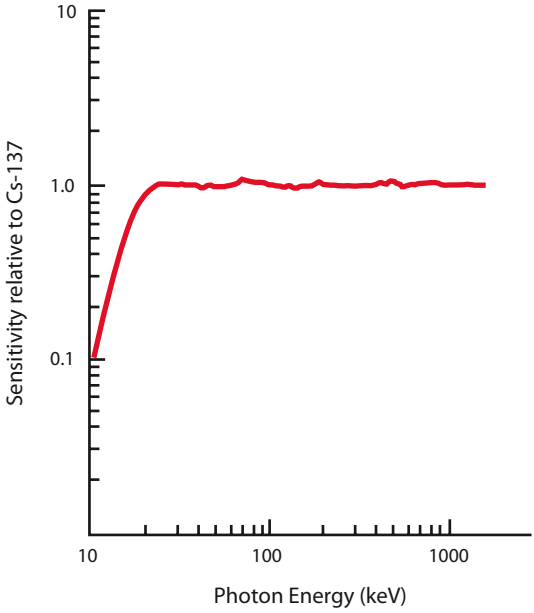

FIG. 7.4. The relative energy-independent response of ionization chamber.

used for calibration of these ion chambers and other survey meters. The sensitivity of these meters is quite linear over a broad range of photon energies relative to ^{137}Cs response except at low energies (Fig. 7.4). These meters can be used for a wide range of exposure readings except at low energies. The output is integrated and averaged over a period of time by the use of an RC circuit, and integration can be made slower or faster by the use of a switch.

Standard ion chambers are used for measurement of moderate to high exposure rate readings (e.g., ^{99}Mo–^{99m}Tc generator, X-ray beam intensity etc.), whereas pressurized ion chambers can be used for measuring low exposure rate readings. Sometimes scintillation detectors that are fabricated in the form of a probe are also used to measure the exposure rates in low to moderate range.

Dose Calibrator

The dose calibrator is an ionization chamber and one of the most essential instruments in nuclear medicine for measuring the activity of radionuclides and radiopharmaceuticals. Since it measures the current produced by activity, it does not have deadtime effects. It is a cylindrically shaped, sealed chamber with a central well and is filled with argon and traces of halogen at high pressure (~5–12 atmospheres). Its operating voltage is about 150 V. A typical dose calibrator is shown in Fig. 7.5.

Because radiations of different types and energies produce different amounts of ionization (hence current), equal activities of different radionuclides generate different quantities of current. For example, the amount of current produced

FIG. 7.5. A typical dose calibrator (Courtesy of Biodex Medical Systems, Inc, Shirley, NY).

by 1 mCi (37 MBq) of ^{99m}Tc differs from that produced by 1 mCi (37 MBq) of ^{131}I. Isotope selectors provided on the dose calibrator are the feedback resistors to compensate for the differences in ionization (current) produced by different radionuclides so that equal activities produce the same reading. In most dose calibrators, isotope selectors for common radionuclides are push-button type, whereas those for other radionuclides are set by a continuous dial. An activity range selector is a variable resistor that adjusts the range of activity (μCi, mCi, Ci, or kBq, MBq, GBq) for display.

In the past, the NRC required the calibration of dose calibrators for constancy, accuracy, and linearity of their operation and geometry of samples and accordingly prescribed specific recommendations for these tests. However, current NRC regulations (10CFR35) require only to have these calibrations performed according to nationally recognized standards or the manufacturers' instructions. In the absence of specific recommendations, the earlier frequency and other related requirements of these calibration tests have been given as follows:

1. Constancy (daily)
2. Accuracy (at installation, annually, and after adjustment or repairs)
3. Linearity (at installation, quarterly, and after adjustment or repairs)
4. Geometry (at installation and after adjustment or repairs)

Constancy

Daily constancy check is performed by measuring a long-lived radioactivity (e.g., ^{137}Cs) in the dose calibrator and observing the variation not to exceed ±10 % relative to the previous day reading. If the variation exceeds ± 10 %, the unit must be repaired or replaced.

Accuracy

Accuracy of the dose calibrator is determined by measuring the activity of at least two long-lived radionuclides (e.g., ^{137}Cs and ^{57}Co) certified by the National Institute of Standards and Technology (NIST) in the dose calibrator and comparing the measured activity with the activity reported by the NIST. The measured value should not differ from the standard value by more than ±10 %. If it exceeds ±10 %, the unit must be repaired or replaced.

Linearity

Decay Method

The linearity test indicates the dose calibrator's ability to measure the activity accurately over a range of values. It is performed by measuring a radioactive source (e.g., ^{99m}Tc), containing the highest activity normally used in the clinical setting, in the dose calibrator at different time intervals until the source decays down to less than 30 μCi (1.1 MBq). The measured activities are plotted against time on a semilog paper and the "best fit" line is drawn (Fig. 7.6). If the deviation of any point from the line exceeds ±10 %, the dose calibrator needs to be replaced, or a correction factor must be applied to the data in the nonlinear region.

Shielding Method

The advantage of this method is that it is less time-consuming and is easy to perform. The method utilizes a commercial kit, called Calicheck, that contains seven concentric tubes or "sleeves." All sleeves except the innermost one are lead-lined with increasing thickness simulating the various times of decay. When an activity source is measured by using first the inner sleeve, followed sequentially by increasingly thick sleeves, the data represent the activities at different decay times. Calibration factors are calculated by dividing the innermost tube reading by each outer tube reading. For subsequent linearity tests, identical measurements are made using the sleeves, and each measurement is multiplied by the corresponding calibration factors. Each corrected sleeve reading should give an identical value, and the average of all values is calculated. If an individual reading exceeds the average value by ±10 %, then the calibrator needs replacement, or a correction factor needs to be applied.

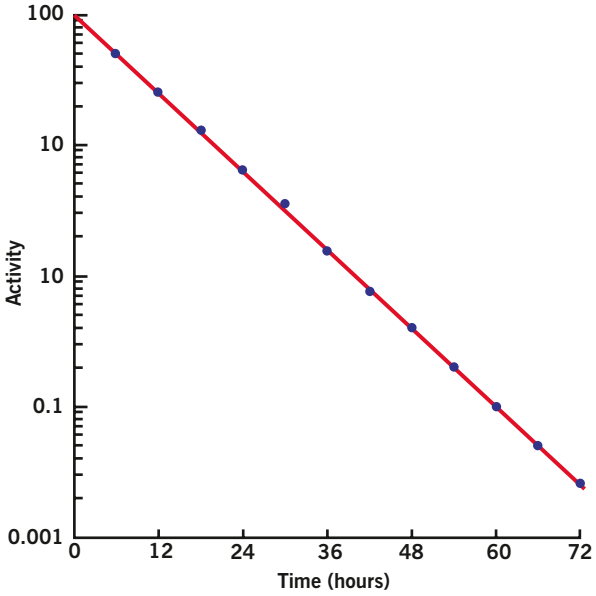

FIG. 7.6. The time-activity curve for decay method.

It should be noted that before the shielding method can be instituted, the linearity test must be first performed by the decay method for a new dose calibrator.

Geometry

Variations in sample volumes or in geometric configurations of the container can affect the accuracy of measurements in a dose calibrator, particularly for low-energy radiations. Thus, 1 mCi (37 MBq) in 1-ml or 30-ml volume, or 1 mCi (37 MBq) in 1-cc syringe, 10-cc syringe, or 10-cc vial, or in containers of different materials (plastic or glass) may give different readings in the dose calibrator. Correction factors must be determined for these geometric variations and applied to the measured activities, if the error exceeds ±10 %.

Pocket Dosimeter

The pocket dosimeter operates on the principle of a charged electroscope equipped with a scale inside. It consists of a quartz fiber electroscope inside the chamber. Initially, the dosimeter is fully charged by means of an external power supply (a dosimeter charger), and the scale then reads zero. After exposure to radiation, charge is lost, and the loss of charge is proportional to the amount of radiation exposure, which is read on the inside scale in mR. This reading can be seen through a viewing window at the end of the dosimeter. After complete discharge of the dosimeter, it can be charged and used again. It is primarily used to determine personnel exposure while working with radiation and has the advantage of giving immediate readings.

These dosimeters are available in full-scale readings of 200 mR, 500 mR, and 1 R. Discharge due to leakage is the major disadvantage of these dosimeters.

Proportional Counter

Proportional counters are gas counters operated in the proportional region of the applied voltage shown in Fig. 7.2. Because of the increased voltage beyond the region of saturation, the electrons released by the initial ionization become energetic enough to cause further ionization of the gas molecules resulting in the amplification of the pulses. These counters are normally hemispherical in shape with various configurations of the anode and the cathode. Proportional counters do not use air as ionizing gas, and instead use a specific gas called P10 (a mixture of 90 % argon and 10 % methane), which is allowed to flow through the counting chamber. Because of the large magnitude of the signals, they operate in pulse mode and are useful in counting α and β particles. Since the specific ionization of α particles is greater than that of β particles, the pulses from these particles are distinguishable. To facilitate the entry of these particles, a thin foil of Mylar is used as a window of the counter. Mylar foil is prone to rupture because of thinness, so caution should be exercised in handling them and not to increase the gas pressure in the counting chamber. The proportional counters are not used as survey meters, but mostly used in various laboratory counting.

Geiger–Müller Counters

The Geiger–Müller (GM) counter operates in the Geiger region of the voltage, as shown in Fig. 7.2. As already mentioned, in this region, an avalanche of ionizations occurs as a result of high voltage. Once an ionization is initiated, the avalanche of ionizations can lead to repetitive discharges unless the process is interrupted by the quenching technique. An electronic technique of quenching can be applied in which the voltage applied to the GM tube is temporarily reduced below the Geiger region until all ion pairs return to their de-excited states. This happens in a few tenths of a millisecond. The original voltage is then restored for the detection of the next event. This technique is no longer in use.

The common technique of quenching is to add a small quantity of a quenching gas to the counting gas. Either organic solvent vapors (e.g., ethyl alcohol, xylene, or isobutane) or halogen gases (chlorine or bromine) are commonly used as the quenching gas. These molecules transfer electrons to the “positive” ion cloud and become themselves ionized. Ionized molecules of the quenching gas migrate to and dislodge electrons from the cathode. When these electrons neutralize the ionized molecules of the quenching gas, energy is released, which causes the dissociation of the molecules of the gas but with no UV emissions to prolong the avalanche. This prevents the continuous discharge of the GM counter. Organic molecules are more effective quenchers but dissociate irreversibly and therefore

FIG. 7.7. **a** A Geiger-Miller survey meter and **b** A pancake probe. (Courtesy of Ludlum Instruments, Inc. Sweetwater, TX).

give a limited lifetime for the GM tube (~10^8–10^{10} pulses). In contrast, dissociated inorganic molecules recombine to form the original molecules, and therefore halogen-quenched GM tubes have infinite useful lifetime.

The probes of GM counters can be either end-window type or side-window type. A GM counter is shown in Fig. 7.7a. The window is made of thin mica (0.01 mm thick), and gases such as argon, methane, helium, and neon mixed with halogen are commonly used as the counting gas. The gas pressure in GM probes is normally kept negative (about 0.8 atmosphere). Different shapes of GM probes are available, such as cylindrical and pancake types (Fig. 7.7b). Some GM probes are provided with a metal cover that stops all β-particles and very low-energy γ-radiations so that only high-energy photons are detected. Without the cover, both β-particles and γ-rays are detected. The GM counter is usually battery operated at a voltage of 500–900 V. Lower voltages are used for smaller tubes, and some special tubes are operated even at 1300 V. The meter connected to the GM probe gives readings in mR/h or counts per minute. Some counters are equipped with audible alarms or flashing light alarms that are triggered by radiation above a preset intensity. The latter counter is often used to monitor the radiation level in work areas and is called an *area monitor*.

The GM probes operate in pulse modes and register each event as a single count displaying the data as counts per minute. However, the individual counts can be summed up by the measuring circuitry and converted to exposure rate (mR/h) for display. Counts per minutes or mR/h are displayed over several decades (e.g. 1, 10, 100, 1000).

The exposure rate (mR/h or counts/min) given by the GM tube for x-rays or γ-rays depends on the energy of the photons, because they primarily interact with

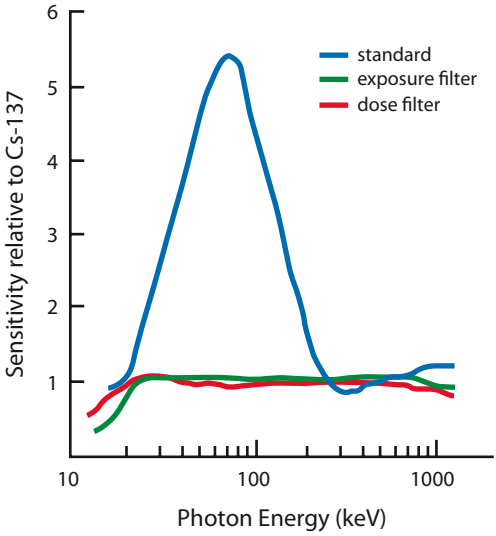

FIG. 7.8. The relative energy-dependent response of the G-M counter.

the walls of the tube rather than with the gas volume. The GM tubes are made of aluminum or steel with atomic number Z higher than that of air. Since at low energies the photons primarily interact with the metal via the photoelectric process, which is proportional to Z^3, the exposure rate measured by the GM counter will be overestimated. On the other hand, at medium energies, the Compton interaction predominates, which is independent of Z and will therefore give correct reading of exposure rate. The GM counters are commonly calibrated for 662-keV photons of ^{137}Cs. The response of different photon energies relative to ^{137}Cs measured by these GM counters is shown in Fig. 7.8. It is seen that the response (exposure) for energies less than 150 keV is overestimated and needs to be corrected. Currently the correction is made by using a filter that can be snap-fitted onto the face of the pancake probe. There are two types of filters, one for exposure and the other for ambient dose equivalent, which flatten the response to within ±20 % relative to 662 keV over the energy range of 33 keV to 1.2 MeV. Alternatively, energy-compensated detectors have been devised in which a thin layer of high Z material such as tin is placed around the inside of the detector. The increased photoelectric absorption of low energy photons in tin significantly flattens the response of the detector. A disadvantage of this detector is that the low energy sensitivity is greatly reduced.

The GM survey meters are more sensitive than ionization chambers by a factor of about ten. Because voltage pulses generated in GM tubes are independent of the energy deposited, they cannot discriminate between energies and types of radiations. These counters are almost 100 % efficient for counting β-particles but have only 1–2 % efficiency for counting γ-and x-rays. The dead time, or resolving time (Chapter 8), of the GM counters is about 80–500 μs. This limits the count

rates to about 15,000–20,000 counts per minute (cpm) for these counters, and at higher activities they tend to saturate, thus losing counts. The GM counters are normally used for area survey for contamination with low-level activity. According to the NRC regulations, these survey meters must be calibrated annually with standard calibrated sources such as ^{137}Cs.

Questions

1. Describe the principles of gas-filled detectors.
2. What are the differences between an ionization chamber and a Geiger–Müller counter?
3. What is the function of a push-button isotope selector on a dose calibrator?
4. Can you discriminate between 140-keV γ-rays, 364-keVγ-rays, and 5-MeV α-particles using a GM counter?
5. What type of instruments would you use for:
   (a) Survey of the laboratory?
   (b) X-ray beam exposure?
   (c) Area survey around x-ray room?
   (d) Spill of 50 μCi (1.85 MBq) of ^{201}Tl?
   (e) Background radiation?
   (f) Radiation survey of a diagnostic x-ray installation?
6. (a) Why are halogen gases added to GM counters?
   (b) What is the typical dead time for GM counters?
   (c) How often do the GM counters need to be calibrated?
   (d) Why cannot the GM counters be used for detecting high-activity samples?
   (e) What are the typical detection efficiencies of the ionization chamber and GM meter?
   (f) When and why is a specific filter used in GM meters?
7. What are the typical voltages applied to the ionization chambers and GM counters?
8. Describe the various tests of the dose calibrator and mention the frequency of each test.

Suggested Readings

Cherry SR, Sorensen JA, Phelps ME. *Physics in Nuclear Medicine*. 3rd ed. Philadelphia: W.B. Saunders; 2003.

Hendee WR, Ritenour R. *Medical Imaging Physics*. 4th ed. New York: Wiley-Liss; 2002.

Knoll, G. *Radiation Detection and Measurement*. 4th ed. New York: Wiley; 2010.

Ouseph PJ. *Introduction to Nuclear Radiation Detectors*. New York: Plenum Press; 1975.

Robinson CV. Geiger–Müller and proportional counters. In: Hine GJ, ed. *Instrumentation in Nuclear Medicine*. New York: Academic Press, 1967:57–72.

8
Scintillation and Semiconductor Detectors

Scintillation Detectors

As stated in Chapter 7, the detection efficiency of γ- and x-rays in gas detectors is very low, because these penetrating radiations travel through the low-density gas with little interaction. To improve detection efficiency for these radiations, solid and liquid scintillation detectors with high density are used. These detectors have the unique property of emitting scintillations or flashes of light after absorbing γ- or x-radiations. The γ- or x-rays interact with scintillation detectors via photoelectric, Compton, and/or pair production mechanisms, whereby the detector molecules are raised to higher energy states through ionization or excitation. These high-energy states return to ground states by emitting light photons. The time to reach the ground state is called the *scintillation decay time*. The light photons produced are converted to an electrical pulse by means of a photomultiplier (PM) tube (described later). The pulse is then amplified by a linear amplifier, sorted by a pulse-height analyzer (PHA), and then registered as a count. Different solid or liquid detectors are used for different types of radiation. For example, sodium iodide detectors containing a trace of thallium (NaI(Tl)) are used for γ- and x-ray detection, whereas organic detectors such as anthracene and plastic fluors are used for β^- particle detection.

In liquid scintillation counting, a β^- emitting radioactive sample and an organic scintillator are dissolved in a solvent. The β^- particle interacts with solvent molecules emitting electrons. The latter interact with the organic scintillator, whereby light photons are produced, which are then directed to two PM tubes coupled in coincidence. A pulse is generated by the PM tube, which is registered as a count, as in the solid scintillation counting.

Organic scintillators usually have a lower density and, hence, a lower detection efficiency than inorganic scintillators. The decay time also limits the efficiency of a detector at high-count rates. The faster decay time allows high-count rate capability. The decay time for organic scintillators is much shorter than that for inorganic scintillators. For example, the decay time for NaI(Tl) is 0.25 μs and that for anthracene is 0.026 μs. The faster decay time permits the use of organic scintillators at higher count rates.

G. B. Saha, *Physics and Radiobiology of Nuclear Medicine,*
DOI 10.1007/978-1-4614-4012-3_8,

TABLE 8.1. Properties of different scintillation and solid-state detectors.[a]

Detectors	Effective Atomic no (Z)	Density (g/cm^3)	Scintillation decay time (ns)	Photon yield (per keV)
NaI(T1)	51	3.67	250	38
BGO	74	7.13	300	6
BaF_2	54	4.89	0.6	2
GSO	59	6.71	50	10
LSO	66	7.40	40	29
YSO	34	4.53	70	46
CsI(T1)	54	4.51	1000	52
LYSO	65	7.2	50	25
YAP	39	5.4	27	18
$LaBr_3$	47	5.3	16	61
CZT	50	5.8	–	–

[a] *BGO* bismuth germanate ($Bi_4Ge_3O_{12}$), *BaF_2* barium fluoride, *LSO* lutetium oxyorthosilicate (Lu_2SiO_5:Ce), *YSO* yttrium oxyorthosilicate (Y_2SiO_5:Ce), *GSO* gadolinium oxyorthosilicate (Gd_2SiO_5:Ce), *LYSO* lutetium yttrium oxyorthosilicate ($LuYSiO_5$:Ce), *YAP* yttrium aluminum perovskite ($YAlO_3$), *$LaBr_3$*: *Ce* lanthanum bromide, *CZT* cadmium zinc telluride

Solid Scintillation Detectors

See Table 8.1 for a summary of the various characteristics of the following detectors.

NaI (Tl) Detector

Pure sodium iodide produces very little scintillation after interaction with γ-radiations at room temperature. However, if it is doped with a trace amount (0.1–0.4 %) of thallium as an activator, NaI(Tl) becomes quite efficient in producing light photons after γ-radiations interact with it. NaI(Tl) molecules are excited or ionized by interaction with γ-rays or x-rays, and the high-energy states return to ground states by emitting light photons. Approximately 20–30 light photons are produced per 1 keV of energy.

The choice of NaI(Tl) crystals for γ-ray detection is primarily due to the high density (3.67 g/cm^3) of the detector and the high atomic number of iodine ($Z = 53$), compared to organic scintillators. However, NaI(Tl) crystals are hygroscopic and fragile, and must be handled with care. Room temperature should not be changed abruptly, because such changes in temperature can cause cracks in the crystal.

Bismuth Germanate Detector

The bismuth germinate (BGO) detector has a higher density and effective atomic number and so higher attenuation coefficient (hence, higher stopping power) for 511 keV photons than NaI(Tl). But it has a slightly longer scintillation decay time (300 ns) compared to NaI(Tl) (250 ns) and its light output is relatively small causing poor energy resolution. However, energy resolution has minimal effect on the spatial resolution of PET, which is mainly determined by the size of the detectors.

Moreover, BGO crystals are not hygroscopic. Because of these factors, BGO is preferred to NaI(Tl) for most positron emission tomography (PET) cameras.

Barium Fluoride Detector

Barium fluoride (BaF_2) is an inorganic crystal that has a very fast decay time (0.8 ns) and offers a suitable detector for time-of flight PET. The photon yield of this crystal is relatively small and it is slightly hygroscopic.

Lutetium Oxyorthosilicate Detector

Lutetium oxyorthosilicate (LSO) doped with cerium is another solid detector that is used for scintillation counting in PET imaging. LSO has a shorter scintillation decay time (40 ns) than BGO that favors the use of a narrow pulse window to cut down random coincidences in PET. Also, its higher light output gives a better energy resolution than BGO. These detectors have high efficiency for photon detection and can be fabricated in the size of a few millimeters. Many commercial manufacturers use LSO detectors in place of BGO detectors in clinical PET scanners and in micro-PET scanners for scanning small animals.

Gadolinium Oxyorthosilicate Detector

Gadolinium oxyorthosilicate (GSO) is a detector that can be used for coincidence counting in PET imaging. Even though it has lower light output and stopping power than LSO, its better energy resolution has prompted some commercial manufacturers to use it in PET scanners. GSO crystals are fragile and great care is warranted in their fabrication.

Yttrium Oxyorthosilicate Detector

Yttrium oxyorthosilicate (YSO) is an inorganic crystal similar to LSO introduced for scintillation counting. The scintillation decay time of YSO is 70 ns and it gives high light output. A combination detector of YSO/LSO has been reported for potential use in simultaneous single photon and coincidence imaging. YSO detects low-energy photons and LSO detects 511 keV photons, and the two pulses are readily separated by pulse shape discriminators.

Yittrium Aluminum Perovskite Detector

Yttrium aluminum perovskite (YAP) doped with cerium (Ce) is a low Z detector with high light output and shorter scintillation decay time of 27 μs, almost ten times shorter than NaI(Tl). It is neither fragile nor hygroscopic and can stand variations in temperatures. Although it has been used for some x-ray imaging, its use in SPECT and PET cameras has been limited.

Lutetium Yttrium Oxyorthosilicate Detector

Lutetium yttrium oxyorthosilicate (LYSO) is a useful detector because of its higher density and atomic number providing greater stopping power. The detection

efficiency of the detector is similar to that of the LSO detector and it has been used in PET scanners by some manufacturers.

Lanthanum Bromide Detector

Lanthanum bromide ($LaBr_3$) has high density and atomic number and reasonably shorter scintillation decay time (16 ns). Its high photon yield and hence its superior energy resolution make it a good candidate for detectors in medical imaging. Like NaI(Tl), it is, however, hygroscopic and needs to be housed in an enclosure.

Solid-State Detectors

Germanium and Silicon Detectors

Solid-state or semiconductor detectors are made of germanium or silicon elements commonly doped with lithium. These detectors are designated as Ge(Li) or Si(Li) detectors, of which the former are commonly used for high-energy γ-ray detection and the latter for α-particle and low-energy radiation detection. Currently, high purity germanium (HPGe) alone without lithium is commonly used. The basic principle of operation of these detectors involves ionization of the semiconductor atoms, as in gas detectors. When radiation interacts with a semiconductor, ionization occurs with the transfer of an electron from the valence band to the conduction band and concomitant creation of a positively charged hole in the valence bond. When an electric field is applied, the electron-hole pairs migrate to the respective electrodes and produce voltage pulses. The pulses are then amplified and counted. The size of the pulse is proportional to the radiation energy absorbed in the detector, but does not depend on the type of radiation. Note that there is no light production and therefore no photomultiplier tube is needed.

Because semiconductors are much denser than gases, they are more efficient for x- and γ-ray detection than gas detectors. Also in semiconductor detectors, each ionization requires only about 3 eV compared to 35 eV in gas detectors. Thus, almost ten times more ions are produced in semiconductor detectors than in gas detectors for a given γ-ray energy, thus yielding a better spectral resolution of γ-ray photons of closer energies. Fabrication of Ge(Li) and Si(Li) detectors is quite time-consuming and expensive. The size of the detectors is also small, which prevents their use in gamma cameras.

Thermal noise at room temperature introduces a high background that can obscure the sample counts, but is reduced at low temperature. Therefore, these detectors are operated at low temperature usually employing liquid nitrogen (–196°C or 77°K). A disadvantage of these detectors is that liquid nitrogen evaporates over time and needs to be replenished periodically, typically weekly. Nowadays HPGe detectors can be kept at room temperature when not used, and cooled when used for counting by means of helium-based cryoelectric and freon-based coolers.

Semiconductor detectors are most useful in differentiating photon energies because of the high-energy resolution, particularly in detecting radionuclidic contamination. These detectors are not in common use in nuclear medicine.

Cadmium–Zinc–Tellurium Detector

Cadmium–Zinc–Tellurium (CZT) detectors are another type of semiconductor made of Cd, Zn, and Te metals, and provide very high efficiency for γ-ray detection because of their high atomic numbers. For reasons of high detection efficiency, these detectors can be made as small as 2 mm thick and 2 mm diameter with almost 100 % efficiency for 100 keV photons. The energy resolution of these detectors is very good (~6 %) for a wide range of γ-ray energies. These detectors are operated at room temperature. The electronics used are similar to those of other scintillation detectors. Different types of handheld probes have been devised for various purposes. One probe, called the Neoprobe 1000, is used for the detection of metastatic sites containing radioactivity (e.g., ^{125}1-labeled monoclonal antibody) during surgery for their removal by incision. Also this detector has been used in gamma cameras manufactured by Spectrum Dynamics and GE Healthcare.

Cesium Iodide (CsI(Tl)) Detector

The CsI(Tl) detector has higher density and hence greater stopping power than the NaI(Tl) detector and also yields more light photons per keV. But its scintillation decay time is very long (1000 ns) resulting in longer dead time for the counting system. The crystal is weakly hygroscopic and does not require hermetic sealing. Unlike NaI(Tl), it can withstand a wide variation in temperature.

Solid Scintillation Counters

A basic solid scintillation counter consists of a scintillation detector, a PM tube, a preamplifier, a linear amplifier, a PHA, and a recording device (Fig. 8.1). The most commonly used scintillation detector in γ-ray counting is NaI(Tl), although BGO and LSO are commonly used in PET, discussed later. Each of these components is described in detail next.

NaI(Tl) Detector

The NaI(Tl) detectors are made of various sizes for different types of equipment. Circular or cylindrical crystals vary from 3.8 to 50 cm in diameter and 0.63–23 cm in thickness. Rectangular crystals of approximate dimension of 45×60 cm are also available. In thyroid probes and well counters, smaller and thicker crystals are used, whereas larger and thinner crystals are employed in scintillation cameras.

Photomultiplier Tube

A PM tube consists of a light-sensitive *photocathode* at one end, a series (usually ten) of metallic electrodes known as *dynodes* in the middle, and an *anode* at the

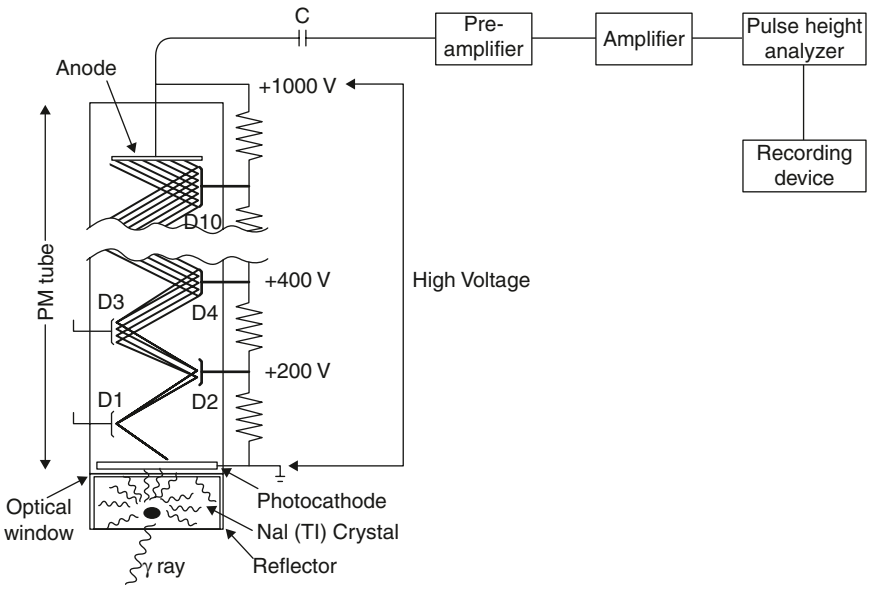

FIG. 8.1. A basic scintillation counter consisting of a NaI(Tl) detector, a photomultiplier (PM) tube, a preamplifier, a linear amplifier, a pulse-height analyzer, and a recording device. The high voltage applied to the PM tube is typically 1000 V.

other end—all enclosed in a vacuum glass tube (see Fig. 8.1). The photocathode is usually an alloy of cesium and antimony or other bialkali metal that releases electrons after absorption of light photons. The PM tube is fixed on to the NaI(Tl) crystal with the photocathode facing the crystal by a special optical grease or connected to the crystal using light pipes.

A high voltage of ~1000 V is applied between the photocathode and the anode of the PM tube in steps of 50–150 V between dynodes (see Fig. 8.1). Dynodes are coated with materials such as Cs . Sb that are good for secondary emission of electrons. When light photons from the NaI(Tl) crystal strike the photocathode, approximately one to three photoelectrons are produced from the photocathode per 7–10 light photons. Each of these photoelectrons is accelerated to the first dynode and emits two to four electrons upon impingement. The accelerated electrons strike the successive dynodes, and more electrons are emitted. The process of multiplication continues until the last dynode is reached, where a pulse of 10^5–10^8 electrons is produced. The pulse is then attracted to the anode and finally delivered to the preamplifier. The amplitude of the pulse is proportional to the number of light photons received by the photocathode and in turn to the energy of the γ-ray photon absorbed in the detector. The applied voltage must be very stable, because slight changes in dynode voltage cause a great variation in electron multiplication factor.

Preamplifier

The pulse from the PM tube is small in amplitude and is initially amplified by a preamplifier. The preamplifier adjusts the voltage of the pulse (pulse shaping) and matches impedance level between the detector and the subsequent circuits so that the pulse is appropriately processed by the system.

Linear Amplifier

A linear amplifier amplifies further the signal from the preamplifier and delivers it to the pulse height analyzer for analysis of its amplitude. The amplification of the pulse is given by the amplifier gain expressed as the ratio of the amplitude of the outgoing pulse to that of the initial pulse from the PM tube. The amplifier gains are given in the range of 1–1000 by gain control knobs provided on the amplifier. The output pulses normally have amplitudes of up to 10 V.

Pulse-Height Analyzer

γ-rays of different energies can arise from a source of the same or different radionuclides or due to scattering of γ-rays in the source and the detector. Thus, in counting a radioactive source, the pulses coming out of the amplifier may differ in magnitude. A PHA is a device that selects for counting only those pulses falling within preselected voltage intervals or "channels" and rejects all others (see Fig. 8.1). Pulses corresponding to γ-ray energies of interest are selected by energy discriminator knobs, known as the *lower level* and *upper level*, or the *baseline* and *window*, provided on the PHA, and are ultimately delivered to the recording devices such as scalers, computers, films, and so on.

There are two modes of counting using PHAs: *differential* and *integral*. In differential counting, only pulses of preselected energies are counted by appropriate selection of lower and upper level knobs (discriminators) or the baseline and window. In scintillation cameras, however, differential counting is achieved by a peak voltage knob and a percent window knob. The peak voltage knob sets the energy of the desired γ-ray, and the percent window knob sets the window width in percentage of the γ-ray energy, which is normally placed symmetrically on each side of the peak voltage.

In integral counting, γ-rays of all energies or all γ-rays of energies above a certain energy are counted by setting the appropriate lower level or baseline and bypassing the upper level or window mechanism.

A PHA normally selects only one range of pulses corresponding to only one γ-ray energy by means of differential counting. Such a PHA is called a single-channel analyzer (SCA). A multichannel analyzer (MCA) is a device that can simultaneously sort pulses into many predetermined voltage ranges or channels, corresponding to different photon energies. By using an MCA, one obtains a simultaneous spectrum of different γ-ray energies from a radioactive source.

Display or Storage

Pulses processed by the PHA can be displayed on a cathode ray tube (CRT) or can be counted for a preset count or time by a scaler-timer device. A rate meter can be used to display the pulses in terms of counts per minute (cpm) or counts per second (cps). In scintillation cameras, pulses can be used to form the image on a CRT and polaroid or x-ray films. These pulses can also be stored in a computer or on a magnetic tape or laser disc for processing later. Nowadays, computer monitor and storage are the mainstay for display and storage of data in nuclear medicine.

Gamma-Ray Spectrometry

Pulses are generated by the PM tube and associated electronics after the γ-ray energy is absorbed in the NaI(Tl) detector. Because γ-rays interact with the NaI(Tl) detector by photoelectric, Compton, and pair production mechanisms, and also because various scattered radiations from outside the detector may interact with the detector, a distribution of pulse heights will be obtained depicting a spectrum of γ-ray energies. Such a γ-ray spectrum may result from a single γ-ray or from many γ-rays in a sample. Different features of this spectrum are discussed here.

Photopeak

In an ideal situation, if the γ-ray photon energy is absorbed by the photoelectric mechanism and each γ-ray photon yields a pulse of the same height, then each γ-ray would be seen as a line on the γ-ray spectrum (Fig. 8.2a). In reality, the photopeak is broader, which is due to various statistical variations in the process of forming the pulses. These random fluctuations arise from the following conditions:

1. Because 20–30 light photons are produced for every keV of γ-ray energy absorbed, there is a statistical variation in the number of light photons produced by the absorption of a given γ-ray energy in the detector. Also, statistically all light photons produced may not strike the photocathode.
2. As already stated, 7–10 light photons are required to release 1–3 photoelectrons from the photocathode. Therefore, the number of photoelectrons that one γ-ray will produce may vary from one event to another.
3. The number of electrons released from the successive dynodes by impingement of each electron from the previous dynode varies from 2 to 4, and therefore pulse heights from the PM tube will vary from one γ-ray to the next of the same energy.

All of the preceding statistical fluctuations in generating a pulse cause a spread in the photopeak (see Fig. 8.2b). A typical spectrum of the 662-keV γ-ray of ^{137}Cs is shown in Fig. 8.3.

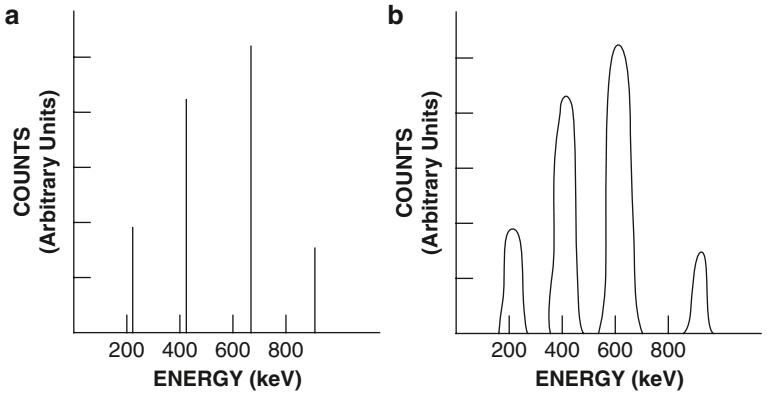

FIG. 8.2. γ-ray spectra. **a** An ideal spectrum would represent the different γ-rays as lines. **b** An actual spectrum showing the spread of the photopeak that is due to statistical fluctuations in the pulse formation.

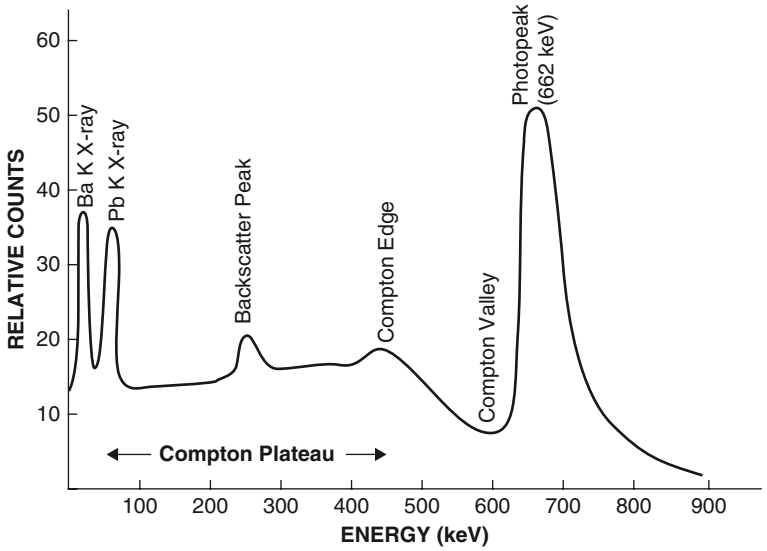

FIG. 8.3. A typical spectrum of the 662-keV γ-ray of ^{137}Cs illustrating the photopeak, Compton plateau, Compton edge, Compton valley, backscatter, characteristic lead *K* x-ray, and barium *K* x-ray peaks.

Compton Valley, Edge, and Plateau

When γ-rays interact with the NaI(Tl) detector via Compton scattering and scattered photons escape from the detector, the Compton electrons result in pulse heights that are smaller than that of the photopeak. The Compton electrons, how-

ever, can have variable energies from zero to E_{max}, where E_{max} is the kinetic energy of those electrons that are produced by the 180° Compton backscattering of the γ-ray photons in the detector. At relatively high photon energy, E_{max} is given by the photon energy minus 256 keV (Eq. 6.3). Thus, the γ-ray spectrum will show a continuum of pulses corresponding to Compton electron energies between zero and E_{max}. The peak at E_{max} is called the *Compton edge*, and the portion of the spectrum below the Compton edge down to about zero energy is called the *Compton plateau* (see Fig. 8.3). The portion of the spectrum between the photopeak and the Compton edge is called the *Compton valley*, which results from multiple Compton scattering of a γ-ray in the detector yielding a narrow range of pulses in this region.

The relative heights of the photopeak and the Compton edge depend on the photon energy as well as the size of the NaI(Tl) detector. At low energies, photoelectric effect predominates over Compton scattering, whereas at higher energies the latter becomes predominant. In larger detectors, γ-rays may undergo multiple Compton scattering, which can add up to the absorption of the total photon energy identical to the photoelectric effect. This increases the contribution to the photopeak and decreases to the Compton plateau.

Characteristic X-Ray Peak

Photoelectric interactions of the γ-ray photons in the lead shield around the detector can lead to the ejection of the *K*-shell electrons, followed by transition of electrons from the upper shells, mainly the *L* shell, to the *K* shell. The difference in binding energy between the *K*-shell electron (~88 keV) and the *L*-shell electron (~16 keV) appears as lead *K* x-ray of ~72 keV. These characteristic x-ray photons may be directed toward the detector and absorbed in it and may appear as a peak in the γ-ray spectrum (see Fig. 8.3). These photons can be reduced by increasing the distance between the detector and the shielding material.

Backscatter Peak

When γ-ray photons, before striking the detector, are scattered at 180° by Compton scattering in lead shielding and housing, and the scattered photons are absorbed in the detector, then a peak, called the *backscatter peak*, appears in the γ-ray spectrum (see Fig. 8.3). For high-energy photons, the backscattered peak appears at 256 keV (see Eq. (6.3)). This peak can be mostly eliminated by increasing the distance between the shield and the detector.

Iodine Escape Peak

Photoelectric interaction of γ-ray photons with iodine atoms of the NaI(Tl) detector usually results in the emission of characteristic *K* x-rays. These x-ray photons may escape the detector, resulting in a peak equivalent to photon energy minus 28 keV (binding energy of the *K*-shell electron of iodine). This is called the *iodine escape peak*, which appears about 28 keV below the photopeak (Fig. 8.4).

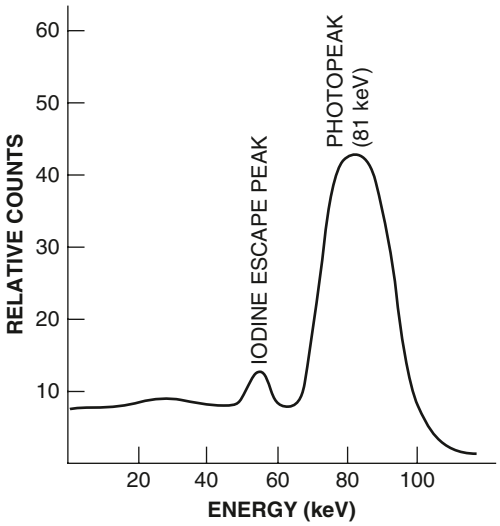

FIG. 8.4. A spectrum of 81-keV γ-ray of ^{133}Xe showing an iodine escape peak.

This peak becomes prominent when the energy of the photon is less than about 200 keV, because, at energies above 200 keV, the iodine escape peak would fall within the width of the photopeak, because of the small differences between the two peaks.

Annihilation Peak

γ-rays with energy greater than 1.02 MeV may undergo pair production in the detector in which a positive-negative electron pair is produced. The β^+-particles are annihilated to produce two 511-keV photons, which appear as photopeaks in the γ-ray spectrum. If, however, one of the 511-keV photons escapes from the detector, then a peak, called the *single-escape peak*, corresponding to the primary photon energy minus 511 keV, will appear in the spectrum. If both annihilation photons escape, then a *double-escape peak* results, corresponding to the primary photon energy minus 1.02 MeV. Larger detectors can prevent the escape of the annihilation radiations.

Coincidence Peak

A *coincidence* or *sum peak* results when more than one photon is absorbed simultaneously in the detector to be considered as a single event. The peak equals the sum of the energies of the photons. Such situations occur with radionuclides that have short-lived isomeric states and thus emit γ-rays in cascade. For example, ^{111}In emits 171- and 245-keV photons, which can result in a sum peak of 416 keV (Fig. 8.5). Sum peaks are also caused by counting high-activity samples in which

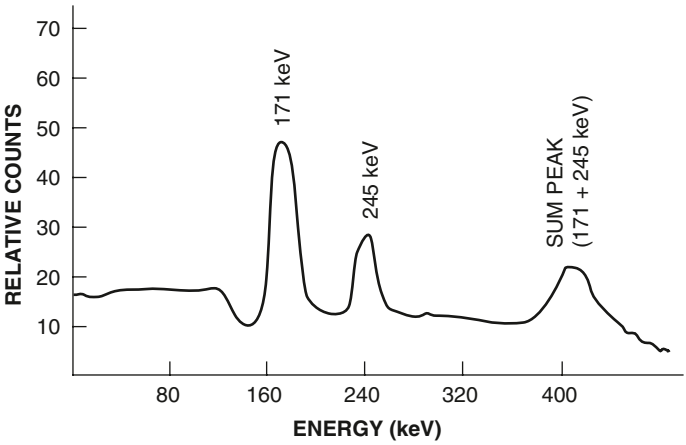

FIG. 8.5. A spectrum of ^{111}In with 171- and 245-keV photons showing a coincidence (sum) peak at 416 keV.

two photons may strike the detector at the same time. These peaks can be reduced by counting the samples at larger distances between the source and the detector or by using smaller detectors so that the likelihood of two photons striking the detector at the same time is reduced. In the case of high-activity samples, the level of activity has to be reduced either by dilution or allowing to decay, in order to reduce the sum peak.

Liquid Scintillation Counters

Low-energy β^--particles are normally absorbed within the source and in the window and walls of the detectors, and therefore β^--emitters are difficult to detect in gas or solid detectors. For this reason, β^--emitting radionuclides are counted using the liquid scintillation technique in which the radioactive sample is mixed with a scintillating material. A sample vial containing the liquid scintillator and the radioactive sample of interest is placed between two PM tubes connected in coincidence (Fig. 8.6). Each PM tube receives the light photons emitted by the interaction of the β^--particle with the scintillator and converts them into a pulse, which is further amplified by an amplifier. The amplitude of the pulses is proportional to the energy of the β^--particles. The amplified pulses are then delivered to the coincidence circuit that contains a PHA to analyze the pulse height for acceptance. A count is registered in the scaler if two pulses of the same height are recorded in both PM tubes simultaneously. Such coincidence counting reduces the background counts due to noise, including terrestrial and cosmic radiations, radioactive patients, etc.

The liquid scintillation solution is prepared by dissolving a primary scintillating solute or fluor and often a secondary fluor in a solvent. The radioactive

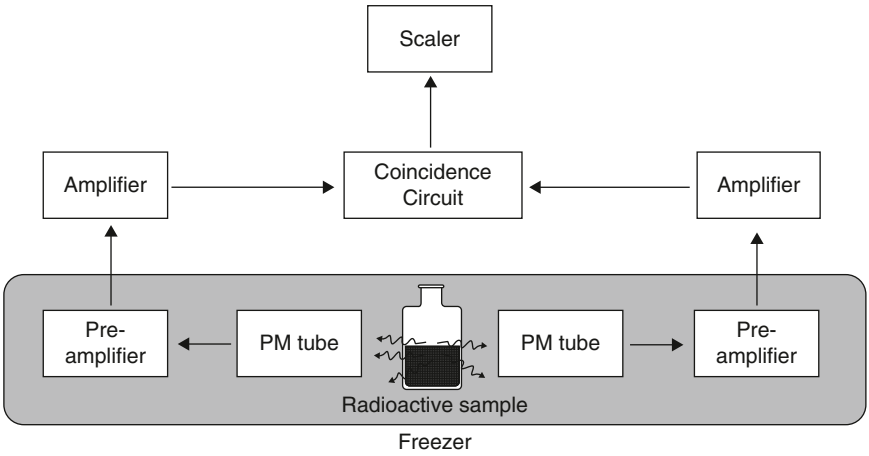

FIG. 8.6. A schematic diagram of a liquid scintillation counting system. Light photons emitted from the sample strike the two photomultiplier tubes to produce pulses. Only coincident pulses are counted.

sample is added to and thoroughly mixed with the scintillating solution for counting. The primary fluors include 2,5-diphenyloxazole (PPO), 2,5 *bis*-2-(5-T-butylbenzoxazolyl)-thiophene (BBOT), and *p*-terphenyl, of which PPO is most commonly used in a concentration of 5 g/L.

Toluene, xylene, and dioxane are the most common solvents that easily dissolve the primary fluor and often the radioactive sample, which is a requirement for a good solvent. These solvents, however, are poorly miscible in water, and therefore their disposal in the sewer system is restricted. For this reason, biodegradable solvents such as linear alkylbenzene and phenylxylylethane are widely used. Counting vials are usually glass or plastic, but the latter is not used when toluene or xylene is used as a solvent because the solvent tends to dissolve plastic.

When radiations pass through the solvent, electrons are released from the solvent molecules after absorption of radiation energies. These electrons transfer energy to primary fluor molecules, which then emit light photons for further processing by PM tubes and associated electronics. The wavelength of these light photons may be somewhat shorter than required for the spectral sensitivity of the photocathode of the PM tube. This mismatch is rectified by adding a secondary fluor or solute, called the *wavelength shifter*, to the scintillating solution. The wavelength shifter absorbs the light photons emitted by the primary fluor and reemits them with a longer wavelength, which is more suitable for the photocathode of the PM tube. The compound 1,4-*bis*-2-(5-phenyloxazolyl)-benzene (POPOP) is most commonly used as a secondary solute in a concentration of about 0.1 %.

An attempt is always made to keep the radioactive sample in solution in the liquid scintillator. Solubilizing agents are added to improve dissolution of specific

samples, and the common example is the hydroxide of Hyamine 10-X used in counting tissue samples.

In liquid scintillation counting, quenching is a problem caused by interference with the production and transmission of light, which ultimately reduces the detection efficiency of the system. Quenching can be of the following types:

1. *Chemical type*, resulting from interference in energy transfer by substances such as samples or extraneous materials (e.g., dissolved O_2)
2. *Color type*, resulting from absorption of light photons by colored substances, such as hemoglobin, before striking the PM tube
3. *Dilution type*, resulting from relatively large dilution of the scintillation mixture, in which case many light photons may be absorbed by the diluted sample.
4. *Optical type*, resulting from absorption of light by a dirty vial containing frost or fingerprints.

Quenching must be corrected to obtain accurate counting of samples, and three methods have been adopted for this purpose, namely, internal standard method, channel ratio method, and external standard method. The readers are referred to reference physics books for details of these methods.

A problem with liquid scintillation counting is the noise due to spontaneous thermal emission of electrons from the photocathode of the PM tube. Background noise also arises from the interaction of light with scintillation solution. Thermal emission of electrons is reduced by refrigeration of the counting chamber to keep the PM tubes at low temperature. But the coincidence counting is the most effective method to reduce the noise.

The liquid scintillation counting systems are provided with automatic sample changers for counting as many as 500 samples. Also, one to five PHAs are available on a liquid scintillation counter, so that β^--particles of different energies can be counted simultaneously by using different baselines and windows on each PHA. The β^--emitters, ^{3}H, ^{14}C, ^{32}P, and ^{35}S, are commonly detected by liquid scintillation counting. Whereas the counting efficiencies of ^{3}H (E_{max} = 0.018 MeV) and ^{32}P (E_{max} = 1.71 MeV) are ~60–70 % and ~100 % respectively, they are negligible for γ- and x-rays.

Characteristics of Counting Systems

Detection of radiation and therefore counting of radioactive samples is affected by different characteristics of the detector and the associated electronics. The following is a discussion of these properties.

Energy Resolution

As already mentioned, even though γ-rays of the same energy are absorbed in the NaI(Tl) detector by the photoelectric effect, pulses of different amplitudes are produced because of the statistical variations in the production of light photons

in the detector and photoelectrons and electrons in the PM tube. This results in the broadening of the photopeak. The width of the peak or the sharpness of the peak (i.e., the energy resolution of the detector) predicts the ability of the NaI(Tl) spectrometer to discriminate between the γ-ray photons of dissimilar energies. A similar situation exists for semiconductor detectors where the number of ionizations may vary from one γ-ray to another of the same energy, leading to the broadening of the peak.

The energy resolution of a system is given by the full width at half-maximum (FWHM) amplitude of the photopeak expressed as a percentage of the photon energy as follows:

$$\text{Energy resolution (\%)} = \frac{\text{FWHM}}{E_\gamma} \times 100 \tag{8.1}$$

where E_γ is the energy of the γ-ray photon. In Fig. 8.7, FWHM is 55 keV for the 662-keV peak of ^{137}Cs; therefore,

$$\text{Energy resolution (\%)} = \frac{55}{662} \times 100 = 8.3\ \%$$

The energy resolution depends on the photon energy. The higher the photon energy, the better the energy resolution (i.e., smaller FWHM), because of the decrease in the percentage of statistical variations in the pulse production. The energy resolution of NaI(Tl) detectors is about 7–10 % for the 662-keV γ-ray of

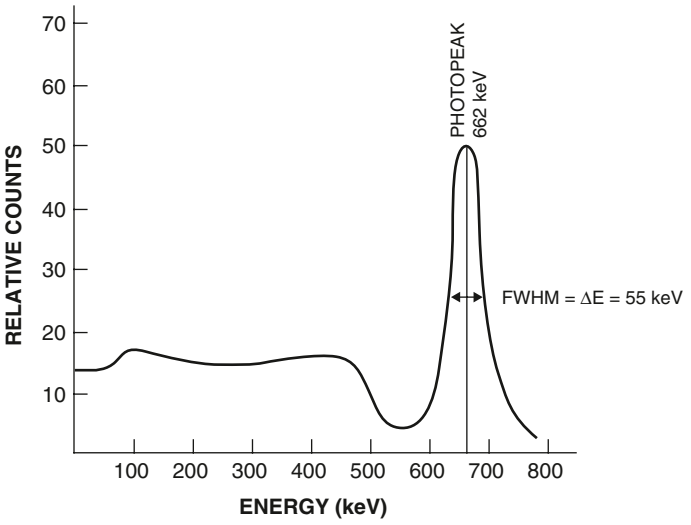

FIG. 8.7. The full width at half maximum (FWHM) of the 662-keV γ-ray of ^{137}Cs in a NaI(Tl) detector.

^{137}Cs and 10–14 % for the 140-keV γ-ray of ^{99m}Tc. In contrast, the energy resolution in Ge(Li) detectors is about 0.42 % for 140-keV γ-rays and about 0.2 % for photons of more than 1 MeV.

Detection Efficiency

The detection efficiency of a counter is given by the observed count rate divided by the disintegration rate of a radioactive sample. The count rate of a sample differs from the disintegration rate because of several factors. Radiations from a source are emitted isotropically around 4π steridians, but only a fraction of all photons emitted strikes the detector, depending on the solid angle subtended by the detector on the source. Also, only a fraction of all photons striking the detector may interact in the detector and produce pulses. Only a fraction of all pulses produces a single photopeak. Furthermore, the count rate is affected by the abundance of a particular radiation from a radionuclide. Considering these factors, the overall counting efficiency of a counter for a radiation is given by the following expression:

$$\text{Efficiency} = f_i \times f_p \times f_g \times N_i \tag{8.2}$$

where f_i is the intrinsic efficiency; f_p is the photopeak efficiency, or photofraction; f_g is the geometric efficiency; and N_i is the abundance of the radiation in question. N_i is available in literature on Tables of Isotopes.

Intrinsic Efficiency

The fraction of all radiations of a given type and energy impinging on the detector that interacts with it to produce pulses is called the *intrinsic efficiency*, f_i, of the detector:

$$f_i = \frac{\text{No. of radiations detected by the detector}}{\text{No. of radiations impinging on the detector}}$$

$$= \frac{\text{All counts under the entire spectrum}}{\text{No. of radiations impinging on the detector}} \tag{8.3}$$

It includes all photons undergoing both photoelectric absorption and Compton scattering. Intrinsic efficiency depends on the type and energy of the radiation and the linear attenuation coefficient (μ) and thickness of the detector. The dependence of intrinsic efficiency on the photon energy and the detector thickness is illustrated in Fig. 8.8. The value of f_i is almost 1 for low-energy γ-rays and thicker detectors. The f_i tends to 0 for high-energy γ-rays and thinner detectors. These conditions apply to all solid scintillation detectors. The intrinsic efficiency of gas detectors is almost unity for α- and β-particles but is about 0.01 (1 %) for γ- and x-rays.

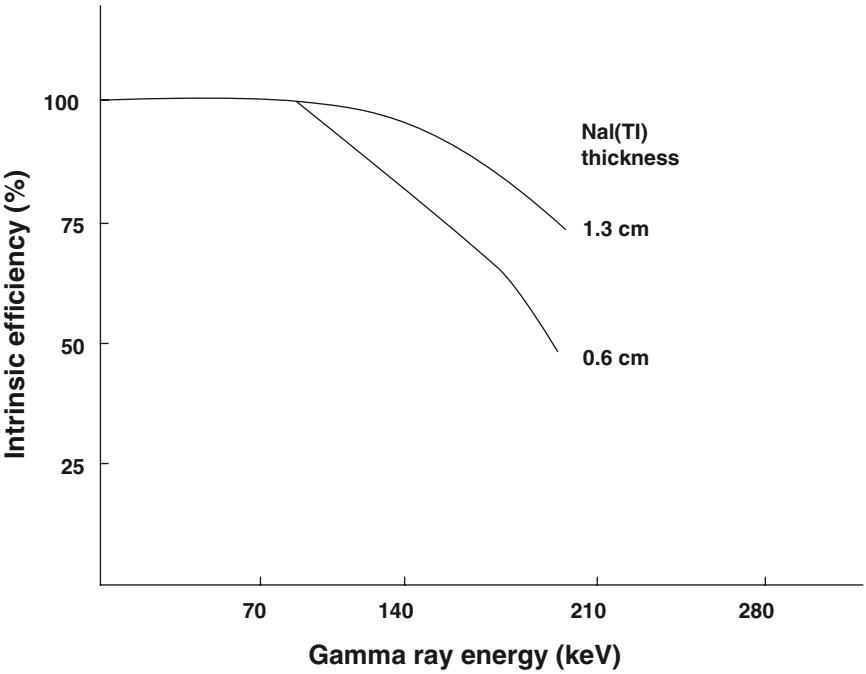

FIG. 8.8. Dependence of intrinsic efficiency on photon energy and detector thickness.

Photopeak Efficiency or Photofraction

The fraction of all detected γ-rays that contributes only to the photopeak is called the *photopeak efficiency*, or *photofraction* (f_p). It is given as the total photopeak area divided by the total area under the entire spectrum:

$$f_p = \frac{\text{All counts under the photopeak}}{\text{All photons detected by the detector}} \tag{8.4}$$

This value is affected by all factors that influence photoelectric effect, such as the size and composition of the detector and γ-ray energy, but is primarily determined by the discriminator settings on the PHA. The f_p increases with increasing window width of the PHA.

Geometric Efficiency

Radiations from a source are emitted uniformly with equal intensity in all directions. If a source of radiation is placed at a distance from a detector, then only a fraction of all radiations emitted from the source will be detected by the detector. This fraction is determined by the solid angle subtended by the detector on the source. The geometric efficiency, f_g, is equal to the number of radiations striking the detector divided by the total number of radiations emitted by the source.

Thus,

$$f_g = \frac{\text{No. of radiations striking the detector}}{\text{Total number of radiations emitted by the source}} \tag{8.5}$$

For a circular detector with radius r, it is equal to the area πr^2 of the detector divided by the total spherical area $4\pi R^2$, where R is the distance between a point source S and the detector D (Fig. 8.9).

$$f_g = \frac{\pi r^2}{4\pi R^2} \tag{8.6}$$

As the distance R between the source and the detector increases, the f_g decreases, according to the inverse square law, that is, $f_g \propto 1/R^2$ (Fig. 8.9a). Thus the f_g at $2R$ is one fourth of the f_g at R. The value of f_g increases with the size of the detector. Also, the finite size of the radiation source affects the f_g values.

When the source and the detector are in close contact, the f_g tends to be about 50% (Fig. 8.9b). In the case of gamma well counters and liquid scintillation counters, the f_g approaches 100 % (Fig. 8.9c).

Dead Time

Each counting system takes a certain amount of time to process a radiation event, starting from interaction of radiation with the detector all the way up to forming a pulse and ultimately recording it. The counter remains insensitive to a second event for this period of time, that is, if a second radiation arrives during this time, the counter cannot process it. This period is called the *dead time*. When the counter recovers after this period, only then can a second radiation be detected. Thus the second event arriving during the dead time is lost. Counts lost during the dead time are called the *dead-time loss*. In scintillation detectors radiations may arrive at the same time and be processed simultaneously to form a single event of amplitude that is equal to the sum of the amplitudes of both events. This is referred to

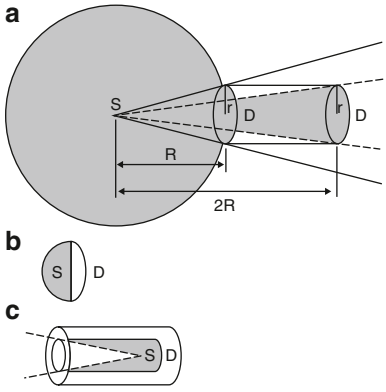

FIG. 8.9. Illustration of geometric efficiency, f_g, of a detector D with a circular area, πr^2, where r is the radius of the detector. **a** The detector D placed at a distance R from the point source S has an f_g four times greater than the f_g when the detector is placed at a distance $2R$. **b** When the source and the detector are in close contact, the f_g is about 50 %. **c** When the source is well inside the detector as in a well counter, the f_g approaches 100 %.

as *pulse pileup*. If one or both of the events were photopeaks originally, then the combined peak will fall outside the PHA window setting and be lost. Dead time loss at high count rates is a serious problem for any counting system and is more so for scintillation cameras due to pulse pileup (see Chapter 11).

The dead time of a counting system may arise from different components of the entire counting system: detector, PHA, PM tube, scaler, computer interface, and so on. While Geiger–Müller (GM) detectors have a longer dead time of 80–500 μs, the typical values for NaI(Tl) and semiconductors are of the order of 0.5–10 μs and for liquid scintillators, ~0.1–1 μs (Cherry et al. 2003).

Based on how successive pulses are processed owing to the dead time, the counting systems fall into two categories: *paralyzable* and *nonparalyzable*. In paralyzable systems, each event sets its own dead time, even if it arrives within the dead time of the previous event and is not counted. Each event prolongs the dead time induced by the previous event, and thus adds to the total dead time of the system, whereby a paralyzable system can become totally unresponsive to process events if the count rate of the source is very high. On the other hand, in nonparalyzable systems, the instrument remains insensitive to successive events for a period of time equal to the dead time, and these events are lost. But unlike paralyzable systems, the dead time is not changed or lengthened. When the system recovers after the detection of the first event, only then is the second event processed and detected. The two types of dead time losses are illustrated in Fig. 8.10.

The paralyzable and nonparalyzable systems can be represented by mathematical relationships among the observed count rate R_o, true count rate R_t, and dead time τ. For nonparalyzable systems,

$$R_t = R_o/(1 - R_o\tau) \tag{8.7}$$

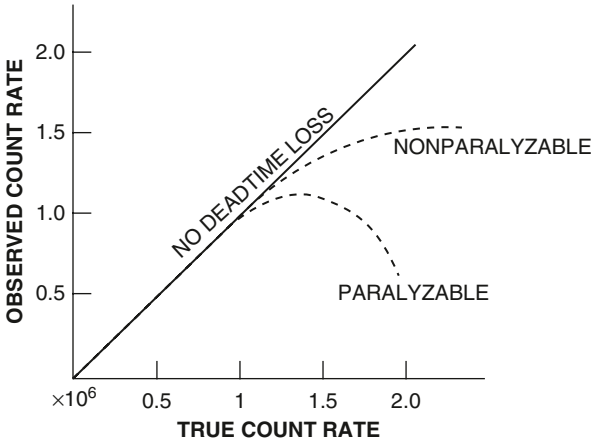

FIG. 8.10. Plot of observed count rates versus true count rates indicating the dead time loss in paralyzable and nonparalyzable systems.

and for paralyzable systems,

$$R_o = R_t e^{-R_t \tau} \tag{8.8}$$

Different components of a radiation detection system can have either paralyzable or nonparalyzable dead time. Scalers and pulse-height analyzers are nonparalyzable systems, whereas radiation detectors themselves are paralyzable systems. Scintillation cameras have both paralyzable and nonparalyzable components of dead time. As can be seen from Eq. (8.8), the radiation detectors become totally paralyzed at very high count rates giving no reading.

Dead time loss is a serious problem for a counting system at high-count rates. Therefore, either count rates must be lowered or corrections must be made to the observed count rates. There are several methods to determine or correct for dead time. An empirical method is to plot the observed count rates as a function of increasing concentrations of known activity. From the plot and Eqs. (8.7) and (8.8), the dead time is calculated for the nonparalyzable or paralyzable system. For subsequent measurements of unknown samples, correction is made to compensate for the dead time loss giving true count rates. Another method uses two radioactive sources, which are counted in the counter individually and together. From these three measurements, one can calculate dead time using appropriate equations (see Cherry et al. 2003). Various techniques, such as use of buffers, in which overlapping events are held off during the dead time, use of pulse pileup rejection circuits, and use of high-speed electronics have been employed to improve the dead time correction.

Gamma Well Counters

The gamma well counter consists of a NaI(Tl) detector with a hole in the center for a sample to be placed and associated electronics such as a PM tube, preamplifier, amplifier, PHA, and scaler-timer. Placing a radioactive sample in the central hole of the detector increases the geometric efficiency (almost 99 %) and hence the counting efficiency of the counter. The NaI(Tl) detectors have dimensions in the range of 5-cm diameter × 5-cm thick to 23-cm diameter × 23-cm thick. Smaller detectors are used for low-energy γ-rays (less than 200 keV), and larger detectors are used for high-energy γ-rays. Most well counters are shielded with about 8.5-cm thick circular lead ring to reduce background from cosmic rays, natural radioactivity such as ^{40}K, or background activity in the work area. A typical well counter detector is shown in Fig. 8.11.

Calibration of Well Counters

It is essential that the dial settings of the discriminators on the PHA are calibrated so that the dial readings correspond directly to the pulse height (i.e., the energy of the γ-ray photon); that is, the dial readings can be read in units of keV. This

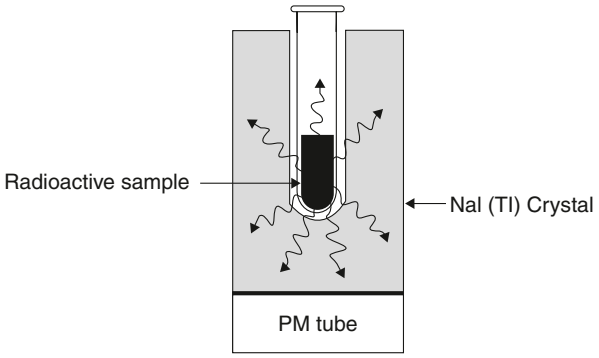

FIG. 8.11. A schematic diagram of a NaI(Tl) well counter with a PM, photomultiplier tube.

calibration is called the *high-voltage* or *energy calibration* of the well counter. The energy calibration is carried out by using the 662-keV photons of ^{137}Cs. After placing a ^{137}Cs source in the well counter, the lower and upper discriminator levels are set at 640 divisions and 684 divisions, respectively, thus assigning the center of the photopeak at 662 divisions corresponding to the 662-keV γ-ray. Starting from low values, the high voltage is increased in small increments for a given amplifier gain until the observed count rate reaches a maximum. The high voltage at the maximum count rate is kept as the operating voltage for subsequent counting of photons of different energies. The discriminator dials are then said to be energy calibrated; for example, each dial unit corresponds to 1 keV at an amplifier gain of 1. Thus, the center of the 140-keV photopeak of ^{99m}Tc can be set at 140 divisions of the discriminator setting, with lower and upper values set as desired. After calibration, well counters should be checked regularly for any voltage drift using a long-lived source, such as ^{137}Cs.

Counting in Well Counters

For relative comparison of count rates between samples, the well counter does not need to be calibrated, provided all samples for comparison have the same volume. In radioimmunoassays, ferrokinetics, blood volume, red cell mass measurements, a standard of the same geometry (volume) and with relatively the same activity is counted along with all samples, and then a comparison is made between each sample and the standard. However, when the absolute activity of a radioactive sample needs to be determined, then the detection efficiency of the counter must be measured for the γ-ray energy of interest using a standard of the radioactive sample of known activity. The photopeak efficiency is determined from the count rate of the standard at the appropriate PHA setting divided by the disintegration rate from the known activity of the standard. The efficiency correction can then be applied to the count rates of samples of unknown radioactivity when counted at the same setting as the standard to give the absolute activity. For absolute activity, the photopeak efficiency must be determined for each photon energy.

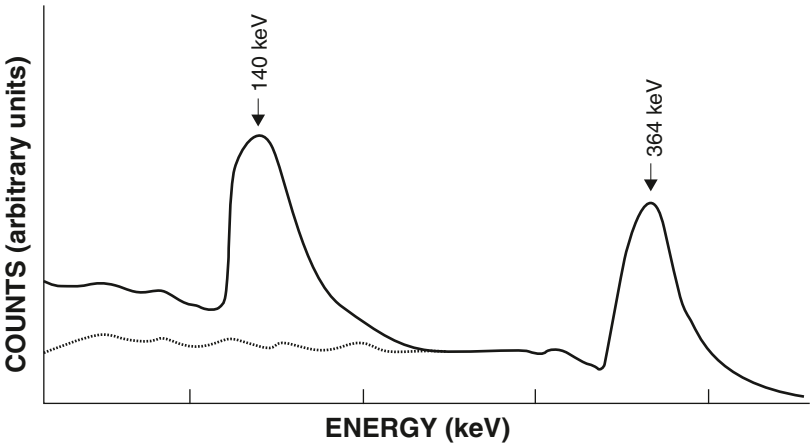

FIG. 8.12. A combined spectrum of the 140-keV γ-ray of ^{99m}Tc and 364-keV γ-ray of ^{131}I. The dotted line under the 140-keV photopeak is the spillover, or crosstalk, contribution from the 364-keV photon.

When multiple γ-rays, either from a single radionuclide or from many radionuclides, are present in a radioactive sample, then the energy spectrum becomes complicated by the overlapping of different photopeaks and also by Compton contributions from the high-energy photons to the low-energy photopeaks. The latter contributions are termed the *spillover*, or *crosstalk contributions*.

Figure 8.12 illustrates an energy spectrum of the 140-keV peak of ^{99m}Tc and 364-keV peak of ^{131}I, in which the Compton contribution from the 364-keV peak to the 140-keV peak is shown. Corrections must be made for this spillover to the 140-keV peak. This is accomplished by counting a sample of pure ^{131}I in both 140-keV and 364-keV discriminator settings and determining the percentage of spillover from the ratio of the counts in the 140-keV photopeak to those in the 364-keV photopeak.

Effects of Sample Volume

The sample volume affects the counting efficiency of well counters. As the sample volume for a given activity is increased, more radiations are lost through the opening of the well without interacting in the detector, and hence, the counting efficiency drops. Therefore, correction factors should be determined for different sample volumes and applied to the measured activity.

Well counters are available with automatic sample changers having provisions of counting as many as 500 samples. Most counters are programmable with computers and provide printouts with various information on counting. The major advantage of the well counter is its high detection efficiency due to increased geometric efficiency, which approaches almost 100 % depending on the volume of

the sample. The detection efficiency of a well counter decreases with increasing photon energy and decreasing detector size. Typically, the overall detection efficiency is close to 100 % for 140-keV photons of ^{99m}Tc and 30–90 % for 364-keV photons of ^{131}I, depending on the detector size.

Thyroid Probe

The thyroid probe is a counter commonly employed to measure the uptake of ^{131}I or ^{123}I in the thyroid gland after the oral administration of a ^{131}I-NaI or ^{123}I-NaI capsule. It consists of a NaI(Tl) detector, 5 cm in diameter by 5 cm in thickness, and other associated electronics, as in a well counter. The operation of the probe is similar to that of a well counter.

One of the differences between the well counter and the thyroid probe is that the latter requires a collimator, which limits the field of view on the thyroid. The collimator is a 20- to 25-cm long cylindrical barrel made of lead and covers the detector as well as the PM tube (Fig. 8.13). This reduces the background activity from the γ-radiations from areas outside the thyroid reaching the detector.

The efficiency of a thyroid probe varies inversely with the square of the distance between the detector and the thyroid. The probe is initially calibrated for photon energies in the same manner as the well counter using the 662-keV γ-ray energy of ^{137}Cs, and then discriminator settings are set for the 364-keV γ-ray of ^{131}I. Attenuation of photons in the thyroid tissues reduces the overall detection efficiency of the probe.

Photons scattered within the thyroid gland by Compton scattering may reach and interact in the detector because they originate in the field of view and are not stopped by the collimator thickness. These scattered photons, however, are excluded from the total measured counts by selecting the appropriate lower and upper discriminator settings on the PHA for the 364-keV γ-ray of ^{131}I.

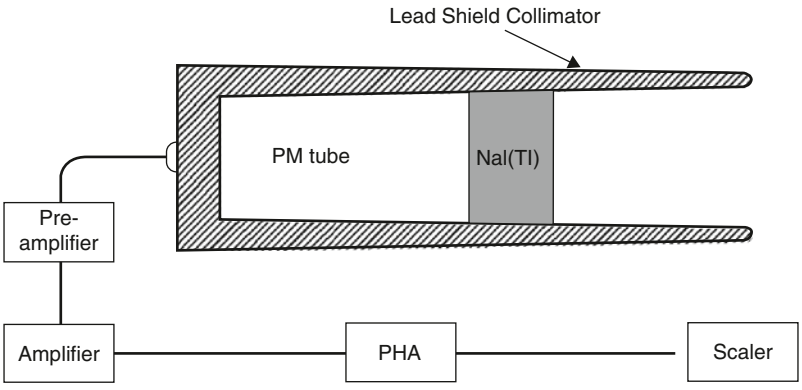

Fig. 8.13. A schematic diagram of a thyroid probe. *PHA* pulse-height analyzer, *PM* photomultiplier.

Thyroid Uptake Measurement

In the thyroid uptake test, a ^{131}I-NaI capsule containing about 10–15 μCi (0.37–0.55 MBq) of ^{131}I is measured in a lucite thyroid phantom at a fixed distance using the thyroid probe and the settings for 364-keV photons of ^{131}I. The thickness and composition of the lucite phantom are equivalent to those of the patient's neck. This count is considered as the standard count. The capsule is then administered to the patient orally, and the thyroid count is obtained at the same distance as the standard count 24 h after administration. The room background count is taken to subtract from the standard count, and the thigh count is taken as background to subtract from the thyroid count. The thyroid uptake is then calculated as follows:

$$\% \text{ uptake} = \frac{(A - B) \times 100}{(C - D)} \tag{8.9}$$

where A is the thyroid count, B is the thigh count, C is the standard count corrected for 24-h decay, and D is the room background. Identical procedures are employed with ^{123}I-NaI using ~300 μCi (11.1 MBq). At times, the 6-h thyroid uptake also is determined depending upon the clinical judgement of the physicians.

Questions

1. Describe the mechanism of γ-ray interaction in the NaI(Tl) detector. In γ-ray counting, why is NaI(Tl) commonly chosen as the detector?
2. (a) Describe the operation of a photomultiplier (PM) tube.
   (b) What is the typical high voltage applied to the PM tube?
   (c) What are the photocathodes commonly made of?
   (d) How many photoelectrons are emitted from the photocathode for each keV of photon energy?
3. (a) Ideally, a photopeak should appear as a line in a γ-ray spectrum. Indicate different factors that contribute to the broadening of the photopeak.
   (b) A photopeak is due to only photoelectric effect of γ-rays, or due to all γ-rays that deposit full energy in the detector. True or false?
4. (a) Describe the function of a pulse-height analyzer (PHA).
   (b) Do the following factors affect the size (pulse height) of the photopeak pulses?
      i. Gain of the amplifier
      ii. High voltage of PM tubes
      iii. Distance between the source and the detector
      iv. Light photons produced in the detector

5. In a γ-ray spectrum, describe the origins of:
   (a) Backscatter peak
   (b) Compton valley
   (c) Characteristic *K* x-ray peak
   (d) Iodine escape peak
   (e) Sum peak
6. (a) Describe the principles of a liquid scintillation counter.
   (b) What is a scintillation solution, and how does it work?
   (c) What is the purpose of using a secondary solute to the scintillation solution?
   (d) What are the most common solvents for liquid scintillation counting?
   (e) Can you count ^{3}H (β^-energy = 0.018 MeV) and ^{14}C (β^-energy = 0.156 MeV) in the same sample using a liquid scintillation counter equipped with three PHAs?
7. (a) Define the energy resolution of a detector.
   (b) For a given detector, the energy resolution of low-energy photons is poorer than that of high-energy photons. True or false?
   (c) For NaI(Tl) detectors, the energy resolution should be less than 10 % for the 662-keV photon of ^{137}Cs. True or false?
8. (a) A point source of ^{99m}Tc is placed 10 cm away from a NaI(Tl) detector that has a diameter of 20 cm. Calculate the geometric efficiency.
   (b) What would be the geometric efficiency if the source were placed on the surface of the detector?
9. (a) Explain the dead time and pulse pileup of a counter.
   (b) What is the distinction between the paralyzable and nonparalyzable systems?
   (c) What are the typical dead times for Geiger–Müller (GM) counters and NaI(Tl) counters?
10. (a) Describe the energy calibration of a NaI(Tl) well counter.
    (b) Why does the count rate differ from the disintegration rate of a sample of a radionuclide?
    (c) How does the sample volume affect the count rate?
11. What are the spillover or crosstalk contributions in a spectrum of several γ-rays? How would you correct for them?
12. A radioactive sample has two γ-ray photons of 130- and 120-keV energies. If a NaI(Tl) crystal has an energy resolution of 10 % at 125 keV, could the two photons be detected as separate photopeaks?
13. Both gas-filled detectors and semiconductor detectors operate by ionization of atoms by radiation. Why do semiconductor detectors give better energy resolution than gas-filled detectors?
14. A patient is given orally a 10-μCi^{131}I-NaI capsule. Before administration, the count rate of the capsule in a thyroid phantom is 297,000 cpm. The 24-hour count rate of the patient's thyroid is 168,000 cpm. If the room background is 200 cpm and the patient's thigh count rate is 1000 cpm, calculate the thyroid uptake.

15. High-activity sources such as radiopharmaceutical dosages and x-ray exposure outputs are better measured with ionization chambers than GM counters and NaI(Tl) well counters. Why?
16. Which of the following counters can detect individual events of the radiation interacting with the detector?
    (a) Ionization chamber
    (b) GM counter
    (c) NaI(Tl) well counter
17. What type of Compton scattering causes the Compton edge of a γ-ray spectrum?
18. Discuss the properties of newer detectors. Explain why LSO is preferably used in PET cameras.

Suggested Readings

Bushberg JT, Seibert JA, Leidholdt EM Jr, Boone JM. *The Essential Physics of Medical Imaging*. 3rd ed. Philadelphia: Lippincott Williams & Wilkins; 2011.

Cherry SR, Sorensen JA, Phelps ME. *Physics in Nuclear Medicine*. 3rd ed. Philadelphia: W.B. Saunders; 2003.

Cradduck TD. Fundamentals of scintillation counting. *SeminNucl Med*. 1973;3:205–223.

Hendee WR, Ritenour ER. *Medical Imaging Physics*. 4th ed. New York: Wiley-Liss; 2002.

Hine GJ. Sodium iodide scintillators. In: Hine GJ, eds. *Instrumentation in Nuclear Medicine*. New York: Academic Press; 1967;I:95–117.

Knoll GF. *Radiation Detection and Measurement*. 4th ed. New York: Wiley; 2010.

Peng CT, Horrocks DL, Alpen EL, eds. *Liquid Scintillation Counting*. New York: Academic Press; 1980; I, II.

Rollo FD, ed. *Nuclear Medicine Physics, Instrumentation and Agents*. St. Louis: Mosby; 1977.

9
Gamma Cameras

The principles of nuclear medicine studies are based on the assessment of radionuclidic distribution in a given organ after in vivo administration of a radiopharmaceutical to distinguish between the normal and abnormal tissues. Such assessment of radionuclide distribution is performed by gamma cameras that primarily comprise NaI(Tl) detectors and the associated electronics described in the previous chapter. The gamma cameras permit the acquisition of both static and dynamic images with better spatial resolution, and can be oriented in any direction around the patient. Various aspects of gamma cameras are discussed below.

Gamma Cameras

The gamma or scintillation camera is an imaging device that is most commonly used in nuclear medicine. It is also called the Anger camera in honor of Hal O. Anger, who invented it in the late 1950s. Gamma cameras detect radiation from the entire field of view simultaneously and therefore are capable of recording dynamic as well as static images of the area of interest in the patient. Various designs of gamma cameras have been proposed and made available, but the Anger camera with a single crystal is by far the most widely used. Although many sophisticated improvements have been made on the gamma cameras over the years, the basic principles of the operation have essentially remained the same.

Principles of Operation

The gamma camera usually consists of several components: a detector, a collimator, PM tubes, a preamplifier, an amplifier, a pulsed-height analyzer (PHA), an *X*-, *Y*-positioning circuit, and a display or recording device. A schematic diagram of a gamma camera is illustrated in Fig. 9.1, and a commercial gamma camera is shown in Fig. 9.2. The detector, PM tubes, and amplifiers are housed in a unit called the *detector head*, which is mounted on a stand. The head can be moved up or down and rotated with electrical switches to position it in the field of view

G. B. Saha, *Physics and Radiobiology of Nuclear Medicine,*
DOI 10.1007/978-1-4614-4012-3_9,

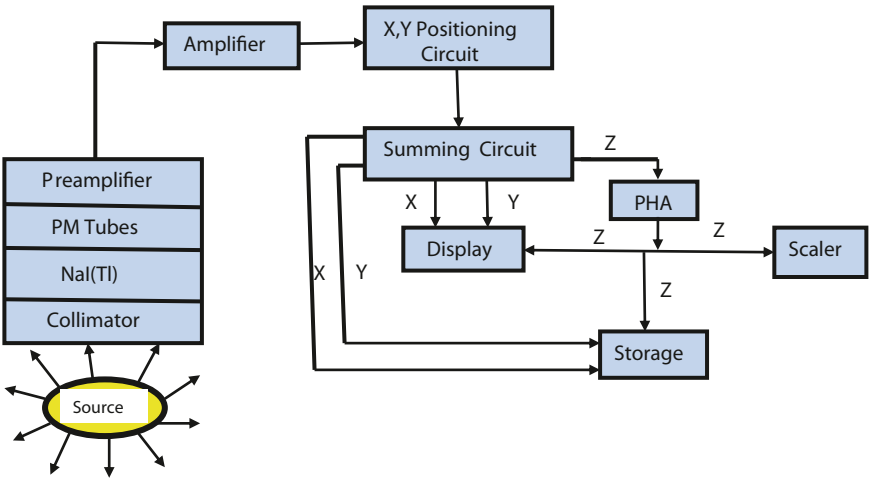

FIG. 9.1. A schematic diagram of a gamma camera. *PHA* pulse-height analyzer; *PM* photomultiplier.

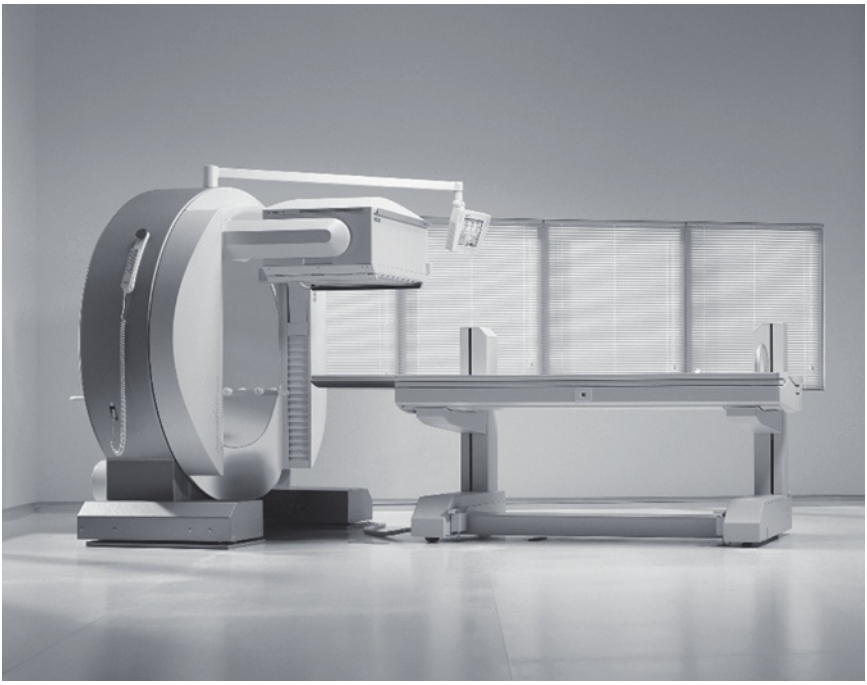

FIG. 9.2. A typical single-head gamma camera. (Courtesy of Siemens Medical Solutions USA, Inc.)

on the patient. The *X*-, *Y*-positioning circuits, PHA, and some recording devices are mounted on a console. In the past, the cameras were operated by switches and dials on the console. Nowadays, much of the operation of the camera is performed by a computer built in it. The computer is run by appropriate software in conjunction with a keyboard, a mouse, and a video monitor. High voltage, window, and photopeaks are all set by the operator's choice of parameters. Acquisition of the data and processing of the data are carried out by the computer. Whereas stationary cameras are permanently installed at desired locations, portable gamma cameras are mounted on wheels for use in situations requiring movement of the camera from room to room, such as to the patient's bedside. Mobile cameras are installed in wheeled vans such that they can be moved to places where gamma cameras are not available for nuclear medicine studies.

The operational principles of a gamma camera are identical to those of solid scintillation counters described in Chapter 8. Basically, γ-rays from a source interact with the NaI(Tl) detector, and light photons are emitted. The latter strike the photocathode of PM tubes, and a pulse is generated, which is then amplified by an amplifier and sorted out by a PHA. Finally, the pulse is positioned by an *X*-, *Y*-positioning circuit on the recording device or stored in the computer, corresponding to the location of γ-ray interaction in the detector (see later).

The functions of PM tubes, preamplifier, amplifier, PHA, and recording devices are the same as described in Chapter 8, and therefore only essential features pertaining to the use of gamma cameras will be highlighted.

Detector

NaI(Tl) crystals are the common detectors used in gamma cameras. In older cameras, circular detectors of a dimension of 25–35 cm in diameter were used, whereas in modern cameras, most manufacturers use rectangular detectors of the size of approximately 45×60 cm, which provide a practical field of view of 40×55 cm. Although the thickness of the detector used varies from 0.63 to 1.84 cm, the optimum thickness of 0.95 cm is used by many manufacturers in the current cameras. Thinner crystals (0.64 cm) are sufficient for low energy radionuclides such as ^{201}Tl, ^{99m}Tc and ^{123}I and used in portable gamma cameras for cardiac studies.

NaI(Tl) crystals are hygroscopic, and absorbed water causes color changes that reduce light transmission to the PM tubes. For this reason, these crystals are hermetically sealed in aluminum containers. Also, the entrance and side of the crystals are coated with a reflective substance (e.g. magnesium oxide) so that light photons are reflected towards the photocathode of the photomultiplier tube.

Increasing the thickness of a detector increases the probability of complete absorption of γ-rays and hence the sensitivity (defined in Chapter 10) of the camera. However, the probability of multiple Compton scattering also increases in thicker detectors, and therefore the *X*, *Y* coordinates of the point of γ-ray interaction can be misplaced. This results in poor resolution of the image of the area of interest. For this reason, thin NaI(Tl) detectors are used in gamma cameras, but this

decreases the sensitivity of the camera, because many γ-rays may escape from the detector without interaction.

Collimator

In gamma cameras, a collimator is attached to the face of the NaI(Tl) detector to limit the field of view so that γ-radiations from outside the field of view are prevented from reaching the detector. Collimators are normally made of material with high atomic number and stopping power, such as tungsten and lead, of which lead is the material of economic choice in nuclear medicine. Two methods are employed to make collimators—the cast method and foil method. In the cast method, holes are made through a single slab of lead, whereas in the foil method, corrugated lead strips are glued together, through which holes are made. They are designed in different sizes and shapes and contain one or many holes to view the area of interest.

Collimators are primarily classified by the type of focusing, although other classifications are also made based on septal thickness and the number of holes. Depending on the type of focusing, collimators are classified as parallel-hole, pinhole, converging, and diverging types; these are illustrated in Fig. 9.3. *Pinhole* collimators are made in conical shape with a single hole and are used in imaging small organs such as the thyroid glands to provide magnified images. *Converging* collimators are made with tapered holes converging to an outside point and are employed to provide magnified images when the organ of interest is smaller than the size of the detector. Images are magnified by converging collimators. *Diverging* collimators are constructed with tapered holes that are divergent outward from the detector face and are used in imaging organs such as lungs that are larger than the size of the detector. The images are minified with these collimators.

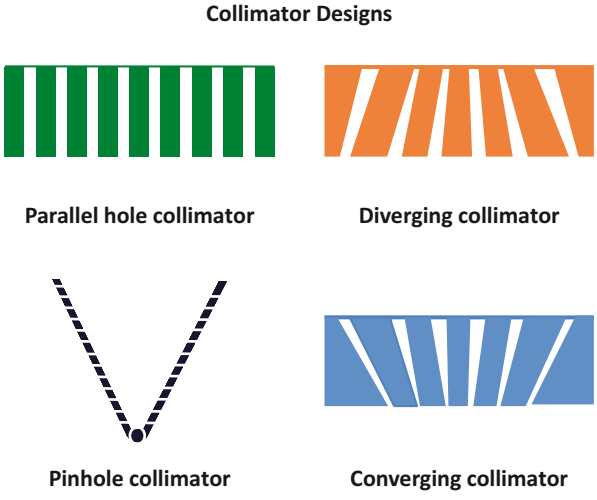

FIG. 9.3. Different designs of collimators.

Parallel-hole collimators are made with holes that are parallel to each other and perpendicular to the detector face and have between 4000 and 46,000 holes depending on the collimator design. These collimators are most commonly used in nuclear medicine procedures and furnish a one-to-one projected image. Because pinhole and converging collimators magnify and the diverging collimators minify the image of the object, some distortion occurs in images obtained with these collimators. Because large field of view (LFOV) cameras are readily available now, diverging collimators are not used in routine nuclear medicine studies.

Parallel-hole collimators are classified as high-resolution, all-purpose, and high-sensitivity type, or low-energy, medium-energy, or high-energy type, depending on the resolution and sensitivity they provide in imaging. High-sensitivity collimators are made with smaller thickness than all-purpose collimators, whereas high-resolution collimators are thickest of all. These characteristics are discussed in detail in Chapter 10.

Several collimators are available that are designed for some specific purposes. *Fan-beam* collimators are designed with holes that converge in one dimension but are parallel to each other in the other dimension. These collimators are primarily used for imaging smaller objects and hence magnify the images. *Cone-beam* collimators are similar to fan-beam collimators and magnify the images except that the holes are designed such that they converge in two dimensions.

In earlier collimators, the holes were made circular, but current designs have square, hexagonal, or even triangular holes with uniform thickness of lead around the opening. These collimators provide better spatial resolution than the circular-hole ones.

Photomultiplier Tube

As in scintillation counters, PM tubes are essential in gamma cameras for converting the light photons in the NaI(Tl) detector to a pulse. Instead of one PM tube, an array of PM tubes are mounted on the back of the detector with optical grease, or in some instances, using lucite light pipes between the detector and the PM tubes. In older cameras, the number of PM tubes used were 19 or 37, whereas most manufacturers utilize 59 PM tubes in modern cameras. In modern gamma cameras, square or hexagonal PM tubes are used for better packing. The output of each PM tube is used to define the *X*, *Y* coordinates of the point of interaction of the γ-ray in the detector by the use of an *X*-, *Y*-positioning circuit (see later) and also is summed up by a summing circuit to form a pulse known as the *Z pulse*. The *Z* pulse is then subjected to pulse-height analysis and is accepted if it falls within the range of selected energies.

X-, Y-Positioning Circuit

Each pulse arising out of the γ-ray interaction in the NaI(Tl) detector is projected at an *X*, *Y* location on the image corresponding to the *X*, *Y* location of the point of interaction of the γ-ray. This is accomplished by an *X*-, *Y*-positioning circuit in conjunction with the PM tubes and a summing circuit. Fig. 9.4 illustrates the

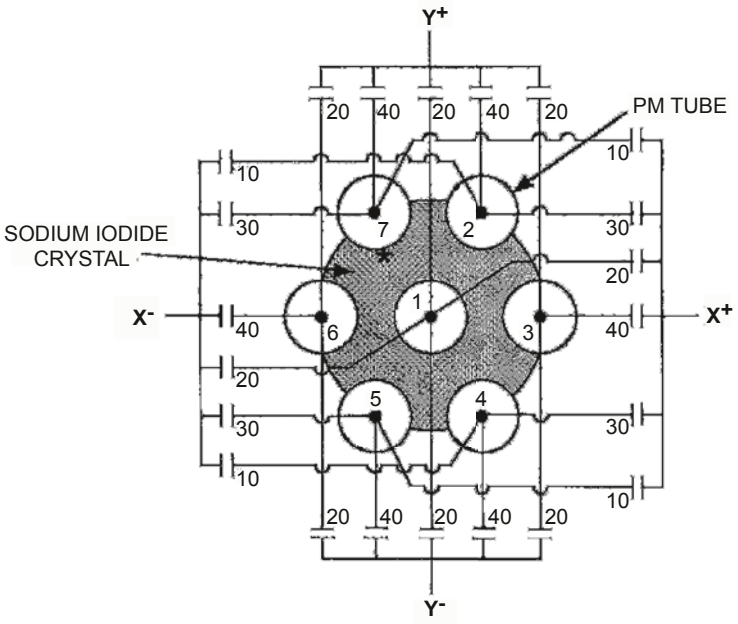

FIG. 9.4 Arrangement of seven photomultiplier (*PM*) tubes to produce *X* and *Y* pulses for the *X*, *Y* location of the γ-ray interaction in the detector. X^+, X^-, Y^+, and Y^- pulses are obtained by summing the output of all PM tubes weighted by capacitors for the location of each PM tube in relation to the site of γ-ray interaction. (Adapted from Anger HO. Scintillation camera. Rev Sci Instr. 1958; 29:27.)

principles of *X*, *Y* positioning of pulses arising from γ-ray interactions in the detector employing seven PM tubes. All PM tubes are connected through capacitors to four output leads representing four directional signals, X^+, X^-, Y^+, and Y^-. The capacitance values are assigned in direct proportion to the location of the PM tube relative to the four signals. Suppose a γ-ray interacts at a location (*) near tube 7. The largest amount of light is received by tube 7, and other tubes receive light in proportion to their distances from the point of interaction. The output signals of PM tubes are weighted by the appropriate capacitance values and then summed to form each of the X^+, X^-, Y^+, and Y^- signals individually. In this case, X^- will be greater than X^+, and Y^+ will be greater than Y^-, because the interaction occurred in the upper left quadrant. The *X*-, *Y*-designating pulses, *X* and *Y*, and the *Z* pulse are then obtained as follows:

$$Z = X^+ + X^- + Y^+ + Y^- \tag{9.1}$$

$$X = \frac{k}{Z}\left(X^+ - X^-\right) \tag{9.2}$$

$$Y = \frac{k}{Z}\left(Y^+ - Y^-\right) \tag{9.3}$$

where k is a constant and k/Z is the amplifier gain. The X and Y pulses are then projected on a display monitor to depict the X, Y coordinates of the point of γ-ray interaction, which in turn corresponds to the coordinates of the location in the field of view where the γ-ray interacted in the crystal. Similarly, these pulses can be stored in the computer in a square matrix so that the data can be processed later to reproduce an image. Details of data acquisition and storage in the computer are given in Chapter 11. Or, they can be projected on an x-ray film. Nowadays, resistors and microprocessors have been used in place of capacitors.

The larger the number of PM tubes, the better the accuracy of the X, Y locations of all pulses on the image; that is, the better the spatial resolution of the image (see Chapter 10).

Pulse-Height Analyzer

After the Z pulses are formed by the summing circuit, the PHA analyzes their amplitude and selects only those of desired energy by the use of appropriate peak and window settings. In many gamma cameras, the energy selection is made automatically by push-button–type isotope selectors designated for different radionuclides such as ^{99m}Tc, ^{131}I, and so on. In modern cameras, isotope peak and window settings are selected by menu-driven algorithm on a computer monitor interfaced with the camera. In some gamma cameras, two or three PHAs are used to select simultaneously two or three γ-rays of different energies. These types of cameras are useful in imaging with ^{111}In and ^{67}Ga that possess two or three predominant γ-rays. The window settings are expressed in percentages of the peak energy and for most studies, a 15 % to 20 % window centered symmetrically on the photopeak is employed.

It should be noted that X and Y pulses are accepted if the Z pulse is within the energy range selected by the PHA. If the Z pulse is outside this range, then X and Y pulses are discarded.

Display and Storage

In a typical nuclear medicine study, data are collected normally for preset counts (e.g., 500,000 counts) or a preset time (e.g., 10 min). Until the mid-1990s, image data were captured on x-ray film or Polaroid film or stored on magnetic tapes, laser disks, and the like. Nowadays, all camera systems use computer memories for storage of image data. The details of storage in computers are given in Chapter 11. In older systems, images were mostly displayed on cathode ray tube (CRT) monitors and at present, all systems commonly use LCD (liquid crystal display) video monitors for better display of images. The computer manipulation of image contrast on LCD monitors provides a better view of images leading to more accurate diagnosis of diseases. The details of display and storage are given in Chapter 11.

Digital Cameras

It is seen from the above description that the *X*- and *Y*-pulses are obtained in analog form and are projected on different display and recording systems. Such analog processing inherently includes instability in pulse formation and results in image nonlinearity and nonuniformity. These are caused by fluctuations in PM tube output due to high voltage (HV) variations, drift in preamplifier output, and variations in PH and *X*-, *Y*-positioning analyses. To circumvent these effects and also for the manipulation of data at a later time, analog data are digitized to be stored in a matrix map in a computer. Digitization of the analog signal is performed by an electronic circuit, called the analog-to-digital converter (ADC). The digitized data are later retrieved for further processing to display on video monitors.

In modern cameras each PM tube output is digitized by the ADC before PH and *X*-, *Y*-positioning analyses. These cameras are called "all-digital" cameras. In these cameras, the gains of all PM tubes are initially optimized by placing a narrow beam of a radioactive source in front of each PM tube and determining the center of the photopeak by adjusting the high voltage of the PM tube with a digital computer. Next, the camera is calibrated, in which a source of interest is positioned in front of each PM tube, and output from each PM tube is sampled, integrated, and digitized by a high-speed ADC in the computer. Each signal is then normalized by dividing it with the sum of all digital signals arising from the same scintillation event. In a two-dimensional array of PM tubes, the normalized digital output $Z_i(X, Y)$ corresponds to the X, Y location of the PM tube i. To determine the location of each signal Z_i, a weighting factor is calculated from the inverse of the uncertainties of X and Y positions, i.e., $1/\Delta X$ and $1/\Delta Y$, that are related to the spatial distribution of Z_i values around the center of the PM tube. The X, Y locations and weighting factors are mapped and stored in reference tables as functions of Z_i values for all PM tubes for positional and Z-pulse analyses of a scintillation event in later imaging studies.

In subsequent patient imaging studies, the output signal of each PM tube from a scintillation event is sampled, integrated, digitized and finally normalized to give Z_i. The location (X, Y) of the scintillation event is then calculated by using the appropriate values of locations and weighting factors in the reference tables in the memory. The digitized $Z_i(X, Y)$ is stored in the X, Y location of the image matrix, if the pulse discrimination does not reject the signal. Since the location of each event is determined by digitizing and analyzing the individual signal from each PM tube, the accuracy of positioning of the signals is greatly improved. For these reasons, the digital cameras provide excellent intrinsic linearity and hence superior spatial resolution in image formation.

Solid State Digital Cameras

Digirad Corporation has made commercially available several gamma cameras using solid state detectors. Initially CZT detectors were used, but later the company replaced them with CsI(Tl) detectors. Each detector head is pixelated with a

dimension of 21 × 16 cm. There are 768 pixels in each head and each pixel (voxel) has a dimension of 6.1 × 6.1 mm. The uniqueness of these cameras is that they do not use PM tubes for pulse formation and use silicon diodes instead. No *X, Y* positioning circuit is used, because each CsI(Tl)/silicon diode element functions as an individual detection system, independent of other elements, and each event of photon interaction in the crystal is positioned in the image matrix corresponding to the location of the element (Early 2005). This provides an excellent spatial resolution and quality of the images in the energy range of 60–300 keV.

Various Digirad camera models include Cardius X-ACT, Cardius 3 XPO (three-head), and Cardius 2 XPO (two-head). Appropriate collimators are required for imaging different organs and photons of different energies. Many units are small and portable. These cameras are commonly used for cardiac SPECT studies with the use of a rotating chair for the patient. During the study, the patient is positioned in the chair in front of the vertically standing camera and the chair rotates at incremental angles with respect to the detector providing desired projections.

Spectrum Dynamics has introduced a gamma camera (D-SPECT) using CZT semiconductor as the detector for cardiac studies. It consists of an array of nine columnar detectors that are arranged in a configuration to conform to the contour of the left side of the patient's chest. Each detector consists of 1024 (16 × 64) 5-mm thick CZT crystals of size 2.46 × 2.46 mm, and can rotate and translate individually to obtain the desired number of angular projections around the patient. The data acquisition is quite fast requiring only two minutes for a gated cardiac study and providing high quality images.

Another gamma camera using CZT crystals has been introduced by GE Healthcare (Discovery NM 530c) primarily for cardiac studies. A focused multi-pinhole collimator is used to improve the detection efficiency and hence sensitivity. The detector and the collimator are held in a fixed position so that many cardiac projections are acquired simultaneously. This camera allows much faster acquisition of data (4–5 min. compared to 15–20 min. for conventional cameras) virtually eliminating the artifacts caused by patient movement and also facilitating dose reduction to the patient. Recently for fusion of anatomical and functional images, a CT unit (LightSpeed VCT) has been incorporated in this system to make an integrated SPECT/CT unit, NM/CT 570c, to provide photon attenuation correction and better delineation of lesions in organs.

Questions

1. (a) Describe the operational principles of a gamma camera.
   (b) The main purpose of a collimator is to limit the field of view of an imaging device for imaging. True or false?
   (c) The purpose of a photomultiplier tube is to convert light photons to an electron pulse. True or false?

(d) The scattered photons are excluded by the proper choice of a collimator. True or false?
(e) Scattered photons are excluded by the proper choice of discriminator settings (windows). True or false?

2. (a) What are the different categories of collimators?
(b) Which collimator is most used in nuclear medicine?
(c) Which types of collimator give image distortion and why?
3. Describe the function of the *X*, *Y* circuit in the gamma camera system.
4. A pulse-height analyzer:
(a) Reduces the background. True or false?
(b) Rejects γ-rays that undergo Compton scattering in the patient and the detector. True or false?
(c) Rejects γ-rays undergoing photoelectric effect in patients. True or false?
(d) Increases the signal-to-noise ratio. True or false?
5. (a) The detection efficiency of a gamma camera increases with the thickness of the detector. True or false?
(b) What are the most common thicknesses of the NaI(Tl) detector used?
(c) A gamma camera detector with a 20-cm field of view is used to image the lungs, which fill 75 % of the image. The camera is set to accumulate 450,000 counts. Calculate the information density.
6. In pulse-height analysis, a 20 % window means 10 % on either side of the photopeak. True or false?
7. Describe how the digital camera works.
8. What is the advantage of a digital camera over an analog camera (Anger type)?
9. Why does a solid-state camera not require a PM tube?

Suggested Readings

Cherry SR, Sorensen JA, Phelps ME. *Physics in Nuclear Medicine*. 3rd ed. Philadelphia: W.B. Saunders; 2003.

Early P. Private communication, 2005.

Erickson J. Imaging systems. In: Harbert J, da Rocha AFG, eds. *Textbook of Nuclear Medicine, Volume I: Basic Science*. Philadelphia: Lea & Febiger; 1984.

Rollo FD, ed. *Nuclear Physics, Instrumentation, and Agents*. St Louis: CV Mosby; 1977.

10
Performance Parameters of Gamma Cameras

The quality and detail of an image obtained by gamma cameras are affected by several parameters associated with these imaging systems. These parameters include spatial resolution, sensitivity, uniformity, and contrast, and they are described here in detail. A brief description of the quality control tests for gamma cameras is also included.

Spatial Resolution

The spatial resolution of a gamma camera is a measure of the ability of the device to faithfully reproduce the image of an object, thus clearly depicting the variations in the distribution of radioactivity in the object (Erickson 1984). The *spatial resolution* of a gamma camera is empirically defined as the minimum distance between two points in an image that can be detected by the system. The overall spatial resolution (R_o) of a gamma camera comprises three components, namely, intrinsic resolution (R_i) of the detection system, collimator resolution (R_g), and scatter resolution (R_s), and is given by

$$R_o = \sqrt{R_i^2 + R_g^2 + R_s^2} \tag{10.1}$$

The smaller numerical values of R_o indicate better resolution and vice versa.

Intrinsic Resolution

Intrinsic resolution, R_i, is the component of spatial resolution contributed by the detector and associated electronics, and is a measure of how well an imaging device can localize an event on the image. Intrinsic resolution arises primarily from the statistical fluctuations in pulse formation that have been discussed in the section entitled Gamma Ray Spectrometry in Chapter 8. The statistical variations in the production of light photons after γ-ray interaction in the detector and varia-

G. B. Saha, *Physics and Radiobiology of Nuclear Medicine,*
DOI 10.1007/978-1-4614-4012-3_10,

tions in the number of electrons emitted from the photocathode and dynodes in the photomultiplier (PM) tubes have significant effects on the intrinsic resolution. In gamma cameras, the *X*, *Y* positioning of the pulses is improved by increasing the number of PM tubes, thus improving the intrinsic resolution. Also, PM tubes with greater quantum efficiency and their improved optical coupling to the detector for greater light collection provide better intrinsic resolution.

Intrinsic resolution improves with higher γ-ray energy and deteriorates with lower energy because greater statistical fluctuations occur in the production of light photons by lower energy photons and vice versa. For example, the 140-keV photons of ^{99m}Tc produce almost twice as many light photons in the detector as the 69- to 80-keV photons of ^{201}Tl and thus result in better intrinsic resolution. However, there is little improvement in intrinsic resolution with photon energy above 250 keV because of multiple scattering of photons within the detector that can result in photoelectric absorption (see below). Intrinsic resolution improves with narrow PHA window settings, because scattered radiations are avoided.

Multiple Compton scattering of a γ-ray photon followed by absorption of all scattered photons in the detector causes uncertainty in the *X*, *Y* location of the original γ-ray interaction and makes the intrinsic resolution, and hence spatial resolution, worse. This effect is worse with thicker detectors and high-energy photons (>250 keV) because of the increased chances of multiple scattering. For this reason, thinner detectors (0.63–1.84 cm) are used in gamma cameras.

Most modern cameras have intrinsic resolution of the order of 4-mm full width at half maximum (FWHM) for 140-keV photons of ^{99m}Tc.

Collimator Resolution

Collimator resolution, also termed the *geometric resolution* (R_g), constitutes the major part of the overall spatial resolution and primarily arises from the collimator design. In general, collimator resolution is worse than intrinsic resolution. As already mentioned in Chapter 9, there are four major collimators: parallel-hole, pinhole, converging, and diverging. Of these, parallel-hole collimators are most commonly used in nuclear medicine.

The different parameters of a typical parallel-hole collimator are shown in Fig. 10.1. The spatial resolution for this collimator is given by the geometric radius of acceptance, R_g:

$$R_g = \frac{d(t_e + b + c)}{t_e} \tag{10.2}$$

where d is the hole diameter of the collimator, b is the distance between the collimator face and the source of radiation, c is the distance between the back face of the collimator and the midplane of the detector, and t_e is the effective length of the collimator holes. The t_e is empirically given by $t_e = t - 2\mu^{-1}$, where μ is the linear attenuation coefficient of the photons in the collimator material (e.g., lead), and t

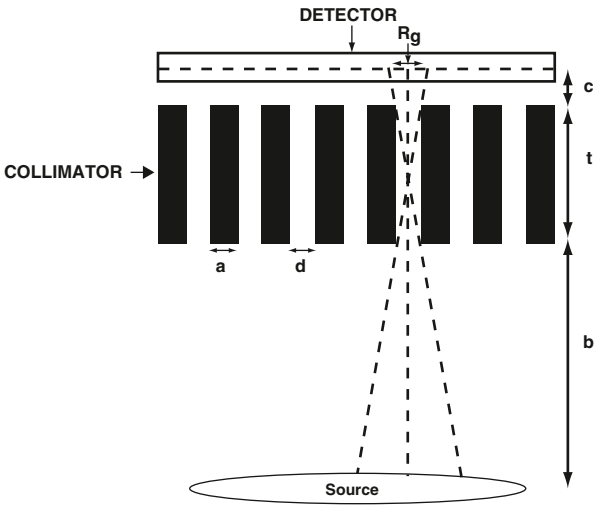

FIG. 10.1. A parallel-hole collimator with thickness t, hole diameter d, septal thickness a, and source-to-collimator distance b. The collimator is attached to a detector whose midplane is at a distance c from the back surface of the collimator. R_g is the collimator resolution.

is the length or thickness of the collimator hole. This corrects for the penetration of the two corners of the holes by the photons.

As seen from Eq. (10.2), the collimator resolution is improved by increasing the length, t, of the collimator holes or by decreasing the diameter, d, of the holes. Thus, long narrow holes provide better spatial resolution. Also, the collimator resolution deteriorates with increasing source-to-collimator distance, b, and is best at the collimator face. Therefore, in nuclear medicine studies, patients should be placed as close to the collimator as possible to provide the best resolution. The effects of various features of parallel-hole collimators on spatial resolution and sensitivity are summarized in Table 10.1.

The thickness a between the holes is called the *septum*. Septal penetration of γ-rays plays an important role in the collimator resolution. High energy photons from outside the field of view can cross the septum and yet interact in the detector, thus obscuring the image. In the collimator design, a primary consideration is to have negligible penetration by these extraneous photons through the septum to

TABLE 10.1. Effect of various features of parallel-hole collimators on their performance.

Increasing	Resolution	Sensitivity
Number of holes	↔	↑
Hole diameter	↓	↑
Hole length	↑	↓
Septal thickness	↑	↓
Source-to-collimator distance	↓	↔

reach the detector. However, it is practically impossible to stop all photons from penetration with any reasonable amount of material without substantial loss of counting efficiency. As a trade-off between penetration and collimator efficiency, a compromise value of 5 % penetration is accepted, and the minimum septal thickness of a parallel-hole collimator can be calculated as

$$a > \frac{6d/\mu}{t_e - (3/\mu)} \tag{10.3}$$

Septal penetration depends on the atomic number Z of the collimator material and is low in high Z material. For cost-effectiveness, lead is commonly preferred for use in the septa. It also depends greatly on the photon energy, and so gamma rays of only ~50–300 keV are suitable for present-day collimators, the most preferable photon energy being 150 keV. At energies below ~50 keV, photons are absorbed in the body tissue, whereas at energies above ~300 keV, septal penetration of the photons can occur. Current collimators are made with appropriate septal thickness for specific photon energies in order to limit septal penetration. Collimators are classified as low energy collimators with a few tenths of a millimeter septal thickness (for up to 140 keV γ-rays) and medium energy collimators with a few millimeter thickness (up to 360 keV photons) (Cherry et al. 2003). Very high energy collimators also are available for counting 511-keV photons. It is understandable that for a given diameter collimator, the number of holes are greater in low energy collimators than in high energy collimators. Various properties of different parallel-hole collimators are given in Table 10.2.

In another classification, collimators are termed high sensitivity and high resolution collimators. Often, these collimators are made with an identical number of holes with identical diameters, but with different thicknesses. Therefore, the high resolution collimators are made with longer holes and the high sensitivity collimators with shorter holes. The spatial resolution for the high sensitivity collimator deteriorates sharply with the source-to-collimator distance. Low energy all purpose (LEAP) collimators are designed with intermediate values of resolution and sensitivity.

TABLE 10.2. Various parallel-hole collimators and their features and properties[a].

Collimator type	Hole diameter (mm)	Hole length (mm)	Septal thickness (mm)	Geometric resolution[b] (mm)	Sensitivity (cpm/μCi)	Optimum energy (keV)
Low energy all purpose (LEAP)	1.43	23.6	0.2	9.1	360	~140
Low energy high resolution (LEHR)	1.11	23.6	0.3	7.5	230	~140
Medium energy	3.02	40.6	1.1–1.4	12.1	288	~280
High energy	4.32	62.8	1.3–3.0	13.8	176	~360
Ultra high energy	3.4	75.0	3.0–4.0	10.4	60	~511

[a] Adapted with permission from Halama J. Quality assurance in gamma camera and SPECT systems. www.medphysicwisc.edu/courses.

[b] At 10 cm from the collimator face

The geometric resolution for pinhole, diverging and converging collimators is expressed by similar but somewhat complex equations, and their details are available from reference books on nuclear physics and instrumentation. In the case of pinhole collimators, the image is magnified and the magnification depends on the ratio of the hole-detector distance to the hole-object distance. The resolution varies over the area of the object along with distortion of the image and the sensitivity falls off with increasing distance from the collimator face. For converging collimators, the image is magnified and the magnification increases with the distance from the collimator face resulting in the deterioration of resolution and an increase in sensitivity, but the image is distorted. For diverging collimators, the situation is opposite to that of the converging collimators. Having the collimator holes diverging away from the detector results in minification of the object to fit into a smaller detector. So distortion occurs, and resolution and sensitivity vary over the object. The fan beam collimator is basically a converging collimator and commonly used for cardiac and brain imaging. It gives better spatial resolution with poorer sensitivity than parallel-hole collimators. The overall system resolutions with different collimators are illustrated in Fig. 10.2.

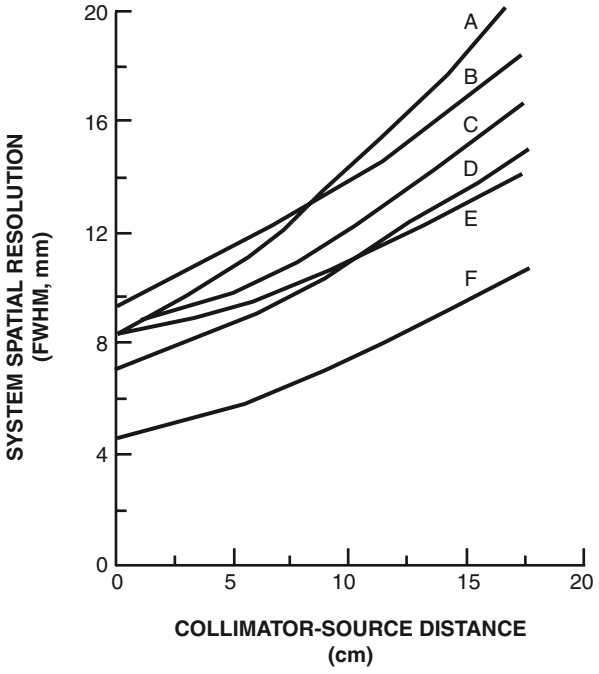

Fig. 10.2. Effect of source-to-collimator distance on overall system resolution for various types of collimators. *A* High sensitivity parallel-hole. *B* Diverging. *C* All purpose parallel-hole. *D* Converging. *E* High resolution parallel-hole. *F* Pinhole. (From Rollo FD, Harris CC. Factors affecting image formation. In: Rollo FD, ed. *Nuclear Medicine Physics. Instrumentation and Agents*. St. Louis: Mosby; 1977. 407. Modified from Moyer RA. J Nucl Med 1974, 15:59.)

Scatter Resolution

Radiations are scattered by interaction with tissue in patients and with the detector. It is possible that some of these radiations are scattered without much loss of energy and fall within the field of view, resulting in pulses of amplitude acceptable within the window set by pulse-height analyzer (PHA). This degrades the overall spatial resolution. This component is called the *scatter resolution* (R_s) and depends on the composition of the scattering medium, the source configuration, and PHA discriminator settings. Scatter increases in heavy patients, and decreasing the PHA window reduces the scatter contribution. The effect of scatter resolution is essentially the same for all collimators (Rollo and Harris 1977).

Evaluation of Spatial Resolution

Bar Phantom

Qualitative evaluation of the spatial resolution of an imaging device can be made by visual inspection of the images obtained using bar phantoms. Bar phantoms consist of four sets of parallel lead bar strips arranged perpendicular to each other in four quadrants in a lucite holder (Fig. 10.3). The widths and spacings of the strips are the same within each quadrant but differ in different quadrants. In all bar phantoms, the thickness of lead should be sufficient to stop photons of a given energy for which spatial resolution is being estimated.

The bar phantom is placed over the detector of a gamma camera. A ^{57}Co flood source (described later under Quality Control) is placed on the top of it and an image is taken. For evaluation of spatial resolution for different photon energies, flood sources of radiations of respective energies should be used. The image of

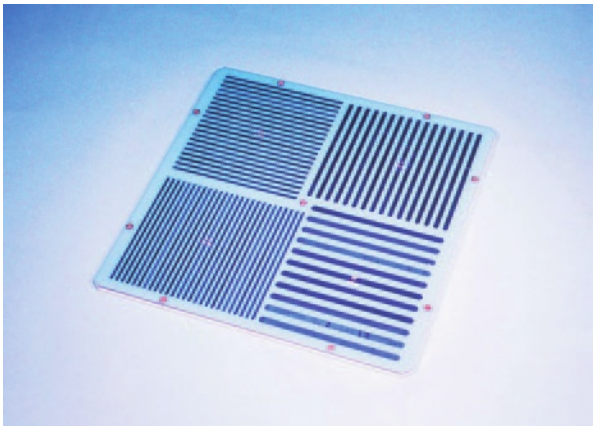

FIG. 10.3. A typical rectangular bar phantom. (Courtesy of Biodex Medical Systems, Inc. Shirely, NY).

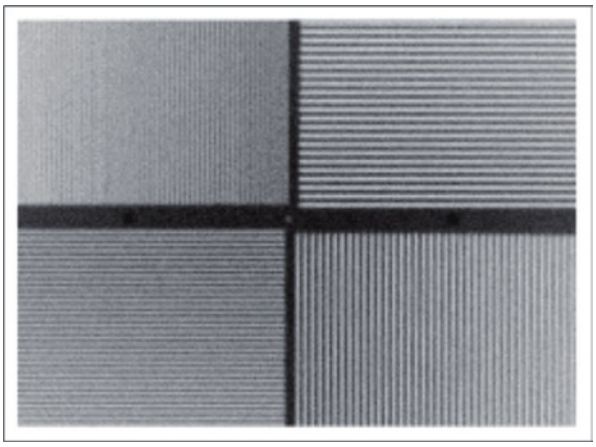

FIG. 10.4. Rectangular bar phantom image obtained using a parallel-hole collimator.

the bar phantom obtained is visually inspected, and spatial resolution is estimated from the smallest strips or spacings distinguishable on the image (Fig. 10.4). Images also can be taken by placing the source of activity at different distances from the collimator to see the changes in spatial resolution with distance (Fig. 10.5). Obviously, this technique is qualitative and does not give a quantitative measure of the spatial resolution.

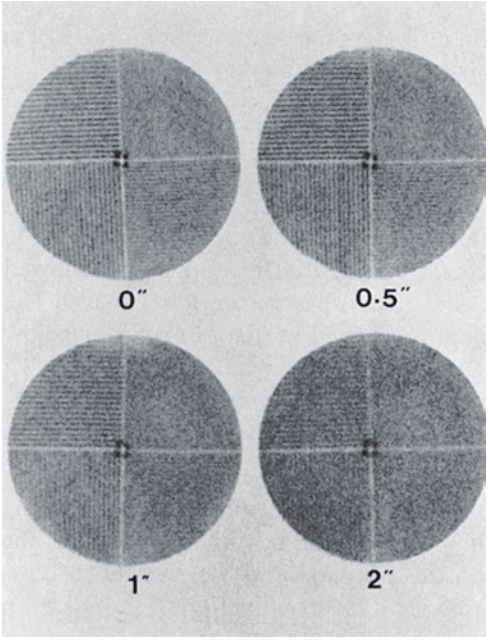

FIG. 10.5. Bar phantom images at different distances from a parallel-hole collimator.

Line-Spread Function

A quantitative method of estimating spatial resolution of a gamma camera is based on the use of a line-spread-function (LSF). A long plastic tubing with a radioactive solution (e.g. ^{99m}Tc) is placed in the field of view at a distance from the detector fitted with a collimator. The gamma camera interfaced with a computer collects and stores the counts (responses) from the line source in a single view, and the computer generates a bell-shaped LSF by plotting the counts at distances from the center of the FOV along the tubing (Fig. 10.6). It shows a distribution of activity with a minimum at the edge of the FOV increasing to a maximum at the center. The FWHM of the LSF gives the spatial resolution of the gamma camera. Similar LSFs can be obtained at different distances from the detector as well as in different media as shown in Figure 10.6. It can be seen that the spatial resolution of a gamma camera deteriorates with increasing source-to detector distance and increasing density of the medium e.g. air versus water. Thus spatial resolution is degraded in patient imaging due to attenuation of photons in body tissues.

Spatial resolution by the LSF method varies with the design of the collimator and is, therefore, different for parallel-hole, converging, and diverging collimators. Also, the FWHM values of the LSF may not represent the true spatial resolution, because the scatter and septal penetration components fall in the tail part of the LSF (i.e., below 50 %) and therefore are not accounted for.

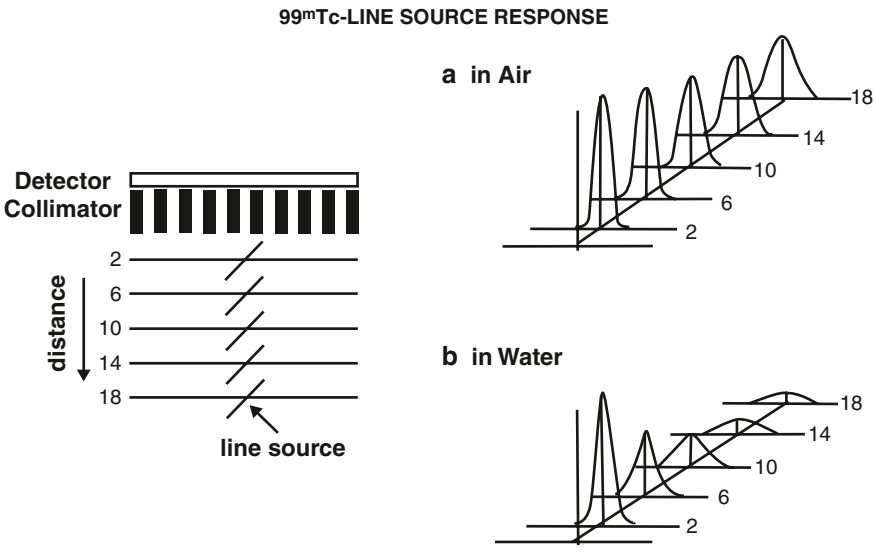

FIG. 10.6. Line spread function of a gamma camera equipped with a low-energy all-purpose parallel-hole collimator obtained in (**a**) air and (**b**) water at different distances using a ^{99m}Tc-line source. Note that the resolution deteriorates in water due to attenuation.

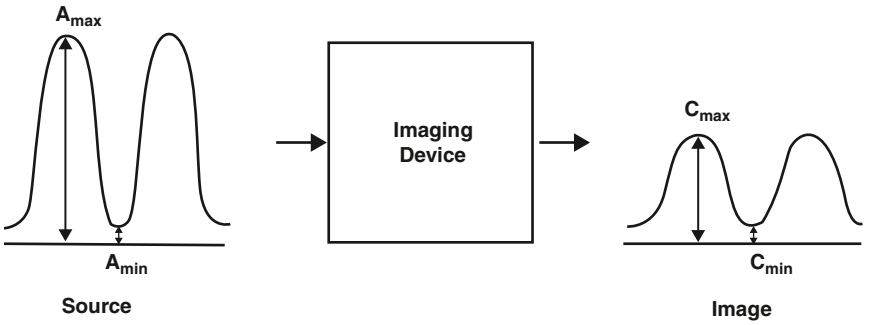

FIG. 10.7. An illustration of the principles of modulation transfer function (MTF) of an imaging system. See text for details.

Modulation Transfer Function

A more complete and quantitative assessment of spatial resolution of imaging devices is made by using modulation transfer function (MTF) (Rollo 1977). The concept of MTF is illustrated in Fig. 10.7. Suppose a source of activity (e.g., a patient) has a sinusoidal distribution with peaks (maximum activity, A_{max}) and valleys (minimum activity, A_{min}), as illustrated in Fig. 10.7. Such a distribution gives a spatial frequency (v) in cycles per centimeter or cycles per millimeter. The contrast, or *modulation* (M_s), in the source activity is given by

$$M_s = \frac{A_{max} - A_{min}}{A_{max} + A_{min}} \tag{10.4}$$

If a perfect imaging device were to image the source faithfully, it would depict the same distribution of activity in the image with A_{max} and A_{min} as in the source activity. Because the imaging devices are not absolutely perfect, it will portray the distribution of activity in the image with C_{max} for the peak and C_{min} for the valley, which are smaller in magnitude than A_{max} and A_{min}. The modulation in the image (M_i) is then expressed by

$$M_i = \frac{C_{max} - C_{min}}{C_{max} + C_{min}} \tag{10.5}$$

The MTF at a spatial frequency v is then calculated as the ratio of M_i to M_s:

$$\text{MTF}(v) = \frac{M_i}{M_s} \tag{10.6}$$

When $M_s = M_i$, MTF = 1. This is true if the sinusoidal cycles are well separated and if the imaging device reproduces the image of each cycle faithfully. Thus, the system with MTF = 1 gives the best overall spatial resolution. When the distri-

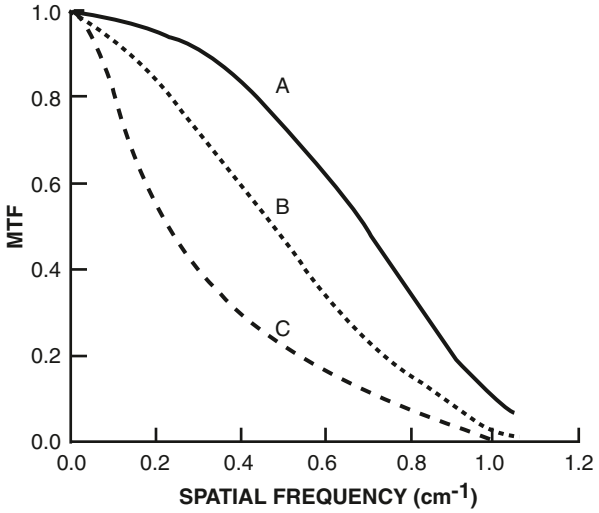

FIG. 10.8. Plot of modulation transfer function (MTF) against spatial frequency. System *A* gives better spatial resolution than systems *B* and *C*, and system *B* provides better resolution than system *C*.

bution of activity is such that spatial frequency increases, the peaks and valleys come closer. When the peaks and valleys are too close, the imaging device cannot delineate them, and the MTF tends to 0, yielding the poorest spatial resolution of the system. The values of the MTF between 0 and 1 give intermediate spatial resolutions. It is important to note that small objects are better imaged at higher frequencies and large objects at lower frequencies.

It has been demonstrated that the MTF is a normalized Fourier transform of the LSF discussed previously. In practice, the source activity distribution is assumed to be composed of line sources separated by infinitesimal distances, and the MTFs are then calculated from the LSFs of all line sources. The mathematical expression of these functions is quite complex and can be found in reference physics books.

Plots of the MTFs against spatial frequencies are useful in determining the overall spatial resolution of imaging devices and are presented in Fig. 10.8 for three imaging systems. It is seen that, at very low frequencies (i.e., larger separation of sinusoidal cycles), the MTFs are almost unity for all three systems; that is, they reproduce equally good images of the radiation source. At higher frequencies (i.e., sinusoidal cycles are too close), system A in Fig. 10.8 gives the best resolution, followed in order by system B and system C.

It is appropriate to mention that whereas the FWHM of the LSF does not account for the scatter and septal penetration of γ-radiations, the MTF takes these two factors into consideration and provides a complete description of the spatial resolution of a system. Furthermore, individual components of an imaging system may have separate MTFs, and they are combined to give the overall MTF, as follows:

$$\mathrm{MTF} = \mathrm{MTF}_1 \times \mathrm{MTF}_2 \times \mathrm{MTF}_3 \cdots \tag{10.7}$$

Problem 10.1
The MTFs at a certain spatial frequency of the detector, PM tubes, and PHA of a gamma camera are 0.8, 0.6, and 0.7, respectively. What is the overall MTF of the camera?

Answer

$$\begin{aligned} \text{MTF} &= 0.8 \times 0.6 \times 0.7 \\ &= 0.34 \end{aligned}$$

Sensitivity

Sensitivity of a gamma camera is defined as the number of counts per unit time detected by the device for each unit of activity present in a source. It is normally expressed in counts per second per microcurie (cps/μCi or cps/MBq). Sensitivity depends on the geometric efficiency of the collimator, the intrinsic photopeak efficiency of the detector, PHA discriminator settings, and the dead time of the system. Intrinsic photopeak efficiency of a detector (Chapter 8), PHA discriminator settings (Chapters 8 and 9), and the dead time (Chapter 8) have been discussed previously. Briefly,

(a) the intrinsic photopeak efficiency of a detector decreases with increasing photon energy and with increasing source-to-detector distance (see Fig. 8.9a) but increases with the thickness of the detector (see Fig. 8.8). Most modern cameras have 0.95 cm thick NaI(Tl) crystals. The photopeak efficiency of these crystals is about 90 % for 140-keV photons of ^{99m}Tc and about 30 % for 364-keV photons of ^{131}I.
(b) A narrow window setting on the PHA reduces the counts measured and therefore compromises the counting efficiency.
(c) Counts are lost when counting a high-activity sample using a device with a long dead time, and hence the counting efficiency is reduced.

Sensitivity of a gamma camera is most affected by the collimator efficiency, which is described next.

Collimator Efficiency

Collimator efficiency, or geometric efficiency (E_g), is defined as the number of γ-ray photons passing through the collimator holes per unit activity present in a source. For parallel-hole collimators (see Fig. 10.1), it is given by

$$E_g = K^2 \cdot \frac{d^4}{t_e^2 (d + a)^2} \tag{10.8}$$

where d is the hole diameter, t_e is the effective length of the collimator hole defined before, and a is the septal thickness. The constant K is a function of the shape and arrangement of holes in the collimator and varies between 0.24 for round holes in a hexagonal array to 0.28 for square holes in a square array.

The collimator efficiency for parallel-hole collimators increases with increasing diameter of the collimator holes and decreases with increasing collimator thickness (t) and septal thickness (a), which is quite opposite to spatial resolution (see Eq. (10.2)). Thus, *for a given collimator, as the spatial resolution of a system increases, its sensitivity decreases, and vice versa*. Accordingly, if high-resolution images are required for a test, then high-resolution collimators should be used, whereas in dynamic studies such as the renal flow measurement, high sensitivity collimators need to be used for increased counts in short-exposure images at the sacrifice of resolution. The sensitivity values of different parallel-hole collimators are given in Table 10.2 Note that collimator efficiency, E_g, for parallel-hole collimators is not affected by the source-to-detector distance for an extended planar source such as radioactive patients; that is, it essentially remains the same at different distances from the detector. Collimator efficiency varies with different types of collimators, and the values are shown as a function of source-to-collimator distance in Fig. 10.9.

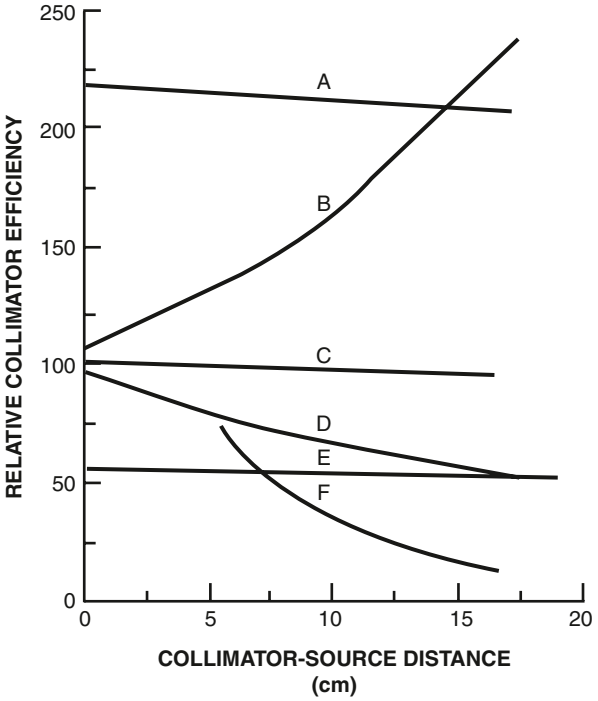

FIG. 10.9. Variation of collimator or geometric efficiency with source-to-collimator distance for various collimators. (*A*) High sensitivity parallel-hole. (*B*) Converging. (*C*) All purpose parallel-hole. (*D*) Diverging. (*E*) High resolution parallel-hole. (*F*) Pinhole. (From Rollo FD, Harris CC. Factors affecting image formation. In: Rollo FD, ed. *Nuclear Medicine Physics. Instrumentation and Agents*. St. Louis: Mosby; 1977. 407. Modified from Moyer RA. J Nucl Med. 1974; 15:59)

Uniformity

It is always expected that a gamma camera should yield a uniform response throughout the field of view. That is, a point source counted at different locations in the field of view should give the same count rate by the detector at all locations. However, even properly tuned gamma cameras produce nonuniform images with count density variations of as much as 10 %. Such nonuniformity adds to the degradation of the spatial resolution of the system.

The nonuniformity in detector response arises from several factors: (a) variations in PM tube response, (b) nonlinearity in *X*, *Y*-positioning of pulses across the field of view, and (c) edge packing. While factor (c) is preventable as discussed below, factors (a) and (b) are the leading causes of deterioration in uniformity and special attention is needed to remedy them.

Pulse-Height Variation

As already mentioned in Chapter 8, there are variations in the light production from γ-ray interaction in the detector, light transmission to PM tubes, and in the pulse formation in PM tubes. These variations result in pulses of different amplitude. Because there are many PM tubes across the detector, the amplitude of the pulses will vary from location to location (i.e., from PM tube to PM tube) across the detector even with a fixed energy window. These variations in PM tube response contribute significantly to the nonuniformity of the detector response.

This part of nonuniformity is corrected by acquiring an image using a well-tuned gamma camera and a ^{99m}Tc point source that is placed at a distance of five times the detector's FOV. An intrinsic image (without the collimator) is acquired using the appropriate window and stored in a 128×128 matrix. The pulse height in each (X, Y) pixel is determined and stored in a 128×128 look-up table. In subsequent patient studies, a microprocessor compares the pulse height in each pixel of the patient image with the corresponding value in the look-up table, and then either moves the energy window or adjusts the pulse height to compensate for the variations. This is performed in real-time during the data collection in patient studies and should be carried out for each radionuclide.

Nonlinearity

The spatial nonlinearities are systematic errors in the positioning of *X*-, *Y*-coordinates of pulses in the image and result from local count compression or expansion. For example, when a radioactive source is moved across from the edge to the center of a PM tube, counts are compressed toward the center. The line sources in front of the PM tubes are found to be bent inward (pincushion distortion) and those between the PM tubes appear to be bent outward (barrel distortion) as illustrated in Fig. 10.10.

The spatial distortions due to nonlinearity are corrected by microprocessors built into modern cameras that use correction matrices. Nonlinearity correction

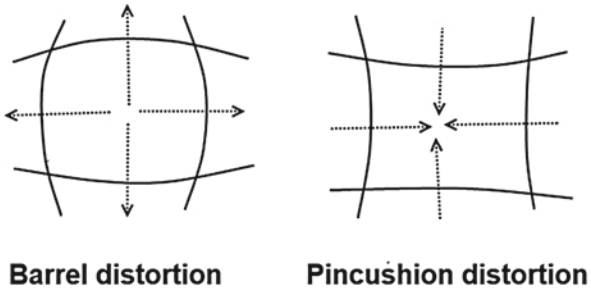

FIG. 10.10. Illustration of *barrel* and *pincushion distortions* of *straight line* objects.

factors are generated by calculating the spatial shift of the observed position of an event from its actual position. An intrinsic image (without collimator) is taken using a line or orthogonal hole test pattern and a source of radioactivity of interest placed at a distance five times the detector's FOV. The test pattern is placed directly on the detector, and an image is stored in a 128×128 matrix. The actual location (X, Y) of each pixel is known and the corresponding location on the image is measured. The variations in X, Y for all pixels are calculated as correction factors and are normally supplied by the manufacturer in the form of a look-up table. These correction factors are subsequently applied in real-time to each detected event to move it to the actual position during patient imaging. This is performed for all events throughout the field.

As stated above, modern cameras include two look-up matrices, the pulse-height correction and the linearity correction, to compensate for variations in the overall uniformity of images. As the camera slowly drifts over time, the correction tables have to be updated for proper correction of the patient scan. The exact frequency of reacquiring the correction tables depends on stability of the camera and varies with the manufacturer. The pulse-height correction tables require more frequent acquisitions, whereas the linearity correction tables are typically performed by a service engineer. Different manufacturers recommend monthly to quarterly acquisition of these correction factor maps.

It should be pointed out that uniformity corrections are mainly for minor variations in PM tube response across the field of view and are not a replacement for proper tuning of the gamma camera. Even though the uniformity corrections at times can correct for large nonuniformities, frequent retuning of the gamma camera is essential as these corrections affect linearity, resolution, and overall sensitivity of the camera. However, in modern cameras, uniformity has improved considerably with better attachment of the PM tubes to the detector and the use of PM tubes with higher quantum efficiency.

Edge Packing

Edge packing is seen around the edge of an image as a bright ring and results in nonuniformity of the image. This results from the fact that more light photons are

reflected near the edge of the detector to the PM tube. Normally a 5-cm wide lead ring is attached around the edge of the collimator to mask this effect. In modern cameras, electronic masking is employed.

Gamma Camera Tuning

Nonlinearity and pulse-height correction factors are generated with properly balanced PM tubes, and for them to work accurately, the PM tubes must be maintained properly balanced or "tuned." Changes can occur over time in the gain of the PM tubes and other electronic circuits that can invalidate these factors. Most modern cameras have circuits to monitor the PM tube gains and automatically can make minor adjustments using uniformity corrections. Still they need routine maintenance of tuning monthly or quarterly.

The methods of tuning of the gamma camera vary from manufacturer to manufacturer. One method of tuning involves the use of a ^{99m}Tc source in front of the camera and then obtaining the pulse-height spectrum for each PM tube. If a photopeak shift in a PM tube is seen from the original value in a PM tube, the preamplifier gain is adjusted. This technique was employed in earlier models of the gamma camera.

Some manufacturers use a split-window technique for each PM tube with two narrow tuning windows set on the high side of the photopeak to minimize the scattered radiation. The source of radiation can be either the radiation from the patient or an external radioactive source, for example, ^{99m}Tc. Counts are collected in the two windows for each PM tube and the ratios are calculated, which are stored in look-up tables and should be constant over time for each well-tuned PM tube. Deviation of the ratio from the constant value in subsequent patient studies indicates a drift in the gain of the PM tube, which is then adjusted electronically.

In another method, once a week each PM tube of the camera is tuned up with a radioactive source followed by illumination of the crystal with a light-emitting diode (LED) attached to each PM tube. The LED is pulsed at a high frequency and the response of each PM tube is recorded as a reference value. Subsequently, the illumination of the detector is carried out daily by the LED optical system, and the PM tube response is measured and compared with the reference value. If there is any drift, the gain is adjusted. Tuning should be performed separately for each radionuclide.

Effects of High Counting Rates

As discussed in Chapter 8, the scintillation cameras suffer count losses at high counting rates due to pulse pileup. Pulse pileup results from the detection by the camera of two events simultaneously as one event with amplitude different from

that of either original event. If one or both of the events are photopeaks, then the amplitude of the new event will be outside the pulse-height window setting and so the event will be rejected resulting in a loss of a count. If, however, two Compton scattered photons are processed together to produce an event equivalent to the photopeak in amplitude, then the event will be counted within the window setting. But the X, Y position of the event will be misplaced on the image somewhere between the locations of the two events. This causes image distortion. Both count loss and image distortion at high count rates must be taken into consideration in evaluating the performance of different cameras.

Several techniques are employed to improve the high count rate performance of a gamma camera. In modern cameras, buffers (or derandomizers) are used in which pulses are processed one at a time, and overlapping events are kept on "hold" until the processing of the preceding event is completed. In some cameras, the dead time is shortened by shortening the time to integrate the signals from the PM tubes. Other cameras use pulse pileup rejection circuits to minimize the count loss and image distortion and thus to improve images, although they tend to increase the dead time of the camera. Recent developments include high-speed electronics that reduce the number of misplaced events and improve the image quality significantly.

Contrast

Contrast of an image is the relative differences in count densities between adjacent areas in the image corresponding to the activity distribution in an object. Contrast (C_0) gives a measure of detectability of an area, for example, abnormal tissue relative to the surrounding tissue and is expressed as

$$C_0 = \frac{A - B}{B} \tag{10.9}$$

where A and B are the count densities recorded over the abnormal tissue and surrounding tissue respectively. The count density B may be from normal tissues or background counts. It is understood from Eq. (10.9) that the greater the difference between the abnormal and the surrounding tissues, the better is the image contrast. Also it can be seen that if additional background is added throughout the image, contrast is reduced, since the numerator remains the same, while the denominator is increased. Lesions on the image are seen as either "hot" or "cold" spots with increased or decreased uptakes of radioactivity in the object meaning that C_0 can be positive or negative and therefore is expressed in absolute values.

Several factors affect the contrast of the image, namely, count density, image noise due to background activity, size of the lesion, and patient motion, and each contributes to the contrast to a varying degree and is briefly discussed below.

Count density: Count or information density is an important factor to improve the image contrast and a minimum number of counts need to be collected for reasonable contrast in the image. The higher the counts in an image, the better is the contrast. Count density depends on the amount of activity administered and the uptake in the organ of interest. Contrast is improved with increasing administered activity and also with the differential uptake between the area of interest and surrounding tissues. The optimum count density is considered to be about 1000 counts/cm^2.

Image noise: Noise is an integral part of images in nuclear medicine impairing the detectablity of lesions and has two forms: systematic or random. Systematic noise pertains to a fixed amount of variation in count rate all across the image distorting the image contrast. This may be caused by system artifacts or may arise from the radioactivity distribution in different overlapping organs such as bladder activity adding the noise to the pelvic bone image with ^{99m}Tc-MDP. Nonuniformities in the gamma camera and tomographic reconstruction of images also result in systematic noise.

Random noise, also called quantum noise, is a major component of image contrast caused by statistical variations of the background counts in and around the image and is given by the standard deviation of the background count B. Thus,

$$Noise = \sqrt{B}$$

We can express it as a fraction of the total background counts contributed to image contrast,which is called the contrast noise, C_N. Thus,

$$C_N = \frac{\sqrt{B}}{B} = \frac{1}{\sqrt{B}} \tag{10.10}$$

The percent contribution of noise is

$$\%C_N = \frac{1}{\sqrt{B}} \times 100 \tag{10.11}$$

With less number of counts, the percent standard deviation is increased compared to higher counts and hence noise is increased degrading the image contrast. Noise originates from random variations of the background count density that is composed of scattered radiations from the patient and the detector, and septal penetration of photons in the collimator. All these counts add to the noise in the image and worsen the contrast. Narrow pulse height analyzer reduces the scattered radiations, but it also reduces the counting efficiency, i.e., sensitivity of the camera. This in turn increases the percent standard deviation of counts due to low counts (Eq. 10.11) and hence the noise. An optimum 15–20 % window centered on the photopeak of interest is customarily used in routine imaging. Septal penetration is mitigated by the choice of appropriate collimators.

Although it is conceptually understandable that reducing noise or background counts minimizes the image contrast, a more appropriate parameter to consider for detectibility of a lesion is the *contrast-to-noise ratio (CNR)*, which is given by

$$CNR = \frac{C_0}{C_N} \tag{10.12}$$

Combining Eqs. (10.9) and (10.10),

$$CNR = \frac{\mathrm{A} - B}{B} \div \frac{1}{\sqrt{B}} = \frac{\mathrm{A} - B}{\sqrt{B}} \tag{10.13}$$

Cherry et al. (2003) have given a detailed discussion of this parameter and its effect on the image contrast. The larger the CNR, the better is the contrast. It is reported that a lesion should have a *CNR* of > 3–5 in order to be detected. For a given imaging setting, a minimum number of counts needs to be collected for reasonable image contrast. Even with adequate spatial resolution of an imaging device, lack of sufficient counts may give rise to poor contrast due to increased noise such that the lesion may be missed. It can be seen from Eq. (10.13), increasing the amount of administered activity or counting for a longer period of time in the case of low administered activity increases the count density and in turn, improves the *CNR* for the area of interest. However, due consideration should be given to the radiation dose to the patient from large amounts of administered activity.

Noise is more problematic in SPECT than in planar imaging, because in SPECT, counts per pixel are less than in planar imaging and also reconstruction in SPECT amplifies the noise. Reconstruction filter has a significant effect on noise and an appropriate filter should be chosen in SPECT. However, in planar imaging, overlapping structures cause more contrast degradation than in SPECT imaging, because in the latter, only images of slices are collected excluding the interfering activities from adjacent slices.

Noise is also affected by the choice of a matrix and so is the contrast. For example, for a given time of data acquisition from a source, the count density per pixel will be lower in a 128×128 matrix than in a 64×64 matrix. This will cause an increase in noise and hence a loss of contrast in a matrix of smaller pixels, which can be mitigated by counting for a longer time. This effect is more prominent in SPECT imaging because of the low count density per projection and hence per pixel, relative to planar imaging. So the choice of an acquisition matrix of appropriate size is essential.

High count rate: At high count rates, pulse pileup can degrade the image contrast. Two Compton events occurring simultaneously may add up to form the photopeak, but the event will be mispositioned somewhere between the two events and hence the distortion of the image.

Size of lesion: Image contrast to distinguish a lesion depends on its size relative to system resolution and its surrounding background. Unless a minimum size of a lesion larger than system resolution develops, contrast may not be sufficient to appreciate the lesion even at higher count density. The lesion size factor depends on the background activity surrounding it and whether it is a “cold” or “hot” lesion. A relatively small size “hot” lesion can be well contrasted against

a lower background, whereas a small "cold" lesion may be missed against surrounding tissues of increased activities.

Patient motion: Patient motion during imaging reduces the image contrast. This primarily results from the overlapping of adjacent areas by the movement of different organs. It is somewhat alleviated by restraining the patients or having them in a comfortable position.

Quality Control Tests for Gamma Cameras

To ensure high quality of images produced by imaging devices, several quality control tests must be performed routinely on gamma cameras. The frequency of tests is daily, weekly, and, for some tests, monthly, quarterly, or even annually. The most common tests are the positioning of the photopeak (peaking), uniformity, spatial resolution and linearity of the camera. These tests can be carried out with the collimator attached to the camera (*extrinsic*) or without the collimator (*intrinsic*), and should be performed for each radionuclide used in a specific clinical study. Various quality control tests and their frequency are given in Table 10.3.

In the intrinsic method, the source of a particular radionuclide containing approximately 100–200 μCi (3.7–7.4 MBq) in a syringe is normally placed at a distance of four to five times the detector field of view to ensure uniform irradiation of the detector (Fig. 10.11a). Because the collimator is removed, the integrity of the collimator cannot be assessed by this method.

In the extrinsic method, a sheet source is used made of plastic containing the radionuclide of interest. Because ^{99m}Tc is most commonly used in nuclear medicine studies, a ^{99m}Tc sheet source can be prepared by adding several millicuries of ^{99m}Tc activity to a water-filled plastic sheet container. The source should be thoroughly mixed and free of air bubbles. Because of the inconvenience of daily preparation of the ^{99m}Tc sheet source and radiation exposure to the technologist during preparation, an alternative solid ^{57}Co sheet source is used, which is commercially available in rectangular or circular forms. ^{57}Co has a longer half-life (~270d) and emits photons of 122 keV and 136 keV, which are equivalent to the 140 keV photons of ^{99m}Tc. These sources, typically made with 10 mCi (370 MBq) of ^{57}Co, are also called *flood* sources and most commonly used for over a period of one to two years. The source is placed on the collimator attached to the detec-

TABLE 10.3. Recommended quality control tests and their frequency.

Test	Frequency
Peaking of photopeak	Daily
Intrinsic or extrinsic uniformity	Daily
Spatial resolution and linearity	Weekly
Center of rotation (See SPECT section later)	Monthly
High-count uniformity calibration	Monthly
Collimator integrity	Semiannually
Overall system performance (see SPECT)	Semiannually

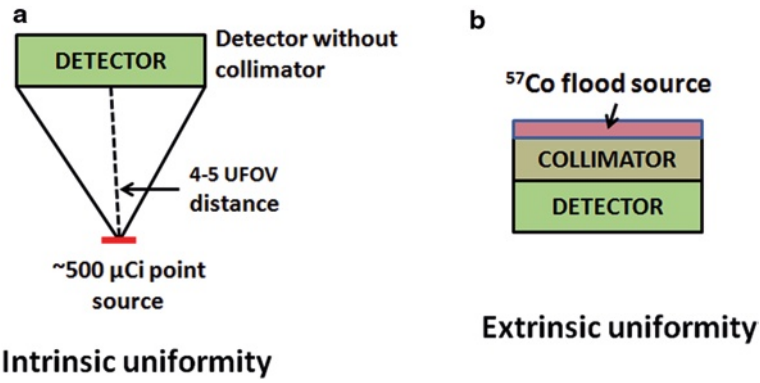

FIG. 10.11. Arrangement of detector, collimator and ^{57}Co flood source. **a** Intrinsic method without collimator. **b** Extrinsic method with collimator.

tor (Fig. 10.11b) and an image is taken. The use of these sources in the extrinsic method provides information on PM tubes as well as any structural imperfections in the collimator. Because ^{57}Co activity decays over time, counting time increases with time to accumulate sufficient counts for the image. An additional problem with ^{57}Co source is the contamination with small amounts of ^{56}Co and ^{58}Co ($t_{1/2}$ = 70–80 days) emitting high energy γ rays (>500 keV). This contamination is more prominent in the new sources, because of the short half-life but fades away over time and can be mitigated by using a medium-energy collimator.

Daily Checks

Positioning of Photopeak

Positioning, often called peaking, of the photopeak must be done daily or as needed for each radionuclide used in the clinical study to center the PHA window on the center of the photopeak. In older analog cameras, a source of radioactivity of interest is placed on the collimator attached to the detector (extrinsic) and the high voltage on the PM tube is adjusted to center the energy window on the photopeak. For ^{99m}Tc, typically 1 mCi (37 MBq) of the activity in a syringe is used as a source for peaking and a 20 % window is set around 140 keV. Peaking for ^{111}In, ^{67}Ga, ^{123}I, ^{201}Tl, and so on must be done separately, as needed.

In modern cameras, peaking is performed automatically by menu-driven protocol-based software provided by the manufacturer. Initially at the time of the camera set-up, the photopeak window is set with a ^{99m}Tc source using the intrinsic method. Subsequently the daily check of the position of the photopeak is performed with a ^{57}Co flood source by the extrinsic method using a low-energy high-resolution collimator. If the peak shift is more than 10 %, the camera must be tuned. Tuning is performed by the computer program by repeaking of the camera with a ^{99m}Tc source placed at least 30 cm away from the detector and without a collimator (intrinsic method). The same method is applied for other radionuclides.

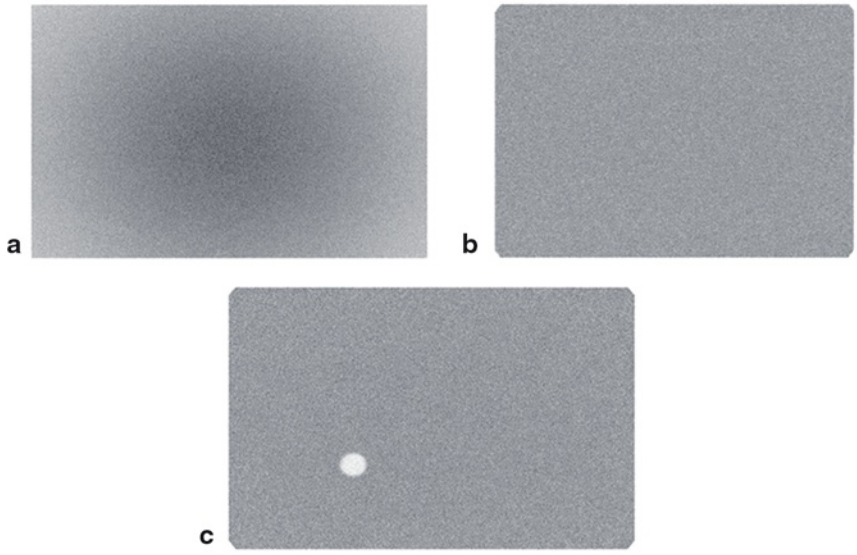

FIG. 10.12. Images of a ^{57}Co flood source. **a** Intrinsic uniformity image showing less activity distribution at the periphery due to greater distance traveled by the photons. **b** Extrinsic uniformity image. **c** Nonuniform extrinsic image showing a defective PM tube.

Uniformity

The uniformity of the detector response is checked daily by either the intrinsic method using a ~100–200 μCi (3.7–7.4 MBq) ^{99m}Tc source or the extrinsic method using a 10 mCi (370 MBq) ^{57}Co flood source, although for convenience the latter method is routinely employed. The flood source is placed on the low-energy high-resolution collimator attached to the detector and an energy window of 20 % is set around the photopeak. An image is acquired with about five million counts and then assessed for uniformity and linearity (tube pattern), integrity of the PM tubes, artifacts and so on by visual inspection (Fig. 10.12). Nonuniformity exceeding 5–10 % is detectable by human eyes. Integral uniformity and differential uniformity are then calculated (see below) for both the useful field of view (UFOV) and central field of view (CFOV). The UFOV is the area of the field of view obtained after masking the edge of the detector to minimize edge packing effect, and the CFOV is the area whose linear dimensions (length x width for rectangular detector, or diameter for circular detector) are reduced to 75 % of those of the UFOV, as illustrated in Fig. 10.13.

According to the NEMA protocol, the intrinsic method is employed to calculate the integral and differential uniformities using a 100–200 μCi (3.7–7.4 MBq) ^{99m}Tc source. Before calculating these parameters, the acquisition matrix is adjusted so that the pixel size is about 6 ± 1.9 mm and then smoothed with a nine-point filter. Integral uniformity (*IU*) is defined by

$$IU = \frac{C_{max} - C_{min}}{C_{max} + C_{min}} \times 100 \qquad (10.14)$$

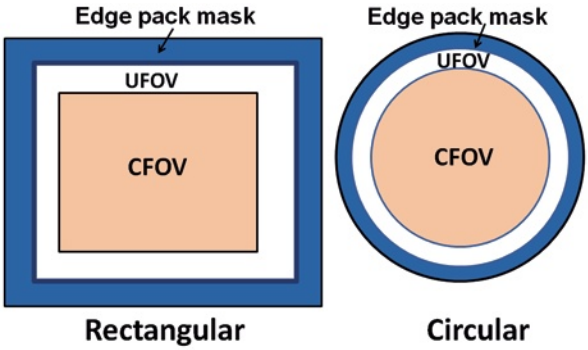

FIG. 10.13. Definition of UFOV and CFOV.

where C_{max} and C_{min} are the maximum and minimum pixel counts across the image. Differential uniformity (DU) is given by

$$DU = \frac{\text{high count} - \text{low count}}{\text{high count} + \text{low count}} \times 100 \tag{10.15}$$

where "high" and "low" are the maximum and minimum differences in counts over five contiguous pixels in all rows and columns of the matrix. The computer program calculates both IU and DU values, which should be less than 4–6 %; otherwise, the camera needs to be tuned. Note that the *IU* is a global parameter, whereas the *DU* is a regional parameter indicating the nonuniformities in pixel counts.

Weekly Checks

Spatial Resolution and Linearity

The spatial resolution and linearity of the gamma camera is checked weekly by using a bar phantom (Fig. 10.3). The bar phantom is placed on the detector head with a low-energy high-resolution collimator attached (extrinsic), and a flood source of ~10 mCi (370 MBq) of ^{57}Co is placed on the top of the bar phantom. An image is taken with approximately 10 million counts and visually inspected to check the linearity and separation of the smallest bars (Fig. 10.4). This is a qualitative method. For a quantitative method, a line spread function must be determined and then FWHM measured as discussed earlier. Although extrinsic tests are done for convenience, intrinsic tests are preferable for better accuracy.

Monthly Checks

High-count-uniformity Calibration

A high-count-uniformity flood image (30 million counts) is acquired extrinsically using a 10 mCi ^{57}Co flood source or intrinsically using 100 μCi (3.7 MBq) ^{99m}Tc.

It is performed monthly or quarterly as recommended by the manufacturer. A very high count uniformity calibration with 100 million counts is carried out annually. These high count flood images are stored and used for nonuniformity correction, as needed, and should be done with each radionuclide used and each collimator employed. Because of the longer time required for high counts to be acquired, data are often collected overnight.

Collimator Integrity

Although collimators made of lead are heavy and robust, they are prone to dent and damage due to the ductile nature of lead. Any dent or damage on the collimator will appear as an artifact on the image taken using it. Collimator is normally encased in a frame and there should be no gap between the frame and the collimator. Although most collimator defects can be seen on extrinsic images, all collimators should be checked by visual inspection at least monthly for their structural integrity as to the hole parameters, bolts, frames and proper fit to the detector head.

Annual, Semiannual, or As-Needed Checks

Tuning of the camera is performed monthly or quarterly by the protocols described earlier. Other essential parameters such as energy resolution, high count rate response, multiwindow registration (e.g., ^{111}In and ^{67}Ga with multiple photons) and sensitivity should be evaluated at least annually or as needed after extensive modification or repair of the camera.

In addition, tests on accessories such as computers, multiformat cameras, scanning tables, rotation of gantry, and so on should be performed periodically. Furthermore, all tests must be documented in a record book with pertinent information, such as the date, time, total counts, window settings, the type of radioactive source, the type of camera, and initials of the technologist performing the tests.

Questions

1. (a) Define the spatial resolution of a gamma camera.
   (b) What are the different components of the spatial resolution?
   (c) A system with a spatial resolution of 5 mm is better than a system with a spatial resolution of 8 mm. True or false?
2. The intrinsic resolution of a gamma camera depends on:
   (a) The thickness of the NaI(Tl) detector. True or false?
   (b) The energy of the γ-ray. True or false?
   (c) The width of the pulse-height window. True or false?
   (d) The number of counts collected. True or false?
3. (a) What is the best photon energy for imaging with a gamma camera?
   (b) Why is a thinner NaI(Tl) detector used in a gamma camera?

(c) Intrinsic resolution improves with higher γ-ray energy. True or false?
(d) Spatial resolution of a gamma camera improves as the number of photomultiplier tubes is increased. True or false?

4. For a gamma camera with a parallel-hole collimator,
   (a) The spatial resolution increases with decreasing detector thickness. True or false?
   (b) The collimator efficiency decreases with increasing collimator length. True or false?
   (c) The spatial resolution increases with decreasing collimator length. True or false?
   (d) High-energy collimators have higher efficiency and resolution than low-energy collimators. True or false?
   (e) The best resolution is obtained at the face of the parallel-hole collimator. True or false?
5. What are the effects of the following factors on the spatial resolution and sensitivity of a gamma camera?
   (a) Photomultiplier (PM) tubes with higher quantum efficiency
   (b) A wider "window" on the pulse-height analyzer (PHA)
   (c) Increasing the activity of ^{99m}Tc from 5 mCi (185 MBq) to 15 mCi (555 MBq)
   (d) Increasing the diameter of the collimator hole
   (e) Adding more tissue between the collimator face and the patient's organ
   (f) Using a diverging collimator
   (g) Increasing the source-to-collimator distance for a parallel-hole collimator
   (h) Using a γ-ray of higher energy, which penetrates the septum of the collimator
6. (a) In routine practice, how is the spatial resolution of a gamma camera checked?
   (b) The full width at half maximum of the line spread function of a gamma camera does not give a true picture of spatial resolution. Why?
   (c) What is the modulation transfer function (MTF) of a system?
   (d) A system gives the best spatial resolution when its MTF is equal to 1. True or false?
   (e) If PM tubes and the PHA of a gamma camera have MTFs of 0.5 and 0.7 at a certain spatial frequency, what is the overall MTF of the camera?
   (f) As the sensitivity of a gamma camera increases, its spatial resolution decreases. True or false?
   (g) The collimator efficiency of a parallel-hole collimator is not affected by the source-to-detector distance. True or false?
7. (a) What is the primary cause of nonuniformity in an image?
   (b) What is edge packing?
   (c) How is the nonuniformity in an image corrected?
8. (a) What is the contrast of an image?
   (b) What are the different factors that affect the contrast of an image?
   (c) How does pulse pileup affect the contrast?

(d) Is contrast or spatial resolution affected by increasing the administered activity?

9. (a) What are the daily and weekly tests performed for gamma cameras?
   (b) What is meant by extrinsic and intrinsic tests?
10. If count density in a lesion is 77,000 and the adjacent background is 35,000, calculate
    (a) The contrast
    (b) The noise, and
    (c) The contrast-to-noise ratio

References and Suggested Readings

Bushberg JT, Seibert JA, Leidholdt EM Jr, Boone JM. *The Essential Physics of Medical Imaging*. 3rd ed. Philadelphia: Lippincott Williams & Wilkins; 2011.

Cherry SR, Sorensen JA, Phelps ME. *Physics in Nuclear Medicine*. 3rd ed. Philadelphia: W.B. Saunders; 2003

Erickson J. Imaging systems. In: Harbert J, da Rocha AFG, ed. *Textbook of Nuclear Medicine. Volume I. Basic Science*. Philadelphia: Lea & Febiger; 1984:105.

Groch MW, Erwin WD. Single-photon emission computed tomography in the year 2001: Instrumentation and quality control. J Nucl Med Technol. 2001;29:12.

Murphy PH. Acceptance testing and quality control of gamma cameras, including SPECT. *J Nucl Med* 1987;28:1221.

Rollo FD. Evaluating imaging devices. In: Rollo FD, ed. *Nuclear Physics, Instrumentation and Agents*. St. Louis: Mosby; 1977:436.

Rollo FD, Harris CC. Factors affecting image formation. In: Rollo FD, ed. *Nuclear Physics, Instrumentation and Agents*. St. Louis: Mosby; 1977:387.

11
Digital Computers in Nuclear Medicine

Digital computers were introduced in nuclear medicine practice in the mid-1960s, but did not become an integral part in both imaging and nonimaging applications until the mid-1970s. In imaging modalities, the computers are used to quantitate the distribution of radiopharmaceuticals in an object both spatially and temporally. Both data acquisition and image processing in scintigraphy are accomplished by digital computers. In nonimaging applications, patient scheduling, archiving, inventory of supplies, management of budget, record keeping, and health physics are just a few examples of what is accomplished with the help of digital computers. Computational capabilities have advanced tremendously over the years and are still evolving, and the utility of a computer is limited only by the limitations of hardware and software.

Basics of a Computer

The basic elements of a computer are a *central processing unit* (CPU), *main memory*, *external storage* and *input/output* (I/O) devices, which are connected to one another by pathways called *buses*. The main memory stores all program instructions and acquired data, while the CPU executes all instructions given in a program. External storage includes floppy disks, CD-ROMs, DVD-ROMs, and hard drives. I/O devices include peripherals such as keyboards, mouse, video monitors, and printers, whose functions are to communicate with the computer for input of the acquired data and output of the processed data. A typical setup of a computer is illustrated in Fig. 11.1.

The signals, i.e., electrical pulses from a scintillation camera, are obtained in analog form and are digitized by the digital computers for further processing and storage. Digital computers operate with *binary* numbers using only two digits, 0 and 1, as opposed to 10 digits 0–9 in the decimal system. The basic unit of the binary system is a *bit* (binary digit) that is either 0 or 1. The binary numbers are expressed by placing 0's and 1's in a row, e.g., 10101, which are equal to a sum of a series of powers of two, as opposed to decimal numbers that are expressed in powers of 10.

G. B. Saha, *Physics and Radiobiology of Nuclear Medicine,*
DOI 10.1007/978-1-4614-4012-3_11,

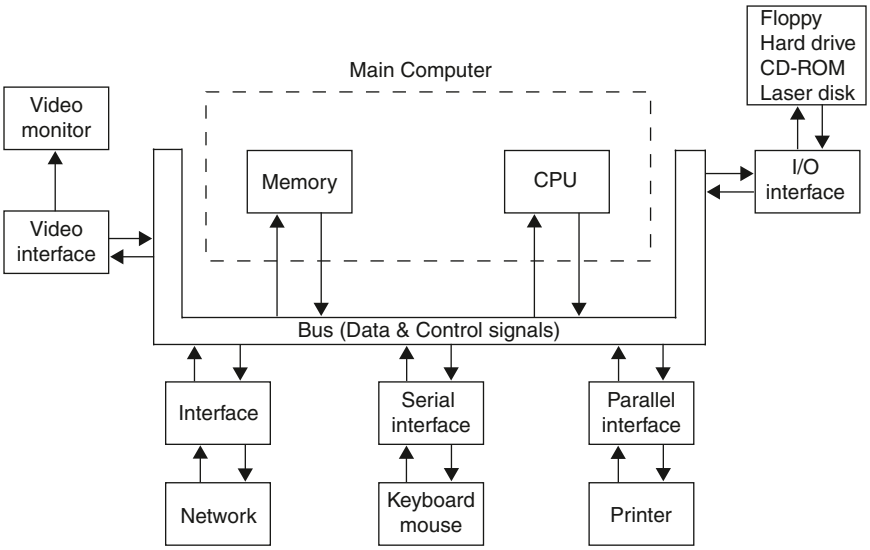

FIG. 11.1. Basic components of a computer.

Thus, the binary number 10101 ($1 \times 2^4 + 0 \times 2^3 + 1 \times 2^2 + 0 \times 2^1 + 1 \times 2^0$) is equal to the decimal number 21, which is given as $2 \times 10^1 + 1 \times 10^0$ in the decimal system.

The bits, 1 and 0, are represented by the "on" or "off" states of many transistor components present in the computer memory. A two-bit number can be expressed in 2^2, or four, ways (00, 01, 10, 11) corresponding to decimal numbers, 0, 1, 2, 3; a three-bit number can be expressed in 2^3, or eight, ways (000, 001, 010, 011, 100, 101, 110, 111) corresponding to decimal numbers 0, 1, 2,…7, and an *n*-bit number can be expressed in 2^n ways corresponding to decimal numbers from 0 to $2^n - 1$. In computer nomenclature, a *byte* of memory is equal to eight bits that can store up to 2^8, i.e., 0–255, units of information. Similarly, a *word* of memory consists of 16 bits or two bytes and can store up to 2^{16}, i.e., 0–65,535, units of information. In newer computers, a word can consist of 32 or 64 bits, allowing more counts to be stored in memory.

Central Processing Unit

The CPU, also called the microprocessor, performs all control, logic, and arithmetic operations in a computer. A computer program is a set of sequential instructions for the computer to perform with essential data inserted whenever appropriate. The CPU retrieves the instructions and data from memory storage, executes the instructions sequentially, and displays or stores the results in appropriate locations. Transfer of data from one location to another is performed by the CPU using buses, which are essentially a set of electrical connections.

How fast a program is executed depends on the speed of the computer operation, which increases with the faster electrical components of the CPU. The ef-

ficiency of the computer operation is further increased by using parallel transfer of data (where many transfers are performed simultaneously) rather than serial transfer (where only one transfer is carried out at a time).

Computer Memory

The memory of a computer is a section assigned for temporary storage of data during the operation of a program. The program instructions and processed data are all stored in the computer memory with the help of the CPU. When the CPU sends data to the memory, it writes the data into the memory. If the CPU retrieves data from the memory, it is then said to read the data from the memory. The memory can be of two types: random access memory (RAM) and read-only memory (ROM). RAM has the advantage of both write and read capacity; however, the data stored in it is lost when the computer is shutoff or the electrical power is lost. With larger RAMs, computation time becomes shorter. On the other hand, data stored in ROMs such as CD-ROMs, DVD-ROMs, etc. cannot be erased by electrical failure or computer shutoff.

External Storage Devices

Floppy disks, hard disk drives, CD-ROMs, DVD-ROMs, magnetic tapes, and optical (laser) disks are varieties of external storage devices that are commonly used for storage of programs and data. Each of them has variable storage space. Hard drives are installed virtually in all computers for internal storage of the programs and data. Floppy disks are commonly used for storing data externally as backup copies, although in some applications programs and data can be stored for input into the computer for execution. While internal or external hard drives have the storage capacity of hundreds of gigabytes, floppy disks can only store up to a few megabytes and are getting out of use. Currently, CD-ROMs are available with capacities of 650–700 MB and DVD-ROMs with 4.7–9 GB. Magnetic tapes and laser optical disks have large storage space in compact form and can be utilized primarily for archiving of patient data that can be retrieved for future reference.

Input/Output Devices

Input/output (I/O) devices are essential for input of the initial data and for output of the processed data. Input and output of data are carried out by the use of acquisition and video interfaces via serial or parallel buses. The keyboard and the mouse are the most common input devices used in computers, although joysticks, light pens, and trackballs are occasionally used as input devices. While the keyboard is essential for the input of alphanumeric data such as patient identification, date, time, and operator's name, the mouse and trackballs are used to select items from the menu. Light pens, a mouse, and touch screens are often used for the selection of regions of interest (ROI) in an image.

Common output devices include display screens (video monitor) for texts, images or graphics, and printers for printing. Display screens normally have a capability of a gray scale or a color scale for comparison between the intensities or amplitudes of different regions of the image.

Operation of a Computer

A computer operates according to instructions provided by an operator. These instructions are given in the form of one or more programs. A collection of programs is called the software, which is developed by specialists according to the specific need for a project. The most essential program for the operation of a computer is the so-called operating system (OS) such as Windows, Unix, and Linux. The utility of the OS is to facilitate communication between the computer and operator's instructions. The operating system transfers the program instructions from the input device to the memory, commands the CPU to carry out the specific instruction and returns the data to the output devices. Other utilities of this system include file transfer from one location to another, storing data in the external storage device, and display of the data.

Data must be provided as input to the computer for processing, and in nuclear medicine they are available in the form of counts or voltage pulses obtained from scintigraphic studies. Data are processed according to instructions in the software program, and the processed data are then stored in computer memory or external storage spaces or displayed on video monitors. The time to complete a task by the computer depends on a number of factors such as the speed of the CPU, the size of the RAM, serial or parallel processing of data, and the data transfer rates of the I/O devices. The faster CPU, the larger size of RAM and the parallel buses provide speedy computation.

Digitization of Analog Data

In nuclear medicine, signals from a gamma camera are acquired in analog form, which are digitized before storing and further processing by the computer. Conversion of analog signals to discrete digital values is performed by the so-called *analog-to-digital converters* (ADCs) and the process is called digitization.

While analog signals are continuous in time, digital signals consist of a fixed number of bits produced by the ADC by sampling a selected number of time points in the analog signal. ADCs are available as 8-, 10-, 12-, or 16-bit depending on the number of bits they produce in the digital signal from the analog signal. While the analog signals can be distorted by the electronic noise, there is some inherent loss of signal information as a result of digitization, i.e., due to different time-point selections during the analog-to-digital conversion. This arises from the fact that there is a likelihood of a small fraction of the signal being lost during the conversion of a continuous analog signal to discrete digital values. However, higher bit ADCs minimize this loss by producing a large number of bits from each

analog signal. The faster ADCs can handle higher count rates. The slower ADCs increase the dead time of the system and hence are good for low count rates only.

Digital-to-Analog Conversion

For video displays, data must be in the analog form, and therefore digitized data must be converted back to analog data. This is performed by units, called the digital-to-analog converters (DACs), similar to the ADCs. DACs are connected to the computer via video interface cards, and the speed of digital-to-analog conversion depends on the speed of various electrical components included in its operation.

Digital Images

Digital images are characterized by two quantities: matrix size and pixel depth. The computer memory approximates the area of the detector in a gamma camera as a square matrix of a definite size that can range from 32×32 to 1024×1024 with 1024 (1 K) to 1,048,576 (1 M) picture elements, called *pixels*, respectively. The size of a matrix is selected by the operator, depending on the type of task to be performed and is approximated to the field of view (FOV). Each pixel corresponds to a specific location in the detector. As discussed in Chapter 9, the *X*- and *Y*-pulses are obtained in the analog form from the photomultiplier (PM) tube, which originate from the interaction of γ-rays in the detector. The *X*- and *Y*-analog pulses are digitized by the ADC and stored in the appropriate pixel of the matrix. How many counts can be stored in a pixel depends on the depth of the pixel, which is represented by a byte or a word. Thus, a 1-byte pixel could record up to 2^8, or 256, events, whereas a 1-word pixel could store up to 2^{16}, or 65,536, events.

The pixel size, which depends on the choice of the matrix size for a study, is an important factor that affects the spatial resolution of a digital image. The field of view is approximated to the matrix size; therefore the pixel size is calculated by dividing the FOV by the number of pixels across the matrix. Thus if an image of 250×250 mm FOV is obtained in a matrix of 128×128 mm, the pixel size would be $250/128 \approx 2$ mm. If the matrix size is changed to 64×64, then the pixel size would be ~4 mm. Often, a *zoom factor* is applied during data acquisition to improve spatial resolution because it reduces the pixel size. Overall, the pixel size d can be calculated as

$$d = FOV/(z \times N) \tag{11.1}$$

where z is the zoom factor (1.2, 2.0, etc.,) and N is the number of pixels across the matrix. The use of a zoom factor of, say, 2, reduces the pixel size by half, improving the spatial resolution, but counts per pixel are reduced thus increasing the noise on the image (see later).

The choice of pixel size and zoom factor is limited by the spatial resolution of the imaging device, particularly in tomographic systems. Ideally, the pixel size

should be less than 1/3 of the expected spatial resolution of the SPECT system, measured at the center of rotation. That is,

$$d \leq FWHM/3 \tag{11.2}$$

where *FWHM* is the full width at half maximum of the line spread function of the imaging system. If the expected system resolution is 12.9 mm, then the pixel size in the matrix should be less than 4.3 mm. Pixel size larger than this limit would degrade the image.

For a typical SPECT gamma camera, the FOV size is 400–500 mm across and the spatial resolution is of the order of 12 mm. Thus, the pixel size in a 64×64 matrix is 400/64 or 500/64 = 6.25 or 7 mm, which is nearly equal to or less than the 1/3 of the spatial resolution of the SPECT system. Thus, a 64×64 matrix should be good enough in most SPECT imaging. Using a 128×128 matrix (pixel size is 3.13 mm, which is much less than 1/3 of the system resolution), would improve the spatial resolution significantly. However, as mentioned before, the counts in each pixel would be reduced by 1/4, as the total counts are distributed over four times the pixels, compared to a 64×64 matrix. Thus the noise increases in the image and so the signal-to-noise ratio decreases causing degradation in image contrast.

Application of Computers in Nuclear Medicine

Digital Data Acquisition

The *X*- and *Y*-signals obtained in scintigraphic studies in nuclear medicine are digitized by ADCs in the computer and stored in one of two ways: (a) *frame mode* and (b) *list mode*. In both modes, a technique of magnification or zooming can be applied, whereby the pixel size is decreased by a zoom factor. Zoom factors typically vary from 1 to 4 in increments of 0.25.

Data acquisition in the frame mode is the most common practice in nuclear medicine and widely used in static, gated, dynamic, and single photon emission computed tomography (SPECT) studies. In this mode, a matrix is chosen that approximates the entire area of the detector so that a position (*X*, *Y*) in the detector corresponds to a pixel position in the matrix. Digitized signals (*X*, *Y*) are stored in the corresponding (*X*, *Y*) positions (pixel) of the matrix of choice in the computer. Every time a new *X*, *Y* signal arrives, it is added to the (*X*, *Y*) pixel (Fig. 11.2a). In this mode, one must specify the size and depth of the matrix, the number of frames per study, and the time of collection of data per frame or total counts to be collected. Data acquisition continues until a preselected time or total count is reached. This mode provides instant images for storage and display.

In the list mode, digitized *X*- and *Y*-signals are coded with "time marks" as they are received in sequence in time, and are stored as individual events in the

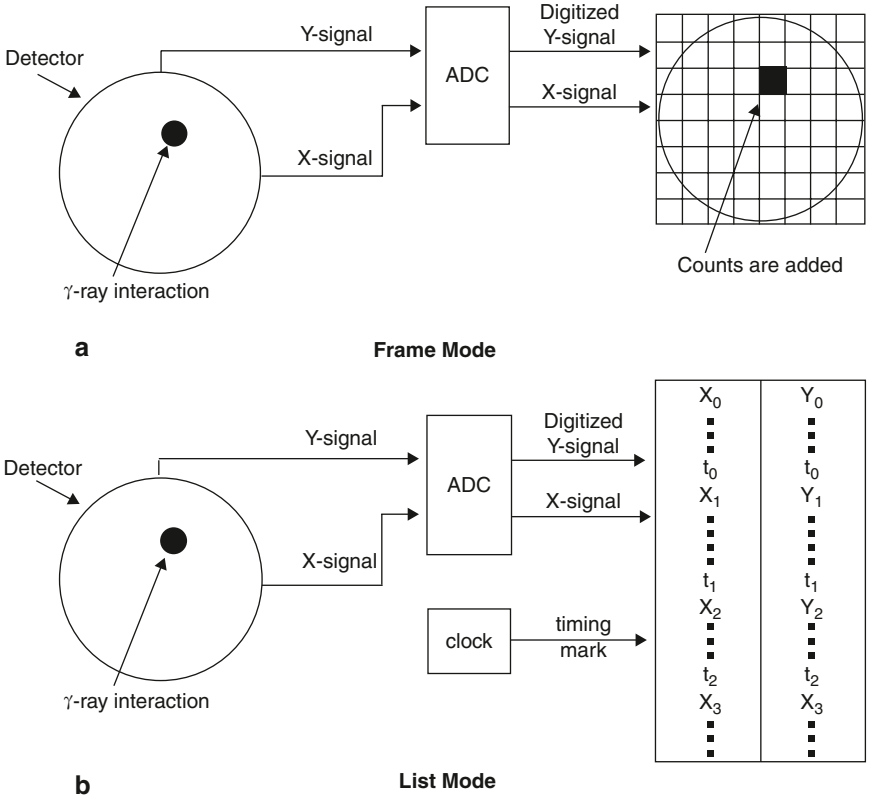

FIG. 11.2. Data acquisition in the frame mode and the list mode.

order they occur (Fig. 11.2b). After the data acquisition is completed, the data can be sorted to form images in a variety of ways to suit a specific need. Data can be manipulated by changing the matrix size and the time of acquisition per frame. Also, physiologic markers, such as the start of a cardiac cycle (e.g., the start of the R-wave) in the gated cardiac studies, can be incorporated in the list mode acquisition. Since the data are listed sequentially without overlapping each other, the bad signals from an arrhythmic cardiac cycle can be discarded, as found appropriate, in the postacquisition reformatting. Although the list mode acquisition provides wide flexibility, its major disadvantages are larger memory space and longer processing time required and unavailability of images during or immediately after the completion of the study.

Static Study

A static study is the collection of data in one view of a region of interest in an object for a preset time or preset total counts. Data are acquired in the frame mode,

and normally the matrix size is specified prior to starting the study. The choice of a matrix size depends on the field of view of the imaging system and the pixel size to give desired image resolution. For all practical purposes, a pixel size of 2–3 mm is considered appropriate for good image resolution. Thus, for large FOV scintillation cameras (>400 mm), one would need a 256×256 matrix to obtain the above pixel size. Because of the high count densities in static views, data acquisition in byte mode may overflow in individual pixels and, therefore, the word mode is usually employed.

Digital images essentially represent the count density in regions of interest in an object. How many counts should be acquired in an image? It depends on how small a region in an image is to be identified and its apparent contrast with the surrounding background. Large and high-contrast objects are easily detectable at low count densities, whereas small and low-contrast objects are difficult to delineate from the statistical noise. Count density should be optimum for desirable contrast.

Dynamic Study

In dynamic studies, a series of images are collected and each image (frame) is acquired over a certain period of time selected by the operator. While the patient's position cannot be changed during the image acquisition, the matrix size and the frame rate (time of acquisition) can be changed. The frame rate can vary from many frames per second to a single frame per hour. The acquisition of image data is buffered such that while one frame is being collected, the previous frame is stored in the external storage device (e.g., disk). Data in dynamic studies can be collected in a sequence of several phases, e.g., 1 frame per second for 1 min, then 1 frame/min for 5 min, followed by 1 frame/10 min for 2 h. The choice of frame rate for a given study depends on the kinetics of the radiotracer through the organ of interest.

The common matrix size used in dynamic studies is 64×64 or 128×128, although some loss of spatial resolution is expected with these matrices. However, 256×256 or larger matrices require larger memory size. Since counts collected per frame are low in number, the data are collected in byte mode, which obviates the need for a large memory space, and normally does not allow pixel counts to exceed 255 with little chance of counts overflow.

Gated Study

The gated study was introduced in the mid-1970s to determine the ejection fraction of the heart by acquiring two images, one at end diastole and the other at end systole. It was later substituted by continuous acquisition of data in multiple sequential images (multiple gated acquisition, MUGA) in each cardiac cycle by gating between successive cycles.

In the MUGA study, the data are acquired in synchronization with the R-wave of the cardiac cycle. The normal heart beat is about 1 beat/second, and the R-R interval is therefore about 1 s, i.e., 1000 msec. First, the R-R interval is divided into

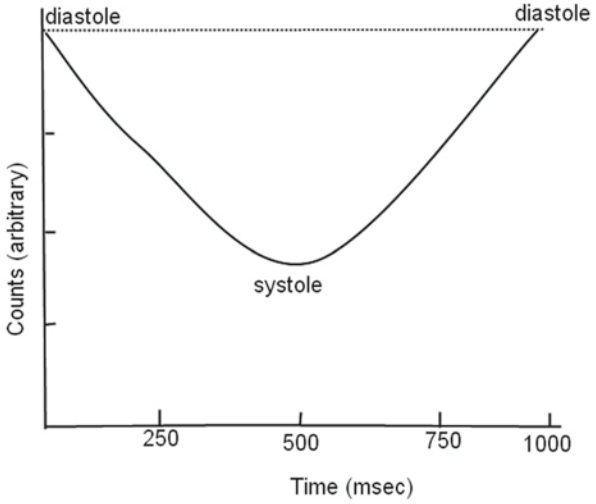

FIG. 11.3. The time-activity curve obtained in a gated study using segments of a QRS cardiac cycle.

several segments or frames (16–32 segments) depending on the number of frames one chooses to obtain. For example, with a choice of 20 frames in the R-R interval, each frame will be 50 msec long. In actual data collection, first the counts are acquired in frame 1 for 50 msec, followed by the collection of counts in frame 2 for another 50 msec, and so on. After completion of counting in all 20 frames, a new R-wave is detected, and the above sequence of counting continues until sufficient counts have been accumulated in each frame. Assuming a count rate of 10,000–20,000 counts/s in a typical cardiac study, each 50 msec frame would accumulate counts of the order of 500–1000. Normally, 64×64 or larger matrices are used for the gated study. A typical plot of the time-activity curve (TAC) is shown in Fig. 11.3, from which the ejection fraction (EF) of the heart is calculated as

$$EF(\%) = \frac{A_d - A_s}{A_d} \times 100 \tag{11.3}$$

where A_d and A_s are the end-diastolic and end-systolic activities.

The heart beat must be regular for the above method to work well. If the heart beat is irregular such as in cardiac arrhythmia, the R-R interval is sufficiently altered and the data become corrupted from R-wave to R-wave. Modern acquisition programs have been devised to reject the bad heart beat cycle. Using the list mode acquisition, bad heart beat data can be sorted out and rejected in postacquisition reformatting.

SPECT is routinely used in nuclear medicine for various organ imaging, particularly cardiac imaging. The gated SPECT study is also employed for the cardiac studies using the typical 20 frames in each R-R interval.

Reconstruction of Images

In planar imaging, the acquired data are displayed in a two-dimensional images without further processing. In tomographic imaging, data are acquired in different angular projections around the patient. The data of each projection are processed further using the methods described in Chapter 12 to reconstruct the images at different depths of the patient's organ in 3-D directions. All reconstruction methods are accomplished by the use of modern computers.

Fusion and Subtraction of Images

It has been a common practice to superimpose image data from one modality onto another for better delineation of lesions on the images. For example, computed tomography (CT) or magnetic resonance imaging (MRI) anatomical images of an organ are fused with the corresponding functional images obtained by SPECT or PET to match the functional abnormalities with the anatomical defects. Computers are well utilized to perform these superimpositions of images.

Another important utility of the computer is the subtraction of background activity from an image or one set of images from another set. An example of the latter is to subtract the interictal images obtained in epilepsy patients using ^{99m}Tc-ethyl cysteinate dimer (ECD) from those obtained in ictal period using the same radiotracer. Resultant difference images provide better delineation of epileptogenic foci in these patients.

Display

Digital images are displayed on video monitors which are either cathode ray tubes (CRT) or flat-panel type liquid crystal display (LCD) monitors. These monitors are characterized by parameters such as spatial resolution, contrast, aspect ratio, luminance, persistence, refresh rate, and dynamic range. The spatial resolution and luminance of LCD monitors are far superior to those of CRTs. These monitors are placed in what is called the workstation where nuclear physicians view, manipulate, and interpret the images using the computer.

Display can be in either grayscale (black and white) or colorscale. In either case, grading of scale is achieved by variations in counts in the pixels in the digital image. In grayscale, the number of counts in the pixel defines the brightness level of a pixel. Thus, the black and white contrast in a digital image is obtained by applying the grayscale.

Color hues are assigned to different pixels corresponding to counts stored in the individual pixels in order to provide contrast between areas on the image. In a gradient colorscale, blue, green, yellow, and red are assigned to pixels in order of increasing counts: blue to the lowest count and red to the highest count. Edges of color bands are blended to produce a gradual change over the full range of the color scale.

Often a grayscale or colorscale bar is shown on the side of the image in order to help the interpreter differentiate the image contrast. Images can be displayed

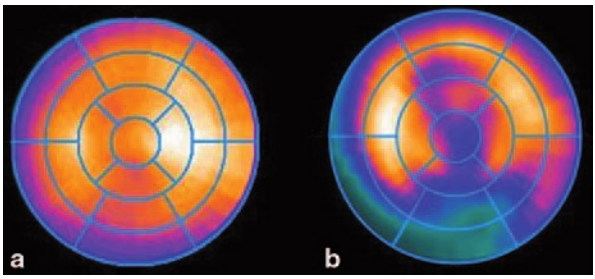

Fig. 11.4. A typical illustration of a bull's eye or polar map. **a** a normal heart, and **b** a heart with infarction. (supplied by Dr S. Shrikanthan of Cleveland Clinic Nuclear Medicine).

in transaxial (transverse), coronal (horizontal long axis), or sagittal (vertical long axis) views individually or simultaneously on the video monitor. On simultaneous display of SPECT images, a point on the image is chosen using the cursor and three images that pass through the point are displayed. New sets of images are obtained by choosing a different point on the image. Such sequential screening of images is helpful in delineating the abnormal areas on images of the patient.

Angular projections around an object computed from the 3-D tomographic data can be displayed in continuous rotation. This presents the image data in a movie or cinematographic (cine) mode, whereby a rotating 3-D image is seen on the monitor screen. This type of presentation identifies the location of a lesion in an organ in relation to other organs in the body.

In cardiac, brain, and respiratory studies, a popular technique called the *bull's eye, or polar map*, is employed in which the activities in each transverse slice are displayed on a circumferential profile. The circumferential profile of each slice is projected on a bull's-eye format where the intensity of a point in the slice represents the magnitude of the activity, and the location of the point represents the radial location of the slice (Fig. 11.4). In polar images, the activity distribution in an object is essentially unfolded from inside out, and three-dimensional data are presented in a two-dimensional format. The major advantage of this technique is that one can identify the location of the defect in relation to adjacent areas on a single image.

Software and DICOM

As already mentioned, software is a collection of instructions for the computer to perform in carrying out a particular imaging study. Different vendors develop software programs, which are proprietary to them to operate their own equipment, and it is difficult to use one vendor's software for another's equipment. Also, there are third-party companies who develop software specific for equipment of a particular vendor. To partially circumvent such situations, one may stick to one vendor all the time using the same software. However, the American College of Radiology and the National Engineering Manufacturing Association (NEMA) jointly sponsored a standard format for the software, called Digital Imaging and Communications in Medicine (DICOM), which all vendors are recommended to

adopt for compatibility among different software. Some of the standards of DICOM formats include image storage, protocols for intertransfer of data between the workstation and PACS (see later), query and retrieval of image data, print, and scheduling of data acquisition. DICOM formats are encoded in binary form. NEMA upgrades DICOM formats from time to time to meet the requirements of advancing technology and the medical community.

Essentially, vendors conform to the DICOM standard in developing their software, although compliance is voluntary. It provides a common format for imaging systems recognized by the hardware and software components of various manufacturers. This allows interoperability in the transfer of images and associated information among multiple vendors' devices. DICOM is very useful in the implementation of PACS (see below).

PACS

The modern networking of computers has offered a great advantage for exchange of information among individuals and organizations. It has been particularly useful for healthcare facilities in exchanging patient information among the physicians and hospitals. One type of network systems implemented in healthcare facilities is called the Picture Archiving and Communication System (PACS) and is solely used for the archiving and exchanging of patient information among health professionals. A PACS consists of devices to produce and store digital images electronically, workstations to view and interpret images, and a networking of these devices at different sites. Appropriate PACS software allows the interpreter to retrieve images from other locations and manipulate and interpret them as needed at his own location, and then return them with a report back to the original locations. In the absence of PACS, one can read the images only at the local facility and cannot transport them electronically to and from other facilities, if needed. PACS has improved the workflow profoundly by facilitating and expediting the transfer of information through network connections among various facilities.

In a radiology department, a small network system called the Radiology Information System (RIS) is normally implemented to maintain all types of workflow, such as image storage, patient scheduling, study type and its time of completion, image reporting, all the billing codes, and so on, within the department. Similarly, hospitals also have the Hospital Information System (HIS) that maintains similar information on patients including their demographic data, laboratory data, clinical history, and medication, and again, scheduling, tracking, reporting, and billing. A PACS can integrate both RIS and HIS for a broader exchange of information among healthcare personnel that will save time and money in healthcare operations. In such an integrated system, a referring physician can retrieve an image of a patient on his/her computer from other locations within the PACS, rather than waiting for the hardcopy from the imaging department. He/She can then correlate the images with the clinical findings with a considerable saving of time. A typical integrated PACS is shown in Fig. 11.5.

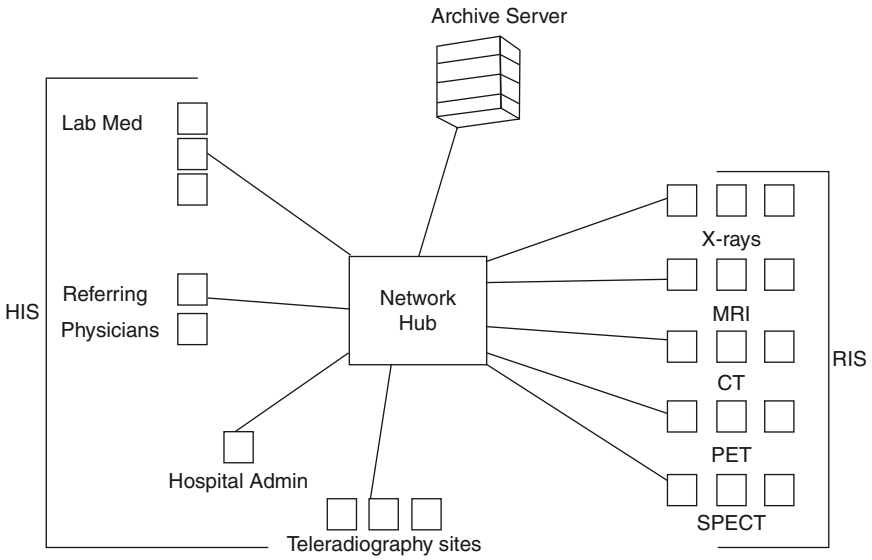

FIG.11.5. A PACS integrating the networks of HIS and RIS.

A PACS can be run by software on different operating systems such as Windows, MAC OS, Linux, or UNIX, although most PACS workstations are PC-based. PACS software must preserve confidentiality of patient information as mandated by the U.S. Hospital Insurance Portability and Accountability Act (HIPAA). The system must be reliable so that its downtime is nil. Also, the integrity of the system should be intact to avoid any medical errors in the patients' information. It should be always and easily accessible to all concerned to avoid delay in patient care. PACS software is constantly evolving to meet the new demands of healthcare professionals, and it is usually upgraded every 6–12 months. Numerous vendors (Siemens Medical, GE Healthcare, Phillips Healthcare, Spectra, Agfa Healthcare, Infinitt, Medweb, etc.) have made commercially available their copyrighted PACS software, which are claimed to be robust, reliable, and user-friendly, with an uptime of more than 99.9 %. A drawback is that there is a lack of a uniform standard among PACS software. It is desirable that the medical community, and perhaps the federal government, come up with a consensus policy similar to DICOM to make PACS uniform among different vendors.

An important application of PACS is in teleradiology which is being implemented throughout the country, and even worldwide between countries connecting through PACS' different healthcare institutions for exchange of patient care information. By virtue of teleradiology, a radiologist or a nuclear physician can retrieve and interpret diagnostic images from a distant hospital and send back the report to the original hospital. This type of practice has resulted in outsourcing practitioners at a lower cost from one country to interpret imaging scans performed in another country, where the practitioner's pay is high.

Questions

1. What is a binary number? Express the decimal number 23 in binary form.
2. What is the difference between RAM and ROM memory?
3. The speed of a computer depends on the size of RAM memory and faster electrical components in the computer. True or false?
4. Why are parallel buses more efficient than serial buses in the computer?
5. Resolution of digital images are poorer than analog images. True or false? Explain why.
6. Which of the two matrices gives better resolution—64×64 or 128×128?
7. Describe the method and advantages and disadvantages of the list mode acquisition and the frame mode acquisition.
8. Which mode would you use—byte mode or word mode—in static studies versus dynamic studies? Explain.
9. What is the essential difference between the Anger type analog camera and the "all-digital" camera?

Suggested Readings

Bushberg JT, Seibert JA, Leidholdt, Jr EM, Boone JM. *The Essential Physics of Medical Imaging*. 3rd ed. Philadelphia: Lippincott, Williams & Wilkins; 2011.

Huang HK (2004). *PACS and Imaging Informatics: Principles and Applications*. New Jersey: Wiley; 2004

Lee K. *Computers in Nuclear Medicine: A Practical Approach*. New York: Society of Nuclear Medicine; 1992.

Royal HD, Parker JA, Holman BL. Basic principles of computers. In: Sandler MP, Coleman RE, Wackers FJT, et al., eds. *Diagnostic Nuclear Medicine*. 3rd ed. Baltimore: Williams and Wilkins; 1995:93.

12
Single Photon Emission Computed Tomography

Tomographic Imaging

Conventional gamma cameras provide two-dimensional planar images of three-dimensional objects. Structural information in the third dimension, depth, is obscured by superimposition of all data along this direction. Although imaging of the object in different projections (posterior, anterior, lateral, and oblique) gives some information about the depth of a structure, precise assessment of the depth of a structure in an object is made by tomographic scanners. The prime objective of these scanners is to display the images of the activity distribution in different sections of the object at different depths and in turn to accurately determine the location of the lesion.

The principle of tomographic imaging in nuclear medicine is based on the detection of radiations from the patient at different angles around the patient. It is called *emission computed tomography* (ECT), which is based on mathematical algorithms, and provides images at distinct depths (slices) of the object (Fig. 12.1). In contrast, in transmission tomography, a radiation source (x-rays or a radioactive source) projects an intense beam of radiation photons through the patient's body, and the transmitted beam is detected by the detector and further processed for image formation.

In nuclear medicine, two types of ECT have been in practice based on the type of radionuclides used: *single photon emission computed tomography* (SPECT), which uses γ-emitting radionuclides such as ^{99m}Tc, ^{123}I, ^{67}Ga, and ^{111}In, and *positron emission tomography* (PET), which uses β^+-emitting radionuclides such as ^{11}C, ^{13}N, ^{15}O, ^{18}F, ^{68}Ga, and ^{82}Rb. SPECT is described in detail in this chapter and PET in Chapter 13.

Single Photon Emission Computed Tomography

The most common SPECT system consists of a typical gamma camera with one to three NaI(Tl) detector heads mounted on a gantry, an online computer for acquisition and processing of data, and a display system (Fig. 12.2). The detector

G. B. Saha, *Physics and Radiobiology of Nuclear Medicine,*
DOI 10.1007/978-1-4614-4012-3_12,

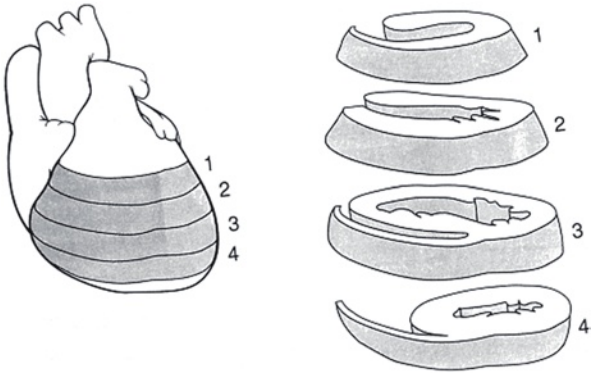

FIG. 12.1. Four slices of the heart in the short axis.

head rotates around the long axis of the patient at small angle increments (3 to 10°) for collection of data over 180 or 360°. The data are collected in the form of pulses at each angular position and normally stored in a 64×64 or 128×128 matrix in the computer for later reconstruction of the images of the planes of interest. Note that the pulses are formed by the PM tubes from the light photons produced by the interaction of γ-ray photons from the object, which are then amplified, verified by X, Y position and PH analyses, and finally stored. Transverse

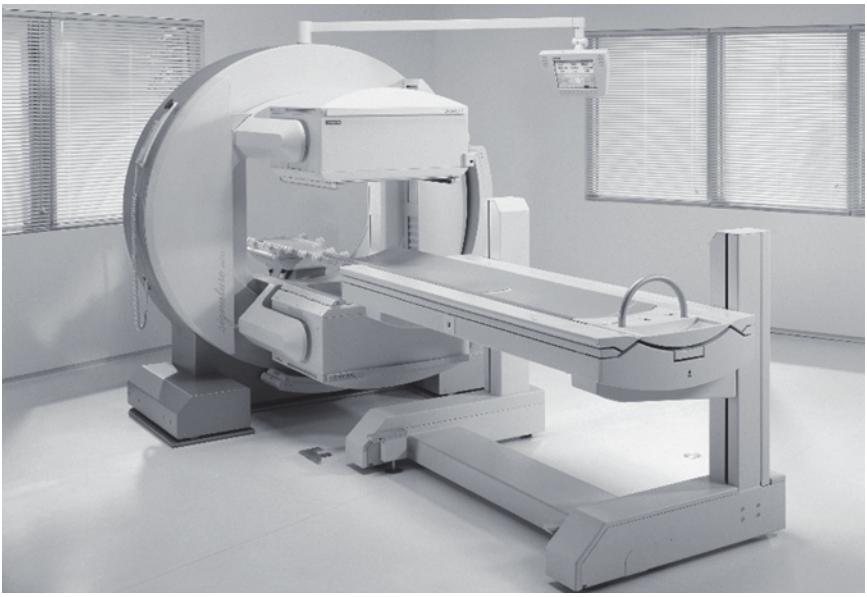

FIG. 12.2. A dual-head SPECT camera, e-CAM model (Courtesy of Siemens Medical Solutions, Hoffman Estates, IL).

Table 12.1. Relationship of sensitivity and time of imaging for 180 and 360° acquisitions for different camera head configurations.

	180° Acquisition		360° Acquisition	
Camera Type	Acquisition time (min)	Relative sensitivity	Acquisition time (min)	Relative sensitivity
Single-head	15	1	15	1
Dual-head (heads at 180°)	15	1	7.5	2
Dual-head (heads at 90°)	7.5	2	7.5	2
Triple-head (heads at 120°)	10	1.5	5	3

(short axis), sagittal (vertical long axis), and coronal (horizontal long axis) images can be generated from the collected data. Multihead gamma cameras collect data in several projections simultaneously and thus reduce the time of imaging. For example, a three-head camera collects a set of data in about one third of the time required by a single-head camera for 360° data acquisition.

Data Acquisition

The details of data collection and storage such as digitization of pulses, use of frame mode or list mode, choice of matrix size, etc., have been given in Chapter 11.

Data are acquired by rotating the detector head around the long axis of the patient over 180 or 360°. Although 180° data collection is commonly used (particularly in cardiac studies), 360° data acquisition is preferred by some investigators, because it minimizes the effects of attenuation and variation of resolution with depth. In 180° acquisition using a dual-head camera with heads mounted in opposition (i.e., 180°), only one detector head is needed for data collection and the data acquired by the other head essentially can be discarded. In some situations, the arithmetic mean $(A_1 + A_2)/2$ or the geometric mean $(A_1 \times A_2)^{1/2}$ of the counts, A_1 and A_2, of the two heads are calculated to correct for attenuation of photons in tissue. However, in 180° collection, a dual-head camera with heads mounted at 90° angles to each other has the advantage of shortening the imaging time required to sample 180° by half (Table 12.1). Dual-head cameras with heads mounted at 90 or 180° angles to each other and triple-head cameras with heads oriented at 120° to each other are commonly used for 360° data acquisition and offer shorter imaging time than a one-head camera for this type of angular sampling.

The sensitivity of a multihead system increases with the number of heads depending on the orientation of the heads and whether 180 or 360° acquisition is made. Table 12.1 illustrates the relationship among sensitivity, time of imaging, and acquisition arc (180 or 360°) for different camera head configurations.

Older cameras were initially designed to rotate in circular orbits around the body. Such cameras are satisfactory for SPECT imaging of symmetric organs such as the brain, but because the body contour is not uniform, such a circular orbit places the camera heads at different distances from various parts of the body in the anterior, lateral, and posterior positions. This causes loss of data and hence loss of spatial resolution in projections. To circumvent this problem, many modern cameras are designed to include a feature called *noncircular orbit* (NCO)

(i.e., to follow the body contour) that moves the camera heads such that the detector remains at the same distance close to the body contour at all angles.

Data collection can be made in either continuous motion or "step-and-shoot" mode. In continuous acquisition, the detector rotates continuously at a constant speed around the patient, and the acquired data are later binned into the number of segments equal to the number of projections desired. In the step-and-shoot mode, the detector moves around the patient at selected incremental angles (e.g., 3°) and collects the data for the projection at each angle.

Image Reconstruction

Data collected in two-dimensional projections give planar images of the object at each projection angle. To obtain information along the depth of the object, tomographic images are reconstructed using these projections. Two common methods of image reconstruction using the acquired data are the backprojection method and the iterative method. Both methods are described below.

Simple Backprojection

The principle of simple backprojection in image reconstruction is illustrated in Fig. 12.3, in which three projection views are obtained by a gamma camera at

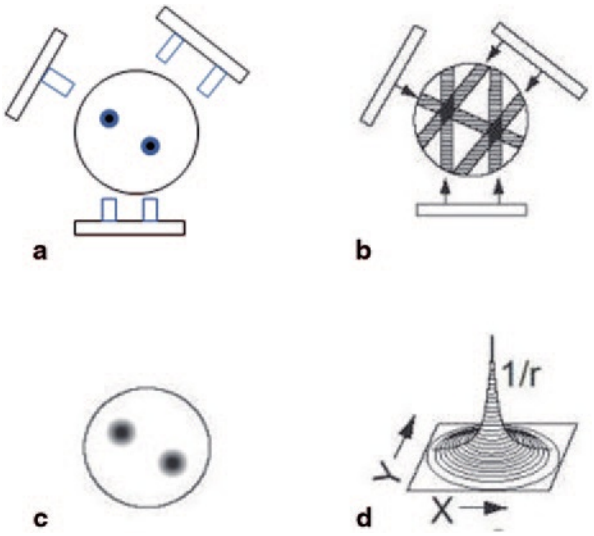

FIG. 12.3. Basic principle of reconstruction of an image by the backprojection technique. **a** An object with two "hot" spots (solid spheres) is viewed at three projections (at 120° angles). Each pixel count in a projection represents the sum of all counts along the straight-line path through the depth of the object. **b** Collected data are used to reconstruct the image by backprojection. **c** When many views are obtained, the reconstructed image represents the activity distribution with "hot" spots. **d** Blurring effect described by $1/r$ function where r is the distance away from the central point.

three equidistant angles around an object containing two sources of activity designated by black dots. In the two-dimensional data acquisition, each pixel count in a projection represents the sum of all counts along the straight-line path through the depth of the object (Fig. 12.3a). Reconstruction is performed by assigning each pixel count of a given projection in the acquisition matrix to all pixels along the line of collection (perpendicular to the detector face) in the reconstruction matrix (Fig. 12.3b). This is called *simple backprojection*. When many projections are backprojected, a final image is produced as shown in Fig. 12.3c.

Backprojection can be better explained in terms of data acquisition in the computer matrix. Suppose the data are collected in a 4×4 acquisition matrix, as shown in Fig. 12.4a. In this matrix, each row represents a slice, projection, or profile of a certain thickness and is backprojected individually. Each row consists of four pixels. For example, the first row has pixels A_1, B_1, C_1, and D_1. Counts in each pixel are considered to be the sum of all counts along the depth of the view. In the backprojection technique, a new reconstruction matrix of the same size (i.e., 4×4) is designed so that counts in pixel A_1 of the acquisition matrix are added to each pixel of the first column of the reconstruction matrix (Fig. 12.4b). Similarly, counts from pixels B_1, C_1, and D_1 are added to each pixel of the second, third, and fourth columns of the reconstruction matrix, respectively.

Next, suppose a lateral view (90°) of the same object is taken, and the data are again stored in a 4×4 acquisition matrix. The first row of pixels (A_2, B_2, C_2, and D_2) in the 90° acquisition matrix is shown in Fig. 12.4c. Counts from pixel A_2 are added to each pixel of the first row of the same reconstruction matrix, counts from pixel B_2 to the second row, counts from pixel C_2 to the third row, and so on. If more views are taken at angles between 0 and 90°, or any other angle greater than 90° and stored in 4×4 acquisition matrices, then the first row data of all these views can be similarly backprojected into the reconstruction matrix. This type of back-projection results in superimposition of data in each projection, thereby forming the final transverse image with areas of increased or decreased activity (Fig. 12.3c).

Similarly, backprojecting data from the other three rows of the 4×4 matrix of all views, four transverse cross-sectional images (slices) can be produced. Therefore, using 64×64 matrices for both acquisition and reconstruction, 64 transverse slices can be generated. From transverse slices, appropriate pixels are sorted out along the horizontal and vertical long axes, and used to form sagittal and coronal images, respectively. It is a common practice to lump several slices together to increase the count density in the individual slices to reduce statistical fluctuations.

Filtered Backprojection

The simple backprojection has the problem of "star pattern" artifacts (Fig. 12.3c) caused by "shining through" radiations from adjacent areas of increased radioactivity resulting in the blurring of the object. Because the blurring effect decreases with distance (r) from the object of interest, it can be described by a $1/r$ function (Fig. 12.3d). It can be considered as a spillover of certain counts from a pixel

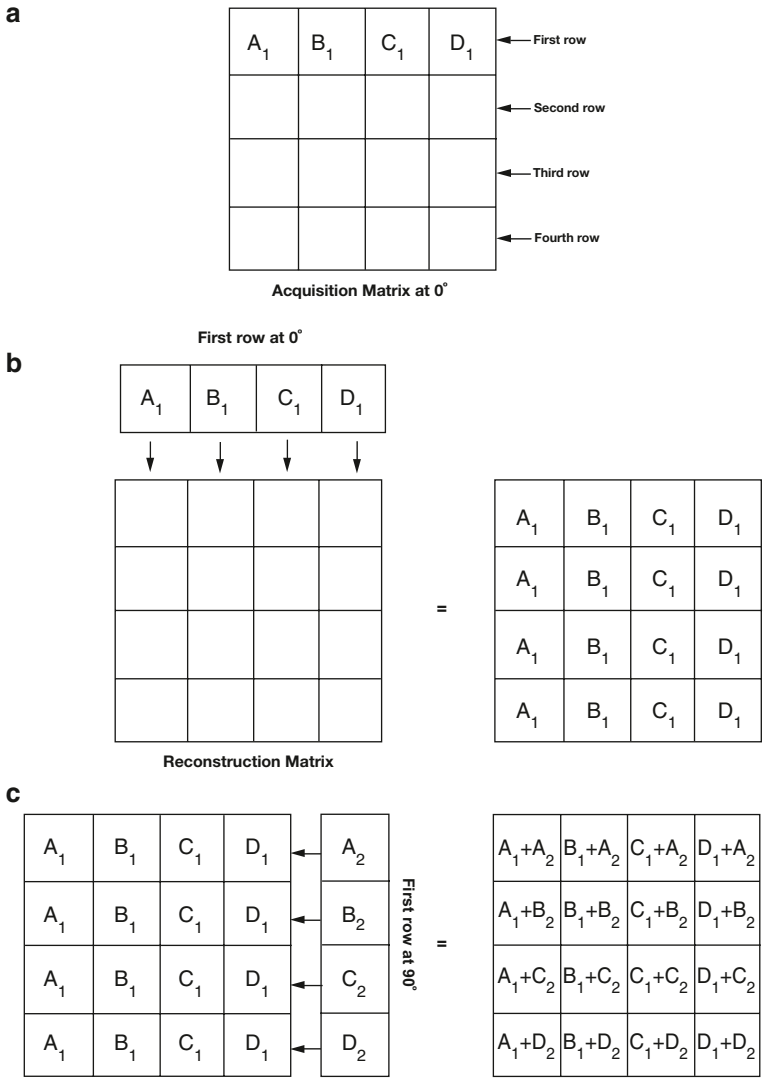

FIG. 12.4. An illustration of the backprojection technique using the data from an acquisition matrix into a reconstruction matrix.

of interest into neighboring pixels, and the spillover decreases from the nearest pixels to the farthest pixels. This blurring effect is minimized by applying a "filter" to the acquisition data, and the filtered projections are then backprojected to produce an image that is more representative of the original object. Such methods are called the filtered backprojection. There are in general two methods of filtered backprojection: the convolution method in the spatial domain and the Fourier method in the frequency domain, both of which are described below.

The Convolution Method

The blurring of reconstructed images caused by simple backprojection is eliminated by the convolution method in which a function, termed "kernel," is convolved with the projection data, and the resultant data are then backprojected. The application of a kernel is a mathematical operation that essentially removes the $1/r$ function by taking some counts from the neighboring pixels and putting them back into the central pixel of interest. Mathematically, a convolved image $f'(x, y)$ can be expressed as

$$f'(x,\ y) = \sum_{i=-N}^{N} \sum_{j=-N}^{N} h_{ij} \odot f_{ij}(x - i,\ y - j) \tag{12.1}$$

where f_{ij} $(x - i, y - j)$ is the pixel count density at the $x - i, y - j$ location in the acquired projection, the h_{ij} values are the weighting factors of the convolution kernel, and $\odot$ indicates the convolution operation. The arrangement of h_{ij} is available in many forms.

A familiar "nine-point smoothing" kernel (i.e., 3×3 size), also called smoothing filter, has been widely used in nuclear medicine to decrease statistical variation. The essence of this technique is primarily to average the counts in each pixel with those of the neighboring pixels in the acquisition matrix. An example of the application of nine-point smoothing to a section of an image is given in Fig. 12.5. Let us assume that the thick-lined pixel with value 5 in the acquisition matrix is to be smoothed. First, we assume a 3×3 acquisition matrix (same as 3×3 kernel matrix) centered at the pixel to be convolved. Each pixel datum of this matrix is multiplied by the corresponding weighting factor, followed by the summation of the products. The weighting factors are calculated by dividing the individual pixel values of the kernel matrix by the sum of all pixel values of the matrix. The result of this operation is that the value of the pixel has changed from 5 to 3. Similarly, all pixels in the acquisition matrix are smoothed, and the profiles are then backprojected.

The spatial kernel described above with all positive weighting factors reduces noise but degrades spatial resolution of the image. Sharp edges in the original image become blurred in the smoothed image as a result of averaging the counts of the edge pixels with those of the neighboring pixels.

Another filter kernel commonly used in the spatial domain consists of a narrow central peak with both positive and negative values on both sides of the peak, as shown in Fig. 12.6. When this so-called edge-sharpening filter is applied centrally to a pixel for correction, the negative values in effect cancel or erase all neighboring pixel count densities, thus creating a corrected central pixel value. This is repeated for all pixels in each projection and the corrected projections are then backprojected. This technique reproduces the original image with better spatial resolution but with increasing noise. Note that blurring due to simple backprojection is removed by this technique but the noise inherent in the data acquisition due

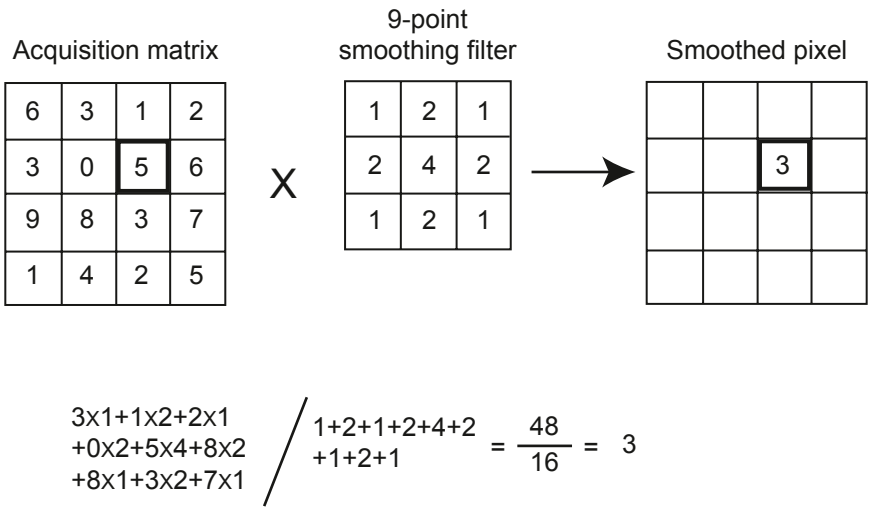

FIG. 12.5. The smoothing technique in the spatial domain using a 9-point smoothing kernel. The thick-lined pixel with value 5 is smoothed by first assuming a 3×3 acquisition matrix (same size as the smoothing matrix) centered at this pixel and multiplying each pixel value of the matrix by the corresponding weighting factor, followed by summing the products. The weighting factor is calculated by dividing the individual pixel value by the sum of all pixel values of the smoothing matrix. After smoothing the value of the pixel is changed from 5 to 3. Similarly all pixel values of the acquisition matrix are smoothed by the nine-point smoothing kernel, to give a smoothed image.

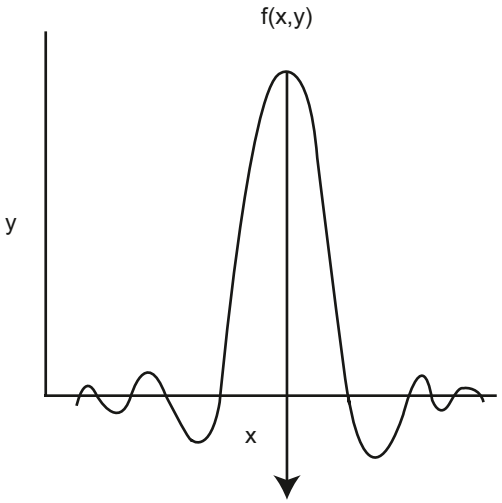

FIG. 12.6. A filter in the spatial domain. The negative side-lobes in the spatial domain cancel out the unwanted contributions that lead to blurring in the reconstructed image.

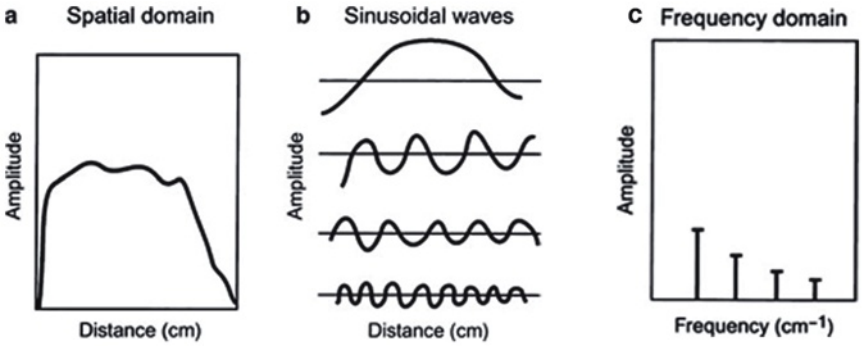

FIG. 12.7. Representation of an object in the spatial and frequency domains. A profile in the spatial domain can be expressed as an infinite sum of sinusoidal functions (the Fourier series). For example, the activity distribution as a function of distance in an organ **(a)** can be composed by the sum of the four sine functions (**b)**. The Fourier transform of this activity distribution is represented in (**c**), in which the amplitude of each sine wave is plotted at the corresponding frequency of the sine wave.

to the limitations of the spatial resolution of the imaging device is not removed but rather enhanced.

The Fourier Method

Nuclear medicine data obtained in the spatial domain (Fig. 12.7a) can be expressed in terms of a Fourier series in the frequency domain as the sum of a series of sinusoidal waves of different amplitudes, spatial frequencies, and phase shifts running across the image (Fig. 12.7b). This is equivalent to sound waves that are composed of many sound frequencies. Thus, the data for each row and column of the acquisition matrix can be considered as composed of sinusoidal waves of varying amplitudes and frequencies in the frequency domain. The process of determining the amplitudes of sinusoidal waves is called the Fourier transformation (Fig. 12.7c) and the method of changing from the frequency domain to the spatial domain is called the inverse Fourier transformation.

The Fourier method of reconstruction can be applied in two ways: either directly or by using filters. In the direct Fourier method, the Fourier transforms of individual acquisition projections are taken in polar coordinates in the frequency domain, which are then used to calculate the values in rectangular coordinates. Inverse Fourier transforms of these profiles are taken to compute the image. The method is not a true backprojection and is rarely used in reconstruction of images in nuclear medicine because of the time-consuming computation.

A more convenient method of reconstruction is the filtered backprojection (FBP) using the Fourier technique. In this method, filters are used to eliminate the blurring function l/*r* that arises from simple backprojection of the projection data. These filters are analogous to tone controls or equalizers in radios or CD

players that act as filters to vary the amplitudes of different frequencies, bass for low-frequency amplitudes and treble for high-frequency amplitudes. In image reconstruction, filters do the same thing, modulating the amplitudes of different frequencies, preserving the broad structures (the image) represented by low frequencies and removing the fine structures (noise) represented by high frequencies.

The Fourier method of filtering the projection data is based on the initial transformation of these data from the spatial domain to the frequency domain, which is symbolically expressed as

$$\mathrm{F}(v_x, v_y) = \mathcal{F} f(x, y) \tag{12.2}$$

where $\mathrm{F}(v_x, v_y)$ is the Fourier transform of $f(x, y)$ and $\mathcal{F}$ denotes the Fourier transformation. Next a Fourier filter, $H(v)$ is applied in the frequency domain; that is,

$$\mathrm{F}'(v) = \mathrm{H}(v) \cdot \mathrm{F}(v) \tag{12.3}$$

where $\mathrm{F}'(v)$ is the filtered projection in the frequency domain, which is obtained as the multiplication product of $\mathrm{H}(v)$ and $\mathrm{F}(v)$. Finally, the inverse Fourier transformation is performed to obtain the filtered projections, which are then backprojected. The results obtained by the Fourier method are identical to those obtained by the convolution method. Although the Fourier method appears to be somewhat cumbersome and difficult to understand, the use of modern computers has made it much easier and faster to compute the reconstruction of images than the convolution method.

Types of Filters

A number of Fourier filters have been designed and used in the reconstruction of images in nuclear medicine. All of them are characterized by a maximum frequency, called the Nyquist frequency, that gives an upper limit to the number of frequencies necessary to describe the sine or cosine curves representing an image projection. Because the acquisition data are discrete, the maximum number of peaks possible in a projection would be in a situation in which peaks and valleys occur in every alternate pixel (i.e., one cycle per two pixels or 0.5 cycle/pixel), which is the Nyquist frequency. If the pixel size is known for a given matrix, then the Nyquist frequency can be determined. For example, if the pixel size in a 64×64 matrix is 4.5 mm for a given detector, then the Nyquist frequency will be

$$\begin{aligned} \text{Nyquist frequency} &= 0.5 \text{ cycle/pixel} \\ &= 0.5 \text{ cycle/0.45 cm} \\ &= 1.11 \text{ cycles/cm} \end{aligned}$$

A common and well-known filter is the ramp filter (name derived from its shape in the frequency domain) shown in Fig. 12.8 in the frequency domain. An undesirable characteristic of the ramp filter is that it amplifies the noise associated

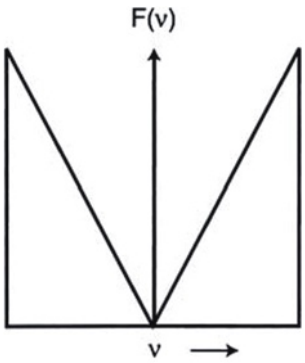

FIG. 12.8. The ramp filter in the frequency domain.

with high frequencies in the image even though it removes the blurring effect of simple backprojection. To eliminate the high-frequency noise, a window is applied to the ramp filter. A window is a function that is designed to eliminate high-frequency noises and retain the low-frequency patient data. Typical filters that are commonly used in reconstruction are basically the products of a ramp filter that has a sharp cut-off at the Nyquist frequency (0.5 cycle/pixel) and a window with amplitude 1.0 at low frequencies but gradually decreasing at higher frequencies. A few of these windows (named after those who introduced them) are illustrated in Fig. 12.9, and the corresponding filters (more correctly, filter–window combinations) are shown in Fig. 12.10.

The effect of a decreasing window at higher frequencies is to eliminate the noise associated with them. The frequency above which the noise is eliminated is

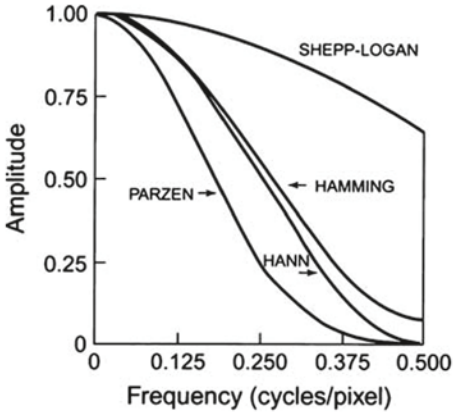

FIG. 12.9. Different windows for reconstruction filters in SPECT. Different windows suppress the higher spatial frequencies to a variable degree with a cutoff Nyquist frequency of 0.5 cycle/pixel.

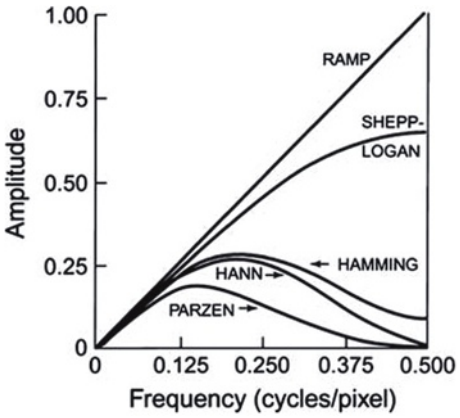

FIG. 12.10. Different filters for SPECT that are obtained by multiplying the respective windows by the ramp filter with cutoff at Nyquist frequency of 0.5 cycle/pixel.

called the cut-off frequency. As the cut-off frequency is increased, spatial resolution improves and more image detail can be seen up to a certain frequency. At a too high cut-off value, image detail may be lost due to inclusion of inherent noise. Thus, a filter with an appropriate cut-off value should be chosen so that primarily noise is removed, and image detail is preserved. Note that the Nyquist frequency is the highest cut-off frequency for a reconstruction filter and typical cut-off frequencies vary from 0.2 to 1.0 times the Nyquist frequency. Filters are selected based on the amplitude and frequency of noise in the data. Normally, a filter with a lower cut-off value is chosen for noisier data as in the case of obese patients and in ^{201}Tl myocardial perfusion studies or other studies with poor count density.

Hann, Hamming, Parzen, and Shepp–Logan filters are all *low-pass* filters because they preserve low-frequency structures, while eliminating high-frequency noise. All of them are defined by a fixed formula with a user-selected cut-off frequency. It is clear from Fig. 12.10 that most smoothing is provided by the Parzen filter and the Shepp–Logan filter produces the least smoothing.

An important low-pass filter that is most commonly used in nuclear medicine is the Butterworth filter (Fig. 12.11). This filter has two parameters: the critical frequency (v_c) and the order or power (n). The critical frequency is the frequency at which the filter attenuates the amplitude by 0.707, but not the frequency at which it is reduced to zero as with other filters. The parameter, order or power n, determines how rapidly the attenuation of amplitudes occurs with increasing frequencies. The higher the order, the sharper the fall. Lowering the critical frequency, while maintaining the order, results in more smoothing of the image.

Another class of filters, the Weiner and Metz filters, enhances a specific frequency response.

Many commercial software packages are available offering a variety of choices for filters and cut-off values. The selection of a cut-off value is important such

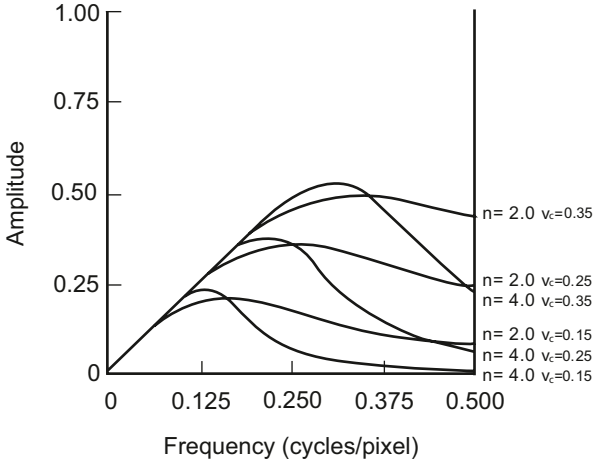

FIG. 12.11. Butterworth filter with different orders and cutoff frequencies.

that noise is reduced and image detail is preserved. Reducing a cut-off value will increase smoothing but will curtail low-frequency patient data and thus degrade image contrast particularly in smaller lesions. No filter is perfect and, therefore, the design, acceptance, and implementation of a filter are normally done by trial and error with the ultimate result of clinical utility.

As already mentioned, filtered backprojection was originally applied only to transverse slices from which vertical and horizontal long axis slices are constructed. Filtering between the adjacent slices is not performed, and this results in distortion of the image in planes other than the transverse plane. With algorithms available in current SPECT systems, filtering can be applied to slices perpendicular to transverse planes or in any plane through the 3-D volume of an object. This process is called volume smoothing. However, because of increased popularity of iterative methods described below, the 3-D volume smoothing is not widely applied.

Iterative Reconstruction

The basic principle of iterative reconstruction involves a comparison between the measured image and an estimated image that is repeated until a satisfactory agreement is achieved. In practice, an initial estimate is made of individual pixels in a projection of a reconstruction matrix of the same size as that of the acquisition matrix, and the projection is then compared with that of the measured image. If the estimated pixel values in the projection differ from the measured values, a correction is calculated from the ratio or difference between the two values for each projection, which is applied to each pixel in the projection to obtain an updated estimated projection for the next comparison with the measured projection. This process is repeated until a satisfactory agreement is obtained between the estimated and actual images. The schematic concept of iterative reconstruction is

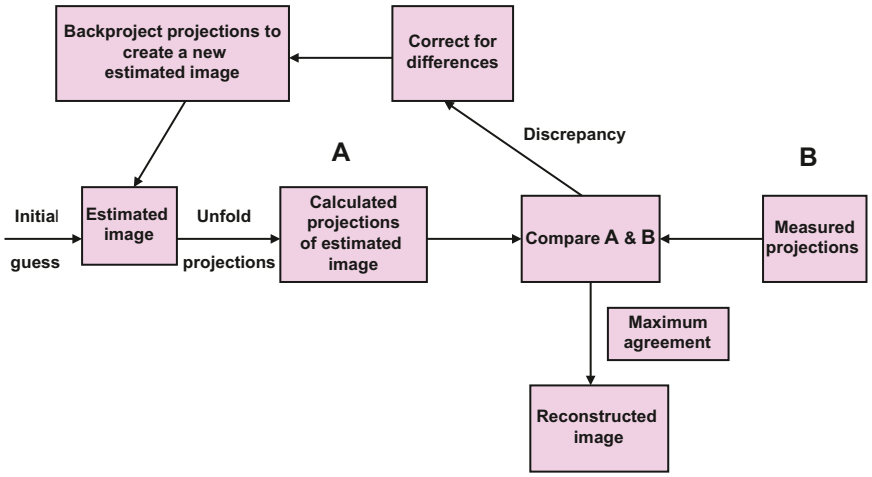

FIG. 12.12. Conceptual scheme of iterative reconstruction.

illustrated in Fig. 12.12. The method makes many iterations requiring long computation time and with the availability of faster computers nowadays, the method is routinely used in image reconstruction in PET, SPECT, CT and MR imaging.

Consider a radioactive source of 5×5 pixel cross-sectional matrix containing varied amount of activity in each pixel as illustrated in Fig. 12.13a. Only three measured projections A, B, and C obtained at different angles are shown with five bins each, which are basically the pixels in a row of the acquisition matrix in line with the source matrix. Since all pixels do not contribute equally, a weighted sum

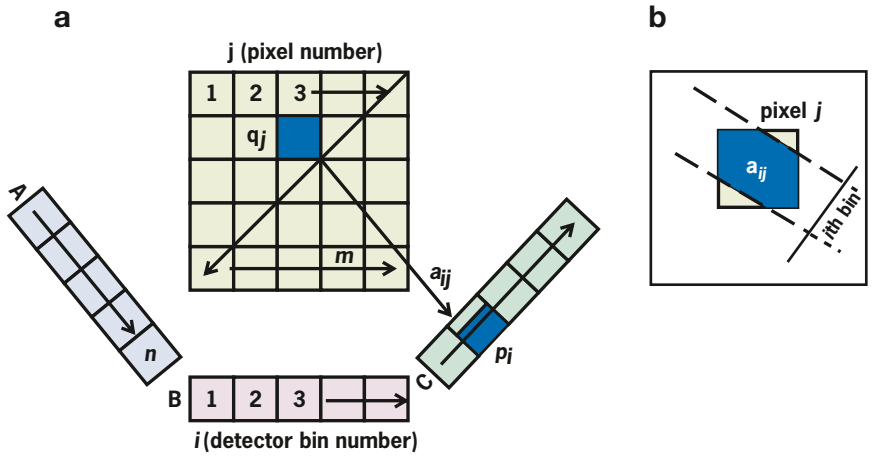

FIG. 12.13. **a** Three projections A, B, and C each with 5 bins taken of a 5×5 cross-sectional matrix. Counts p_i is the weighted sum of counts contributed by each pixel in a row of acquisition matrix, as given by Eq. (12.4). **b** Concept of weighting factor, a_{ij}.

of the contributions from each pixel makes up the measured activity p_i in the ith bin, that is,

$$p_i = \sum_{j=1}^{m} a_{ij} q_j \tag{12.4}$$

where q_j is the counts (activity) in the jth pixel and a_{ij} is the probability that an emission from pixel j is recorded in the ith bin. The concept of a_{ij} is illustrated in Fig. 12.13b, which is given by the shaded area of the pixel j along the ith bin.

In Equation (12.4), the measured values of p_i are known, whereas those of q_j in the true image are not known and need to be determined by the iterative method. Initially some arbitrary positive estimates of q_j (0, 1, and so on) are assumed in each pixel of the image matrix. Then the values of q_i are calculated by the adding the values of q_j for the ith bin at an angular projection. q_i is compared with p_i, and if there is no acceptable agreement, corrections based on their ratio (p_i/q_i) or difference ($p_i - q_i$), are applied to each pixel along the ith projection (backprojection) to obtain an updated estimate of the image. This is repeated for each bin of each projection (A, B, and C, etc) to complete one iteration. Many iterations are performed until an acceptable agreement between the measured and estimated images is achieved. The ratio technique is called the *maximum likelihood-expectation maximization* (MLEM) method and the difference method is called the *additive simultaneous iterative reconstruction technique* (ASIRT). Mathematically, they are expressed as follows:

For MLEM:

$$q_j^{k+1} = \frac{q_j^k}{\sum_i^n a_{ij}} \sum_i^n \frac{a_{ij} p_i}{\sum_j^m a_{ij} q_j^k} \tag{12.5}$$

For ASIRT:

$$q_j^{k+1} = q_j^k + \frac{1}{\sum_i^n a_{ij}} \sum_i^n \frac{(p_i - \sum_j^m a_{ij} q_j^k)\, a_{ij}}{\sum_j^m a_{ij}} \tag{12.6}$$

where k is the iteration number. In the MLEM method, the data are considered a Poisson distribution and in the ASIRT method, they are assumed to be a Gaussian distribution. A flow chart of sequential steps of the iterative method is shown in Fig. 12.14.

The main feature of the iterative method is to update the estimated image during each iteration to agree with measured image, and requires many iterations to achieve a satisfactory agreement demanding a lengthy computation time. To expedite the iteration process, the ordered subset expectation maximization (OSEM) algorithm has been introduced, which is a modification of MLEM, in that projections are grouped into a number of subsets separated by some fixed projection angles. The number of projections are grouped equally in each subset. For example, if there are 48 projections, they can be divided into eight subsets,

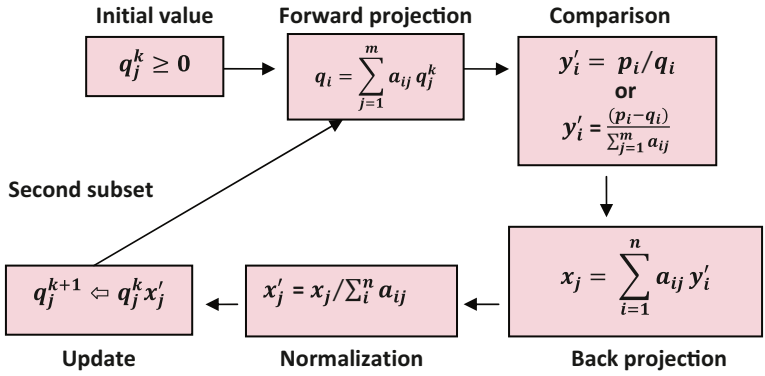

FIG. 12.14. A flow chart of sequential steps in iterative reconstruction algorithm.

each containing six projections. The projections in each subset are not contiguous but are spread over all angular projections so that the first subset will contain projections 1, 7, 13, 19, and so on, and the second set will have projections 2, 8, 14, 20 and so on, and so goes for the remaining subsets. For each subset, MLEM is applied, and the expected projection values are computed from the estimation of pixel values in all projections in the subset and compared with the measured image. The variance in p_i/q_i or $(p_i - q_i)$ is applied to the pixel values to give the next subset. This is repeated for all subsets. After all subsets are processed, a single iteration is considered complete. Such iteration is repeated until an expected agreement is achieved between the estimated and measured images. It has been shown that if there are n subsets and, once all subsets are used in a single iteration of OSEM, an estimate is produced which is similar to that obtained by n iterations of MLEM using all projections (Hudson and Larkin 1994). It is this property of OSEM that accelerates the computation process, and, in general, the computation time decreases when more projections are included in each subset. However, there is a tendency of having more image variance with increasing number of subsets when compared to MLEM. So an optimum number of subsets need to be chosen.

To illustrate the OSEM method, consider an example of a 2×2 true image whose pixel values are 2, 4, 6, and 8, which are *not* known and need to be determined (Fig. 12.15). However, the measured p_i values at 4 projection angles (6 and 14 at 0°, 10 at 45°, 8 and 12 at 90°, and 10 at 135°) are known. In the OSEM method, initially the first estimate of the image is assumed with some arbitrary values of, say, 4, 4, 4, and 4 in each pixel. Instead of 4, any other positive values can be assigned. The pixel values in the two columns at the 0° projection are added to give q_i values of 8 and 8. The ratios, p_i/q_i, are calculated as $8/8 = 1.0$ and $12/8 = 1.5$ (comparison). The pixel values in each column are then corrected by these ratios (backprojection): $4 \times 1 = 4$, $4 \times 1 = 4$; and $4 \times 1.5 = 6$ and $4 \times 1.5 = 6$, resulting in the first subset. Next, the q_i values are calculated for the 90° projection by adding the pixel values in each row, that is, $4 + 6 = 10$ and $4 + 6 = 10$ and the p_i/q_i values are $6/10 = 0.6$ and $14/10 = 1.4$. The pixel values are corrected to

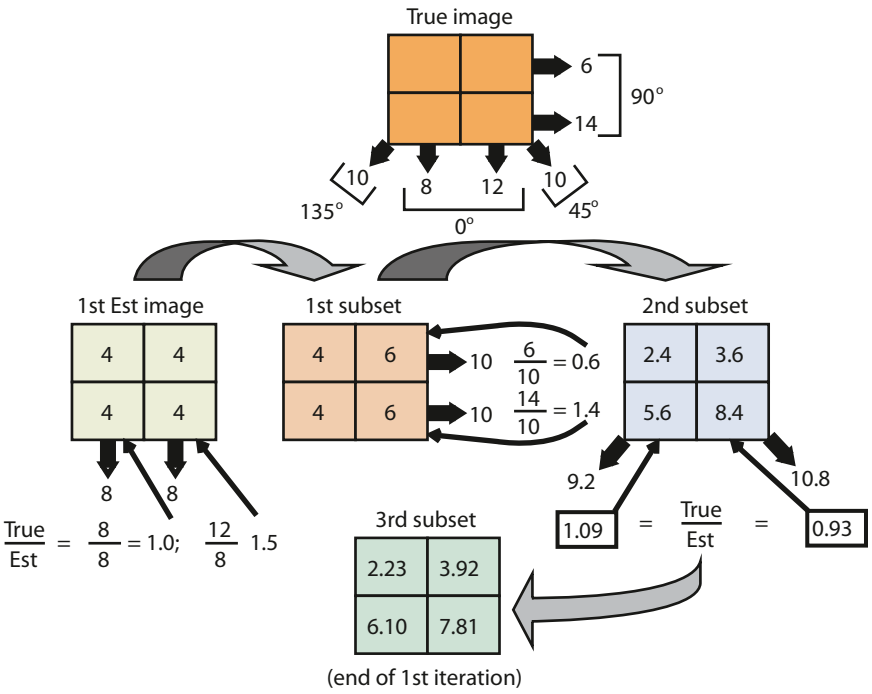

FIG. 12.15. Illustration of iterative reconstruction of an image represented by a 2×2 image. Known are *i*th bin values (sum), 8 and 12 at 0° projection, 10 at 45° projection, 14 and 6 at 90° projection, and 10 at 135° projection. Initially an estimate of the image in a 2×2 matrix is assumed with arbitrary values of 4 in each pixel. From these values, the estimated *i*th bin values are calculated for a given projection, e.g., 8 and 8 at 0° projection. The ratios of true to estimated values are calculated as 1.0 and 1.5, which are then applied to update the estimated image which becomes the 1st subset. The estimated *i*th bin values are calculated for a next projection (90° projection) and the ratios are calculated and applied to generate the next subset. When comparison of all bin values of all projections is made, an iteration is complete. Iterations are repeated until an acceptable agreement is achieved between the estimated image and measured image.

give the second subset with values as $4 \times 0.6 = 2.4$, $6 \times 0.6 = 3.6$, $4 \times 1.4 = 5.6$ and $6 \times 1.4 = 8.4$. For the third subset, the diagonal pixel values at 45 and 135° projections are added, the p_i/q_i values calculated and corrections are applied. This is the end of the first iteration, and iterations are repeated for better agreement. Refer to the references (Hudson and larkin 1994; Shepp and Verdi 1982) for a detailed description of the iterative methods.

Corrections for detection efficiency variations, noise component, random coincidences, scatter coincidences, and photon attenuation are made prior to reconstruction in the FBP method. In the MLEM or OSEM method, these factors are incorporated a priori in the estimated image and need not be applied separately. In general, iterative reconstruction methods do not produce artifacts that are ob-

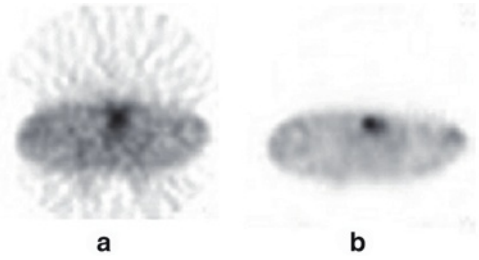

FIG. 12.16. Comparison of filtered backprojection and iterative OSEM method with attenuation correction.

served with the FBP method and provide a better signal-to-noise ratio in regions of low tracer uptake (Fig. 12.16). Overall, iterative methods provide high-quality images and are routinely used in image reconstruction in PET and SPECT. Despite many improvements in the OSEM method, it is a big challenge to have good-quality images in obese patients.

Another algorithm, the row-action maximum likelihood algorithm (RAMLA), has been proposed as a special case of OSEM requiring sequences of orthogonal projections, which lead to faster convergence than OSEM itself.

SPECT/CT

Accurate medical diagnosis of human disease can be made if both anatomical and functional status of the patient's disease is known. In the interpretation of nuclear medicine studies, physicians always like to have a comparison between high-resolution CT or MR images and low-resolution PET or SPECT images for accurate localization of lesions. In PET and SPECT imaging, in vivo measurement of organ physiology, cellular metabolism, and perfusion and other functional status of the organ is made. However, these studies have poor resolution due to poor photon flux and lack anatomical detail. On the other hand, computed tomography (CT) or magnetic resonance (MR) imaging provide excellent spatial resolution with high anatomical detail, but little functional information.

Efforts are made to co-register the two sets of images, in which the matrix size, voxel intensity, and rotation are adjusted to establish one-to-one spatial correspondence between the two images. Various techniques of such alignment are employed, and co-registered images are displayed side by side with a linked cursor indicating spatial correspondence, or may be overlaid or fused using the gray or color scale. The major drawback of these alignment techniques arises from positional variations of the patient scanned on different equipment and at different times. Furthermore, patient motion, voluntary or involuntary, adds to the uncertainty in the co-registration. Even with the sophisticated algorithm, a misalignment of 2–3 mm is not uncommon.

To overcome the problem of positional variations in alignment of images from different equipment, a dual-modality system has been introduced, in which a

SPECT camera and a CT scanner are combined into a single system for imaging the patient in the same clinical setting. Both units are mounted on the same gantry, with the SPECT camera in the front and the CT scanner in the back, and use a common imaging table. The two units are mounted fixed, therefore the centers of the scan fields of SPECT and CT scanners are separated by a fixed distance, called the displacement distance. The axial travel range of the scanning table varies with different designs of the manufacturers. The scan field is limited by the maximum travel range of the table minus the displacement distance.

The details of CT scanners are found in standard textbooks on CT and only a brief summary is given here. The CT scanner consists of an x-ray producing tube that contains a cathode filament and a rotating tungsten anode. When a high voltage (kV) is applied to the filament, electrons are emitted from it, which strike the rotating anode producing brehmsstralung and characteristic K x-rays. These radiations are then focused to an intense beam to project toward the object of irradiation. The beam energy typically ranges from 70 to 140 keV in energy depending on the high voltage applied. When a beam is projected through a patient, the transmitted beam is detected by detectors on the opposite side of the body and processed to produce signals that are stored in a matrix of choice (64×64, 128×128, etc.) in a computer. The stored data are further processed to form the image of different organs.

The detectors in CT scanners are made of materials such as ceramics, gadolinium oxysulfide, gemstone, etc and in some units, xenon gas. X-rays interact with these detector materials and produce visible light that is processed by a photodiode producing a signal. Normally a large number of such detectors are arranged in a full ring or in a partial ring in the form of an arc around the patient. In the full ring system, the detectors are fixed in 360° around the patient and the x-ray tube rotates around (Fig. 12.17a), whereas in the partial ring, both the detectors and the x-ray tube are mechanically tied together in 180° opposition in the gantry and the two together rotate around the patient (Fig. 12.17b). The detected data are acquired in seconds and stored in a matrix of choice (64×64, 128×128, etc.) in a computer. The stored data are then processed to reconstruct subject images in different projections. Currently multislice CT scanners are available providing 6, 16, 64 or 128 slices. In *helical* or *spiral* CT scanners, the patient table moves along the body while the x-ray tube rotates around the body, resulting in a spiral pattern of motion of the x-ray tube around the subject. This technique reduces the time of scanning to a few seconds.

When x-rays are projected through the patient's body, they are attenuated by the tissues at varying degrees depending on the density of the tissues. The transmitted beam produces different shadows of the tissues on the detection system (x-ray film, computer etc.) due to varied attenuation, which are often obscured by the shadow of the adjacent organs or tissues. This problem can be overcome by having separate images at two x-ray energies, e.g., 70 and 140 keV, and removing the shadow intensity from the intended image by coregistration using software algorithm. However, to avoid performing duplicate studies in different settings, manufacturers install two x-ray tubes in the same CT scanner (Sie-

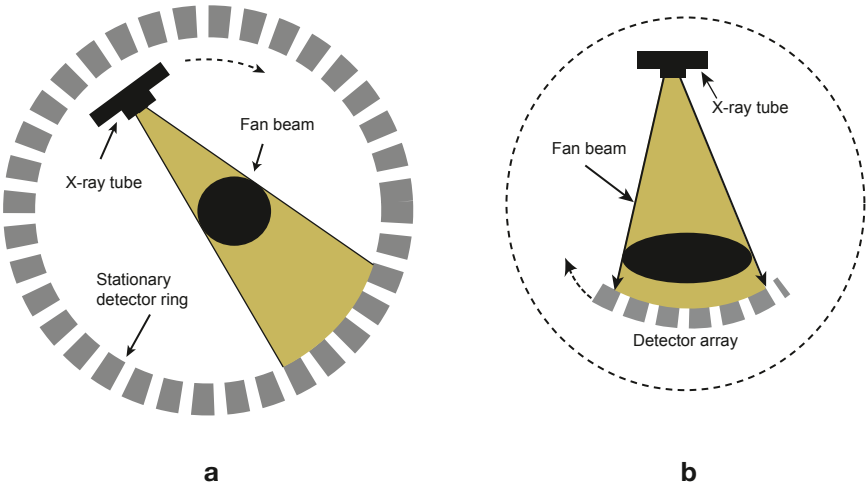

FIG. 12.17. **a** Full ring x-ray unit. **b** Partial ring x-ray unit.

men's Somatom) to operate at two energies separately or in some CT scanners (GE Healthcare's Lightspeed) with a single x-ray tube, which can be switched between two energies in a fraction of a second. These dual energy CT scanners reduce scan time lessening the radiation exposure to the patient and provide high contrast images.

Commercial SPECT/CT scanners are marketed by GE Healthcare (Discovery NM/CT 670), Philips Healthcare (BrightView XCT), Siemens Healthcare (Symbia T16) and Digirad (Cardius X-ACT). Some features of SPECT/CT scanners from three manufacturers are presented in Table 12.2, and Siemen's Symbia TruePoint SPECT/CT scanner is illustrated in Fig. 12.18.

Either CT or SPECT imaging can be performed first, followed by the other. For example, CT images are taken first with the organ of interest in the CT field of view. Next, the scan table with the patient in the same position is moved to the center of the SPECT FOV and images are taken. Both CT (anatomical) and SPECT (functional) images are reconstructed and then fused together by applying appropriate alignment algorithms. Various vendors provide commercially available fusion software, namely, Syngo of Siemens Healthcare, Extended Brilliance Workspace of Philips Healthcare, MIM of MIMVISTA, and Centricity of GE Healthcare. Because the position of the patient on the table does not change, both CT and SPECT images are aligned very accurately and the overall accuracy is improved by 20–25 % compared to either modality alone.

A major advantage of including CT in the dual-modality is that the CT data can be utilized in attenuation correction of SPECT data, which is particularly useful in cardiac perfusion imaging. Apparent perfusion defects are often seen in the anterior wall in women due to breast position and in the inferior wall in men, and soft-tissue attenuation also shifts between rest and stress images. As will be described later, attenuation correction using CT transmission data compensates

TABLE 12.2. Some features of SPECT/CT scanners from three manufacturers.

Manufacturers	GE Healthcare	Philips Healthcare	Siemens Healthcare
Model	Discovery NM/CT 670	BrightView XCT	Symbia T16
Crystal dimension (cm)	N/S	47×59.3	59.1×44.5
Thickness (mm)	9.5 or 25.4	9.5 or 19.1	9.5 or 15.9
No of PMTs	59	59	59
Attenuation corr.	Yes	CT-AC	Yes, CT-AC
UFOV (cm)	54×40	40.6×54	53.3×38.7
Max count rate, cps	≥460	350	310
Dead time, (μsec)	N/S	1.3	Proprietary
FWHM, CFOV (mm) (Intrinsic)	3.8	3.3	3.3
FWHM, CFOV, mm at 10 (cm) (extrinsic)	7.4	7.4	7.5
System sensitivity, LEHR (cpm/μCi)	160	168(3/8); 188(3/4)	202
Integral UFOV (%)	≤3.6	2.5	≤3.7
Differential UFOV (%)	≤2.3	2	≤2.7
Contouring (WB)	Automatic	Full or semi-automatic	Automatic
CT detectors	BrightSpeed Elite 16	High Res flat panel	UltraFast Ceramic
kV range	80–140	120	80–130
mA range	10–440	5–80	20–245
Scan field (cm)	50	47	50
No of slices	16	140	16
LC resolution	5 mm at 0.3% at 13.3 mGy	5 mm at 0.5% with 40 mm slice	5 mm at/16.6 mGy at 100 mAs
Std HC Resol. (2% MTF)	8.5 lp/cm at x-y 19.6 lp/cm at z	5 lp/cm at 10% MTF	≥15.6 lp/cm
CTDI(dose/100 mAs) B/16 cm phantom	Head 19.6 mGy; body 9.9 mGy	3 mGy/100 mAs	14.1 mGy at center with 100 kV

Adapted with permission from Imaging Technology News: www.itnonline.com.

for these artifacts more accurately in a shorter time than using the conventional sealed source transmission data. Such CT transmission attenuation correction can be applied to other organ imaging as well.

Factors Affecting SPECT

Photon Attenuation

γ-Ray photons are attenuated in body tissue while passing through a patient. The degree of attenuation depends on the photon energy, the thickness of tissue, and the linear attenuation coefficient of the photons in the tissue. If I_0 is the number of photons emitted from an organ and I is the number of photons detected by the gamma camera, then

$$I = I_0 e^{-\mu x} \tag{12.7}$$

where μ is the linear attenuation coefficient of the photon in tissue and x is the depth of tissue traversed by the photon (Fig. 12.19b). Photons originate from

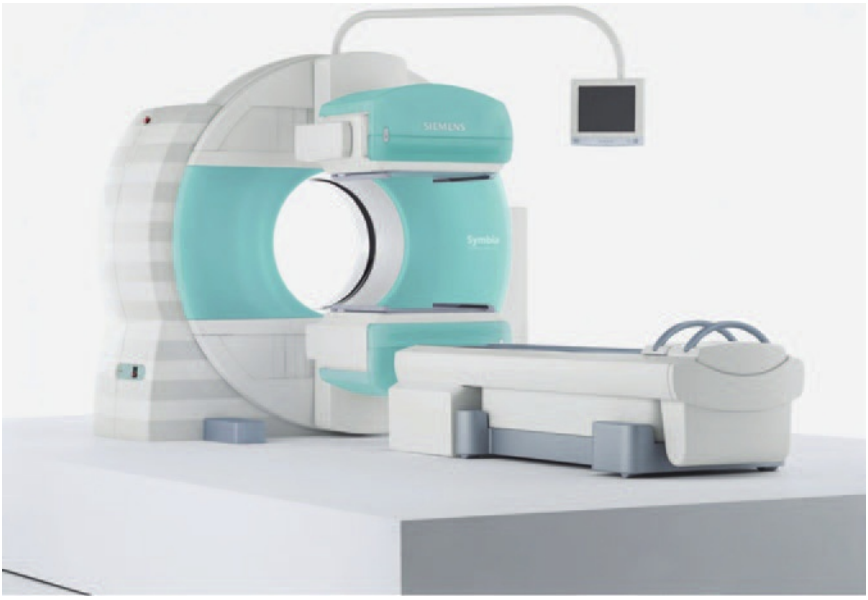

FIG. 12.18. A SPECT/CT camera, Symbia model (Image/photo courtesy of Siemens Medical Solutions USA, Inc, Malvern, PA).

different depths of tissue, which are not exactly known, and so are attenuated to different extents (Fig. 12.19a). Attenuation causes a gradual decrease of count density from the edge to the center of the image (Fig. 12.20a). If SPECT images are reconstructed from these attenuated profiles without correction, artifacts are seen. Attenuation corrections are difficult to apply to the attenuated photons due to lack of knowledge about I and x in Eq. (12.7). Attempts have been made over the years to devise methods of attenuation correction in SPECT imaging, with particular attention to estimate the values of I and x, and given below is a brief description of the commonly used ones.

Attenuation Correction Methods

In SPECT imaging, two techniques are employed to estimate I_0. One is to obtain two counts in opposite projections and then taking the arithmetic mean of the two, or secondly, taking their geometric mean. This is accomplished by acquiring SPECT data in 360° and sorting the counts in opposite projections to calculate the arithmetic or geometric mean. The arithmetic mean is given by

$$I_t = \frac{(I_a + I_b)}{2} \tag{12.8}$$

where I_a and I_b are the measured attenuated counts in the opposite projections. Similarly, the geometric mean is given by

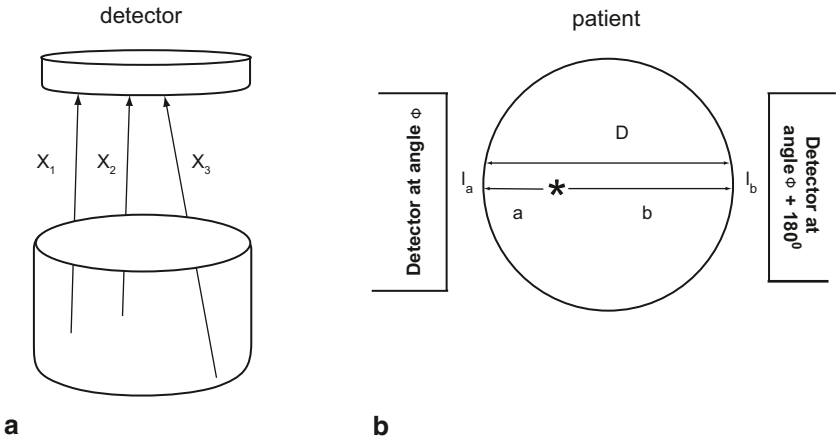

FIG. 12.19. **a** Illustration of photons traveling different depths of tissue, thus suffering variable attenuation. **b** Two photons traversing distances a and b are detected by the two detectors oriented at 180°. Attenuation correction can be applied by taking the geometric mean of the two counts I_a and I_b and using the total thickness D of the tissue in place of a and b separately.

$$I_g = (I_a \times I_b)^{1/2} \tag{12.9}$$

Considering Fig. 12.19 and applying Eq. (12.7), Eq. (12.9) becomes

$$\begin{aligned} I_g &= (I_a \times I_b)^{1/2} = (I_{a0}e^{-\mu a} \times I_{b0}e^{-\mu b})^{1/2} = (I_{a0} \times I_{b0})^{1/2}e^{-\mu(a+b)/2} \\ &= (I_{a0} \times I_{b0})^{1/2}e^{-\mu D/2} \end{aligned} \tag{12.10}$$

where I_{a0} and I_{b0} are the unattenuated counts detected in opposition and D is the total thickness of the tissue. For parallel-hole collimators, which are most commonly used in SPECT imaging, the photon intensity does not change with distance, i.e., I_{a0} and I_{b0} are approximately equal. Then Eq. (12.10) becomes

$$I_0/I_g = e^{\mu D/2} \tag{12.11}$$

Equation (12.11) is the attenuation correction factor that is applied to the geometric mean counts to obtain the unattenuated correct counts. For the arithmetic mean, assuming a uniform uptake of the tracer and a constant μ value for all tissues, the attenuation correction factor is

$$I_0/I_t = \mu D_i/(1 - e^{-\mu D_i}) \tag{12.12}$$

Equations (12.11) and (12.12) are applied for attenuation corrections using geometric and arithmetic means of SPECT projection data. For ^{99m}Tc studies, a value

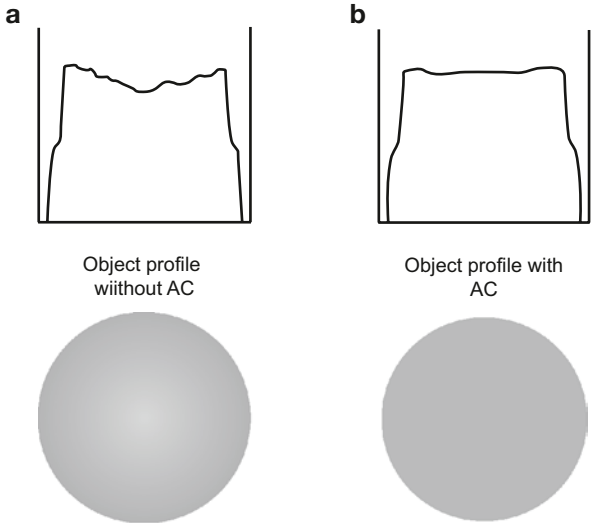

FIG. 12.20 **a** Object profile without attenuation correction showing decreased distribution of activity at the center. **b** The same object profile with attenuation correction.

of 0.12 cm^{-1} is assumed for μ, and D_i is empirically estimated from standard body shape and size. Corrections are applied to the measured projections, which are then used for reconstruction of the images by filtered backprojection. A simulated picture of attenuation corrected image is shown in Fig. 12.20b.

Chang Method: In the Chang method, an improvement has been made to the above method in that attenuation corrections are made after reconstruction of the image rather than before image reconstruction. The travel path D_i for each pixel at projection i is estimated from the contour of the image, and a constant value of μ is assumed for all tissues. *A*ttenuation correction factors are calculated for individual pixels by Eq. (12.11) or (12.12) depending on the geometric or arithmetic mean used. The attenuation correction is then applied to each pixel in the reconstructed image. This method works reasonably well for organs such as brain and abdomen, where the attenuating tissue can be considered essentially uniform. However, the situation is complicated in areas like thorax, where μ varies due to close proximity of various organs, and the Chang method is difficult to apply.

Transmission method: A plausible method for attenuation correction in SPECT is the transmission method. The SPECT system uses a transmission source of a radionuclide that is mounted opposite to the detector such as is an x-ray tube in computed tomography. The detector collects the transmission data to correct for attenuation in emission data. For ^{99m}Tc imaging, common transmission sources are gadolinium-153 (^{153}Gd) (48 keV, 100 keV) and ^{57}Co (122 keV), whereas for ^{201}Tl imaging, americium-241 (^{241}Am) (60 keV) and ^{153}Gd are used in different configurations. In one common configuration, a well-collimated line source is

FIG. 12.21. Illustration of attenuation correction of cardiac SPECT image reconstructed by filtered backprojection. **a** Cardiac SPECT images without attenuation showing deficient activity in the inferior wall. **b** The same images with attenuation correction using the CT transmission method showing improvement in count density in the inferior wall.

mounted that is translated across the plane parallel to the detector face to collect transmission data. The line source is scanned at each angular stop during the SPECT data collection to apply attenuation correction to each angular projection.

Typically, a blank scan is obtained without the patient in the scanner. The data from this scan are used for all subsequent patients for the day. Then a transmission scan is obtained with the patient in the scanner before the emission scan is acquired. The ratio of counts of each pixel between the blank scan and the transmission scan is the attenuation correction factor for the pixel, which is applied to the emission pixel data obtained next. This is done for each patient for the day. Because the patient is positioned separately in the two scans, error may result in the attenuation correction.

Because the transmission and emission photons have different energy, it is possible that SPECT cameras can be used to collect both transmission and emission data simultaneously using separate discriminator settings. However, one should keep in mind that there is spillover of scattered high-energy photons (i.e., with reduced energy) into the low-energy photopeak window. The transmission data are used to calculate the attenuation factors, which are then applied to the emission data. It should be noted that in the iterative reconstruction method, the attenuation factor is taken into consideration in the estimated image and it is perhaps the best approach for attenuation correction in SPECT.

In SPECT/CT, the CT transmission data are utilized for attenuation correction, with an advantage of fast data collection in less than a minute thus improving the patient throughput. In the CT technique, typically a blank CT scan is taken without the patient in the scanner at the beginning of the day and is used for subsequent patient studies for the day. Next, the CT transmission scan of the patient is taken and an attenuation correction map is generated from the ratios of counts of each pixel of the blank and the patient transmission scans. After the CT scan, the scanning table with the patient in the same position is moved to the SPECT scanning field and the emission scan is obtained. Factors from the map are then applied to the corresponding pixels in the patient's emission scan for attenuation correction. A typical patient scan is shown in Fig. 12.21 with and without attenuation correction.

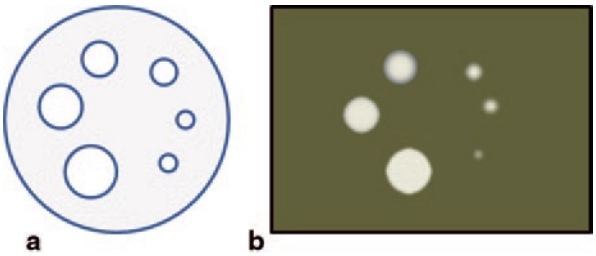

FIG. 12.22. An illustration of partial volume effect. **a** Cross-section of a cylindrical phantom with six holes of different sizes. **b** PET images of the cylindrical holes filled with activity demonstrating partial volume effect.

Note that the attenuation depends on photon energy and, therefore, correction factors derived from ~70 keV CT x-ray scans must be scaled to the energy of single photons of the radionuclide used (e.g., 140 keV of ^{99m}Tc) by applying a scaling factor defined by the ratio of mass attenuation coefficient of the photons in tissue to that of 70 keV photons. This factor is assumed to be the same for all tissues except bone, which has a slightly higher mass attenuation coefficient. Because the position of the patient does not change in CT transmission and PET emission scans, the error in positional misalignment of pixels between the two scans is minimized. The CT transmission method provides essentially noiseless images.

Several factors introduce errors in CT attenuation correction factors. One is the respiratory motion of the thorax during scanning that causes mismatch in the fusion of SPECT and CT images. These effects are minimized by multislice CT scanning and a short scanning time (~25 s), with a breath hold at end expiration. Also, contrast agents affect the CT attenuation factors because contrast-enhanced pixels overestimate attenuation. Some investigators advocate not using contrast agents and others suggest the use of water-based contrast agents to mitigate this effect.

Partial-Volume Effect

Partial-volume effects are inherent flaws of all imaging devices, because no imaging device has perfect spatial resolution. These effects make the intensity values in images differ from their actual values and so images appear to be different. They are caused by two phenomena—the 3D image blurring introduced by the finite spatial resolution of the imaging device and the tissue fraction effect (Soret et al. 2007). In 3D image blurring, the activity from a region is spilled out to the adjacent regions, reducing the activity in the region of interest and causing smearing effect on the edge. Because of the finite spatial resolution and if the size of a "hot" region surrounded by a "cold" background is smaller than 2–3 times the spatial resolution of the imaging device, the activity around the object is smeared over a larger area than its actual size. While the total counts are preserved, the object appears to be larger and to have a lower activity concentration than it actually has (Fig. 12.22). Similarly, a cold spot relative to a hot background will appear

smaller with higher activity concentration, caused by spill-in of the activity from the hot area.

The tissue fraction effect arises from sampling of the emission data from the voxels in the matrix. Clearly, the count density in each voxel is the mean of count densities of all different types of underlying tissues in that voxel. This will lead to an overestimation of activity in the voxel in question and the image would appear having increased activity. This effect is more prominent at the edge of the image and with larger pixels or (larger slices), because they will have greater chance of mixing of different tissues. For example, the choice of larger pixels or slices in tumor imaging may underestimate the actual activity due to possibility of mixing of tumor and necrotic or background tissues.

The standard uptake value (SUV) is an important parameter in tumor imaging by SPECT or PET that indicates the degree of metabolic activity of a tumor. It is widely used as a follow-up indicator to assess the outcome of therapeutic treatment of tumors. It is calculated from the administered activity (A), the tumor region (R) and the body weight or surface area (W) and given as

$$SUV = \frac{R}{A} \times W \tag{12.13}$$

The value of R depends on several factors such as the size and shape of the tumor, surrounding tissues, image sampling and spatial resolution of the reconstructed image and thus is affected by the partial-volume effect. This in turn will affect the SUV value of the tumor.

The partial-volume effect is a concerned issue for smaller structures in images, and correction factors need to be applied for the overestimation or underestimation of the activities in them. There are several methods for the partial-volume correction, and one simple method uses a correction factor, called the recovery coefficient, which is the ratio of the reconstructed count density to the true count density of the region of interest. The recovery coefficient can be determined by measuring the count densities of spheres of different sizes in a phantom containing the same activity in each sphere. Spheres of sizes both larger and smaller than the spatial resolution of the system are used. Coefficients are calculated by dividing the measured activity of each sphere with the true activity. Fig. 12.23 presents the recovery coefficients for objects of different sizes. The recovery coefficient is 1 for the larger objects meaning that partial–volume effect does not affect the larger objects. However, recovery coefficients are usually measured using phantoms, which may not be a true representative of human body.

Center of Rotation

The center of rotation (COR) parameter is a measure of the alignment of the opposite views (e.g., posterior versus anterior or right lateral versus left lateral) obtained by the SPECT system. The COR must be accurately aligned with the center of the acquisition matrix in the computer. If the COR is misaligned, then a

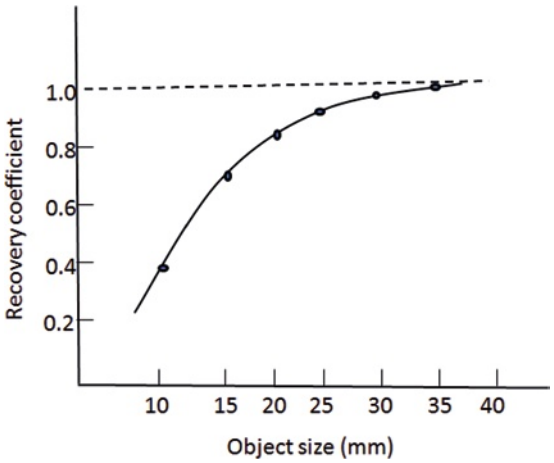

FIG. 12.23. Recovery coefficients as a function of object size.

point source would be seen as a "donut" on the image (Fig. 12.24). Thus, an incorrect COR in a SPECT system would result in image degradation. For example, an error of 3 mm in the alignment of COR is likely to cause a loss of resolution of ~30 % in a typical SPECT system (Todd-Pokropek 1983).

The misalignment of COR may arise from improper shifting in camera tuning, mechanics of the rotating gantry, and misaligned attachment of the collimator to the detector. The COR off by more than one pixel may cause degradation in the reconstructed image. It is essential that the COR alignment is assessed routinely in SPECT systems to avoid potential degradation in spatial resolution. Manufacturers provide detailed methods of determining COR alignment for SPECT systems, which should be included in the routine quality control procedure. Currently, manufacturers include the COR alignment in their maintenance services.

Sampling

It is understood that the larger the number of projections (i.e., small angular increment), the less is the star or streaking effect and hence the image quality is better. However, this requires a longer acquisition time. Ideally, for accurate reconstruction, the number of angular projections should be at least equal to the size of the acquisition matrix (e.g., 64 angular projections for a 64×64 matrix or 128 projections for a 128×128 matrix). A fewer number of projections may not erase the streaking effect. How many angular projections should be taken over 180° or 360° to reconstruct the images accurately depends on the spatial resolution of the camera. As a general rule, 120–128 projections (using a 128×128 matrix) are needed for large organs such as lungs and liver, whereas 60–64 projections (using a 64×64 matrix) are sufficient for smaller organs such as head and heart. Typi-

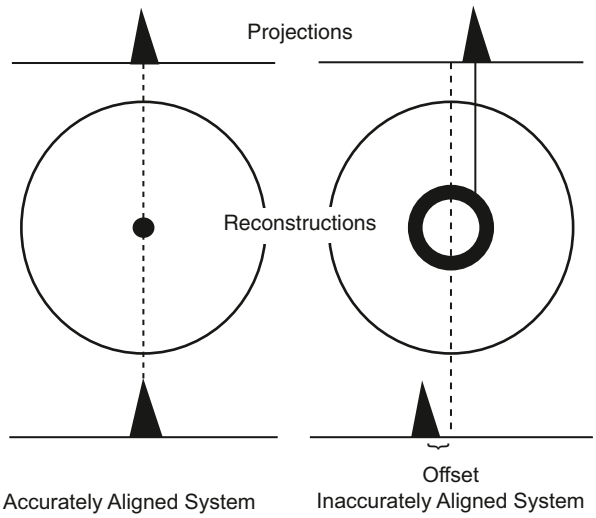

FIG. 12.24. An illustration of the effect of a misaligned center of rotation. A "donut"-shaped image appears from inaccurately aligned center of rotation. (From Todd-Pokropek A. The mathematics and physics of emission computerized tomography (ECT). In: Esser PD, Westerman BR, editors. *Emission Computed Tomography*. New York: Society of Nuclear Medicine; 1983; 3.)

cally, angular sampling at 6° intervals for 360° acquisition or at 3° intervals for 180° acquisition are commonly used for most SPECT systems.

Scattering

Radiations are scattered in patients, and the scattered photons, depending on the energy and angle of scattering, may strike the detector. Scattering may occur in the detector itself, and also within or outside the FOV. Normally, most of these scattered photons fall outside the photopeak window and are rejected. However, a fraction of these photons whose energy falls within the photopeak window will be counted, but their (*X*, *Y*) positions remain uncertain causing degradation of the image resolution. In SPECT imaging, more than 95% of the 140 keV photons of ^{99m}Tc are scattered in the patient and pose a serious problem. Scatter correction should be applied to improve the spatial resolution of images.

There are a few methods of scatter correction, of which the most common method is the use of two windows: a scatter window and a photopeak window. The scatter window is set at a lower energy than the photopeak window. As an example, Fig. 12.25 shows the two windows for ^{99m}Tc studies–the low energy window (scatter window) set at 45–75 keV and the photopeak at 125–160 keV. The photopeak contains scatter, which is shown by the area B, and is estimated from the counts in the scatter window shown by the area A. Since the area A and area

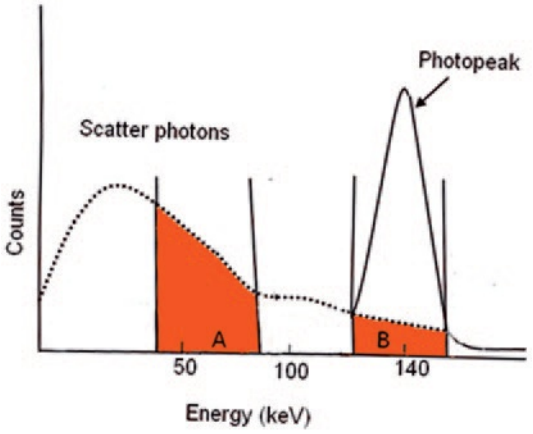

FIG. 12.25. Two-window set up for scatter correction. See text for details.

B are not the same, a scaling factor must be applied to A to estimate B, which is determined experimentally using a phantom of known size and the same window settings. The scatter counts in the scatter window are corrected and subtracted from the photopeak counts for each projection to obtain the scatter-corrected projections, which are then used for reconstruction. The scatter spectrum is variable in energy; therefore, to have more accurate scatter corrections, multiple scatter windows can be used. Scatter corrections are made prior to attenuation correction, because the former are amplified during the latter operation. Overall, scatter correction adds noise to the reconstructed image.

Performance of SPECT Cameras

Performance of SPECT cameras is assessed by evaluating several parameters such as spatial resolution, sensitivity, and contrast, which are discussed below.

Spatial Resolution

Spatial resolution of a SPECT camera is affected by all the factors discussed in Chapter 10. Typically, it consists of intrinsic resolution, collimator resolution, scatter resolution, angular sampling, and the type of reconstruction filter. Because of 3-D orientation, SPECT images have both axial and transaxial spatial resolutions. The axial spatial resolution refers to the resolution along the axis of rotation of the camera heads, whereas the transaxial spatial resolution indicates the resolution across the transverse FOV perpendicular to the axis. Spatial resolution of a SPECT system is measured by using a point source of ^{99m}Tc placed at the center

of the FOV and at several axial and transverse locations, and then taking the SPECT images. Images are reconstructed using the ramp filter, from which the point-spread-functions (PSF) are derived. Alternatively, line sources can be used to generate the line-spread-functions, as described in Chapter 10. The FWHM values of the PSFs or LSFs give the spatial resolution of the system. Typical spatial resolution obtained with a LEHR collimator varies from 3.8 to 7.9 mm at the center of the FOV and from 7.4 to 7.9 mm at a radius of 10 cm of the FOV. Normally, planar images have better resolution than the SPECT cameras. Spatial resolution deteriorates but sensitivity increases with increasing slice thickness. As a trade-off between spatial resolution and sensitivity, an optimum slice thickness should be chosen.

Sensitivity

The sensitivity of an imaging system is always desired to be higher for better image contrast. All factors that affect the conventional cameras also affect the SPECT systems in the same manner, as discussed in Chapter 10.

The sensitivity of SPECT cameras is measured for each detector head by placing about 1 mCi of ^{99m}Tc in a petri dish and counts are acquired for a certain time for each detector head using a specific collimator, normally the LEHR parallel-hole collimator. Counts are divided by the counting time to give sensitivity in cpm/μCi or cpm/MBq. It is often customary to use volume sensitivity for SPECT cameras, which is measured by using a cylindrical polypropylene phantom of size 20 × 20 cm and outer thickness of about 1 cm, filled with a volume of radioactivity, normally ^{99m}Tc, of uniform concentration. The activity should be low enough to avoid count losses due to dead time and pulse pile-up. Data are acquired in a desired number of projections (64 or 128) using the collimator of interest (normally LEHR parallel-hole collimator) for a certain time. Volume sensitivity is calculated in cpm/μCi-cc or cpm/MBq-cc, by dividing the total counts of all projections with the counting time and the volume of activity in the cylinder.

The sensitivity of gamma cameras varies from 160 to 200 cpm/μCi for LEHR parallel-hole collimators. The SPECT systems are designed for greater sensitivity so that high counts can be accumulated for images of thin slices of an organ in a reasonable time. For conventional two-dimensional planar images of good contrast, about 500,000 counts are required. Thus, if each sectional image (i.e., slice) of an organ requires 500,000 counts for the same contrast as in a conventional image, and if there are, for example, 20 sectional images of an organ of interest, then 10 million counts would be needed for the entire organ. For most SPECT systems using low-energy all-purpose collimators, 5–20 million counts are acquired. Total counts may be increased by either counting for a longer period or by administering more activity. However, long counting is inconvenient for the patient and administering a larger amount of activity increases the radiation dose to the patient.

Other Parameters

Other important parameters to evaluate include effects of high-count rates, uniformity, and contrast of images. These parameters have been discussed in detail in Chapter 10 for conventional gamma cameras and are equally applicable to multihead SPECT cameras.

Quality Control Tests for SPECT Cameras

Daily Tests

Photopeaking and Uniformity

The daily photopeaking and uniformity tests for SPECT cameras are the same as for conventional gamma cameras described in Chapter 10 with more stringent requirements. These tests must be done for each head of the system. In SPECT systems, nonuniformities are substantially magnified by the FBP reconstruction method causing a ring artifact in the image particularly at the center of rotation. To achieve uniformity on SPECT images, UFOV nonuniformity should be less than 1 %. Ideally this can be achieved by acquiring at least 30 million counts for 64×64 images or 120 million counts for 128×128 images. For practical reasons, however, 5 million counts for large FOV cameras and 3 million counts for small FOV cameras are appropriate. For Siemens e-Cam cameras, acquisition of 5 million counts in a 1024×1024 matrix is recommended.

Weekly Tests

Spatial Resolution

For single-head or multihead SPECT cameras, spatial resolution for each head is checked by using bar phantoms in the same manner as conventional gamma cameras described in Chapter 10. In determining spatial resolution by the intrinsic method, the two detectors must be kept apart at maximum radius, and a ^{99m}Tc point source is placed in a source holder on the rear bed mechanism provided by the manufacturer. The bar phantom is placed on the detector, and the bed is raised to a maximum height.

Center of Rotation

The COR corrections are performed weekly or bi-weekly using the computer software provided by the manufacturer. To begin COR corrections, the camera face must be parallel to the axis of rotation. Generally, a point or line source is placed in the FOV of the camera and then SPECT scans of the source are obtained for 360°. The software analyzes the scans and determines if the COR is within acceptable limits.

Nowadays, many manufacturers provide a phantom using 5-point sources for low-energy high-resolution collimators or 3-point sources for medium-and high-energy collimators. The phantom with the sources in position is placed on the patient table. SPECT data are collected for 360° in a circular orbit of 20 cm, when the detector heads are in 180° configurations. In the case of 90° configurations, the default radius is applied as given by the manufacturer. In a proper COR-corrected system, the point sources should be visible in all projection images.

This method is also used to check the head alignment and noncircular orbit configuration in multihead camera systems with the computer software.

Quality Control Tests for CT Scanners

As with any imaging devices, proper preventive maintenance and quality control tests of CT scanners must be performed to achieve optimum image quality on a regular schedule. These tests are mandatory for accreditation of the CT scanners by the American College of Radiology and are published in the form of guidelines (www.acr.org). The frequency of these tests may be daily, weekly, monthly, semi-annually or annually depending on the type of parameter to be evaluated. Parameters such as tube voltage, mA setting, the uniformity of image, noise, and accuracy of CT numbers are evaluated daily. The CT numbers are a function of the linear attenuation coefficient of tissue and assigned to each pixel of the tissue image in Hounsfield units (HU) relative to that of water which is given a value of 0. The water CT number is measured using a uniform water phantom in the scan field and should be within $\pm$ 5 HU. All these measurements are menu-driven by manufacturer's algorithm and the results are given in PASS/FAIL display.

Noise and field uniformity are affected by, among others, detector sensitivity, matrix size, slice thickness, scattered radiation, software algorithm, electrical components, and patient size. They are assessed by scanning a phantom at different slice thicknesses and increasing mAs. Regions of interest (ROI) are measured at the center and the edge of the image. Equal CT numbers in both areas indicate image uniformity. A variation in the CT numbers is the noise that is calculated as percentage of image contrast in CT numbers and should be within $\pm$ 3 HU. This test should be performed daily. Other parameters such as slice thickness, spatial resolution, contrast resolution, linearity, laser alignment, and mechanical operation are performed monthly, semi-annually, or annually as recommended by the manufacturers. Phantoms are made of Plexiglass in different designs for use in measuring a specific parameter. The details of these tests are given in standard textbooks on CT and on the ACR website.

Since radiation dose imparted to the patient during a CT study is a great concern for cancer risk, regular quality control tests must be instituted for the optimum operation of the CT scanner to afford an acceptable radiation dose to the patient. This is commonly done by measuring a CT dose index (*CTDI*), which is defined as the cumulative dose along the patient's axis for a single tomographic

image. A head phantom of polymethyl methacrylate is used for head dose and a body phantom of the same material for the body dose. The dose is measured by an ion chamber or a thermoluminiscent dosimeter at the center and different peripheral locations, and *CTDI* is calculated as an integral of all values along the slice, divided by the width of the axial field (no of slices x width of the slice). *CTDI*s vary with kV and mA and must be evaluated at least semi-annually. The American College of Radiology (ACR 2007) recommends maximum *CTDI* values of 6 rad (60 mGy) for brain, 3.5 rad (35 mGy) for for adult abdomen, and 2.5 rad (25 mGy) for pediatric (5-yr old) abdomen.

During a CT study, the patient receives the radiation absorbed dose over the field of view and so the patient dose is calculated by multiplying *CTDI* with the length (L) of the scan field in centimeter ($CTDI \times L$). This product is called *dose length product* (*DLP*) and is given in mGy-cm. *DLP* is calculated for each study by the CT computer using appropriate software algorithm and printed in the output. In order to estimate the risk for the patient, the effective dose is calculated in rem (mSv) by multiplying the *DLP* of the scan field with the tissue weighting factor (W_T) of the tissue in the field (see Chapter 14).

Questions

1. Describe the principles of single photon emission computed tomography (SPECT).
2. Explain how SPECT images are reconstructed by the filtered backprojection technique.
3. Elucidate different factors that affect SPECT images.
4. What is the optimum angular sampling for the SPECT system?
5. How does the center of rotation affect the SPECT image and from what does it originate? What is the ideal location of COR in a 64×64 matrix?
6. With a multihead camera, does the sensitivity of an imaging device increase or decrease?
7. What are the different types of common filters used in the reconstruction of images in SPECT?
8. Which of the following acquisition matrices would give better spatial resolution: a 64×64 matrix or a 128×128 matrix?
9. What are the different factors that affect the uniformity of an imaging device? Describe the methods to improve uniformity.
10. In the filtered backprojection method, the Fourier method is preferred to the convolution method. Why?
11. What is edge packing and how is it rectified?
12. High-frequency data represent noise in SPECT image reconstruction. True or False?
13. A filter with a low cut-off frequency should be used for noisy data and low count density studies in order not to curtail image detail. True or False?

14. A gamma camera has a NaI(Tl) detector of 38-cm diameter. Data of a study are acquired in a 64×64 matrix. What is the Nyquist frequency?
15. Describe the OSEM method of reconstruction of SPECT images.
16. Partial volume effects mostly affect the (a) larger object or (b) smaller object?
17. What are the common values of spatial resolution and sensitivity?
18. For SPECT imaging, what should be the limit for nonuniformity?
19. What are CTDI and DLP? How are they measured?

References and Suggested Readings

American College of Radiology (www.acr.org)

Bacharach SL. Image analysis. In: Wagner HN Jr, Szabo Z, Buchanan JW, eds. *Principles of Nuclear Medicine*. Philadelphia: W.B. Saunders; 1995;393–404.

Brooks RA, DiChiro G. Theory of image reconstruction in computed tomography. *Radiology*. 1975;117:561–572.

Bruyant P. Analytic and iterative reconstruction algorithms in SPECT. *J Nucl Med*. 2002;43:1343.

Cherry SR, Sorensen JA, Phelps ME. *Physics in Nuclear Medicine*. 3rd ed. Philadelphia; W.B. Saunders: 2003.

English RT, Brown SE. *Single Photon Emission Computed Tomography: A Primer*. 2nd ed. New York: Society of Nuclear Medicine; 1990.

Groch MW, Erwin WD. Single-photon emission computed tomography in the year 2001: Instrumentation and quality control. *J Nucl Med Technol*. 2001;29:12.

Groch MW, Erwin WD. SPECT in the year 2000: Basic principles. *J Nucl Med Technol*. 2000;28:233–244.

Hudson HM, Larkin RS. Accelerated image reconstruction using ordered subsets of projection data. *IEEE Trans Med Imaging*. 1994;13:601.

Jaszczak RJ, Coleman E. Single photon emission computed tomography (SPECT): Principles and instrumentation. *Invest Radiol*. 1985; 20:897–910.

Madsen MT. Introduction to emission CT. *Radiographics*. 1995;15:975–991.

Rollo FD, ed. *Nuclear Medicine Physics, Instrumentation, and Agents*. St. Louis: Mosby; 1977.

Shepp LA, Vardi Y. Maximum likelihood reconstruction for emission tomography. *IEEE Trans Med Imaging*. 1982;MI-1:113.

Soret M, Bacharach SL, Buvat I. Partial-volume effect in PET tumor imaging. *J Nucl Med*. 2007;48:932.

Todd-Pokropek A. The mathematics and physics of emission computerized tomography (ECT). In: Esser OD, ed. *Emission Computed Tomography*. New York: Society of Nuclear Medicine; 1983:3.

13
Positron Emission Tomography

Positron emission tomography (PET) is based on the detection in coincidence of the two 511-keV annihilation radiations that originate from β^+-emitting sources, such as the patient containing β^+-emitting radioactivity. Positrons are annihilated in body tissue and produce two 511-keV annihilation photons that are emitted in opposite directions (180°). Two photons are detected in an electronic time interval, called "coincidence time window", by two detectors connected in coincidence. Conversion of 511-keV photons to light photons in the detector, formation of a pulse by the PM tube, and pulse-height analysis follow the same principles as in conventional gamma cameras. Detectors are arranged in the array of several rings to have the organ of interest in the field of view. Data collected over 360° simultaneously around the body axis of the patient are used to reconstruct the image of the activity distribution in the slice of interest. Because the two opposite photons are detected in a straight line, no collimator is needed to limit the field of view, and the technique is called the *electronic collimation*.

PET Radiopharmaceuticals

Many positron-emitting radionuclides are produced in a cyclotron, but only a few are used in preparing radiopharmaceuticals for PET studies. The production method and characteristics of the most common ones are listed in Tables 5.1 and 13.1. While all of these are used in developing new PET radiopharmaceuticals, only ^{18}F, ^{13}N, ^{82}Rb radiopharmaceuticals are used clinically. Readers should refer to reference books on the synthesis of PET radiopharmaceuticals. ^{82}Rb-RbCl and ^{13}N-ammonia are used for myocardial perfusion imaging, whereas ^{18}F-fluorodeoxyglucose is used for metabolic imaging of the heart and brain, and various types of cancers. Some promising PET radiopharmaceuticals for potential clinical use are ^{18}F-fluorodopa for Parkinson disease, and neuroendocrine tumors, ^{18}F-fluorothimidine (FLT) for tumor imaging, ^{18}F-fluoromisonidazole (FMISO) for imaging hypoxic tumors, ^{11}C-choline for colon cancer, ^{11}C-methionine for

This chapter is adapted from Saha (2010, Chapter 2–5).

G. B. Saha, *Physics and Radiobiology of Nuclear Medicine,*
DOI 10.1007/978-1-4614-4012-3_13,

TABLE 13.1. Characteristics of PET radionuclides.

Radionuclides	Half-life	Mode of decay (%)	$E_{\beta+\max}$(MeV)
^{11}C	20.4 min	β^+(100)	0.970
^{13}N	10 min	β^+(100)	1.2
^{15}O	2 min	β^+(100)	1.74
^{18}F	110 min	β^+(97) EC (3)	0.64
^{68}Ga	68 min	β^+(89) EC(11)	1.90
^{82}Rb	75 s	β^+(95) EC(5)	3.15
^{124}I	4.2 d	β^+(23) EC(77)	2.14

brain tumor, ^{18}F-florbetapir for amyloid plaque imaging in Alzheimer's patient, ^{18}F-HX4 for hypoxic tumor imaging and so on.

Detectors in PET Scanners

Several types of scintillation detectors are available for PET scanners and their properties are illustrated in Table 8.1. NaI(Tl) was initially used in earlier PET scanners, but nowadays commercial manufacturers mostly use BGO, LYSO and LSO detectors because of their favorable characteristics in pulse production. All three detector materials are not hygroscopic obviating the need for hermetic sealing. They all have high stopping power (high density and linear attenuation coefficient), but LSO and LYSO have shorter scintillation decay time (40 ns and 50 ns, respectively) than BGO (300 ns) and have higher light output (30 photons and 25 photons vs. 6 photons). However, due to the intrinsic property, the energy resolution of these detectors is poor. It is to be noted that LSO and LYSO contain a naturally occurring radioisotope of its own, ^{176}Lu, with an abundance of 2.6 % and a half-life of 3.8×10^8 years. This radionuclide decays by emission of β^- rays and x-rays of 88–400 keV. However, the activity level is low enough to ignore radiation exposure from ^{176}Lu, and its photon energy lower than 511 keV does not cause a major problem in PET imaging.

GSO has been used in PET scanners by some manufacturers, despite its lower light output and stopping power than LSO. These crystals are fragile and require great care in fabrication.

BaF_2 has the shortest decay time of 0.6 ns and is primarily used in time-of-flight PET scanners that are rarely used clinically.

Semiconductors such as lithium-activated germanium and silicon (Ge(Li) and Si(Li)) detectors are used for photon detection. Photons eject an electron from the atomic orbital following an interaction with these materials and create a positively charged hole in the atom. The electron-hole pair moves as current, when a high

voltage is applied. These are called photodiodes and do not require any PM tube for amplification of pulses. High voltage application causes some electron multiplication in the detector, but in the absence of PM tubes, a large electron multiplication does not occur. The output signal is therefore weaker than the conventional PM tube signal resulting in poorer detection efficiency and so they are not used in PET scanners. A separate category of semiconductor detectors are cadmium-zinc-tellurium (CZT) or cadmium-tellurium (CdTe) that have relatively high atomic numbers (high stopping power) and excellent energy resolution (~5 %). Currently, the CZT detector has been used in commercial PET scanners offering high resolution and low noise images and promising a great potential for future use.

PM Tubes and Pulse-Height Analyzers

Like conventional cameras, PET scanners use PM tubes and pulse-height analyzers (PHA) for determining the locations of the origin of pulses and their amplitudes. As mentioned in Chapter 8, PM tubes convert light photons arising from the interaction of γ-rays in detectors to pulses, which are used to determine the *X*-, *Y*-positions of the two detectors that detect the two 511-keV photons (discussed later), and the PHA is used to check if the pulse height is within the acceptable range, which is normally set at 350 to 650 keV for 511-keV annihilation photopeak in PET scanners.

PET Scanners

In original PET scanners, many detectors (hundreds to thousands), each connected to a photomultiplier tube, are arranged in multiple circular, hexagonal, or orthogonal rings. The number of rings in PET scanners, and the number of crystals per ring vary with the manufacturer. The number of rings and, hence, the width of the array of rings define the axial field of view. Despite the advantage of good resolution with these scanners, the use of many PM tubes and packing them with as many detectors is very costly and impractical. To circumvent this problem, blocks of detectors connected to fewer PM tubes have been designed, which are described below.

Block Detectors

In modern PET scanners, the *block detector* is used, in which small detectors are created by making partial cuts on the front surface of a block of detector crystal and each block detector is coupled on the back side to 2–4 PM tubes. A schematic block detector is shown in Fig. 13.1. Typically, each block is about 3 cm deep and grooved into 6 × 8, 7 × 8, or 8 × 8 elements by partial cuts through the crystal

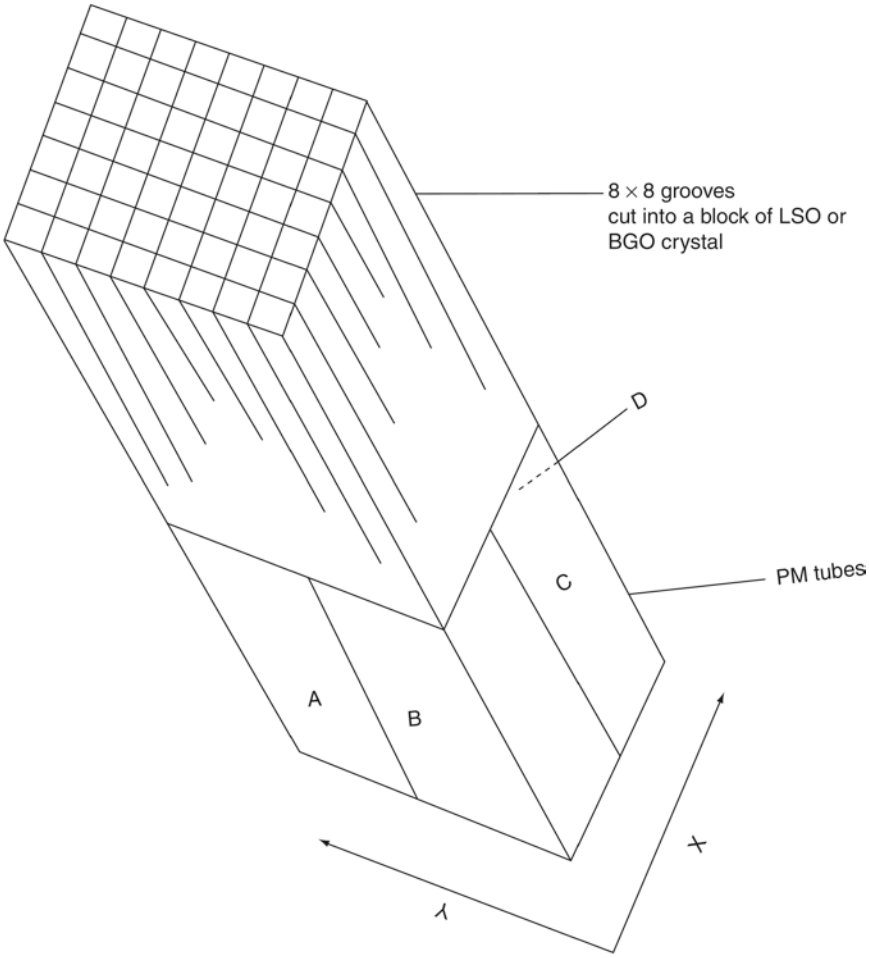

FIG. 13.1. A schematic block detector is segmented into 8×8 elements, and four PM tubes are coupled to the block for pulse formation. The pulses from the four PM tubes (*A*, *B*, *C*, and *D* signals) determine the location of the element in which 511-keV γ-ray interaction occurs, and the sum of the four pulses determines if it falls within the energy window of 511 keV.

with a saw. Each element is considered a small detector. The cuts are made at varying depths, with the deepest cut at the edge of the block. The cuts are filled with opaque reflective materials to prevent spillover of light between elements. The size of each detector varies from 3 to 6.5 mm and is one of the important parameters that determine the spatial resolution.

The block detectors are arranged in an array of full or partial rings with a diameter of 80–90 cm. The full ring array may be in the form of a circular or hexagonal shape. Two configurations of block detectors adopted by several manufacturers are shown in Fig. 13.2. Siemens mCT has 32,448 crystals arranged in 192 block

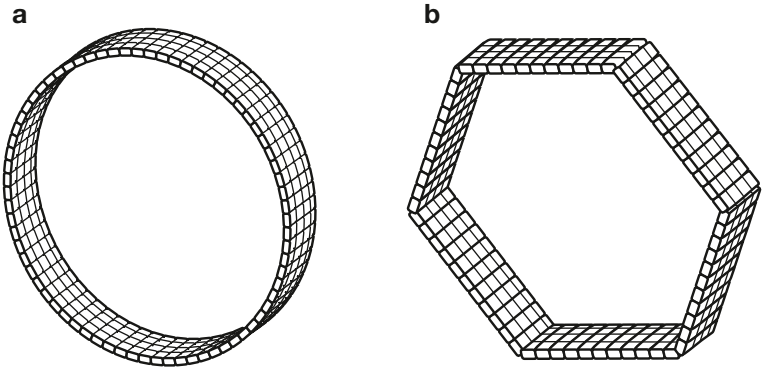

FIG. 13.2. Two configurations of PET scanners. **a** A circular full ring scanner. **b** A hexagonal array of quadrant-sharing panel detectors.

detectors with four PM tubes per block, whereas in Philips Healthcare's Gemini TF Big Bore scanner, 28,336 crystals coupled to 420 PM tubes are arrayed in 28 pixelar modules.

Coincidence Timing Window

In ideal coincidence counting in PET, the two 511-keV annihilation photons should be detected by the two detectors exactly at the same time. In reality, however, one photon may arrive at one detector earlier than the other in the opposite detector. This uncertainty in detection time is called the timing resolution or coincidence timing window. The timing resolution results from the difference in pulse formation in the detector primarily due to statistical variations in gain and scintillation decay time of the detector. Furthermore, there is a time delay in the arrival of one photon relative to the other, because of the difference in distances traveled by the two photons, particularly if the annihilation occurs at the edge of the FOV. This also adds to the timing resolution. For a whole-body scanner with a diameter of 1 m, the maximum distance traveled by one photon can be as large as 1 m, and the other photon travels almost no distance, if the annihilation occurs at the edge of the FOV. Because the velocity of light is 3×10^8 m/s, the difference in the arrival times of the two photons is about 3–4 ns (time to travel 1 m). This is the limit of timing resolution of a PET scanner with 1-m diameter.

After annihilation, two timing signals A and B are formed with timing width, say τ, depending on the scanner system. Signal B may arrive at one detector just τ ahead of (Fig. 13.3a) or τ behind (Fig. 13.3b) the arrival of signal A, and both signals will be counted in coincidence. This is the extreme limit, and all other annihilation events overlapping in their time widths (Fig. 13.3c) will be counted as coincident events. Thus the timing resolution or coincidence timing window has to be a minimum of 2τ. The typical coincidence timing window of conventional PET scanners is set at 6–20 ns.

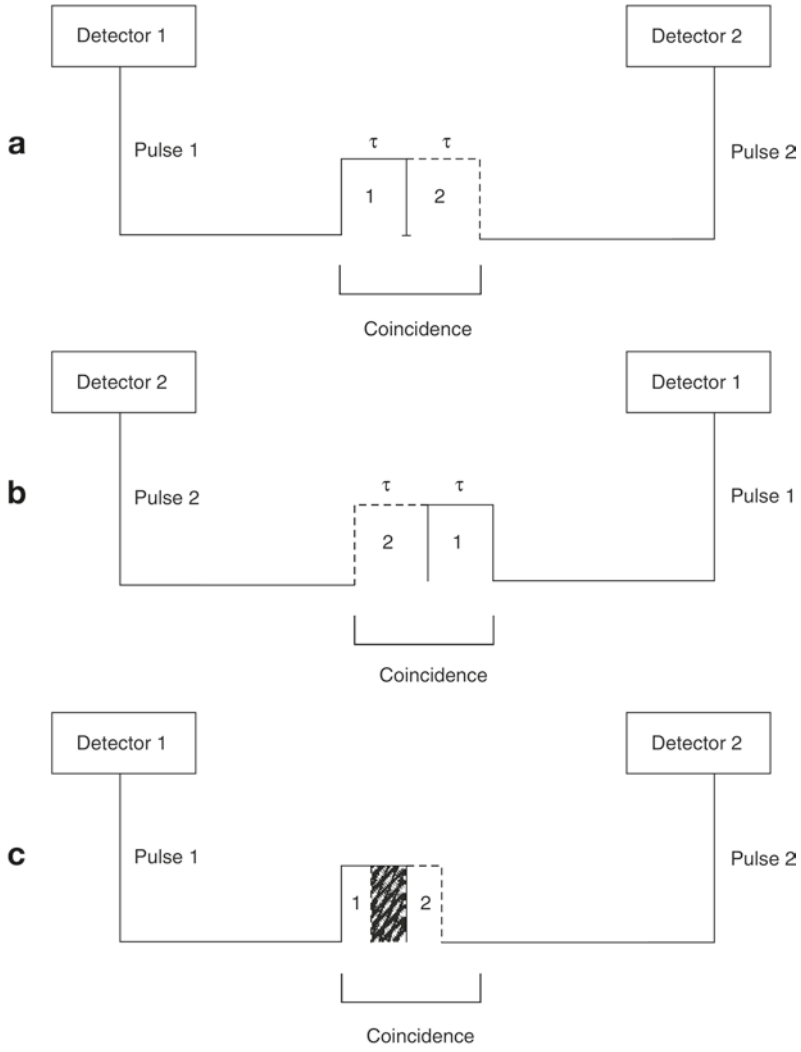

FIG. 13.3. Two time signals with time width τ define the coincidence timing window of 2τ. **a** *Pulse 2* (*dashed line*) of time width τ arrives at the opposite detector just after the arrival of *Pulse 1* (*solid line*) of time width τ at one of the detector pair, overlapping only at the edge and two events are counted in coincidence. **b** *Pulse 2* of time width τ arrives at one of the detector pair exactly prior to the arrival of *Pulse 1* of time width τ at the other detector, overlapping only at the edge and two events are counted in coincidence. **c** *Pulse 2* overlaps *Pulse 1* partially or completely depending on the time of arrival of the pulses at the detector pair, and two events are counted in coincidence. Both *A* and *B* indicate that the timing window of the coincidence circuit must be at least 2τ to detect all events in coincidence.

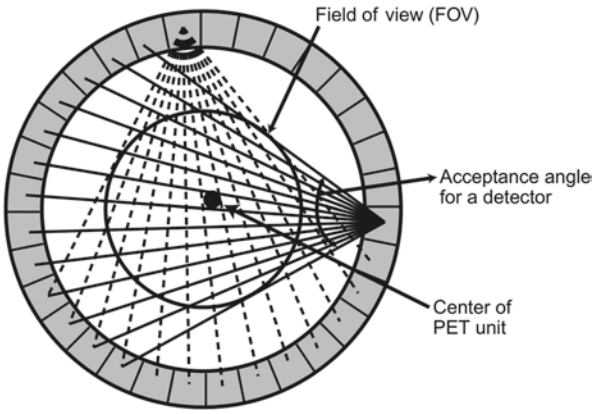

FIG. 13.4. The transverse field of view determined by the acceptance angles of individual detectors in a PET scanner. Each detector is connected in coincidence with as many as half the total number of detectors in a ring and the data for each detector are acquired in a "fan beam" projection. All possible fan beam acquisitions are made for all detectors, which define the *FOV* as shown in the figure. (Reprinted with the permission of the Cleveland Clinic Foundation.)

In a PET scanner, each detector element is connected by a coincidence circuit with a time window to a set of opposite detector elements (both in plane and axial). The number of opposite detectors can vary from one to a maximum of half the total number of detectors present in a ring. Each detector element can be connected in coincidence to a maximum of half the total number N of opposite detector elements ($N/2$). Note that less than $N/2$ detectors can also be connected. As shown in Fig. 13.4, depending on the number of opposite detectors connected, each detector element has a number of projections that define an *angle of acceptance*. These angles of acceptance for all detector elements in the ring form the transaxial FOV. The angle of acceptance increases with the number of opposite detector elements connected in coincidence and, hence, the FOV.

PET/CT Scanners

Parallel to SPECT/CT systems, PET/CT has been developed, in which functional PET images are fused with anatomical CT images to provide more accurate diagnosis of human diseases. In a PET/CT unit, both scanners are mounted on a common gantry with the CT unit in the front and PET unit in the back attached to the CT unit (Fig. 13.5). Typically, this is opposite to the SPECT/CT arrangement in which the SPECT camera is placed in the front and the CT unit in the back. Both units use the same scanning table. As in SPECT/CT, the centers of the PET FOV and CT FOV are separated by a fixed distance, called the displacement distance. The horizontal travel range of the scanning table varies with the designs of the

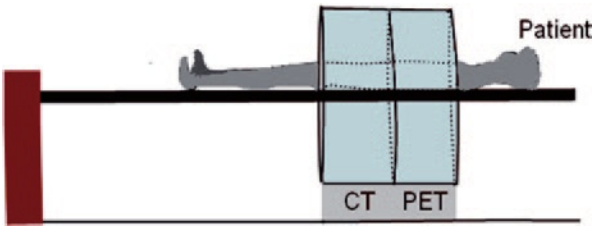

FIG. 13.5. Schematic design of a PET/CT scanner.

scanners. The actual scan field is the maximum travel range of the scanning table minus the displacement distance. Typically, a CT scan is taken first of the patient on the scanning table and in the CT scan field. The table with the patient in the same position is moved to the PET scan field and imaging is performed. Note that ^{18}F-FDG is administered 60–90 min prior to scanning, and low-intensity 511-keV photons in the patient do not interfere with the CT scan, because of the high intensity of the CT x-ray beam. Fusion of the two sets of images is performed by using commercial software as discussed under SPECT/CT. As described later, CT transmission data are used to calculate the attenuation factors for the PET emission data. The principle of attenuation correction is the same as described in SPECT/CT, based on the ratios of pixel data of a blank and the patient's CT transmission scans. Factors affecting the attenuation corrections are discussed later.

Because the position of the patient on the table does not change, both CT anatomical and PET functional images can be fused with accurate alignment providing better accuracy in detection of diseases. The overall accuracy of diagnosis increases by 20–25 % with PET/CT compared to either modality alone. Because CT scanning is fast, the total scanning time is significantly reduced, and the patient throughput is increased. Because of the increased reimbursement, whole-body imaging with PET/CT for accurate diagnosis of various cancers has become the standard of practice. The sale of PET/CT units worldwide has outpaced that of PET scanners with the sale of the latter dwindling.

Three manufacturers dominate the PET/CT markets: Siemens Healthcare, GE Healthcare, and Philips Healthcare. Each company has introduced several models in the market, making many technical improvements over the years. Current available PET/CT cameras have highly sophisticated features affording good quality images. The physical features of three PET/CT scanners from three manufacturers are listed in Table 13.2 and a commercial PET/CT scanner is shown in Fig. 13.6.

PET/MR Scanners

On the heels of success with PET/CT in clinical imaging, interest has grown considerably for similar application of PET/MR as a clinical diagnostic modality. MR provides anatomic and structural images with submillimeter spatial resolution of-

TABLE 13.2. Some features of commercial PET/CT scanners[a].

Model/product name	GE healthcare	Philips healthcare	Siemens healthcare
	Discovery PET/CT 710	Gemini TF Big Bore (PET/CT)	Biograph mCT
Gantry dimensions, H × W × D (cm)	192 × 226.1 × 140	219 × 239 × 223.7	204 × 234 × 136
Weight (kg) (lb)	4,916	4,007	3,980 with TrueV
Patient port (cm)	70	85	78
Transmission source	CT attenuation correction	CT	CT
Vertical travel (cm)	2.5–20.5 below isocenter	40	53–96
Acquisition modes	3-D, 4-D	3-D, 4-D TOF	3-D
Number of detectors	24	28 pixelar modules	192 with TrueV
Number of image planes	47	45 or 90	109 with TrueV
Number of crystals	13,824	28,336	32,448 with TrueV
Number of PMTs	1,024 (256 quad-anode)	420	4/block
Physical axial FOV (cm)	15.7	18	21.6 with TrueV
Detector material	LBS[b]	LYSO	LSO
Crystal size (mm)	4.2 × 6.3 × 25	4 × 4 × 22	4 × 4 × 20
System sensitivity—3-D (kcps/uCi/cc/LLD) (NEMA 2001)	7 cps/KBq	6,700 cps/MBq @ 10 cm >18,000 with TOF	9.5/435 keV with TrueV
Transverse resolution @ 1 cm, mm (NEMA 2001)	4.9 VUE	4.7	4.4
Axial resolution @ 1 cm, mm (NEMA 2001)	5.6 VUE	4.7	4.5
Peak noise equivalent count rate (kcps) (NEMA 2001) 3D	130 @ 29.5 kBq/ml	90 @ 14 kBq/ml (240 with TOF)	175 @ 28 kBq/ml
Scatter fraction—3-D (NEMA 2001)	37 %	26%	<34 %
Type of CT detector	Volara XT Digital DAS	Solid State—GOS	Ultra Fast Ceramic
kV-range/mA-range	700 or 800 mA	90–140 kVp/20–500 mA	80–140 kV/20–800 mA
CTDI (dose/100 mAs) B/16 cm phant	Axial head: 18 mGy Axial body: 8 mGy	10.17 mGy/100 mAs	40/64 slice 9.3 mGy 128 slice 8.5 mGy
Standard HC resolution (2 % MTF)	17.1 lp/cm	12 lp/cm	16.4 lp/cm
Number of slices	16, 64, 128	16	40, 64 or 128
Reconstruction time: std/high res/topo	16 FPS/35 FPS	Up to 20 images per sec	Up to 40 images per sec

[a]Reprinted with permission from Imaging Technology News: www.itnonline.com.
[b]*LBS* lutetium based scintillator

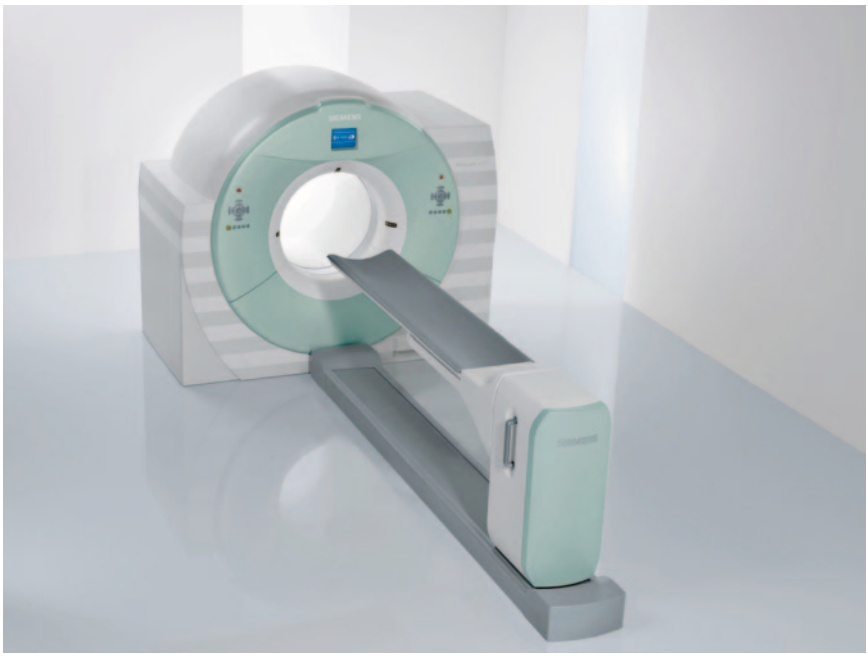

FIG. 13.6. A PET/CT scanner, Biograph mCT. (Image/Photo courtesy of Siemens Medical Solutions USA, Inc., Malvern, PA).

fering a better soft-tissue contrast than CT. MR also has the great advantage of using magnetic radiofrequency, thus eliminating the radiation dose to the patient. The following is a brief description of currently available PET/MR scanners.

Principles of MR Imaging

It is beyond the scope of this book to describe in detail the principles of magnetic resonance (MR) imaging and the readers are referred to specific textbooks on MR imaging. The following is a brief summary of the subject.

MRI is based on the magnetic property of atomic nuclei. Protons and neutrons have magnetic moments due to inherent angular momentum and spin haphazardly (Fig. 13.7a). Nuclei containing even numbers of protons and neutrons possess no net magnetic moment, because of the cancellation of the individual magnetic moments by the even number of nucleons. Nuclei containing odd number of protons or neutrons, however, possess a net magnetic moment that has both a magnitude and a direction and behave like magnets. When these nuclei (or spins, as they are commonly called) are placed in a large external magnetic field (B_0), they align themselves (at a slight angle) in either parallel or antiparallel direction to the magnetic field and also precess (rotate) at a frequency proportional to the strength of the field (Fig. 13.7b). The parallel spins remain in the lower energy state and

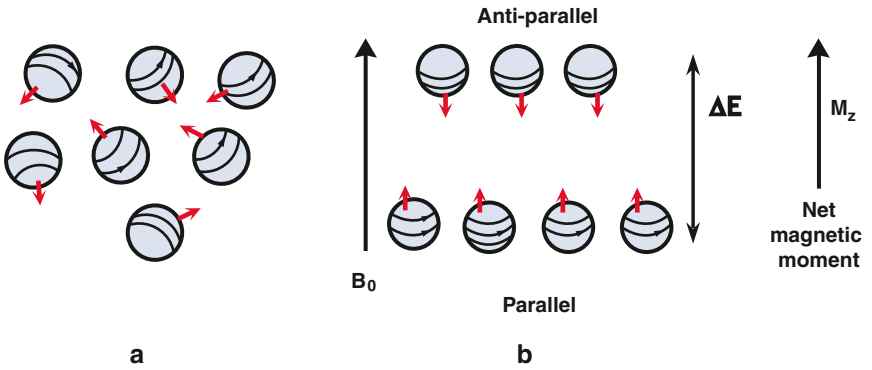

FIG. 13.7. **a** Free protons spin randomly and their magnetic moments cancel each other, with a residual momentum due to an unpaired proton, if any. **b** When an external magnetic field, B_0, is applied, the protons orient themselves in either *parallel* or *antiparallel* direction to the field B_0. The number of *parallel* protons are slightly larger than *antiparallel* ones, thus creating a net magnetic moment in the direction of B_0. The energy difference between the two groups is ΔE.

the antiparallel ones in the high energy state, the energy difference being ΔE. Normally a slightly greater number of spins exist in parallel direction and they increase with the increase in magnetic field strength. These excess spins result in a net magnetization (M_z) with a measurable magnetic moment parallel to the field of B_0 and they are said to be at equilibrium in the Z direction. If a radiofrequency pulse (RF), which is an oscillating electromagnetic field normally termed B_1, is applied perpendicular to B_0 at the precessional (resonant) frequency of the nuclei, the latter absorb energy from the RF field and make a transition to the high energy state. As a result, the longitudinal magnetization (M_z) flips towards the transverse plane (X–Y plane) at different angles depending on the strength of the RF pulse, thus causing transverse magnetization (M_{xy}). RF pulses that cause 90° flipping are called 90° pulses and produce maximum possible transverse magnetization (Fig. 13.8) and are commonly used in MR imaging. If a 180° pulse is applied, it will invert M_z to $-M_z$ i.e. the longitudinal magnetization will be inverted in the opposite direction (Fig. 13.8).

Hydrogen atoms have one proton in the nucleus and are abundant in the living body mostly in the form of water (70 %), with the remainder in tissues and fat. When a patient is placed in a magnetic field (B_0) as in a MR machine, the tissues become magnetized due to excess parallel protons or spins that align with B_0 and remain at equilibrium. When an RF pulse (commonly 90° pulse) is applied perpendicular to B_0, the equilibrium of longitudinal magnetization is perturbed as a result of energy absorption from the RF field by the excess parallel spins of the nuclei, and the magnetization vector orients to the transverse or X–Y plane (at 90° for the 90° pulse). All nuclei remain in phase coherence, meaning magnetization vectors of all neighboring nuclei point to the same direction with maximum mag-

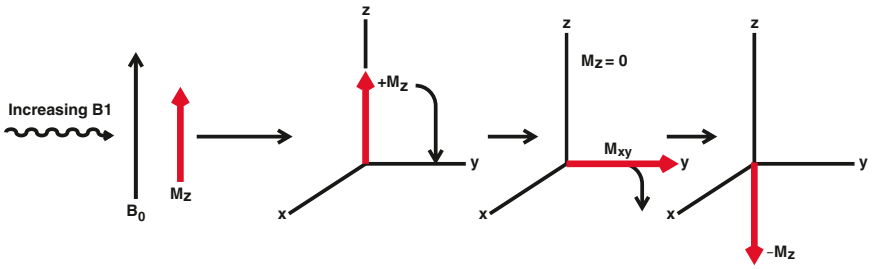

FIG. 13.8. When a radiofrequency pulse (RF), B_1, is applied to the M_Z (longitudinal magnetization) in the presence of B_0, M_Z flips towards the transverse plane (X–Y) plane at different angles depending on the strength of B_1. RF pulse that causes 90° flipping produces maximum transverse magnetization M_{xy}. If a 180° pulse is used, $+M_Z$ becomes $-M_Z$.

netization. If a receiver coil is placed perpendicular to the external field B_0, the transverse magnetization (maximum M_{xy}) induces a current or a sinusoidal MR signal in the receiver coil according to Faraday's law of induction. This signal is called *free induction decay* (FID) signal and its size increases with the strength of the magnetic field B_0 and the magnitude of the RF pulse (B_1). As the RF field is switched off, the FID signal decays resulting in the return of all nuclei to the original state they had before. This return is called *relaxation* of the nuclei. Two types of basic relaxation occur in tissues simultaneously, T1 and T2, and both contribute to the decay of the MR signal.

In T1 relaxation, nuclei give off their excess energy by spin-lattice interaction to the surrounding molecular structures (lattice) and start to regrow magnetization along B_0, finally reaching the original value of maximum longitudinal magnetization at equilibrium. The rate of this regrowth is characterized by a tissue relaxation parameter called T1, which is defined by the time to recover 63 % of the maximum longitudinal magnetization following a 90° pulse (Fig. 13.9). T1 values depend on the vibrational frequencies and hence the physical characteristics of the molecules such as solid or liquid states, or stationary or moving structures.

In T2 relaxation following the shut-off of the RF pulse, all nuclei lose their phase coherence over time due to the random collision among neighboring nuclei (spin-spin interaction) thus losing energy to return to the original state of random phase. Random collision is caused by varying precessions of the nuclei at different velocities because of the small inhomogeneities of the magnetic field intrinsic to the structure of the tissues and also of the external field B_0. The dephasing results in a fast exponential decay of the MR signal characterized by the time T2, which is given by the time interval between peak transverse signal and 37 % of the peak (1/e) (Fig. 13.10).

T1 values increase with higher magnetic field and are normally much longer than T2 values for most tissues. Both T1 and T2 values depend on the composition of tissues. For example, fat has a short T1 and fluid (cerebrospinal fluid, cyst, etc.) has longer T1, so fat is seen as bright, whereas fluid appears as dark. Other tissues fall within the range between the two. On the other hand, mobile

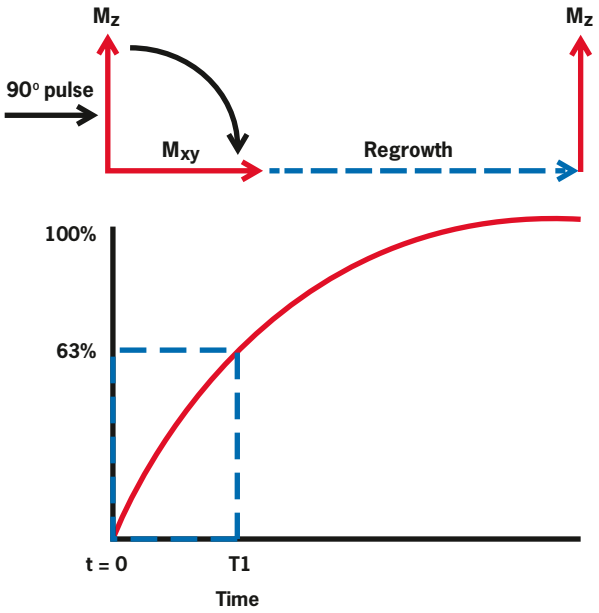

FIG. 13.9. Following a 90° RF pulse, longitudinal magnetization M_Z is converted to zero at *X–Y* plane, but returns to equilibrium exponentially. It occurs through spin-lattice interaction with a relaxation constant T1, which is the time when 63 % of M_Z is recovered.

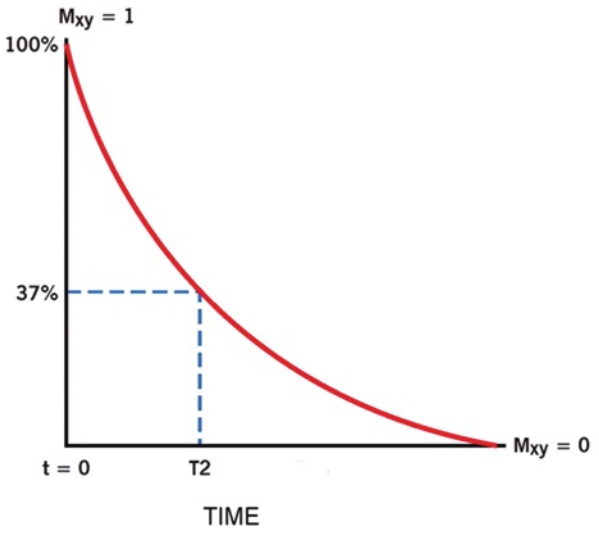

FIG. 13.10. Following a 90° RF pulse, M_Z flips to *X–Y* plane (M_{xy}), which loses phase coherence due to spin-spin interaction in tissues and inhomogeneity of the external field. The FID signal decays exponentially with a time constant T2, during which the signal decays to 37 %.

molecules such as blood exhibit a long T2, whereas nonmoving structures like bone have a short T2.

MR signals depend on proton density, T1 and T2 relaxation time constants of different tissues in the body. One can obtain sufficient contrast between tissues by manipulating the timing, order, polarity and repetition frequency of RF pulses and B_0. Tailoring of these parameters is alluded to as pulse sequence, the application of which depends on the type of tissue being imaged. Three major types of pulse sequences are spin echo (SE), inversion recovery (IR) and gradient recalled echo (GRE), the details of which are available in standard physics books. In spin echo pulse sequence, a 90° pulse is applied to cause transverse magnetization in tissues, followed by a 180° pulse to reverse it to the longitudinal magnetization. When all spins are rephased, an RF "echo" (a measureable MR signal) is produced and the time between the 90° pulse and the peak of the echo is called the time of echo (TE). The time between two successive 90° pulses is called the repetition time (TR). A spin-echo sequence of a short TR (e.g., 250–1000 ms) and a short TE (less than 25 ms) highlights the T1 difference in tissues and is called T1-weighting, whereas a combination of a long TR (2500–6500 ms) and a long TE (more than 75 ms) emphasizes T2 differences in tissues and hence the T2-weighting. In an IR pulse sequence, an 180° pulse is applied causing net longitudinal magnetization along the –Z direction that moves towards equilibrium along the +Z direction due to spin-lattice interaction. But a 90° pulse is applied before reaching equilibrium whereby the longitudinal magnetization flips to the X–Y plane ultimately producing a FID signal. This technique is used to generate contrast between tissues with very different T1 values by adjusting the inversion recovery time (the time between the inversion 180° pulse and the 90° pulse). In GRE pulse sequence, small angle RF pulses (typically 20–60°) are applied in rapid succession to tissues. The technique is useful in eliminating the artifacts arising from respiratory motion by having a breath-hold acquisition. A given pulse sequence is chosen on the basis of tissue characteristics defined by the T1 and T2 relaxation times and proton density.

Paramagnetic contrast agents, commonly gadolinium chelates such as Gd-DTPA, when injected intravenously, accumulate in extra vascular space over time and shorten both T1 and T2 values. But at a commonly used concentration of these contrast agents, better contrast are obtained in T1- weighted images.

MR scanner

An MR scanner is made up of coils of special metal alloys shaped in a cylindrical bore and cooled by liquid helium. Electric current is applied through the coils, which induces a constant magnetic field along the bore of the magnet. The magnets used in most clinical machines are superconducting magnets. In open MR systems commonly used for claustrophobic patients, two disc-shaped magnets are positioned with a gap in between to accommodate patients. An RF coil is used to perturb the magnetization of the atomic nuclei. The same coil or separate coils are used to receive the echo signals from the tissue. Integrated in machines are a patient table, magnetic shielding, and various monitoring equipment and, of course,

a dedicated computer. Currently, the maximum available field strength of the clinical MR machines is 3.0 T, whereas it is limited to 1.2 T in open MR systems.

Commercial PET/MR Scanners

Integration of PET with MR into a single unit faces several hurdles, which have been overcome over the years to some degree. First, the commonly used photomultiplier tubes are sensitive to the radiofrequency of the magnetic field causing artifacts in PET images, now they are replaced by magnetic field-insensitive avalanche photodiodes. Next, compact PET detectors must be designed and shielded to incorporate into the MR unit so that radiofrequency does not interfere with the PET data processing. Unlike PET/CT where simultaneous PET and CT data acquisitions are not feasible because of the crossover of pulses, an integrated PET/MR offers an advantage of simultaneous data acquisition since the radiofrequency pulse and the radiation pulse do not interfere with each other, thus reducing the time of scanning. Since unlike CT imaging, there is no x-ray attenuation in MR imaging for attenuation correction in PET, a new way of attenuation correction need to be devised. Also in the absence of radiation from MR unit, PET/MR offers a low radiation dose to the patient.

Although small animal PET/MR scanners have been developed some time ago, only recently clinical units have been introduced. GE Healthcare, Siemens Healthcare, and Philips Healthcare have each developed PET/MR scanners of their own based on different designs but using the same basic principle. The GE scanner basically consists of two separate systems—PET/CT and MR, and the patient is scanned on each unit separately following transportation from one modality to the other. The two images are fused by algorithm, but the technique suffers from inadequate accuracy in alignment due to possible variation in patient position in two modalities. Furthermore, because of the CT unit, the radiation burden on the patient is relatively higher with the GE scanner. This unit has been approved by the US FDA for clinical use.

Philips Healthcare has introduced Ingenuity TF PET/MRI scanner, in which TF PET and 3-T MR units are positioned at a distance of 2.5 m at opposite ends. A floor–based bed is incorporated between the two scanners that can be turned around 180° to position the patient in either scanner. The patient is scanned sequentially in both scanners and two images are fused more accurately because of the proper alignment of the scanners with the scanning bed.

In Siemens whole-body Biograph mMR scanner, PET and MR units are completely integrated such that data acquisition in both scanners is accomplished simultaneously. The PET detectors are made of avalanche LSO photodiodes that are ingeniously imbedded into the 3-T MR coils. The block detectors contain a cooling feature for optimal PET performance and also a special shielding is incorporated in the system to eliminate radiofrequency interference with the PET data acquisition and processing. Furthermore, low attenuation material has been employed in what is called total imaging matrix (TIM) coils and the table in the MR system to minimize the attenuation of PET signals. Simultaneous data acquisition matching in time and position provides most accurate fusion of images and

FIG. 13.11. A PET/MR scanner, Biograph mMR. (Image/Photo courtesy of Siemens Medical Solutions, USA, Inc., Malvern, PA)

reduces the time of scanning significantly. Biograph mMR has been approved by the US FDA for clinical use, while the Philips scanner is not yet. Siemen's Biograph mMR is shown in Fig. 13.11 and its physical and technical parameters are given in Table 13.3. MR, PET and fused PET/MR images of a section of the whole body of a patient are shown in Fig. 13.12.

Mobile PET or PET/CT

Largely because of the low patient volume and high cost, many community hospitals cannot afford PET or PET/CT scanners, but can take advantage of mobile PET or PET/CT that provides PET scanning services to different locations. PET or PET/CT scanners and necessary accessories are installed in sturdy vans, along with nuclear pharmacy facilities. The mobile unit moves to different clients' facilities on different days depending on the schedule. The patient's schedule and delivery of PET tracers must be well coordinated to provide efficient services. The owner of the mobile unit must have a license from appropriate authorities to

TABLE 13.3. Various physical and technical parameters of Biograph mMR scanner.[a]

MR unit		
Operating field strength		3 T
Magnet type		Niobium-Titanium
Field stability over time		<0.1 ppm/h
Weight (with cryogens)		6300 kg
Magnet length		163 cm
Bore size		60 cm
System length cover to cover		199 cm
FOV		5–500 mm
Slice thickness 2D		0.1–200 mm
Partition thickness 3D		0.05–20 mm
Highest in-plane resolution		9 μm
PET unit		
Crystal material		LSO
Crystal element dimension		4×4×20 mm
Crystal elements per block		64
Avalanche Photodiodes (APDs)		9 per block
Detector ring diameter		656 mm
Blocks per detector ring		56
Transaxial FOV		594 mm
Crystal elements per ring		448
Number of detector rings		64
Total number of crystal elements		28672
Axial FOV		25.8 cm
Spatial resolution, standard processing		
(344×344)- Axial	FWHM @ 1 cm (mm)	≤4.8
	FWHM @ 10 cm (mm)	≤7.2
Spatial resolution—transverse (average of radial and tangential)		
(344×344)	FWHM @ 1 cm (mm)	≤4.7
	FWHM @ 10 cm (mm)	≤5.2
Scatter fraction		≤42%
Sensitivity (cps/kBq)		≥12
Peak NEC rate (kcps) measured ≤22 kBq/cc		≥155

[a] Data supplied by Annemarie Grammens, Siemens Healthcare.

operate the mobile PET/CT and also a letter of agreement between the client and the licensee to provide the service. The van must meet the Department of Transportation's overload regulations, and the rules and regulations of fire safety and security of local authorities.

Micro-PET

For research animal imaging, clinical PET scanners with a large bore give poor spatial resolution. Micro PET scanners with a smaller bore and, hence, smaller in overall size (to be fitted in small rooms) have been developed by several manufacturers. The typical bore diameter is about 16 cm. The spatial resolution can

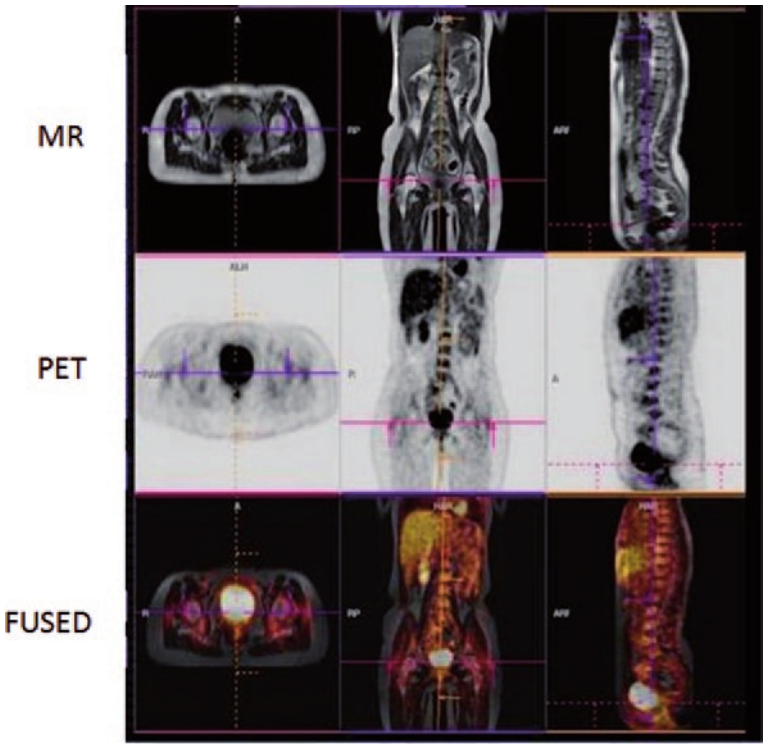

FIG. 13.12. Whole body *MR*, *PET* and fused PET/MR images of a patient. (Supplied by Annemarie Grammens, Siemens Healthcare)

be obtained as small as 1 mm with the use of LSO detectors. These scanners are useful for drug evaluation in animals.

Dual- and Triple-Head Gamma Cameras

Conventional dual-head and triple-head gamma cameras (Fig. 12.2) can be utilized as PET cameras by connecting the appropriate heads with a coincidence circuitry. The typical time window is ~12 ns for dual-head and ~10 ns for triple-head cameras. In SPECT mode, the cameras are used with collimators, whereas in PET mode, collimators are removed, and therefore they can be used in either mode as needed. These cameras are attractive to community hospitals because of their low cost with the scope of PET imaging.

These cameras suffer from a disadvantage of low sensitivity due to low detection efficiency of NaI(Tl) crystal for 511-keV photons. To improve sensitivity, thicker crystals of sizes 1.6 to 2.5 cm have been employed in some cameras, with a resultant increase in coincidence photopeak efficiency of only 3–4 %, with

concomitant degradation of spatial resolution. There is a significant camera dead time loss and pulse pile-up of counts in PET mode in the absence of a collimator because the number of detectors are only two or three unlike thousands in PET cameras. Overall, the spatial resolution of a multihead camera is poorer than that of a dedicated PET scanner. The use of these cameras is fading due to popularity of PET cameras.

Data Acquisition

In PET imaging, two 511-keV annihilation photons are detected in coincidence by two opposite detectors along a straight line, called the *line of response* (LOR). In a full ring system, data are collected in 360° simultaneously, whereas in the partial ring system, the rings are rotated around the patient for 360° data acquisition. There are three steps in PET data acquisition. First, the location of the detector pair in the ring is determined for each coincident event. Next, the pulses are analyzed by PHA to check if they are within the energy window set for 511 keV. Finally, the position of the LOR is determined in polar coordinates to store the data in computer memory.

Because each detector is connected to many opposite detectors in coincidence, which detector pair detected a coincidence event must be determined. As in gamma cameras, the position *X, Y* of each detector in the ring is determined by

$$X = \frac{(C + D) - (A + B)}{A + B + C + D} \tag{13.1}$$

$$Y = \frac{(A + D) - (B + C)}{A + B + C + D} \tag{13.2}$$

where A, B, C, D are the pulses from the four PM tubes attached to the block, as shown in Fig. 13.1.

Next, the four pulses (A, B, C, and D) are summed up to give a *Z* pulse, which is then checked by the PHA if its amplitude is within the energy window set for the 511-keV photons. If it is outside the window, it is rejected; otherwise, it is accepted for storage.

The last step in data acquisition is the storage of the data in the computer. Unlike conventional planar imaging where individual events are stored in a (*X*, *Y*) matrix, the coincidence events in PET imaging are stored in the form of a *sinogram*. Consider an annihilation event occurring at the * position in Fig. 13.13a. The coincidence event is detected along the LOR indicated by the arrow between the two detectors. It is not known where along the line of travel of the two photons the event occurred, because they are accepted within the set time window (say, 12 ns) and their exact times of arrival are not compared. The only information we have is the positions of the two detectors in the ring that registered the event,

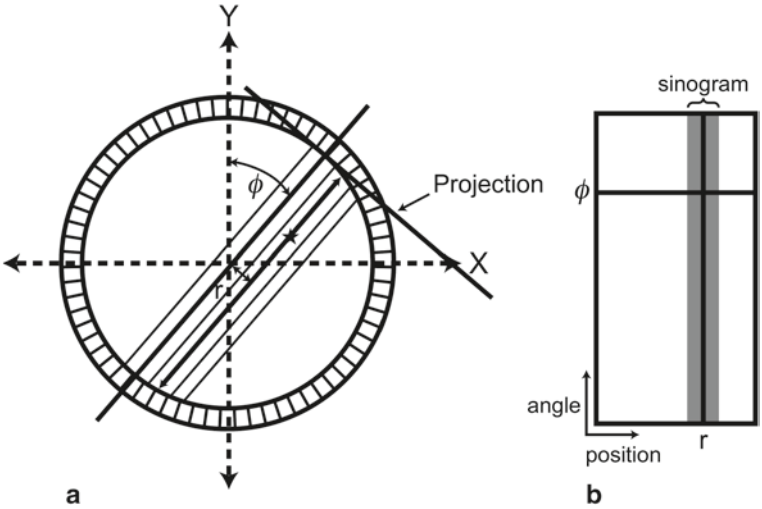

FIG. 13.13. PET data acquisition in the form of a sinogram. **a** Each LOR datum is plotted in (r, ϕ) coordinates. **b** Data for all r and ϕ values are plotted to yield the sinogram indicated by the shaded area (only a part is shown). (Reprinted with the permission of the Cleveland Clinic Foundation)

that is, the location of the LOR is established by the (X, Y) positioning of the two detectors. Many coincidence events arise from different locations along the LOR and all are detected by the same detector pair and stored in the same pixel, as described below.

For data storage in sinograms, each LOR is defined by the distance (r) of the LOR from the center of the scan field (i.e., the center of the gantry) and the angle of orientation (ϕ) of the LOR (i.e., the angle between r and the vertical axis of the field). A matrix of an appropriate size is chosen defined by the r, ϕ coordinates, rather than by X-, Y-coordinates used in SPECT data acquisition, and counts in each LOR are stored in the corresponding pixel in the matrix. If we plot the distance r on the x-axis and the angle ϕ on the y-axis, then the coincidence event along the LOR (r, ϕ) will be assigned at the cross-point of r and ϕ values (Fig. 13.13b). In a given projection, adjacent detector pairs constitute parallel LORs (at different r values in Fig. 13.13a) at the same angle of orientation. The plot of these LORs will be seen as a horizontal row at angle ϕ. Similarly LORs from different projections (i.e., at different angles ϕ) for the same r values can be plotted, which will give a vertical line. When all projections around the field of view are considered, the plot of the LORs at different projection angles and r values will result in the shaded area in Fig. 13.13b, which is called the sinogram. A typical normal sinogram is shown in Fig. 13.14.

The sinogram represents a single slice of data for a transverse FOV obtained from a single ring of the PET scanner. PET data are acquired directly into a sinogram in a matrix of appropriate size in the computer. Each pixel corresponds to a

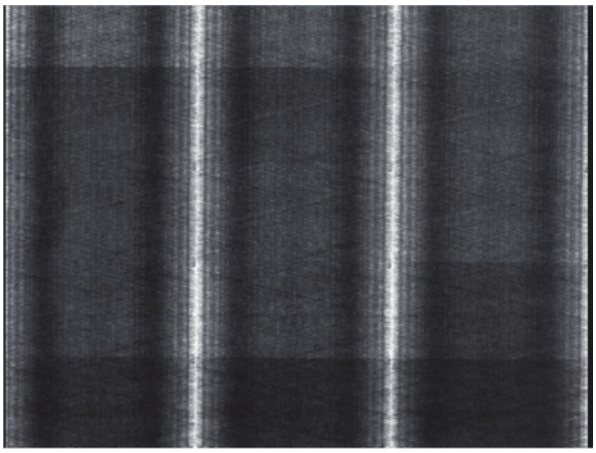

FIG. 13.14. A typical normal sinogram indicating all detectors are working properly.

particular LOR characterized by (r, ϕ) containing all coincidence counts detected by the detector pair along the LOR. Data can be collected in both static and dynamic imaging using either the frame mode or the list mode, described in Chapter 11.

Because PET scanners are axially fixed, whole-body imaging is accomplished by the use of a computer-controlled bed-table that moves along the axis of the scanner. The whole-body scan of the patient is obtained at different axial positions of the bed.

Time of Flight Method

The time of flight (TOF) PET technique is based on the measurement of time difference in the arrival of the two 511 keV annihilation photons at the detectors, as illustrated in Fig. 13.15. Suppose two detectors are equidistant x from the center of FOV (CFOV) and a positron is annihilated in the patient at position at a distance Δx from the CFOV. One of the 511 keV photons will travel x + Δx and the other will travel x – Δx. Since the photons travel at speed of light (c), the difference in time (Δt) of arrival of the two photons at the detectors is 2 Δx/c. Note that the photons from the center of FOV arrive at the detectors simultaneously (Δx = 0). The uncertainty in the annihilation location is usually much smaller than the diameter D of the patient (with good timing resolution). The signal-to-noise ratio (SNR) increases with improved timing resolution and is proportional to D/Δx i.e., 2D/(c.Δt). For a 40-cm subject and with a timing resolution of 0.6 ns, the SNR (sensitivity) increases by a factor of 4.4. With fast electronics and scintillators, and also a shorter time window, TOF PET scanners can measure the time difference Δt fairly accurately and provide high resolution images and better localization of the lesion. Furthermore, the TOF method reduces the scanning time.

Decades ago, the TOF PET scanners were introduced using fast detector like cesium fluoride (CsF) or barium fluoride (BaF_2) to allow high count rates, but

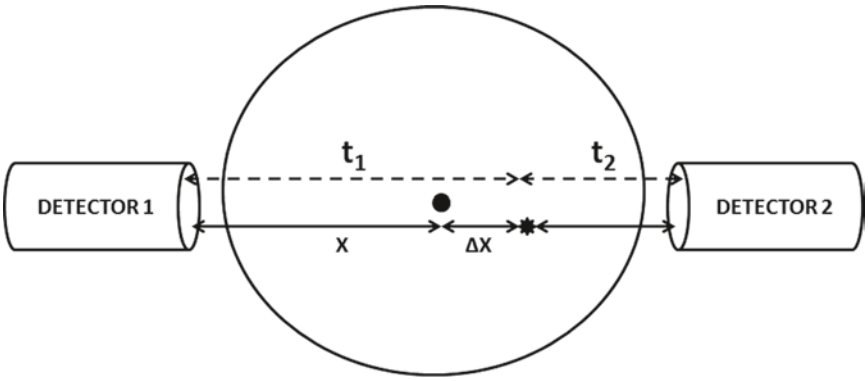

FIG. 13.15. An illustration of the time of flight (TOF) technique in PET. The time difference (t_1–t_2) in the arrival of two 511 keV photons is related to Δx. Using TOF information, the location of annihilation of positron is determined within a spatial range of ($c.\Delta t$)/2, where c is the velocity of light.

spatial resolution and sensitivity were poorer than those of conventional PET scanners with BGO, because of poor light production. With the advent of improved scintillators like LSO, LYSO and $LaBr_3$, along with more efficient and reliable PM tubes, TOF is reemerging as the accepted technique in commercial PET scanners. Philips Healthcare is marketing Big Bore Gemini TF PET scanners based on the TOF technique. Current TOF scanners offer better spatial resolution and sensitivity because of increased light production in the detector material and the shorter timing resolution. Moreover, this technique improves the image quality in heavy patients, compared to the conventional PET scanners that lead to a loss of counts at high count rates as well as an increase in scattered counts.

Two-Dimensional Versus Three-Dimensional Data Acquisition

Coincident counts detected by a detector pair are called the *prompts* which include true, random, and scatter events described later (Fig. 13.16). To eliminate random and scatter events, annular septa (~1 mm thick and radial width of 7–10 cm) made of tungsten or lead are inserted between rings in multiring PET scanners (Fig. 13.17a). The septa act as do parallel hole collimators in gamma cameras. They mostly allow direct coincidence events to be recorded from a given ring and prevent random and scatter from other rings. This mode of data collection is called two-dimensional (2-D) acquisition. The use of septa reduces the contribution of scattered photons from 30 to 40 % without septa to 10–15 %. To improve sensitivity, detector pairs in two adjacent or nearby rings are also connected in coincidence. Such cross-coincidence connections can be made at most among five adjacent rings. Coincidence events detected by the detectors connected in the same ring are called the *direct plane* events, whereas those detected by detectors interconnected between different rings are called the *cross plane* events. Although

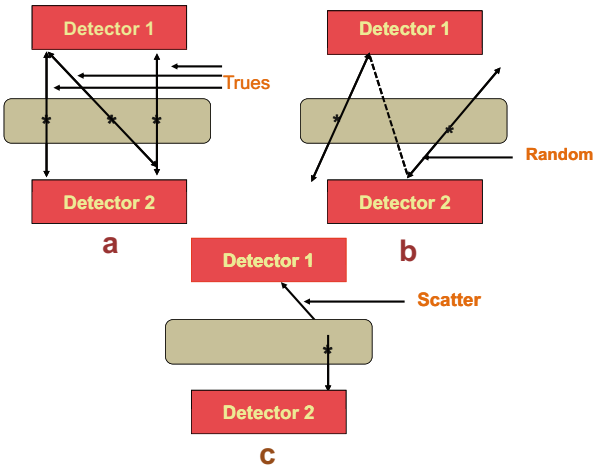

FIG. 13.16. **a** True coincidence events. **b** Random coincidence events detected by two detectors connected in coincidence along the dotted line. The two 511-keV photons originate from different positron annihilations. **c** Scattered coincidence events. One or both of the 511 keV photons from the same annihilation event may be scattered with little loss of energy and may fall within the PHA window and also within the coincidence time window to be detected as a coincidence event by two detectors.

the cross plane events increase the sensitivity, they degrade the spatial resolution as a trade-off. The overall sensitivity in 2-D acquisition is 2–3 % at best.

To improve further the sensitivity of PET scanners, the three-dimensional (3-D) acquisition is employed in which the septa are retracted, or they are not included in the scanner (Fig. 13.17b). In this mode, all events detected by detectors in coincidence in all rings are counted including random and scatter events, and the sensitivity in the 3-D mode increases four- to eightfold over 2-D acquisition. The incidences of random and scatter can be reduced by having a smaller angle of acceptance; that is, a detector is connected to a fewer number of opposite detectors.

Image Reconstruction

Image reconstruction of 2-D PET data is accomplished by the same filtered backprojection and iterative methods that have been described in detail under SPECT in Chapter 12. In PET, the LORs in a sinogram are back-projected by the Fourier method. In the iterative method, the projections are estimated by determining the weighted sum of the activities in all pixels along a LOR across the estimated image, and then compared with the measured projection.

The reconstruction of images from 3-D data is complicated by a very large volume of data, especially in a multiring scanner. The direct application of the filtered backprojection and iterative methods to these data is difficult, and so

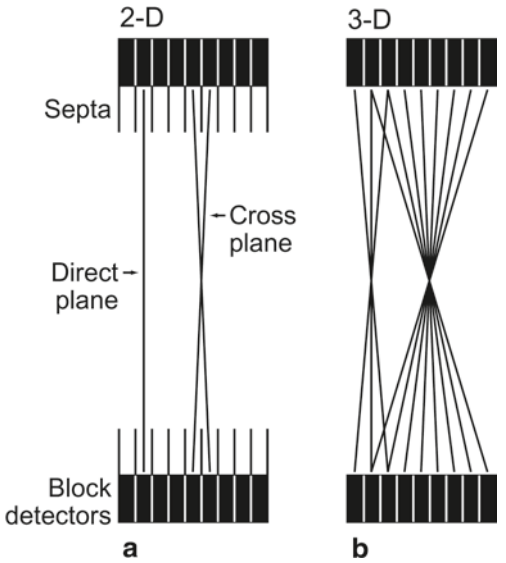

FIG. 13.17. **a** *2-D* data acquisition with the septa placed between the rings so that true coincidence counts are obtained avoiding random events and scatters. Detectors connected in the same ring give direct plane events. However, detectors are connected in adjacent rings and cross plane data are obtained as shown. **b** When septa are removed, the *3-D* data acquisition takes place, which includes random and scatter events along with true events. (Reprinted with the permission of the Cleveland Clinic Foundation.)

the 3-D sinogram data are rebinned into a set of 2-D equivalent projections by assigning axially tilted LORs to transaxial planes intersecting them at their axial midpoints. This method is called the single slice rebinning method (SSRB). In another method, called the Fourier rebinning (FORE) method, rebinning is performed by applying the Fourier method to each oblique sinogram in the frequency domain. This method is more accurate than the SSRB method because of the more accurate estimate of the source axial location. After rebinning of 3-D data into 2-D data, either the filtered backprojection or iterative method is applied.

Factors Affecting PET

As in gamma cameras, PET acquisition data are affected by photon attenuation, variation in detection efficiency of the detectors, scatter coincidences, partial volume effect, and dead time. These factors are already discussed under SPECT and therefore only subtle points pertinent to PET data will be highlighted here. In addition, PET data are affected by some unique factors such as random coincidence and parallax error (radial elongation), which will be discussed below.

Normalization

There are 10,000–32,000 detectors arranged in blocks, and coupled to several hundred PM tubes in modern PET scanners. Practically, as in gamma cameras, the detection efficiency varies from detector pair to detector pair due to variation in the gain of PM tubes and location of the detector in the block, resulting in nonuniformity of the PET data. Data are corrected for this factor by using what is called *normalization* or uniformity correction. In normalization of PET data, all detectors are exposed uniformly to a 511-keV photon source (e.g., ^{68}Ge source), without an object in the field of view, and data are collected in the 2-D or 3-D mode. The normalization factors F_i are calculated for individual pixels as

$$F_i = \frac{A_{mean}}{A_i} \tag{13.3}$$

where A_{mean} is the mean of all pixel counts and A_i is the counts in the ith pixel. The observed count C_i in the ith pixel from the patient is then normalized by

$$C_{norm,i} = C_i \times F_i \tag{13.4}$$

where $C_{norm,i}$ is the normalized count in the ith pixel. The normalization data collection requires a long time (~6–8 h) and is normally carried out overnight. These factors are obtained weekly or monthly and most vendors offer algorithms to obtain them routinely.

Photon Attenuation Correction

Chang method: The two 511-keV photons in PET can traverse different thicknesses of tissues before detection and are attenuated to a different degree similar to situations discussed under SPECT. If the two photons traverse a and b thicknesses of tissues of an organ (Fig. 13.18), then the attenuation correction P for each pixel (i.e., each LOR) is given by

$$P = e^{-\mu a} \times e^{-\mu b} = e^{-\mu(a+b)} = e^{-\mu D} \tag{13.5}$$

where μ is the linear attenuation coefficient of 511-keV photons in tissue and D is the total thickness of the organ. When photons traverse various organs, differences in linear attenuation coefficients and organ thicknesses must be taken into consideration. Then Eq. (13.5) becomes

$$P = e^{-\sum_{i=1}^{n} \mu_i D_i} \tag{13.6}$$

As in SPECT, Eq. (13.5) has been employed to correct for attenuation in brain PET imaging, based on the assumption of uniform density of tissue and a con-

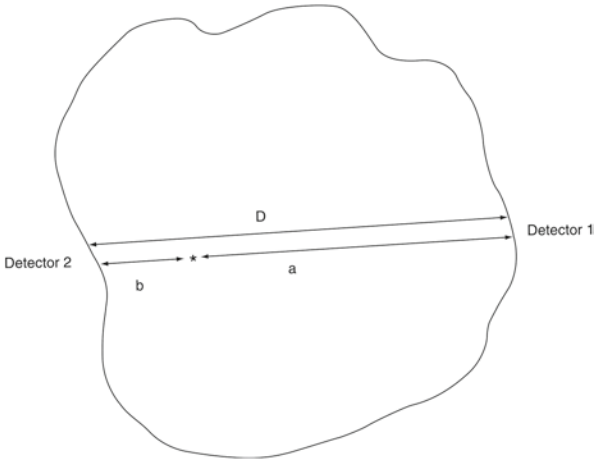

FIG. 13.18. Two 511-keV annihilation photons traverse thicknesses *a* and *b* of tissues of an organ. However, attenuation of the two photons depends on the total thickness D of the organ regardless of *a* and *b*.

stant μ for 511-keV photons in tissue (Chang method). However, the method tends to cause artifacts due to underestimation of attenuation in the thorax area.

Transmission scan method: The transmission scan method was widely used for attenuation correction of PET emission scan data before PET/CT was introduced. In this method, normally a ^{68}Ge source is used to obtain the transmission scan in dedicated PET imaging. The source is placed in a holder mounted at the edge of the scanner bore and the holder is rotated by a motor so that data detected by all detector pairs can be acquired. Normally, a blank scan is obtained at the beginning of the day without any object or patient in the scanner. These blank scan data are used for all subsequent patients for the day. Next a transmission scan is obtained with the patient in the scanner for each patient. The ratios of the counts in each pixel (i.e., each LOR) between the blank scan and the transmission scan are calculated for each patient. The emission scan is taken with the patient in the same position as in the transmission scan to minimize errors in correction factors, and then each LOR datum is corrected for attenuation by applying the corresponding ratio. It takes 20–40 min for acquisition of the transmission scan depending on the source strength. Normally the transmission scan is performed before the emission scan to avoid interference of radiations from the administered radioactivity. Other approaches include post-injection transmission scanning (transmission scan after the emission scan) and simultaneous emission/transmission scanning, but each method suffers from various disadvantages of its own.

CT transmission scan method: In PET/CT, the CT transmission scan is utilized for attenuation correction, which takes less than a minute thus improving the patient throughput, and it has become the method of choice. As mentioned in the SPECT/CT technique, typically at the beginning of the day, a blank CT

scan without the patient in the scanner is obtained, which is later used for subsequent patient studies for the day. Next, the CT transmission scan of each patient is taken with the patient in the CT scan field before the emission scan, and an attenuation correction map is generated from the ratios of counts of each pixel (i.e., LOR) of the blank scan and the transmission scan. Because the PET and CT units are fixed on the same gantry, the patient remains in the same position on the table, which is then moved to the PET scan field for the emission scan. Factors from the attenuation map are subsequently applied to each LOR in the patient's emission scan. The CT transmission method provides essentially noiseless PET images.

Attenuation depends on photon energy; therefore correction factors derived from ~70-keV CT x-ray scans must be scaled to the 511-keV photons of PET by applying a scaling factor defined by the ratio of mass attenuation coefficient of 511-keV photons to that of 70-keV photons. This factor is assumed to be the same for all tissues except bone, which has a slightly higher mass attenuation coefficient. As mentioned in the SPECT/CT section, the respiratory motion of the thorax during scanning and intravenous contrast agents affect the CT attenuation factors. Use of breath hold and water-based contrast agents helps mitigate these effects.

Attenuation correction in PET/MR: Unlike in PET/CT imaging, MR does not have radiation to be attenuated and also a transmission source cannot be installed because of the space constraint in PET/MR scanners, so a new approach is needed to apply attenuation correction (AC) to PET images in PET/MR. An inherent difficulty arises from the fact that air and bone do not produce any MR signal, whereas soft-tissues do. Several approaches have been proposed mostly for brain imaging, although methods for torso imaging are evolving. A common technique for AC in PET/MR is segmentation of MR images. In this method, a transmission scan is obtained using a ^{68}Ge source or a CT scan to generate an attenuation map that is coregistered with the MR image (commonly T1-weighted images which are best for delineating anatomy). The MR image is then segmented in different tissue types such as bone, fluid, air in paranasal sinuses, and brain tissues. Appropriate linear attenuation coefficient values (μ) at 511 keV are then assigned to these tissues.

In another plausible approach, an atlas-based method is used, in which an atlas comprises a template MR image together with a corresponding attenuation label image. A template MR image is generated from the average of co-registered MR images from multiple subjects (atlas). The label image could be a MR image segmented into different tissue classes (e.g., air, bone, and soft tissue) or a co-registered attenuation map from a PET transmission scan or a CT scan with continuous attenuation values. The template MR image is coregistered with the MR image of a patient, and when the transformation is applied to the atlas attenuation image, a patient-specific attenuation map is obtained. Although these methods offer reasonable attenuation correction for brain imaging, it is quite complicated and challenging to apply them in whole body imaging. The issue is further com-

plicated by truncation effects extending beyond the MR field, presence of MR surface coil in PET imaging field, etc.

Random Coincidences

Random coincidence events occur when two unrelated 511-keV photons, arising from two different positron annihilation events, are detected by a detector pair within the same time window (Fig. 13.16b). Random coincidences are largely minimized in 2-D acquisition by septa, whereas in 3-D acquisition in the absence of septa, their contribution is high causing loss of image contrast. They increase with increasing pulse-height window, coincidence time window, and activity (varies as the square of the activity; see Eq. (13.7) below), and can be reduced by decreasing these variables. Also increasing the ring diameter reduces the random coincidences.

Corrections for random coincidences can be made by separately measuring two single count rates, R_1 and R_2, of a radioactive source by each of the detector pair and by using the following equation,

$$R_c = 2\tau R_1 R_2 \tag{13.7}$$

where τ is the coincidence time window and R_c is the random count rate that is to be subtracted from the prompt count rate to obtain the true coincidence count rate. In another method, two coincidence circuits are employed in which one is set at a standard coincidence timing window (e.g., 12 ns) and the other at a delayed time window (say, delayed by 55 ns). In the latter case, the coincidence timing window is set at 55–67 ns, and only counts arriving within 55 ns and 67 ns will be counted using the same pulse-height window in both cases. The counts in the standard time window contain true, scatter, and random events, whereas in the delayed time window, only random events and no true or scatter coincidence events are recorded, because true and scatter photons from the same annihilation decay arrive at the detectors within the short coincidence time window. The random counts will be the same in both coincidence and delayed coincidence windows. The true counts are then obtained by subtracting the delayed window counts from the standard window counts. Use of faster electronics and a shorter coincidence time window are some of the physical techniques that are used to minimize random events. In another method, a very high radioactive source is counted by the PET scanner over time until the radioactivity is reduced to a level where no random event is recorded. Random events are calculated by subtracting the low activity counts (true plus scatter) from the high activity counts (true plus scatter plus random).

Scatter Coincidences

Annihilation radiations may undergo Compton scattering while passing through the body tissue and, due to high energy of 511 keV, they are mostly scattered for-

ward without much loss of energy (Hoffman and Phelps 1986). Such scattering may also occur in the detector material itself. These scattered photons may fall within the coincidence time window (Fig. 13.16c) and be detected by the detector pair. One or both of the 511 keV photons from the same annihilation event may be scattered. Note that coincident counts of scattered photons from two separate annihilation events will be considered as random counts. Scatter counts may comprise both single or multiple scatterings of the photons. Background of the image is increased by these radiations with concomitant loss of image contrast. Scattering increases with the density and depth of tissue, the density of the detector material, the activity, and the pulse-height window. Quantitative measurements such as SUV may be inaccurate due to scatter coincidences.

There are several methods recommended for the scatter correction for PET images. As in SPECT imaging (Chapter 12), a simple two energy window method can be employed using the standard 511-keV photopeak window and a low energy window below the photopeak to estimate scatter coincidences. The technique assumes that the low energy window counts are scattered counts and they are extrapolated to the scatter counts under the photopeak after proper weighting for the difference in spatial distribution. The weighted scatter counts are then subtracted from the measured photopeak counts to obtain the corrected counts for use in the reconstruction of images. However, this technique increases data processing time and the noise in the image. In some studies, the triple window technique has been employed using two overlapping low energy windows with a common upper energy level just below the photopeak window with reasonable success.

Most of the current scatter correction algorithms are based on theoretical models of scatter events. In one model, after random corrections for all projections, a Guassian or parabolic fit is applied to the scatter distribution outside the photopeak area and the function is extrapolated under the photopeak to estimate the scatter contribution, which is then subtracted from the projections for image reconstruction. This method works reasonably well in 2D PET studies in brain, but results in inaccurate scatter correction in areas of high attenuation such as thorax with arms down.

In the convolution method, a scatter function is measured from a point source, which is then used to convolve with the source distribution to estimate the scatter data. An iterative method is used, whereby scatter estimate is improved after each iteration. The scatter estimate is then subtracted from the image data. The method takes into account the scatter dependence on the position of the organ and detection angle, and is computationally efficient.

Another method involves the use of the Monte Carlo calculation to separate the scattered and true events in the measured projections. A reconstructed image is formed from the measured data, which is then positioned in a simulated 3D scanner for tracking photons by the Monte Carlo method. Each interaction of photon in the scattering medium (e.g. patient) and its detection in the block detector is traced, and the total and scattered events are estimated. The latter is subtracted from the former to give the unscattered events. This method, however, does not take into account the scatter from outside the source.

Narrowing the pulse-height window reduces the scattered events significantly. The use of septa in 2-D acquisition reduces the scatter events considerably, but in 3-D acquisition, this becomes a problem. In modern PET scanners, the scatter fraction is around 15 % in 2-D acquisition, whereas it can be as high as 60 % in 3-D acquisition.

Dead Time

The effects of dead time and pulse pile-up have been discussed in Chapter 8. The effects of high-count rates on the performance of gamma cameras have been discussed in Chapter 10. These effects equally apply to the counting of 511-keV annihilation photons in PET imaging. The correction for dead time loss is made by measuring the observed count rates as a function of increasing concentrations of activity. The dead time is calculated from these data and then applied to actual data obtained in the patient's scanning. Uses of high-speed electronics, buffers, and pulse pile-up rejection circuits are some of the techniques that are employed to improve dead time loss.

Radial Elongation

Radial elongation, also called the parallax error or radial astigmatism, occurs from LORs that are off-centered. As shown in Fig. 13.19, the two 511-keV photons originating along the actual LOR (solid line) may strike the detectors tangentially at the back of the detector and form a coincident event. But the *X*, *Y* positioning of the detectors is defined by the dashed line some distance *d* away from the actual LOR. This effect results in some blurring of the image due to unknown depth of interactions, and worsens with the LORs farther away from the center of the FOV and with a thicker detector. However, as can be seen from Fig. 13.19, the use of a larger diameter of the ring improves this effect. Correction can be made for this effect by measuring light in the front and back of each detector and using the difference to measure the depth of the photon interaction in the detector.

Performance of PET Scanners

Spatial Resolution

The spatial resolution of a PET scanner is defined by several factors that are discussed below.

Detector size. In the absence of collimators, unlike in SPECT, the intrinsic resolution R_i is the predominant factor in spatial resolution, which is related to the detector size *d* in multidetector PET scanners. It is normally given by *d* at the face of the detector and by *d/2* midway between the two detectors.

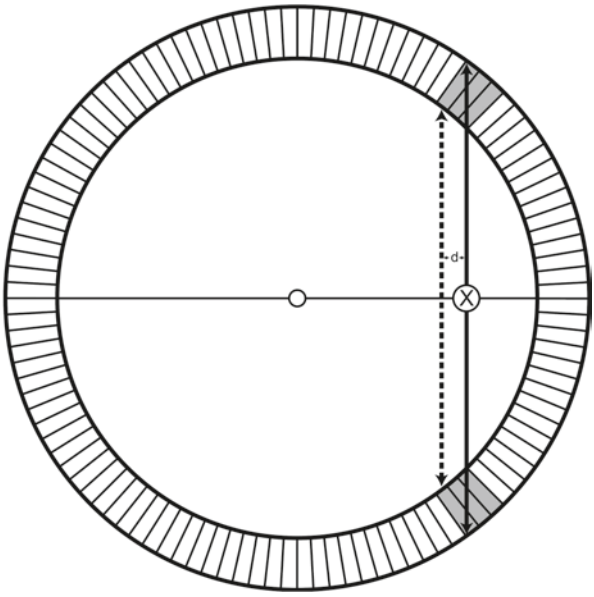

FIG. 13.19. An illustration of radial elongation. An off-center event (*solid line*) strikes the back of the detector pair tangentially. The *X*-, *Y*-positioning of the detectors (*dashed line*) is a distance *d* away from the actual location of the positron annihilation, causing the blurring of the image. (Reprinted with the permission of the Cleveland Clinic Foundation.)

Positron range. A positron with energy travels a distance in tissue losing energy before it almost comes to rest and then combines with an electron to produce two 511-keV photons. The locations of positron emission and annihilation are separated by the effective range of the positron (Fig. 13.20), which adds to the uncertainty of *X*, *Y* positioning of the detector pair. This error R_p increases with the positron energy and decreases with the tissue density. This value is reported to be 0.2 mm for ^{18}F and 2.6 mm for ^{82}Rb in tissue (Tarantola et al. 2003).

Noncolinearity. Positrons at the end of their range still possess some residual momentum and, therefore, the two annihilation photons are not emitted exactly 180°, but at slight deviation. This deviation from 180° is ± 0.25° at maximum. Because of this deviation, the LOR is displaced from the point of annihilation (Fig. 13.21) and, thus, an error R_a is introduced in the spatial resolution of the PET scanner. This value deteriorates with the diameter of the ring and is estimated to be

$$R_a = 0.0022D \tag{13.8}$$

Reconstruction method. If the filter backprojection method is used for reconstruction, the choice of filter with a selected cut-off frequency degrades spatial resolution. This error (K_r) is reported to be a factor of 1.2–1.5 depending on the type of filter used.

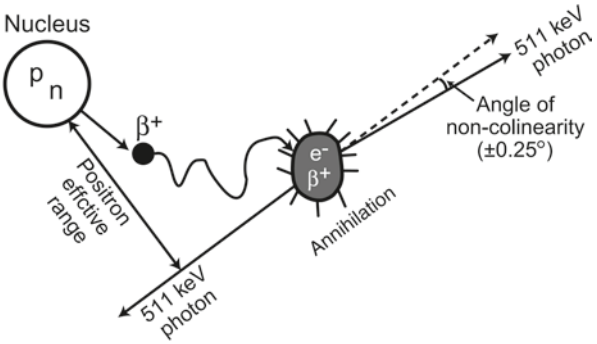

FIG. 13.20. Positrons travel a distance before annihilation in the absorber and the distance increases with positron energy. Because positrons with different energies travel in *zigzag* directions, the effective range is the shortest distance between the nucleus and the direction of 511-keV photons. This effective range degrades the spatial resolution of the PET scanner. (Reprinted with the permission of the Cleveland Clinic Foundation.)

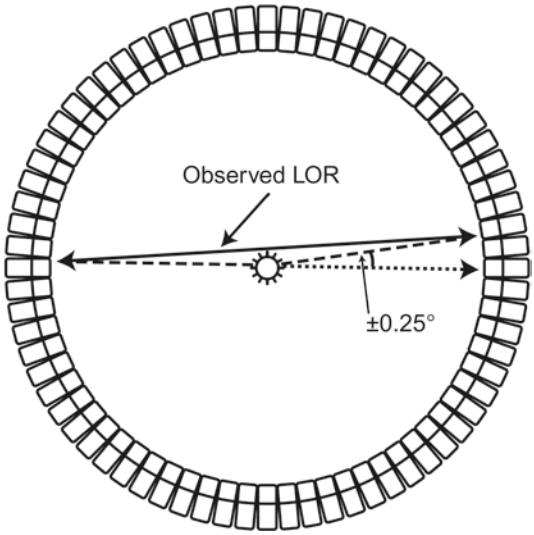

FIG. 13.21. Noncolinearity of 511-keV annihilation photons. Because there is some residual momentum associated with the positron, the two annihilation photons are not emitted exactly at 180°, but at a slight deviation from 180°. Two detectors detect these photons in a *straight line*, which is slightly deviated from the original annihilation line. The maximum deviation is ±0.25°. (Reprinted with the permission of the Cleveland Clinic Foundation.)

Location of the detector The use of block detectors rather than single detectors introduces an error in the (*X*, *Y*) positioning of the detector pair, which causes degradation of the spatial resolution. This value (R_l) is approximately 2.2 mm for BGO detectors, and somewhat less for LSO detectors.

Combining all these factors, the spatial resolution of a PET scanner is given by

$$R = K_r \times \sqrt{R_i^2 + R_p^2 + R_a^2 + R_l^2} \tag{13.9}$$

The transverse spatial resolution typically ranges from 4 to 5 mm at 1 cm and the axial spatial resolution from 5 to 6 mm at 1 cm for commercial PET scanners. The transverse resolution is best at the center of FOV and worsens toward the periphery of the scanner.

Sensitivity

The sensitivity of a PET scanner is defined by the number of counts per unit time for each unit of activity and is normally given in counts per second per microcurie (or megabecquerel) (cps/μCi or cps/MBq). Commercial vendors give this in units of volume sensitivity, kcps/μCi/cc or cps/Bq/cc. Sensitivity depends on the geometric efficiency, detection efficiency of the detector, pulse-height window, and dead time of the detector. These factors have been discussed in detail in Chapter 10 for conventional cameras. However, the geometric efficiency needs further consideration because of the specific configuration of the PET scanners. The geometric efficiency depends on the distance d between the detector and the source, the diameter D of the ring, and the number of rings n in the scanner. Increasing the distance d and the diameter D reduces the solid angle subtended by the detector at the source and, thus, decreases the geometric efficiency. With all these factors taken into consideration, the sensitivity S of a single-ring PET scanner is given by (Budinger 1998)

$$S = \frac{A \cdot \varepsilon^2 \cdot e^{-\mu t} \cdot 3.7 \times 10^4}{\pi D^2} (\text{cps}/\mu\text{Ci}) \tag{13.10}$$

where A is the detector area seen by a point source to be imaged, ε = detector efficiency, μ = linear attenuation coefficient of 511 keV photons in detector material, t is the thickness of the detector, and D is the diameter of the ring. The sensitivity increases with the number of rings in the scanner.

The sensitivity of the PET scanners is 6–10 cps/kBq in 3-D acquisition due to the absence of septa between the rings. However, it contains a large number of random and scatter coincidences. The sensitivity in 2-D aquisition is even lower.

Noise Equivalent Count Rate

As discussed in Chapter 10 under contrast, noise degrades the image contrast and primarily arises from the statistical variation of the count rates. Noise is given by $1/\sqrt{N}$, where N is the count density. An important parameter related to noise is the noise equivalent count rate (*NECR*) that is given by

$$NECR = \frac{T^2}{T + S + R} \tag{13.11}$$

where T, S, and R are the true, scatter, and random coincidences, respectively. It serves as a parameter to compare the performances of different PET scanners. Image noise can be minimized by maximizing *NECR*.

Quality Control Tests for PET Scanners

Daily Tests

Sinogram Check

This is normally carried out by using a standard 20-cm long cylindrical phantom containing a positron emitter (normally a 1–3 mCi (37–111 MBq) ^{68}Ge source). It is mounted on the patient table and centered both vertically and horizontally in the field of view. This arrangement allows uniform exposure to radiations of all detectors to provide a uniform sinogram. Initially, a reference blank sinogram is obtained during the last setup of the scanner. Subsequently, a blank sinogram is taken daily before the patient study is started on each day. This daily sinogram is then compared with the initial blank sinogram. The difference between the two sinograms is characterized by a quantity called average variance, which is calculated by the square sum of the differences of the relative detector efficiencies between the two scans weighted by the inverse variances of the differences. To obtain the average variance, the sum is then divided by the number of detectors. When this value exceeds 2.5, recalibration is needed, whereas for a value greater than 5.0, manufacturer's service is warranted (Buchert et al. 1999). Normally, in modern PET cameras, this is carried out by the manufacturer's menu-driven software.

Weekly Tests

Normalization

As mentioned before, normalization corrects for nonuniformities in the acquired PET data. It is accomplished by using a standard 20-cm long cylinder containing 1–3 mCi (37–111 MBq) ^{68}Ge activity accurately positioned at the center of the FOV. All detectors are uniformly exposed to radiations in the absence of any object in the FOV. From the acquired 2-D or 3-D data, the correction factors are calculated for each detector by dividing the average counts of all detector pairs by each individual detector pair count (i.e., along the LOR; (Eq. 13.3)). These factors are saved and later applied to corresponding detector pairs in the acquired emission data of the patient (Eq. 13.4). Usually, normalization factors need to be taken weekly or monthly, although some manufacturers recommend quarterly. For better statistical accuracy, long hours of counting (6–8 h) are necessary, and often, overnight data

acquisition is made. Data acquisition and calculation of normalization factors and their storage are carried out by the manufacturer's menu-driven software.

Quality Control Tests for MR Scanners

Like any other imaging device, several quality control (QC) tests are carried out at regular intervals for optimum operation of MR scanners to afford good images. Some tests are performed daily, while others weekly or annually. Specifications of tests for MR equipment and their frequencies are performed according to recommendations by the American College of Radiology (ACR) for the purpose of accreditation (www.acr.org). The regular QC tests for optimum operation of MR equipment include, but not limited to, the following:

1. Geometric accuracy: Measuring lengths on the images between locations in the phantom, and comparing them with the true values of those lengths, (daily or weekly)
2. High-contrast spatial resolution: A measure of ability of the MR unit to delineate structures on the image. Measured on the image by the resolution of holes in the MR phantom. (daily or weekly)
3. Slice thickness: Provides the accuracy of slice thickness by comparing the measured and prescribed slice thicknesses. (annually)
4. Slice position accuracy: Measuring the difference between the prescribed and actual positions of specific slices using 45° cross wedges in the ACR phantom, which appear as bars on the image. (annually)
5. Uniformity: Verifying the constant signal response throughout the scanned volume of the phantom filled with only water. Measured by using a large ROI on the phantom image and characterized by percent integral uniformity (see Eq. 10.13). (daily)
6. Percent signal ghosting: Artifacts caused by a faint copy (ghost) of the imaged object appearing superimposed on the image, displaced from its true location.
7. Low-contrast detectability: Assessing the extent to which objects of low contrast are discernible in the images using a phantom having a set of low contrast objects of varying size and contrast.

These tests are performed using a specifically designed phantom, called the ACR phantom, approved by the ACR. The phantom is filled with a water solution of various paramagnetic ions such as manganese, nickel and copper and positioned at the center of the magnet. Scanning is performed for all tests with preset scan parameters such as pulse sequence, timing parameters (TR, TI, and TE), flip angle, matrix size, field of view, RF power setting, slice thickness, number of acquisition, and other relevant parameters. The details of these tests are available from the ACR and the American Association of Physicists in Medicine (AAPM 1990).

Important performance tests include magnetic field homogeneity, radiofrequency (RF) calibration, softcopy (monitor) fidelity, and evaluation of the QC program, which are performed annually. In addition, site planning is important to consider so that the metallic objects are not present to interfere with the magnetic field, and RF interference from outside sources should be avoided. Also, the MR unit should be inspected thoroughly for its physical and mechanical integrity. For ACR accreditation of a MR unit, a certified MR physicist must verify all the QC and performance tests.

Accreditation of Nuclear Medicine and PET Facilities

To standardize different diagnostic methodologies in the USA with a goal to improve patient care, US Congress has passed a law requiring all imaging facilities, institutional or stand-alone, to be accredited by qualified accrediting organizations. Following in the same context, the Centers for Medicare and Medicaid Services (CMS) and private insurers such as Blue Cross and Blue Shield and United Healthcare demand such accreditation of imaging facilities for reimbursement for patient care. For nuclear imaging facilities, there are two major accreditation organizations—The American College of Radiology and the Intersocietal Commission on Accreditation for Nuclear Medicine Laboratories (ICANL), which set standards and criteria for accreditation. The major focus of these organizations is to improve the quality of patient care through perpetual monitoring of the optimal operation of the imaging equipment and continuing education and training of both professionals and personnel working in the facility. A nuclear medicine facility needs to apply to one of these organizations for accreditation submitting all required data and information along with appropriate fees. If satisfied upon proper scrutiny of the application, the organization grants accreditation to the nuclear medicine facility. The entire department or a specialty section of the department such as nuclear cardiology can apply separately for accreditation, provided it fulfills the requirements. Although the goal of both organizations is the same, but there are differences in their requirements and standards for accreditation. The ICANL has two standards for nuclear laboratories: (1) Nuclear Medicine including PET and (2) Nuclear Cardiology. A facility can be a single site or a conglomerate of many sites under the same management. The ICANL requires a medical director who is an authorized user by an Agreement State or the NRC and a licensed and board certified nuclear physician with sufficient knowledge in administration, nuclear medicine technology and patient care. A technical director is also required by the ICANL for accreditation, who must be board certified and licensed and has sufficient knowledge in technology and patient care. All other physicians, technologists, medical physicists, and nuclear pharmacists must be board certified in their respective profession or have sufficient training and experience. All professionals must obtain continuing education as frequently as required by the ICANL. The types of board certification and specific requirements for continuing education are available on www.icanl.org.

Protocols must be established in writing about general activities as well as clinical procedures in compliance with the NRC and Agreement State regulations and must be updated at least annually. Similar protocols must be established for the quality control of equipment and instruments used in the facility. The equipment and instrumentation must be in good working condition, checked routinely for proper functioning and records must be kept on file. The ICANL recommends that at least 600 studies be performed annually at each facility to maintain proficiency in study interpretation and performance. In the application, one needs to submit a certain number of case studies for each category such as brain PET, cardiac PET, cardiac SPECT, other general nuclear medicine, etc. The specific number of normal and abnormal cases required for submission in the application is available at www.icanl.org. The quality control data of equipment and phantom images also need to be submitted, along with various protocols for patient studies and applicable fees. An agreement by the medical director to follow the terms and conditions of the ICANL must accompany the application. The ICANL can make random visit to verify the compliance of the facility with the commitment made in the application. Accreditation is granted for three years and renewable upon reapplying with required information.

In contrast, the ACR emphasizes on the quality control of equipment, phantom studies, and radiopharmaceutical procedures along with patient studies in the nuclear medicine department. In their accreditation protocol, the ACR has developed four modules: Module 1 for planar studies, Module 2 for SPECT studies, Module 3 for nuclear cardiology studies and Module 4 for PET studies. The PET module has three submodules: oncology, brain and cardiology. All modules have some common requirements related to the quality control of equipment, radiopharmaceutical and laboratory environment, but have specific requirements for each module in regard to the patient studies in the disease group assigned.

All nuclear physicians and technologists are required to be board certified in nuclear medicine or have training and experience in their respective profession as specified by the ACR. They also are required to obtain specific hours of continuing education to maintain proficiency in profession. A nuclear medicine physicist is required by the ACR to perform all quality control tests of all imaging equipment in the nuclear medicine facility. The physicist has to be board certified or have adequate training and experience and receive continuing education as mandated by the ACR.

There are two steps in the ACR application process for nuclear medicine facilities. First, the facility submits information about the practice, including policies, procedures, personnel qualifications and equipment used for each modality along with applicable fees. If the ACR considers the application complete, it then notifies the facility to proceed with the second step in which the ACR asks to submit clinical and phantom data along with a variety of instructions. Clinical images for each type of study, both normal and abnormal with bar-coded labels, and techniques employed in obtaining the images must be submitted. Other pertinent information for submission includes reporting of interpretation, radiopharmaceutical procedures, radiation safety and laboratory safety, and recent State or NRC audit along with any violation, if any, and its response. For every modality, two

studies—one normal and one abnormal, must be submitted in a format following the ACR Practice Guidelines and Technical Standards, along with physician's interpretation report. The images are then reviewed by qualified reviewers designated by the ACR. The second step must be completed in 90 days following the receipt of notification from the ACR.

An important part of the accreditation is the annual report of the medical physicist on the quality control of all equipment using designated phantoms prescribed by the ACR. The ACR-recommended phantom is the Jaszczak Deluxe Flangeless ECT phantom (available from Data Spectrum), which is used for both SPECT and PET studies. Data on uniformity, spatial resolution, center of rotation, noise and contrast obtained using this phantom for each imaging device following the ACR instructions must be certified by the medical physicist and submitted to the ACR for review. The phantom images are reviewed and scored by a panel of expert physicist for their quality based on the standard values of the parameters set by the ACR.

After review of all data, if the facility meets all requirements satisfactorily, accreditation is granted to the facility for a three year period and can be renewed by reapplication. If there is any deficiency in any aspect of the application, the ACR will notify the facility indicating the deficiency and make recommendations to correct it and reapply. The ACR reserves the right to visit the facility anytime during or after the accreditation process, to verify the information submitted in the application and to monitor the compliance with accreditation standards. The details of the information needed for the ACR accreditation application are available on www.acr.org.

Facilities having PET/CT and PET/MR scanners have to fulfill additional requirements for CT and MR scanners, which are similar to those for nuclear medicine and PET facilities. Readers are referred to the websites of the ICANL and the ACR.

Questions

1. Describe the principles of positron emission tomography.
2. How is the attenuation of annihilation photons corrected for in PET?
3. Attenuation of photons is directly proportional to the thickness and density of the material through which they pass and inversely proportional to photon energy. True or False?
4. How do random and scatter radiations affect PET images? What are the methods for correcting these effects?
5. What are the typical values of spatial resolutions of PET scanners?
6. What is the cause of the partial-volume effect and how would you rectify it?
7. What are the most common radionuclides used in PET?
8. Explain why ^{13}N-ammonia gives better spatial resolution than ^{82}Rb in the PET imaging of myocardium.
9. What are the factors that affect the spatial resolution of a PET scanner?

10. What are the initial steps that are taken in the reconstruction of 3-D data?
11. The overall sensitivity of PET scanners in 3-D acquisition is four to eight times higher than in 2-D acquisition. Why?
12. What is the daily quality control test for a PET scanner?
13. The sensitivity of a PET scanner increases with the size of the detector. True or False?
14. Explain why LSO detectors are preferred to BGO detectors.
15. Transverse resolution is worse at the center of the field of view than away from the center. True or False?
16. Describe the basic principles of MR imaging.
17. What are the advantages and disadvantages of PET/MR and PET/CT?
18. Define T1 and T2 relaxation times in MR imaging.
19. Normally T1 is longer than T2 in MR imaging. True or False?
20. What is the effect of Gd-DTPA on T1 and T2?
21. The spatial resolution of PET is better than that of MR. True or False?
22. Define CT dose index (CTDI) and dose-length product (DLP) in CT imaging.
23. Describe how attenuation correction is made in PET/MR imaging.

References and Suggested Readings

AAPM Repost No 28. Quality assurance methods and phantoms for magnetic resonance imaging. *Med Phys*. 1990; 17:287.

ACR Technical Standarr for Diagnostic Medical Physics Performance Monitoring of Magnetic Resonance Imaging (MRI) Equipment. Revision 2009; www.acr.org.

American College of Radiology. *CT and MRI Accreditation Program Requirements*.2011.

Bacharach SL. Image analysis. In: Wagner HN Jr, Szabo Z, Buchanan JW, eds. *Principles of Nuclear Medicine*. Philadelphia: W. B. Saunders; 1995:393–404.

Buchert R, Bohuslavizki KH, Mester J, et al. Quality assurance in PET: Evaluation of the clinical relevance of detector defects. *J Nucl Med*. 1999;40:1657.

Budinger TF. PET instrumentation: what are the limits? *Semin Nucl Med*. 1998;28:247.

Bushberg JT, Siebert JA, Leidholdt Jr, EM, Boone JM. *The Essential Physics of Medical Imaging*. 3rd ed. Philadelphia; Lippincott: 2011.

Cherry SR, Dahlbom M. PET: Physics, instrumentation, and scanners. In: Phelps ME. *PET: Molecular Imaging and Its Biological Applications*. New York; Springer: 2004.

Cherry SR, Sorensen JA, Phelps ME. *Physics in Nuclear Medicine*. 3rd ed. Philadelphia; W. B. Saunders: 2003.

Hoffman EJ, Phelps ME. Positron emission tomography: Principles and quantitation. In: Phelps ME, Mazziotta J, Schelbert H, eds. *Positron Emission Tomography and Autoradiography: Principles and Applications for the Brain and Heart*. New York: Raven; 1986:237–286.

Keim P. An overview of PET quality assurance procedures: Part I. *J Nucl Med Techol*. 1994;22:27–34.

Koeppe RA, Hutchins GD. Instrumentation for positron emission tomography: Tomographs and data processing and display systems. *Semin Nucl Med*. 1992;22:162–181.

Saha GB. *Basics of PET Imaging*. 2nd ed. New York; Springer: 2010.

Tarantola G, Zito F, Gerundini P. PET instrumentation and reconstruction algorithms in whole-body applications. *J Nucl Med*. 2003;44:756.

14
Internal Radiation Dosimetry

Radiation can cause detrimental effects on human tissues, and these effects depend on various factors, such as dose, dose rate, time of exposure and so on. This chapter describes the method of calculating absorbed doses in various organs from radionuclides ingested internally either purposely (e.g., medical procedures) or accidentally.

Radiation Units

Three units of measure are related to radiation: the roentgen (R) for exposure, the rad (radiation absorbed dose) for absorbed dose, and the rem (roentgen equivalent man) for dose equivalent.

The *roentgen* is the amount of x- or γ-radiation that produces ionization of one electrostatic unit of either positive or negative charge per cubic centimeter of air at 0 °C and 760 mm Hg, standard temperature and pressure (STP). Because 1 cm^3 air weights 0.001293 g at STP and a charge of either sign carries 1.6×10^{-19} C or 4.8×10^{-10} electrostatic units, it can be shown that

$$1\ \mathrm{R} = 2.58 \times 10^{-4}\ \mathrm{C/kg} \tag{14.1}$$

It should be noted that the roentgen applies only to air and to x- or γ-radiations. Because of practical limitations of the measuring instruments, the R unit is applicable only to photons of less than 3 MeV energy.

The *rad* is a more universal unit. It is a measure of the energy deposited per unit mass of any material by any type of radiation. The rad is specifically defined as

$$1\ \mathrm{rad} = 100\ \mathrm{ergs/g\ \ absorber} \tag{14.2}$$

Since 1 joule (J) = 10^7 ergs,

$$1\ \mathrm{rad} = 10^{-2}\ \mathrm{J/kg} \tag{14.3}$$

G. B. Saha, *Physics and Radiobiology of Nuclear Medicine,*
DOI 10.1007/978-1-4614-4012-3_14,

Another radiation unit is *kerma* (acronym for kinetic energy released in matter) which is defined as the sum of initial kinetic energies of all charged particles liberated by uncharged ionizing radiation per unit mass of material. For all practical purposes, kerma and rad are identical.

In SI units, the *gray* (Gy) is the unit of radiation absorbed dose and kerma and is given by

$$1 \text{ Gy} = 100 \text{ rad} \tag{14.4}$$

$$= 1 \text{ J/ kg absorber} \tag{14.5}$$

It can be shown that the energy absorbed per kilogram of air due to an exposure of 1 R is

$$1 \text{ R} = 86.9 \times 10^{-4} \text{ J/kg in air}$$

Therefore,

$$1 \text{ R} = 0.869 \text{ rad in air}$$

or,

$$1 \text{ R} = 0.00869 \text{ Gy in air}$$

$$\text{Note that for soft tissue, } 1\text{R} = 0.96 \text{ rad} = 0.0096 \text{ Gy}$$

The rad is not restricted by the type of radiation or absorber or by the energy or intensity of the radiation. It should be understood that the rad is independent of the weight of the material. This means that a radiation dose of 1 rad (0.01 Gy) is always 1 rad (0.01 Gy) in 1, 2, or 10 g of the material. However, the integral absorbed dose is given in units of gram-rad (g · rad or g · Gy) and calculated by multiplying the rad (Gy) by the mass of material. For example, if the radiation dose to a body of 45 g is 10 rad (0.1 Gy), then the integral radiation dose to the material is 450 g · rad (or 4.5 g · Gy); however, the radiation dose is still 10 rad (0.1 Gy).

The dose equivalent unit, *rem*, has been developed to account for the differences in effectiveness of different types of radiation in causing biological damage. In radiobiology, the rem is defined as

$$\text{rem} = \text{rad} \times \text{RBE} \tag{14.6}$$

where RBE is the relative biological effectiveness of the radiation. It is defined as the ratio of the dose of a standard radiation to produce a particular biological response to the dose of the radiation in question to produce the same biological response. Radiations of 250 KV x-rays are normally chosen as the standard radiation because of their widespread use. RBE varies with the linear energy transfer (LET) of the radiation, radiation dose, dose rate, and the biological system in which RBE is determined.

TABLE 14.1. Radiation weighting factors.

Type and energy range		Radiation weighting factors (W_r)
Photons, all energies		1
Electrons, muons, all energies		1
Neutrons, energy	<10 keV	5
	10 to 100 keV	10
	>100 to 2 MeV	20
	>2 to 20 MeV	10
	>20 MeV	5
Protons, other than recoil protons, energy >2 MeV		5
Alpha particles, fission fragments, heavy nuclei		20

Adapted with permission from ICRP Publication 60: *1990 Recommendations of the international commission on radiological protection*. New York: Pergamon Press; 1991.

In radiation protection, RBE is replaced by the *radiation weighting factor*, W_r, to account for differences in effectiveness of various radiations in causing biological damage. The rem is then defined as

$$\text{rem} = \text{rad} \times W_r \tag{14.7}$$

The International Commission on Radiological Protection (ICRP) has suggested the W_r values for different radiations, which are listed in Table 14.1 (ICRP 60 1991). These values depend on the LET of the radiation. When a radiation dose comes from several radiations, the total dose equivalent is calculated by adding the absorbed doses from individual radiations multiplied by the W_r of each radiation.

In the past, the W_r values were called *quality factors* (QF), which are somewhat different from the W_r values. The US Nuclear Regulatory Commission (NRC) still adopts these values for regulatory purposes, and the values are listed in Table 14.2.

In SI units, the dose equivalent is expressed in *sievert*, which is defined as

$$1 \text{ sievert (Sv)} = 100 \text{ rem} \tag{14.8}$$

In practical situations, all these radiation units are often expressed in milliroentgens (mR), millirads (mrad), and millirems (mrem), which are 10^{-3} times the units, roentgen, rad, and rem, respectively. In SI units, the equivalent quantities are milligrays (mGy) and millisieverts (mSv). A rad is also commonly expressed as centigray (cGy), one-hundredth of a gray.

TABLE 14.2. Quality factors for different radiations.

Type of radiation	QF
X-rays, γ-rays, β-particles	1.0
Neutrons and protons	10.0
α-Particles	20.0
Heavy ions	20.0

Dose Calculation

The radiation absorbed dose depends on a number of factors: (1) the amount of radioactivity administered; (2) the physical and biological half-lives of the radioactivity; (3) the fractional abundance of the radiation in question from the radionuclides; (4) the biodistribution of radioactivity in the body; and (5) the fraction of energy released from the source organ that is absorbed in the target volume, which is related to the shape, composition, and location of the target. The physical characteristics of a radionuclide are well established. Information concerning the biodistribution of ingested radioactivity can be obtained from various experimental studies in humans and animals. The factors four and five are variable from one individual to another and, therefore, they are approximated for a "standard" or "average" 70-kg man.

Radiopharmaceuticals administered to patients are distributed in different regions of the body. A region of interest for which the absorbed dose is to be calculated is considered the "target," whereas all other regions contributing to the radiation dose to the target are considered "sources." The source and the target become the same when the radiation dose due to the radioactivity in the target itself is calculated.

Radiation Dose Rate

Suppose a source volume r contains A μCi of a radiopharmaceutical emitting several radiations. If the ith radiation has energy E_i and a fractional abundance N_i per disintegration, then the energy absorbed per hour (dose rate) by a target of mass m and volume v from the ith radiation emitted by the source volume r is given by

$$\begin{aligned} R_i(\text{rad/h}) &= A/m(\mu\text{Ci/g})N_i E_i(\text{MeV/disintegration}) \\ &\quad \times \left[3.7 \times 10^4 \text{ disintegrations}/(\text{s} \cdot \mu\text{Ci})\right] \\ &\quad \times (1.6 \times 10^{-6} \text{ erg/MeV}) \\ &\quad \times (0.01 \text{ g} \cdot \text{rad/erg}) \\ &\quad \times (3600 \text{ s/h}) \\ &= 2.13(A/m)N_i E_i \end{aligned}$$

The above equation is valid for nonpenetrating radiations only, meaning all energy is absorbed in the absorber. For penetrating radiations, total or part of the radiation energy may be absorbed in the absorbing material. If the target and the source are not the same, then a factor must be introduced to account for the partial absorption, if any, of the radiation energy. Thus,

$$R_i(\text{rad/h}) = 2.13(A/m)N_i E_i \phi_i(v \leftarrow r) \tag{14.9}$$

Here $\phi_i(v \leftarrow r)$ is called the *absorbed fraction* and is defined as the ratio of the energy absorbed by the target volume v from the ith radiation to the energy emitted by the ith radiation from the source volume r. This is a critical factor that is dif-

ficult to evaluate, because the absorbed fraction ϕ_i depends on the type and energy of the radiation, the shape and size of the source volume, and the shape, composition, and distance of the target volume. However, in the case of β-particles, conversion electrons, α-particles, and x- and γ-rays of energies less than 11 keV, all of the energy emitted by a radionuclide is absorbed in the volume r larger than 1 cm. Then, ϕ_i becomes 0, unless v and r are the same, in which case $\phi_i = 1$. For x- and γ-rays with energies greater than 11 keV, the value of ϕ_i decreases with increasing energy and varies between 0 and 1, depending on the energy. The values of ϕ_i are calculated by statistical Monte Carlo methods on the basis of fundamental mechanisms of interaction of radiation with matter, and are available in standard textbooks on radiation dosimetry, particularly the medical internal radiation dose (MIRD) pamphlets published by the Society of Nuclear Medicine.

The quantity $2.13N_iE_i$ is a constant for the ith radiation and is often denoted by Δ_i. Thus,

$$\Delta_i = 2.13\ N_i E_i \tag{14.10}$$

The quantity Δ_i is called the *equilibrium dose constant* for the ith radiation and has the unit g · rad/(μCi · h) based on the units chosen in Eq. (14.9). It should be pointed out that since β-particles are emitted with a distribution of energy, the average energy $\bar{E}_\beta$ of β-particles, which is equal to one-third of E_{max} of the particle, is used in the calculation of Δ_i. Thus, Eq. (14.9) becomes

$$R_i(\text{rad/h}) = (A/m)\Delta_i\phi_i(v \leftarrow r) \tag{14.11}$$

The activity A will change due to the physical decay and biological elimination of the radiopharmaceutical, and therefore the dose rate will also change. If A_o is the initial administered activity, then the activity localized in an organ is a fraction f of A_o. Assuming an effective exponential change in A with time, Eq. (14.11) can be written as

$$R_i(\text{rad/h}) = (f \cdot A_o/m)\Delta_i e^{-\lambda_e t}\phi_i(v \leftarrow r) \tag{14.12}$$

Here λ_e is the effective decay constant of the radiopharmaceutical, and t is the time over which the original activity has decayed.

Cumulative Radiation Dose

The cumulative radiation dose D_i to the target due to the ith radiation of the radionuclide during the period $t = 0$ to t can be obtained by integrating Eq. (14.12). Thus,

$$\begin{aligned} D_i(\text{rad}) &= (f \cdot A_o/m)\Delta_i\phi_i(v \leftarrow r)\int_0^t e^{-\lambda_e t}dt \\ &= (f \cdot A_o/m)\Delta_i\phi_i(v \leftarrow r)\frac{1}{\lambda_e}(1 - e^{-\lambda_e t}) \\ &= 1.44(f \cdot A_o/m)\Delta_i T_e\left(1 - e^{-\lambda_e t}\right)\phi_i(v \leftarrow r) \end{aligned} \tag{14.13}$$

Here, T_e is the effective half-life of the radiopharmaceutical in hours (discussed in Chapter 3). If $t = \infty$, that is, the radiopharmaceutical is completely eliminated, then the exponential term $e^{-\lambda_e t}$ approaches zero and the absorbed dose in Eq. (14.13) may be written as

$$D_i(\text{rad}) = 1.44(f \cdot A_o/m)\Delta_i T_e \phi_i(v \leftarrow r) \tag{14.14}$$

If the radionuclide has n radiations with energies $E_1, E_2, \ldots E_n$ and fractional abundances $N_1, N_2, \ldots N_n$ per disintegration, then the total dose D can be obtained by summing Eq. (14.14) over all radiations. Thus,

$$D(\text{rad}) = 1.44(f \cdot A_o/m)T_e \sum_{i=1}^{n} \Delta_i \phi_i(v \leftarrow r) \tag{14.15}$$

This summation can also be applied to Eq. (14.12) for the dose rate R_i. The total dose to the target from different sources of radiations can be calculated by summing Eq. (14.15) over all sources.

In the MIRD pamphlets, the values of Δ_i have been compiled on the basis of various nuclear characteristics of the radionuclide in question. The ϕ_i values have been calculated on the basis of different sizes and compositions of the targets receiving the radiation dose and the radiation characteristics of the radionuclide. In MIRD pamphlet no. 11, Eq. (14.15) has been substituted by

$$D(\text{rad}) = \tilde{A} \cdot S \tag{14.16}$$

where

$$\tilde{A} = 1.44 \times f \cdot A_o \times T_e \tag{14.17}$$

$$S = \sum_{i=1}^{n} \Delta_i \phi_i / m \tag{14.18}$$

The quantity $\tilde{A}$ is called the *cumulated activity* and has the unit of μCi · h. The quantity S is called the *mean absorbed dose per cumulated activity* and has the unit of rad/μCi · h. These two quantities are further discussed next.

Factors Affecting $\tilde{A}$

The cumulated activity $\tilde{A}$ in Eq. (14.17) is given as

$$\tilde{A} = 1.44\, f \cdot A_o T_e$$

This is calculated on the assumption that the radiopharmaceutical localizes in the organs instantaneously and cleared by both physical decay and biological elimination.

There are situations when the uptake of the tracer is gradual and the clearance also is slow. In these cases,

$$\tilde{A} = 1.44 f \cdot A_o T_e (T_Q / T_U) \tag{14.19}$$

where T_U is the biological uptake half-time, T_e is the effective excretion halftime (Eq. 3.12) and T_Q is the effective uptake half-time. T_Q is calculated by Eq. (3.12) using the physical half-life T_P and the biological uptake halftime T_U.

Two other situations can occur when the uptake is instantaneous, but the T_P of the radionuclide is greater than the biological half-life T_B, or T_B is greater than T_P.

When $T_P >> T_B$, the cumulated activity is given by

$$\tilde{A} = 1.44\, f \cdot A_o T_B \tag{14.20}$$

If the tracer is excreted by several excretion routes such as urinary excretion, fecal excretion, etc., the fraction of activity excreted and the effective halftime of each mode are used to calculate the fractional cumulated activity of each mode, which are then summed to calculate the total cumulated activity.

When $T_B >> T_P$, the cumulated activity is calculated as

$$\tilde{A} = 1.44\, f \cdot A_o T_P \tag{14.21}$$

In this case, there is no biological excretion.

The *S* Values

The mean absorbed dose per cumulated activity, S, is more appropriately expressed as

$$S(v \leftarrow r) = \frac{1}{m} \sum_{i=1}^{n} \Delta_i \phi_i (v \leftarrow r) \tag{14.22}$$

where the symbols v and r represent the target and the source, respectively. The calculation of these values is quite laborious. The MIRD Committee of the Society of Nuclear Medicine calculates these values for radiopharmaceuticals commonly used in nuclear medicine and publish them periodically. Table 14.3 includes a partial list of S values for ^{99m}Tc obtained from MIRD pamphlet no. 11.

Problem 14.1
Calculate the absorbed dose to the lungs from the administration of 4 mCi (148 MBq) ^{99m}Tc-MAA particles, assuming that 99 % of the particles are trapped in the lungs. The value of S for the lungs is 5.2×10^{-5} rad/μCi · h. Assume that the ^{99m}Tc activity is uniformly distributed in the lungs and

TABLE 14.3 S[a], mean absorbed dose per unit cumulated activity (rad/μCi · h)[b] for ^{99m}Tc.

	Source organs										
Target organs	Bladder content	Stomach content	Kidneys	Liver	Lungs	Ovaries	Red marrow	Spleen	Testes	Thyroid	Total body
Adrenals	1.5E-07	2.7E-06	1.1E-05	4.5E-06	2.7E-06	3.3E-07	2.3E-06	6.3E-06	3.2E-08	1.3E-07	2.3E-06
Bladder wall	1.6E-04	2.7E-07	2.8E-07	1.6E-07	3.6E-08	7.2E-06	9.9E-07	1.2E-07	4.8E-06	2.1E-09	2.3E-06
Bone (total)	9.2E-07	9.0E-07	1.4E-06	1.1E-06	1.5E-06	1.5E-06	4.0E-06	1.1E-06	9.2E-07	1.0E-06	2.5E-06
Stomach	2.7E-07	1.3E-04	3.6E-06	1.9E-06	1.8E-06	8.1E-07	9.5E-07	1.0E-05	3.2E-08	4.5E-08	2.2E-06
Kidneys	2.6E-07	3.5E-06	1.9E-04	3.9E-06	8.4E-07	9.2E-07	2.2E-06	9.1E-06	4.0E-08	3.4E-08	2.2E-06
Liver	1.7E-07	2.0E-06	3.9E-06	4.6E-05	2.5E-06	5.4E-07	9.2E-07	9.8E-07	3.1E-08	9.3E-08	2.2E-06
Lungs	2.4E-08	1.7E-06	8.5E-07	2.5E-06	5.2E-05	6.0E-08	1.2E-06	2.3E-06	6.6E-09	9.4E-07	2.0E-06
Marrow (red)	2.2E-06	1.6E-06	3.8E-06	1.6E-06	1.9E-06	5.5E-06	3.1E-05	1.7E-06	7.3E-07	1.1E-06	2.9E-06
Ovaries	7.3E-06	5.0E-07	1.1E-06	4.5E-07	9.4E-08	4.2E-03	3.2E-06	4.0E-07	0.0	4.9E-09	2.4E-06
Skin	5.5E-07	4.4E-07	5.3E-07	4.9E-07	5.3E-07	4.1E-07	5.9E-07	4.7E-07	1.4E-06	7.3E-07	1.3E-06
Spleen	6.6E-07	1.0E-05	8.6E-06	9.2E-07	2.3E-06	4.9E-07	9.2E-07	3.3E-04	1.7E-08	1.1E-07	2.2E-06
Testes	4.7E-06	5.1E-08	8.8E-08	6.2E-08	7.9E-09	0.0	4.5E-07	4.8E-08	1.4E-03	5.0E-10	1.7E-06
Thyroid	2.1E-09	8.7E-08	4.8E-08	1.5E-07	9.2E-07	4.9E-09	6.8E-07	8.7E-08	5.0E-10	2.3E-03	1.5E-06
Total body	1.9E-06	1.9E-06	2.2E-06	2.2E-06	2.0E-06	2.6E-06	2.2E-06	2.2E-06	1.9E-06	1.8E-06	2.0E-06

[a] Adapted by permission of the Society of Nuclear Medicine from Snyder, et al. *"S" absorbed dose per unit cumulated activity for selected radionuclides and organs.* MIRD pamphlet no. 11. New York: Society of Nuclear Medicine; 1975

[b] Divide by 3.7 to convert to SI unit (Gy/MBq · h).

45 % of the activity is cleared from the lungs with a biological half-life of 3 h and 55 % with a biological half-life of 7 h.

Answer
The half-life of ^{99m}Tc = 6 h. The effective half-life of two biological clearances are

$$T_{e1} = \frac{3 \times 6}{3 + 6} = 2\,\text{h}$$

$$T_{e2} = \frac{7 \times 6}{7 + 6} = 3.2\,\text{h}$$

Using Eq. (14.17)

$$\begin{aligned}\tilde{A} &= 1.44 \times 4000 \times 0.99 \times (0.45 \times 2 + 0.55 \times 3.2) \\ &= 15,200\ \mu\text{Ci} \cdot \text{h}\,(0.562\ \text{GBq} \cdot \text{h})\end{aligned}$$

Using Eq. (14.16)

$$\begin{aligned}D &= \tilde{A}\ S \\ &= 15200 \times 5.2 \times 10^{-5} \\ &= 0.79\ \text{rad} \\ &= 790\ \text{mrad}\ \ (7.9\ \text{mGy})\end{aligned}$$

Radiation Dose in SI Units

The radiation dose in System Internationale (SI) units due to the administration of a radiopharmaceutical can be calculated by assuming a source volume r containing A MBq of the radiopharmaceutical that emits several radiations. If the ith radiation has energy E_i and a fractional abundance N_i per disintegration, then the energy absorbed per hour by a target of mass m and volume v from the ith radiation emitted by the source volume r (dose rate) is given by

$$\begin{aligned}R_i(\text{Gy/h}) = {} & A/m(\text{MBq/g}) N_i E_i(\text{MeV/disintegration}) \\ & \times 10^6\ \text{disintegrations}/(\text{s} \cdot \text{MBq}) \\ & \times (1.6 \times 10^{-6}\ \text{erg/MeV}) \\ & \times (1 \times 10^{-4}\ \text{g} \cdot \text{Gy/erg}) \\ & \times (3600\ \text{s/h}) \\ = {} & 0.576(A/m) N_i E_i\end{aligned}$$

When the target and the source are not the same, the absorbed fraction $\phi_i(v \leftarrow r)$ must be taken into account. Thus,

$$R_i(\text{Gy/h}) = 0.576(A/m)N_i E_i \phi_i(v \leftarrow r) \tag{14.23}$$

The quantity 0.576 $N_i E_i$ is a constant and can be denoted by Δ_i as in Eq. (14.10). Thus

$$\Delta_i = 0.576\ N_i E_i \tag{14.24}$$

With this value of Δ_i, Eqs. (14.11) to (14.18) are equally applicable to radiation doses in SI units. It should be understood that the equations in SI units contain a constant $\Delta_i = 0.576 N_i E_i$ and activities expressed in MBq and has the unit of Gy · g/ MBq · h, whereas the equations in rad units contain the equilibrium dose constant $\Delta_i = 2.13 N_i E_i$ and activities expressed in microcuries. Also note that A should be equal to $f\,\mathrm{A_o}$, if $\mathrm{A_o}$ is the initial administered activity.

Table 14.4 presents radiation absorbed doses from various radiopharmaceuticals to different organs in adults. All values have been obtained from package inserts except those noted by footnotes.

Effective Dose Equivalent and Effective Dose

Historically, the whole-body dose or total body dose was used to evaluate the relative radiation risks of different procedures involving radiations. This quantity is calculated according to the MIRD method by using the *S* factor for the whole body as the source organ as well as the target organ. This value does not take into consideration the effect of tissue sensitivity to radiation.

In 1977 the ICRP introduced the concept of effective dose equivalent (EDE) to take into account the different sensitivity of tissues to radiation (ICRP 26). The tissues weighting factor (W_T) for an organ was defined as the ratio of the whole-body dose, which would cause a certain probability of cancer induction to the absorbed dose in that organ which would cause the same probability of cancer induction in that organ. For example, a dose of 3 rem to the whole body causes some probability of cancer induction; a dose of 100 rem to the thyroid causes the same numerical probability of thyroid cancer induction. Then the W_T for thyroid is equal to 0.03.

The *effective dose equivalent* (H_E) is defined as the sum of weighted dose equivalents in all tissues and organs, and is calculated as

$$H_E = \sum_T W_T H_T \tag{14.25}$$

where W_T is the tissue weighting factor for an organ and H_T is the dose equivalent (rem) to the organ. H_E can be explicitly written as

$$H_E = \sum_T W_T \sum_r W_r \times (\text{rad})_{T,r} \tag{14.26}$$

where $(\text{rad})_{T,r}$ is the absorbed dose to tissue T from radiation of type r and W_r is the radiation weighting factor discussed earlier.

TABLE 14.4. Radiation absorbed doses in adults for various radiopharmaceuticals.

Radiopharmaceuticals	Organ	Dose	
		rad/mCi	mGy/GBq
^{99m}Tc-pertechnetate	Thyroid	0.130	35.1
	Upper large intestine	0.120	32.4
	Lower large intestine	0.110	30.0
	Stomach	0.051	13.8
	Ovaries	0.030	8.1
	Testes	0.009	2.4
^{99m}Tc-sulfur colloid	Liver	0.335	91.2
	Spleen	0.210	57.4
	Red marrow	0.028	7.4
^{99m}Tc-DTPA	Bladder wall (2 h void)	0.115	31.1
	Kidneys	0.090	24.3
	Gonads	0.011	3.0
^{99m}Tc-MAA	Lungs	0.220	59.5
	Kidneys	0.011	3.0
	Liver	0.018	4.9
	Ovaries	0.008	2.2
	Testes	0.006	1.6
^{99m}Tc-MDP	Bone	0.035	9.5
	Bladder wall	0.130	35.1
	Kidneys	0.040	10.8
	Red marrow	0.026	7.0
	Ovaries	0.012	3.2
	Testes	0.008	2.1
^{99m}Tc-sestamibi (Cardiolite)	Gall bladder	0.067	18.1
	Upper large intestine	0.100	27.0
	Lower large intestine	0.180	48.6
	Heart (wall)	0.017	4.6
	Kidneys	0.067	18.1
	Ovaries	0.053	14.3
	Bladder wall	0.140	37.8
^{99m}Tc-mercaptoacetylglycyl-glycylglycine (MAG3)	Bladder wall	0.480	129.7
	Lower large intestine	0.033	8.9
	Gall bladder	0.016	4.3
	Kidneys	0.014	3.8
	Ovaries	0.026	7.0
^{99m}Tc-HMPAO (Ceretec)	Brain	0.026	7.0
	Thyroid	0.100	27.0
	Kidneys	0.130	35.1
	Gall bladder	0.190	51.4
	Lachrymal gland	0.258	69.7
^{99m}Tc-tetrofosmin (at rest) (Myoview)	Gall bladder	0.180	48.7
	Upper large intestine	0.113	30.5
	Lower large intestine	0.082	22.2
	Heart (wall)	0.015	4.1
	Kidneys	0.046	12.4
	Ovaries	0.035	9.5
	Bladder wall	0.071	19.2

TABLE 14.4 (continued)

Radiopharmaceuticals	Organ	Dose	
		rad/mCi	mGy/GBq
^{99m}Tc-ECD (Neurolite) (2 h void)	Brain	0.020	5.4
	Kidneys	0.027	7.3
	Gall bladder	0.091	24.6
	Upper large intestine	0.061	16.5
	Liver	0.020	5.4
	Ovaries	0.020	5.4
	Bladder wall	0.110	29.8
	Testes	0.008	2.2
^{99m}Tc-mebrofenin (Choletec)	Liver	0.047	12.7
	Lower large intestine	0.474	128.1
	Upper large intestine	0.364	98.4
	Gall bladder	0.137	37.0
	Bladder	0.029	7.8
	Red marrow	0.034	9.1
	Ovaries	0.101	27.3
^{99m}Tc-DMSA	Bladder wall	0.070	18.9
	Kidneys	0.630	170.3
	Liver	0.031	8.56
	Red marrow	0.022	5.86
	Ovaries	0.013	3.60
	Testes	0.007	1.80
^{131}I-iodide	Thyroid	1300.00	3.5×10^5
	Liver	0.48	130.00
	Ovaries	0.14	37.8
^{131}I-MIBG	Bladder wall	2.960	800.0
	Liver	2.920	789.2
	Spleen	2.180	589.2
	Heart (wall)	1.410	381.1
	Adrenal medulla	0.780	210.8
	Kidneys	0.330	89.2
	Ovaries	0.270	73.0
^{123}I-iodide	Thyroid	13.00	3513.5
	Testes	0.02	5.4
^{111}In-pentetreotide (OctreoScan)	Kidneys	1.807	488.4
	Liver	0.407	110.0
	Spleen	2.460	664.9
	Bladder wall	1.007	272.2
	Ovaries	0.163	44.1
^{111}In-capromab pendetide (ProstaScint)	Liver	3.700	1000.0
	Spleen	3.260	881.1
	Kidneys	2.480	670.3
	Red marrow	0.860	232.4
	Testes	1.120	339.0
	Prostate	1.640	443.2
^{111}In-WBC	Spleen	26.000	7027.0
	Liver	38.000	10270.0
	Red marrow	26.000	7027.0
	Skeleton	7.280	1967.6
	Ovaries	3.800	1027.0
^{82}Rb-RbCl	Kidneys	0.032	8.6
	Heart (wall)	0.007	1.9
^{18}F-NaF	Bone surface	0.150	40.0
	Bladder wall	0.810	220.0
	Red marrow	0.15	40.0

TABLE 14.4 (continued)

Radiopharmaceuticals	Organ	Dose	
		rad/mCi	mGy/GBq
^{201}Tl-thallous chloride	Heart	0.500	135.1
	Kidneys	1.200	324.3
	Liver	0.550	148.6
	Thyroid	0.650	175.7
	Testes	0.500	135.1
^{18}F-FDG[a]	Brain	0.070	18.9
	Heart	0.220	59.5
	Bladder wall	0.700	189.2
	Spleen	0.140	37.8
	Ovaries	0.063	17.0
	Uterus	0.085	23.0
^{67}Ga-gallium citrate	Liver	0.46	124.3
	Red marrow	0.58	156.7
	Spleen	0.53	143.2
	Upper large intestine	0.56	151.4
	Lower large intestine	0.90	243.2
	Gonads	0.26	70.2
^{153}Sm-lexidronam (Quadramet)	Bone surfaces	25.000	6756.8
	Red marrow	5.700	1540.0
	Bladder wall	3.600	973.0
	Kidneys	0.065	17.6
	Ovaries	0.032	8.6
	Liver	0.019	5.1
^{89}Sr-strontium chloride (Metastron)	Bone surfaces	63.0	17000.0
	Red marrow	40.7	11000.0
	Lower bowel	17.4	4700.0
	Bladder wall	4.8	1300.0
	Ovaries	2.9	800.0
	Kidneys	2.9	800.0
^{90}Y-ibritumomab tiuxetan (Zevalin)[b]	Spleen	27.2	7350.0
	Liver	16.0	4320.0
	Lungs	7.6	2050.0
	Bladder wall	3.3	890.0
	Red marrow	2.2	590.0
	Kidneys	0.8	220.0
	Other organs	1.5	400.0
^{123}I-tositumomab (Bexxar)	Thyroid	10.027	2710.0
	Kidneys	7.252	1960.0
	Upper large intestine	4.958	1340.0
	Heart wall	4.625	1250.0
	Red marrow	2.405	650.0
	Bladder wall	2.368	640.0
	Ovaries	0.925	250.0
	Brain	0.481	130.0
	Total Body	0.888	240.0
^{133}Xe-xenon	Lungs	0.008	2.2

[a] From Stabin MG, Stubbs JB, Toohey RE. Radiation dose estimates for radiopharmaceuticals. Radiation internal dose information center, Oak ridge institute for science and foundation; 1996.

[b] From Wiseman GA, Kormehl E, Leigh B, et al. Radiation dosimetry results and safety correlations from ^{90} Y-ibritumomab tiuexetan radioimmunotherapy for relapsed or refractory non-Hodgkin's lymphoma. Combined data from four (4) clinical trials. *J Nucl Med* 2003;44:465.

TABLE 14.5. Tissue weighting factors W_T.

Tissue	W_T for EDE[a]	W_T for ED[b]
Gonads	0.25	0.20
Breast	0.15	0.05
Thyroid	0.03	0.05
Bone surfaces	0.03	0.01
Bone marrow (red)	0.12	0.12
Lung	0.12	0.12
Colon	not given	0.12
Stomach	not given	0.12
Bladder	not given	0.05
Liver	not given	0.05
Esophagus	not given	0.05
Skin	not given	0.01
Remainder	0.3	0.05
Total Body	1.0	1.0

[a] W_T values from 10CFR20. NRC adopted these values from ICRP 26 (1977)

[b] Adapted with permission from ICRP 60. 1990 *Recommendations of International Commission of Radiological Protection.* New York: Elsevier, 1991

The effective dose equivalent provides an overall risk estimate for an individual exposed to radiation, which is computed from dose equivalent to each organ that is weighted for tissue sensitivity. For assessment of risk versus benefit, the effective dose equivalent is a more appropriate parameter than the whole-body dose, because it takes into consideration the different tissue sensitivities of the organ. The W_T values are assigned such that their sum equals one. These W_T values from ICRP 26 have been adopted by the NRC (10CFR20).

In 1990, ICRP adopted a different set of W_T values and renamed the effective dose equivalent as simply the effective dose (ED) (ICRP 60). Table 14.5 summarizes the W_T values recommended by ICRP for both EDE (ICRP 26) and ED (ICRP 60). Some W_T values are different and some are the same in the two schema, whereas others are not given in the EDE scheme. Because the radio sensitivity of tissues varies with age, the effective dose is age dependent. Table 14.6 lists the effective doses in adult humans from different nuclear medicine studies using various radiopharmaceuticals (ICRP 80, 1999).

Pediatric Dosages

Because the risk of carcinogenesis due to radiation exposure is higher in children and adolescents than in adults, efforts are continually made to minimize the radiation exposure by optimizing the administered dosage of radiopharmaceuticals in nuclear medicine diagnostic studies. Over the years, different groups of

Table 14.6 Effective doses from various radiopharmaceuticals in nuclear medicine

Radiopharmaceuticals	Effective dose[a]	
	rem/mCi	mSv/MBq
^{99m}Tc-pertechnetate	0.048	0.013
^{99m}Tc-sestamibi (exercise)	0.030	0.008
^{99m}Tc-MAA	0.004	0.001
^{99m}Tc-tetrofosmin (exercise)	0.026	0.007
^{99m}Tc-DTPA aerosol	0.022	0.006
^{99m}Tc-MDP	0.022	0.006
^{99m}Tc-red blood cell (RBC)	0.026	0.007
^{99m}Tc-imininodiacetic acid (IDA) derivatives	0.063	0.017
^{99m}Tc-DTPA	0.019	0.005
^{99m}Tc-dimercaptosuccinic acid (DMSA)	0.033	0.009
^{99m}Tc-sulfur colloid	0.033	0.009
^{99m}Tc-white blood cell (WBC)	1.330	0.36
^{99m}Tc-HMPAO	0.033	0.009
^{99m}Tc-ECD	0.041	0.011
^{99m}Tc-glucoheptonate	0.019	0.005
^{99m}Tc-MAG3	0.026	0.007
^{111}In-WBC	0.133	0.036
^{111}In-DTPA	0.078	0.021
^{111}In-pentetreotide	0.185	0.050
^{123}I-NaI (35 % uptake)	0.814	0.220
^{131}I-NaI (35 % uptake)	88.80	24.00
^{201}Tl-TlCl	0.814	0.22
^{18}F-FDG	0.070	0.019
^{67}Ga-citrate	0.370	0.100
^{123}I-MIBG	0.048	0.013
^{131}I-MIBG	0.052	0.014
^{82}Rb-RbCl	0.013	0.003

[a] Adapted with permission from ICRP publication no. 80. New York: Pergamon Press; 1999.

practitioners offered these dosages of different radiophamaceuticals in a list form, that were calculated on the basis of body weight, body surface area, combination of weight and area, and simple fraction of adult dosage. Lassmann et al. (2009) published a pediatric dosage card for calculation of the dosage of radiopharmaceuticals to be administered to pediatric patients. It is calculated by multiplying a baseline activity (assumed to be the activity administered to a 3 kg child) with a multiplication factor. The multiplication factor is a complex value derived from the body weight, adult dosage, and type of radiopharmaceutical. In addition, for each study, a minimum dosage has been recommended irrespective of the calculated dosage. The multiplication factors are given in Table 14.7 and the baseline activity and minimum dosage are presented in Table 14.8.

In the United States, a Pediatric Nuclear Medicine Dose Reduction Workgroup composed of interested professionals from different professional societies like the Society of Nuclear Medicine, the Society for Pediatric Radiology and the American College of Radiology, has been formed. This group held many conferences, surveys, and seminars to establish criteria for pediatric dosages, and finally in

TABLE 14.7 Multiplication factor for baseline activity

Weight (kg)	Class A	Class B	Class C
3	1	1	1
4	1.12	1.14	1.33
6	1.47	1.71	2
8	1.71	2.14	3
10	1.94	2.71	3.67
12	2.18	3.14	4.67
14	2.35	3.57	5.67
16	2.53	4	6.33
18	2.71	4.43	7.33
20	2.88	4.86	8.33
22	3.06	5.29	9.33
24	3.18	5.71	10
28	3.47	6.43	13
32	3.77	7.29	14
36	4	8	16
42	4.41	9.14	19
46	4.65	10	21
50	4.88	10.71	23

Adapted with permission from Lassmann et al. The new EANM paediatric dosage card. Eur J Nucl Med Mol Imaging 2009;36:540.

TABLE 14.8 Baseline activity for different radiopharmaceuticals

Radiopharmaceuticals	Class	Baseline activity (MBq)	Minimum dosage (MBq)
^{123}I	C	0.6	3
^{123}I-MIBG	B	28	80
^{131}I MIBG	B	5.6	35
^{18}F FDG (2D)	B	25.9	26
^{18}F FDG (3D) in children	B	14	14
^{18}F-Fluorine (2D)	B	25.9	26
^{18}F Fluorine (3D) in children	B	14	14
^{67}Ga citrate	B	5.6	10
^{99m}Tc-colloid (gastric reflux)	B	2.8	10
^{99m}Tc-colloid (liver/spleen)	B	5.6	15
^{99m}Tc-DMSA	A	17	15
^{99m}Tc-DTPA (abnorm. renal)	B	14	20
^{99m}Tc-DTPA (normal kidney)	A	34	20
^{99m}Tc-ECD (brain perfusion)	B	32	110
^{99m}Tc-IDA	B	10.5	20
^{99m}Tc-MAG3	A	11.9	15
^{99m}Tc-MDP	B	35	40
^{99m}Tc-pertechnetate (cysto)	B	1.4	20
^{99m}Tc-RBC	B	56	80
^{99m}TcMAA	B	5.6	10
^{99m}Tc sestamibi/tetrofosmin rest scan 2-day protocol	B	42	80
^{99m}Tc sestamibi/tetrofosmin stress scan 2-day protocol	B	42	80
^{99m}Tc sestamibi/tetrofosmin rest scan 1-day protocol	B	28	80
^{99m}Tc sestamibi/tetrofosmin stress scan 1-day protocol	B	84	80

Adapted with permission from Lassmann et al. The new EANM paediatric dosage card. *Eur J Nucl Med Mol Imaging* 2009; 36:540

Table 14.9 North American guidelines for radiopharmaceutical dosages in children and adolescents[a].

Radiopharmaceutical	Recommended dosage	Minimum dosage MBq (mCi)	Maximum dosage MBq (mCi)
^{123}I-MIBG	5.2 MBq/kg (0.14 mCi/kg)	37 (1.0)	370 (10.0)
^{99m}Tc-MDP	9.3 MBq/kg (0.25 mCi/kg)	37 (1.0)	
^{18}F-FDG	Body 3.7–5.2 MBq/kg (0.10–0.14 mCi/kg), brain 3.7 MBq/kg (0.10 mCi/kg)	37 (1.0)	
^{99m}Tc-DMSA	1.85 MBq/kg (0.05 mCi/kg)	18.5 (0.5)	
^{99m}Tc-MAG3	Without flow study 3.7 MBq/kg (0.10 mCi/kg), with flow study 5.55 MBq/kg (0.15 mCi/kg)	37 (1.0)	148 (4.0)
^{99m}Tc-IDA	1.85 MBq/kg (0.05 mCi/kg)	18.5 (0.5)	
^{99m}Tc-MAA	2.59 MBq/kg (0.07 mCi/kg) if ^{99m}Tc is used for ventilation, 1.11 MBq/kg (0.03 mCi/kg) if no ^{99m}Tc is used for ventilation study	14.8 (0.4)	
^{99m}Tc-pertechnetate	(Meckel diverticulum imaging) 1.85 MBq/kg (0.05 mCi/kg)	9.25 (0.25)	
^{18}F-sodium fluoride	2.22 MBq/kg 0.06 mCi/kg)	18.5 (0.5)	
^{99m}Tc-pertechnetate (for cystography)	No weight-based dosage		37 (1.0) for each bladder-filling cycle
^{99m}Tc-sulfur colloid:			
For oral liquid gastric emptying	No weight-based dosage	9.25 (0.25)	37 (1.0)
For solid gastric emptying	No weight-based dosage	9.25 (0.25)	18.5 (0.5)

[a]Adapted with permission of the Society of Nuclear Mediicine from: Gelfand et al. J Nucl Med 2011; 52(2):318. Table 1

2010 came up with a consensus guideline for these dosages. The dosages have been obtained on the basis of body weight, taking into consideration several factors including the body surface area, the radiopharmaceutical, and using a low energy high resolution collimator in SPECT studies. Gelfand et al. (2011) has reported these recommended dosages in MBq/kg for the most commonly used radiopharmaceuticals, which must be multiplied by the body weight of the patient in order to calculate the actual dosage to be administered. The values are given in Table 14.9. This method does away with the weight-based multiplication factors stipulated in the current EANM report (Lassmann et al. 2009). The consensus group also recommended for each radiopharmaceutical a minimum dosage for optimum detectability of lesions and a maximum dosage to reduce the radiation dose to the patient. It is further recommended that the practitioners should adjust the dosage for patients heavier than 70 kg and also for different types of scanners (SPECT and PET).

Questions

1. Calculate the absorbed dose to the thyroid gland of a hyperthyroid patient from a dosage of 30 mCi ^{131}I, assuming 60 % uptake, a biological half-life of four days for thyroid clearance of ^{131}I, and S equal to 2.2×10^{-2} rad/μCi · h.
2. Calculate the dose in rems and sieverts to a tumor that received 35 rads (0.35 Gy) from neutron therapy (radiation weighting factor = 10 for neutrons).
3. What is the difference between the effective dose equivalent and effective dose?
4. Identify as true or false if the following affect the absorbed fraction of a γ-emitting radionuclide:
   (a) γ-ray energy
   (b) Shape of the target organ
   (c) Composition of the target organ
   (d) Amount of the radioactivity present in the source
   (e) Shape of the source organ
5. Does the mean absorbed dose per cumulated activity, S, depend on:
   (a) Absorbed fraction
   (b) Target mass
   (c) Photon energy
   (d) Photon abundance
6. What is the important parameter that is considered in adjusting the activity to be administered to children compared to adults for a nuclear medicine test?
7. Calculate the cumulated activity $\tilde{A}$ in a 55-g source organ containing 3 mCi (111 MBq) of ^{99m} Tc ($t_{1/2}$ = 6 h) with a biological $t_{1/2}$ = 14 h.
8. A target organ has a mass of 35 g and contains 1 mCi (37 MBq) of a radionuclide emitting a β^--particle with $\Delta_1 = 0.3$ g rad/μCi · h and $\phi_1 = 1.0$, and a γ-radiation with $\Delta_2 = 0.2$ g rad/μCi · h and $\phi_2 = 0.35$. Calculate the mean absorbed dose per cumulated activity.
9. An external beam deposits 360 ergs of energy in 3 g of tissue. What is the radiation dose in rad and cGy?
10. Explain why the concept of effective dose was introduced.
11. The absorbed doses are 10 rad (10 cGy) to organ A, 5 rad (5 cGy) to organ B, and 6 rad (6 cGy) to organ C from each radiation from a 20 mCi (370 MBq) source containing two radiations having radiation weighting factors, W_r, as 1 and 10. The tissue weighting factors of organs A, B, and C are 0.30, 0.22, and 0.46, respectively. Considering the contribution from other organs negligible, calculate the effective dose.

References and Suggested Readings

Federal Register. *Code of Federal Regulations.* 10CFR20. Washington, DC: US Government Printing Office; 1996

Fourth International Pharmaceutical Dosimetry Symposium, CONF-85113, Oak Ridge, Tenn.; November, 1985.

International Commission on Radiation Protection. 1990 Recommendations of the International Commission on Radiological Protection; *ICRP 60.* New York: Pergamon Press; 1991.

International Commission on Radiation Protection. Radiation Doses to Patients from Radiopharmaceuticals. *ICRP 80.* New York: Pergamon Press; 1999.

International Commission on Radiological Protection. *Radiation Dose to Patients from Radiopharmaceuticals ICRP 53.* New York: Pergamon Press; 1988.

Kereiakes JG, Rosenstein M. *Handbook of Radiation Doses in Nuclear Medicine and Diagnostic X-ray.* Boca Raton, FL: CRC Press; 1980.

Snyder WS, et al. *"S" absorbed dose per unit cumulated activity for selected radionuclides and organs.* MIRD pamphlet no. 11. New York: Society of Nuclear Medicine; 1975.

Snyder WS, Ford MR, Warner GG. *Specific absorbed fractions for radiation sources uniformly distributed in various organs of a heterogeneous phantom.* MIRD pamphlet no. 12. New York: Society of Nuclear Medicine; 1977.

Stabin MJ. *Fundamentals of Nuclear Medicine Dosimetry.* New York: Springer; 2008.

15
Radiation Biology

The subject of radiation biology deals with the effects of ionizing radiations on living systems. During the passage through living matter, radiation loses energy by interaction with atoms and molecules of the matter, thereby causing ionization and excitation. The ultimate effect is the alteration of the living cells. Radiation biology is a vast subject, and it is beyond the scope of this book to include the full details of the subject. The following is only a brief outline of radiation biology, highlighting the mechanism of radiation damage, radiosensitivity of tissues, different types of effect on living matter, and risks of cancer and genetic effects from radiation exposure.

The Cell

The cell is the building unit of living matter and consists of two primary components: the nucleus and the cytoplasm (Fig. 15.1). All metabolic activities are carried out in the cytoplasm under the guidance of the nucleus.

The nucleus contains chromosomes, which have a threadlike structure of two arms connected by a centromere (Fig. 15.2). Chromosomes are formed of genes, which are the basic units of heredity in the cells of all living species. Genes are composed of deoxyribonucleic acid (DNA) molecules. The structural relationship of DNA molecules, genes, and chromosomes is shown in Fig. 15.2. The sequence of genes in the chromosome characterizes a specific chromosome. Two categories of cells—namely, germ cells (reproductive cells such as oocytes and spermatozoa) and somatic cells (all other cells)—are based on the number of chromosomes they contain. Whereas germ cells contain n number of individual chromosomes, somatic cells contain $2n$ number of chromosomes in pairs, where n varies with species of the animal. In humans, n is equal to 23; therefore, there are 23 chromosomes in germ cells and 46 chromosomes in somatic cells.

In the cytoplasm of the cell exist four important organelles—ribosomes, endoplasmic reticula, mitochondria, and lysosomes—that carry out the cellular metabolic activities. Ribosomes are made up of protein and ribonucleic acid (RNA) and are responsible for protein synthesis in living matter. Endoplasmic reticula

G. B. Saha, *Physics and Radiobiology of Nuclear Medicine,*
DOI 10.1007/978-1-4614-4012-3_15,

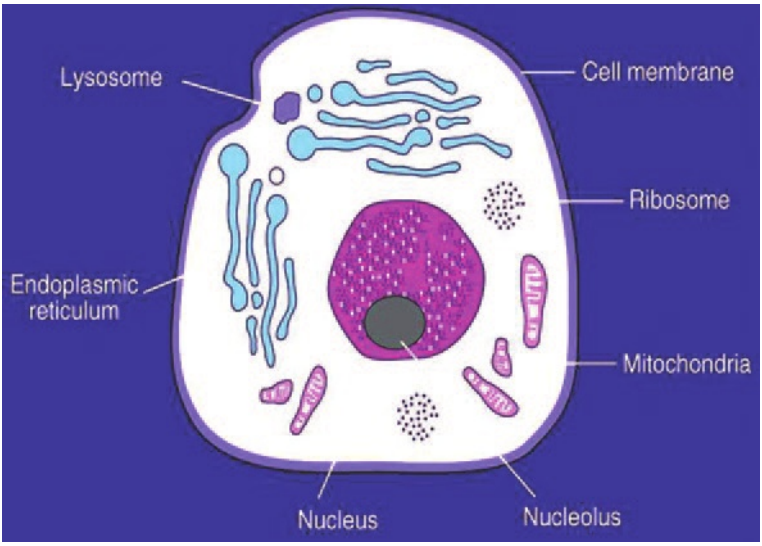

FIG. 15.1. Structure of a typical mammalian cell.

FIG. 15.2. Structural relationship of chromosomes, genes, and DNA molecules.

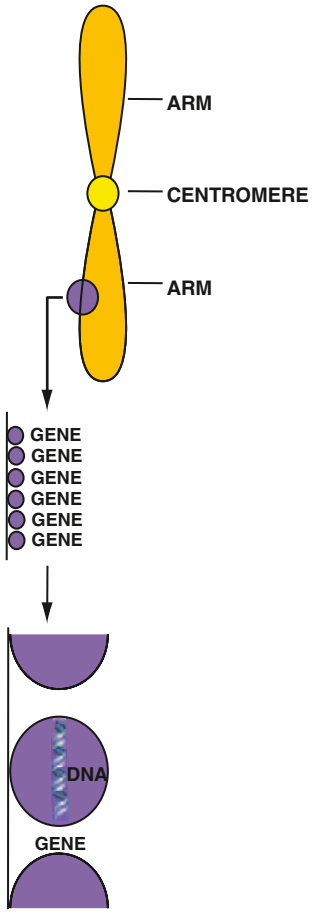

are tubular structures mostly responsible for protein synthesis. Mitochondria are ellipsoidal structures with a central cavity and contain specific enzymes to oxidize carbohydrate and lipid to produce energy. Lysosomes are small organelles in the cytoplasm that contain enzymes capable of lysing many nutrients and cells.

The entire cytoplasm is enclosed within a cell membrane made of lipids and proteins. Its primary function is to selectively prohibit or permit the passage of substances into and out of the cell.

The growth of living matter is caused by proliferation of cells by cell division—a process in which a cell divides into two cells. The cell division of somatic cells is called *mitosis* and that of germ cells is called *meiosis*. Both mitosis and meiosis, designated as M, consist of four phases: *prophase*, *metaphase*, *anaphase*, and *telophase*. Each of these phases involves the rearrangement of the number of chromosomes and represents the progression of cell division (Fig. 15.3) and is described below.

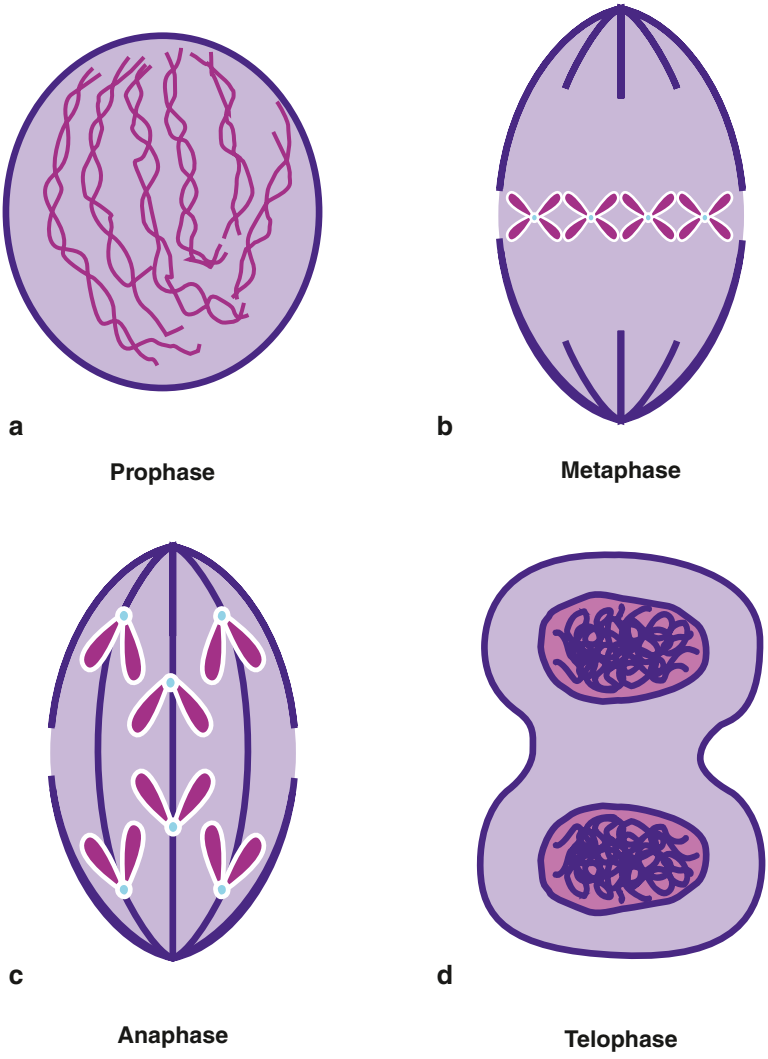

Fig. 15.3. Different phases of mitosis. See text for details.

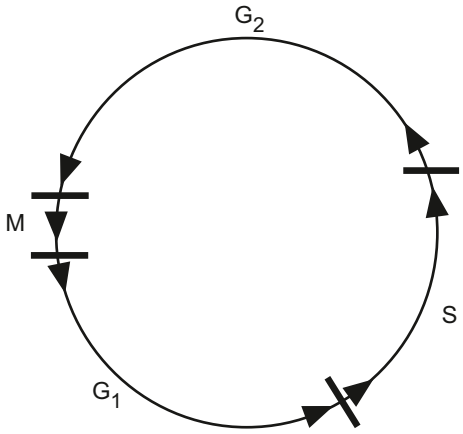

FIG. 15.4. The cell cycle. *S* is the DNA synthesis phase. *M* is the period of mitosis during which the prophase, metaphase, anaphase, and telophase take place. G_1 is the period between the telophase and *S*, and G_2 is the period between *S* and the prophase.

In prophase, the chromosome thickens in the shape of a dumbbell with a constriction at the center, called centromere. The nuclear membrane breaks open, leading to the mixture of cytoplasm and nuclear material, and spindles made of fibers are formed extending from one end (pole) of the cell to the other. Next in the metaphase, the chromosomes move to and line up at the central (or equatorial) plane of the cell, and the centromeres divide into two, each attaching to the spindle. Anaphase then follows and two chromatids move to the two poles of the cell. The last step of cell division (telophase) involves the deconvolution of the chromosomes leading to the regeneration of the nuclear membrane and nucleoli around both poles. Division of cytoplasm (cytokinesis) sets in, and ultimately two daughter cells are formed.

Before cell division, each cell undergoes a long period, termed *interphase*, in which DNA molecules are synthesized. In DNA synthesis, two new DNA molecules are produced from each DNA molecule, which are exact replicas of the original DNA molecule. This period of DNA synthesis is designated the "S" phase, which takes place around the middle of the interphase. The period between the telophase and the S phase is termed G_1, and the period between the S phase and the prophase is termed G_2 (Fig. 15.4). During the G_1 and G_2 periods, no functional activity related to cell division occurs. The period of the entire cell cycle including the M and S phases varies with the types of cells. The S phase normally is the longest and G_1 is the most variable phase in the cell cycle. The duplicate DNA molecules lead to two identical chromosomes during mitosis, which are termed sister chromatids.

One important difference between mitosis and meiosis is that in meiosis, for a given series of cell division, every alternate cell division skips DNA synthesis, thus keeping the number of chromosomes the same in germ cells.

Effects of Radiation

DNA Molecule

The nucleus of the cell is the most sensitive part to radiation and this sensitivity has been attributed to the DNA molecule. To understand the effect of radiation

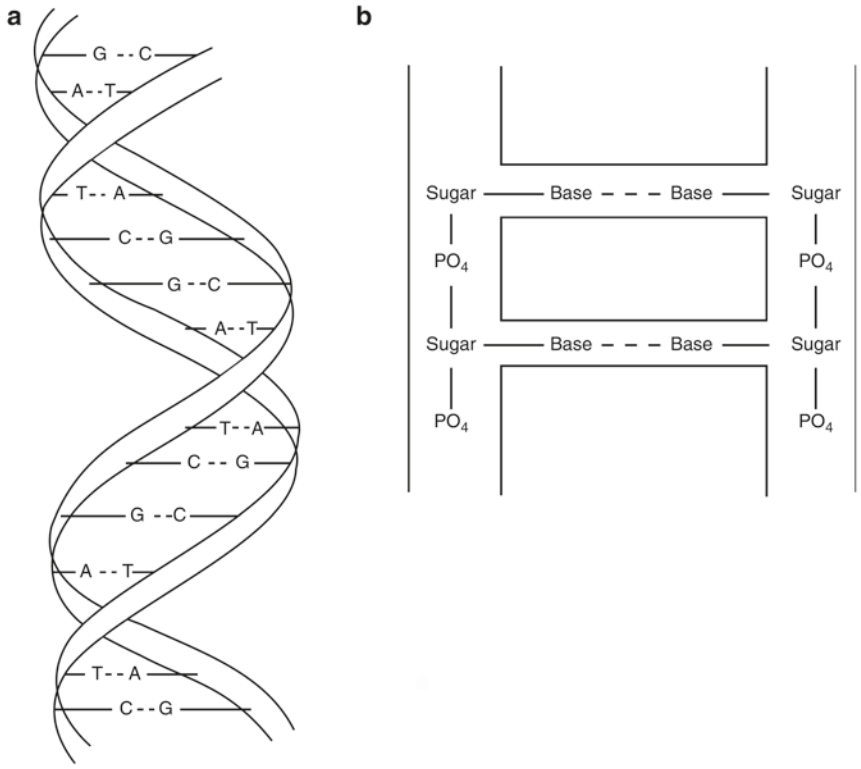

FIG. 15.5. **a** Double-helical structure of DNA molecule composed of four bases: adenine (*A*), guanine (*G*), thymine (*T*), and cytosine (*C*). **b** Configuration of a DNA molecule: strands are formed by sugar molecules bonded by phosphate groups. The rungs of the ladderlike structure are formed by bases connected to each other by the hydrogen band (*dashed line*) and to the sugar molecule on the strands on both sides.

on the DNA molecule, a knowledge of its structure is essential. It has a double-helical structure consisting of two strands, which are like the two rails of a ladder (Fig. 15.5a). The strands are composed of sugars interlinked by phosphate bonds. The two strands are connected to each other by rungs made of four bases: thymine (T), adenine (A), guanine (G), and cytosine (C) (Fig. 15.5b). The bases are bonded to the sugar molecule on the strands on both sides, and are paired to each other by hydrogen bonds. These four bases are arranged in a very specific manner to form a specific gene in every living species and provide the unique characteristics to these species.

Radiation damage to the DNA molecule can be due to

(a) Loss of a base
(b) Cleavage of the hydrogen bond between bases
(c) Breakage of one strand of the DNA molecule (single strand)
(d) Breakage of both strands of the DNA molecule (double strand)

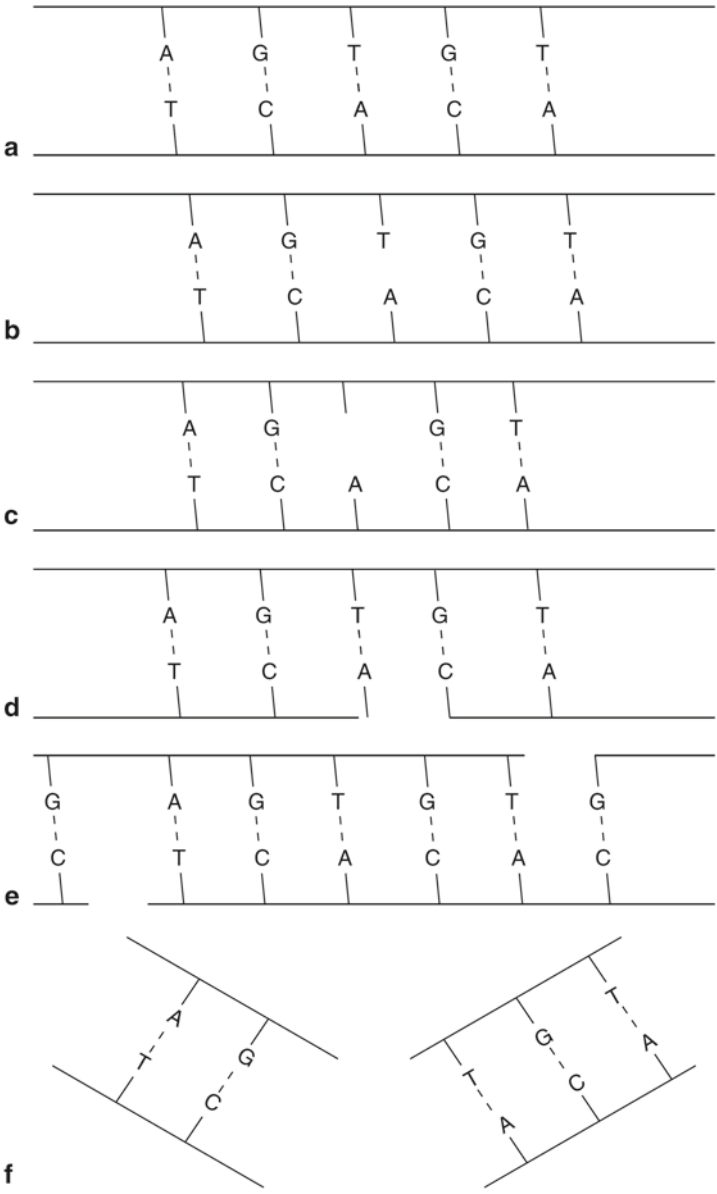

FIG. 15.6. Illustration of radiation effects on DNA molecules: **a** Normal DNA molecule; **b** hydrogen bond is broken without the loss of the base; **c** hydrogen bond is broken with the loss of the base *T*; **d** single strand break that can repair; **e** double strand breaks which are well separated and can repair; **f** double strand breaks that are too close to repair.

These radiation effects on DNA molecules are illustrated in Fig. 15.6. These changes result in so-called *mutations*, which have adverse effects on the genetic codes. The number of mutations increases with increasing radiation exposure. At low-dose exposures, the breaks are single stranded and can be repaired by joining the broken components in the original order. At higher exposures, however, double strand breaks occur and the odds for repair decrease. Also, high-LET radiations cause more damage to the DNA molecule because of the double strand breaks. If the cell is not repaired, it may suffer a minor functional impairment or a major consequence (cell death). If DNA damage occurs in germ cells, future offspring may be affected.

Chromosome

Chromosomes are likely to be affected by mutations of the DNA molecules. However, chromosomes themselves can be cleaved by radiation producing single or double breaks in the arms. These structural changes are called *aberrations*, anomalies, or lesions. These aberrations are categorized as chromatid aberrations and chromosome aberrations. In chromatid aberrations, irradiation occurs after DNA synthesis prior to mitosis and thus only one chromatid will be affected. On the other hand, in chromosome aberrations, irradiation occurs after mitosis prior to DNA synthesis and hence the broken chromatids will be duplicated producing daughter cells with damaged chromosomes.

Whether chromosome aberrations are induced by single-strand breaks or double-strand breaks in the structure determines the fate of the cell. In single-strand breaks, the chromosome tends to repair by joining the two fragments in a process called *restitution*, provided sufficient time is allowed. The cell becomes functionally normal and replicates normally (Fig. 15.7a). However, if the fragments are replicated during DNA synthesis prior to restitution, two strands with centromeres and two strands without centromeres will be produced. Random combination of these fragments will then produce acentric and dicentric chromatids as illustrated in Fig. 15.7b. Such chromosomes suffer severe consequences due to the mismatch of genetic information.

If radiation produces single-strand breaks in two separate chromosomes, then there are four ways of recombining the broken ends as shown in Fig. 15.8. The dicentric and acentric combinations (Fig. 15.8a) are similar to those formed after replication of single strands in the same chromosome shown in Fig. 15.7b. However, these cells suffer severe consequences because of the mismatch of genetic information from two separate damaged chromosomes. The translocation is a process in which two fragments—one with a centromere from one chromosome and one without a centromere from another chromosome—combine to form a new chromosome (Fig. 15.8b). In another scenario, radiation can cause two breaks in one arm of a chromosome, resulting in three fragments, only two of which combine with the loss of the third. Such a process is called deletion (Fig. 15.9a). Translocation and deletion, although not as harmful to the cell, cause late effects such as carcinogenesis and hereditary effects due to mismatch or loss of genetic

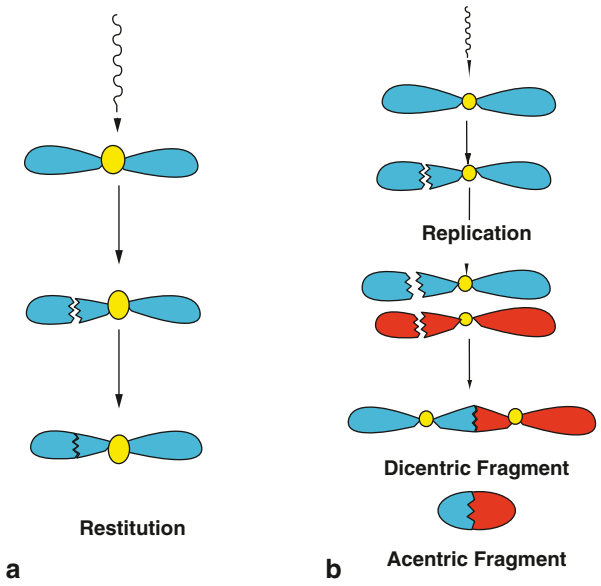

FIG. 15.7. **a** Illustration of restitution, in which the fragments produced by a single-strand break in one arm of the chromosome by radiation join together to produce the original chromosome. **b** Formation of dicentric and acentric chromosomes by combination of the fragments, after replication from a single-strand break in a chromosome.

material. An alternative to deletion is the combination of all three fragments into a chromosome with changes along the broken line as shown in Fig. 15.9b. This process is called inversion, which has all the original genetic material except a change in the sequence of genes and hence is not as detrimental to the cell.

Repair of chromosomes after irradiation depends on the sites of break in the DNA molecule or the chromosome, the total radiation dose, the dose rate, and the LET of the radiation. Chromosome aberrations by double-strand breaks occur more frequently at high-dose rates than at low-dose rates because of less time to repair and fewer chances of combining two fragments in correct sequence of genes. High-LET radiations cause more double-strand breaks in chromosomes than low-LET radiations, and thus repair becomes difficult in the former. For example, α-particles, protons, and neutrons will cause more chromosome aberrations than γ-rays.

Direct and Indirect Actions of Radiation

The DNA molecule of a cell is the most sensitive target to radiation. Radiation damage to the cell can be caused by the direct or indirect action of radiation on the DNA molecules. In the direct action, the radiation hits the DNA molecule directly, disrupting the molecular structure (Fig. 15.10). Such structural change leads to cell damage or even cell death. Damaged cells that survive may later induce carcinogenesis or other abnormalities. This process becomes

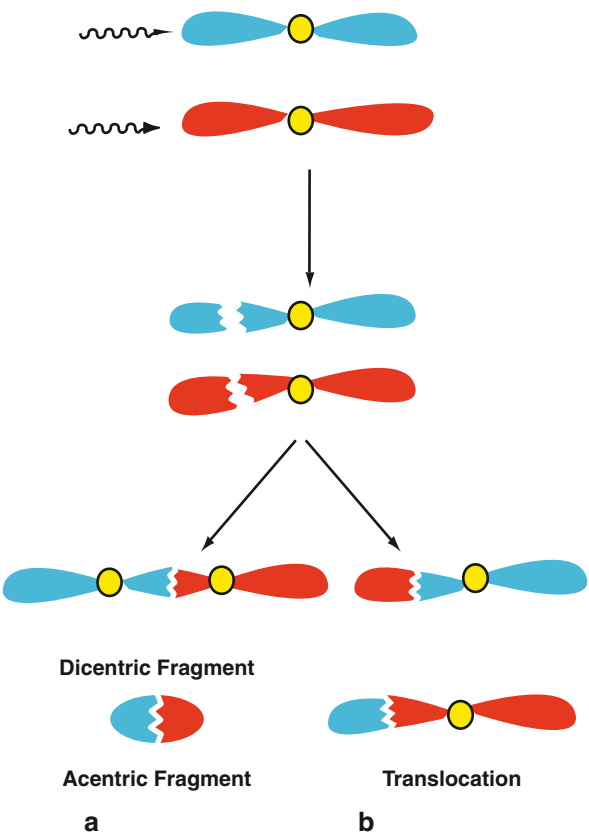

FIG. 15.8. Single-strand breaks in one arm of each of two separate chromosomes. Combination of these four fragments leads to dicentric and acentric chromosomes **a** or translocation **b**.

predominant with high-LET radiations such as α-particles and neutrons, and high radiation doses.

In the indirect action, the radiation hits the water molecules, the major constituent of the cell, and other organic molecules in the cell, whereby free radicals such as perhydroxyl ($HO_2\bullet$) and alkoxy ($RO_2\bullet$) are produced. A variety of reactions that can occur after radiation interacts with water molecules is shown below.

$$H_2O + \text{energy} \rightarrow H_2O^+ + e^-$$
$$H_2O + e^- \rightarrow HOH^-$$
$$H_2O^+ \rightarrow H^+ + OH\bullet \text{ (free radical)}$$
$$HOH^- \rightarrow OH^- + H\bullet \text{ (free radical)}$$
$$H^+ + OH^- \rightarrow H_2O$$
$$H\bullet + OH\bullet \rightarrow H_2O$$
$$OH\bullet + OH\bullet \rightarrow H_2O_2$$
$$H\bullet + O_2 \rightarrow HO_2\bullet \text{ (perhydroxyl radical)}$$

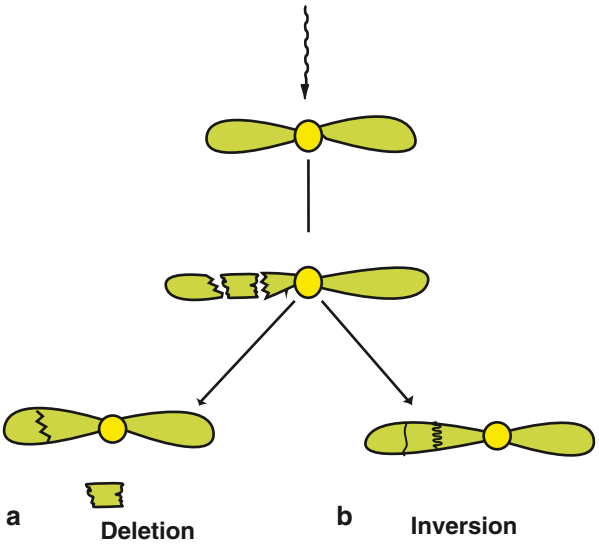

FIG. 15.9. Two breaks in one arm of a chromosome producing three fragments. **a** In deletion, two of the fragments combine with the loss of the third, or **b** in inversion, all three fragments combine with the interchange of positions.

Free radicals are characterized by an unpaired electron in the structure, which is very reactive, and therefore reacts with DNA molecules to cause a molecular structural damage (Fig. 15.10). Hydrogen peroxide, H_2O_2, is also toxic to the DNA molecule. The result of indirect action of radiation on DNA molecules is the impairment of function or death of the cell. The number of free radicals produced by ionizing radiation depends on the total dose but not on the dose rate. It has been found that the majority of radiation-induced damage results from the indirect action mechanism because water constitutes nearly 70 % of the composition of the cell.

Radiosensitivity of Cells

In living matter, there are two types of cells: differentiated and undifferentiated. Undifferentiated cells do not have any specific physiologic function except to develop into mature cells. They undergo mitosis and serve as the precursors for mature cells. In contrast, all mature cells are differentiated and perform specific functions in the living body. For example, red blood cells (RBCs) are mature and differentiated cells performing the function of oxygen carriers, whereas erythroblasts are undifferentiated cells that develop into RBCs through mitosis.

According to the law of Bergonié and Tribondeau, undifferentiated cells that are undergoing active mitosis are most sensitive to radiation, and differentiated

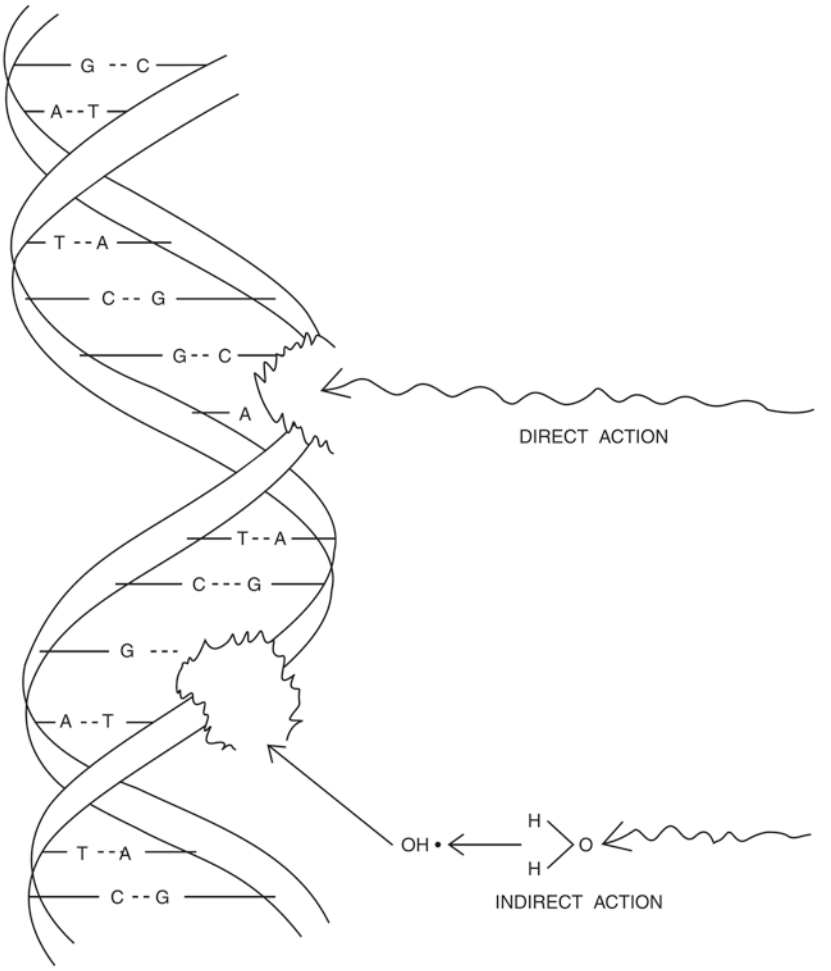

FIG. 15.10. Illustration of direct and indirect action of radiation on the DNA molecule. In direct action, radiations hit the DNA structure directly, whereas in indirect action, radiations produce free radicals in the cytoplasm, which react adversely with the DNA molecule to cause structural damage.

or mature cells are least affected by radiation. For example, in a sample of mixed RBCs, erythroblasts are most damaged and mature RBCs are least affected by radiation. Undifferentiated cells that are killed by radiation may be replaced by new cells, but those that survive with defective DNAs can induce late effects, such as cancer (see later). In contrast, the S phase of DNA synthesis in the cell cycle is least radiosensitive. Radiosensitivity is best assessed by cell death. For differentiated cells, it means loss of cellular function, whereas for undifferentiated cells it means loss of reproductivity.

TABLE 15.1. Different types of cells and their radiosensitivity.

Types of cells[a]		Radiosensitivity
VIM	Mature lymphocytes	Highly sensitive
	Erythroblasts	
	Spermatogonia	
DIM	Myelocytes	Relatively sensitive
	Intestinal crypt cells	
	Basal cells of epidermis	
MCT	Osteoblasts	Intermediate sensitivity
	Spermatocytes	
	Chondroblasts	
	Endothelial cells	
RPM	Spermatozoa	Relatively resistant
	Granulocytes	
	Erythrocytes	
	Osteocytes	
FPM	Nerve cells	Highly resistant
	Muscle cells	
	Fibrocytes	

Adapted from Casarett AP. Radiation Biology. Englewood Cliffs, NJ: Prentice-Hall; 1968:168–169.

[a] *VIM* vegetative intermitotic, *DIM* Differentiating intermitotic, *MCT* multipotential connective tissue, *RPM* reverting postmitotic, *FPM* fixed postmitotic.

Groups of cells and their relative radiosensitivity are listed in Table 15.1. As can be seen, lymphocytes, though mature cells, are most sensitive to radiation, owing to a large nucleus; nuclear material is more radiosensitive. Nerve cells and muscle cells are totally differentiated cells and therefore are highly resistant to radiation. The tissue or organ that contains more radiosensitive cells will be highly radiosensitive and vice versa. For example, bone marrow containing radiosensitive erythroblasts is very radiosensitive, whereas nerves and muscles containing radioresistant cells are less radiosensitive. Following irradiation of blood, depressed blood counts are observed as follows: lymphocytes on the same day, granulocytes in 3 days, platelets in 6 days, and RBCs in 10 days.

Cell Survival Curves

When mammalian cells are irradiated, not all cells are affected to the same extent. Different factors such as the total dose, the dose rate, the LET of the radiation, the particular stage of the cell cycle (M, G_1, S, or G_2) and the type of cell will affect the radiation-induced damage. Some cells may die and some will survive. The cellular response to radiation is illustrated by what is called the *cell survival curve*. It is obtained by plotting the dose along the linear *X*-axis and the surviving fraction along the logarithmic *Y*-axis. Surviving cells are those cells that retain all reproductive as well as functional activities after irradiation, whereas the death of

cells is indicated by the loss of their function in differentiated cells and by the loss of reproductive activity in undifferentiated cells. It should be noted that thousands of grays are needed to kill differentiated cells, whereas only hundreds of grays are needed for undifferentiated cells.

Typical cell survival curves are shown in Fig. 15.11. For high-LET radiations such as α-particles and low-energy neutrons, the survival curves are nearly a straight line starting from the lowest doses. In contrast, for low-LET radiations (e.g., x- and γ-radiations), the survival curve exhibits an initial shoulder, followed by a straight line. This straight line portion on the semilog plot is an exponential curve on a linear plot. This curve based on a *multitarget model* is characterized by three parameters: D_0 (dose at which 37 % of cells survive), the extrapolation number n, and the quasithreshold dose D_q, and they are related by the expression

$$\log_e n = D_q / D_0 \tag{15.1}$$

The quasithreshold dose, D_q, is the dose given by the width of the shoulder of the curve. The D_q indicates that, at low doses, almost all cells repair after irradiation, and cell killing is minimal, which is due to very limited radiation damage to the cell.

D_0 is determined from the slope of the straight line portion of the survival curve. It is the dose that kills 63 % of the total number of cells. The value of D_0 is a measure of radiosensitivity of a given type of cell. For example, a large value of D_0 for a type of cell means that the cells are less radiosensitive and vice versa.

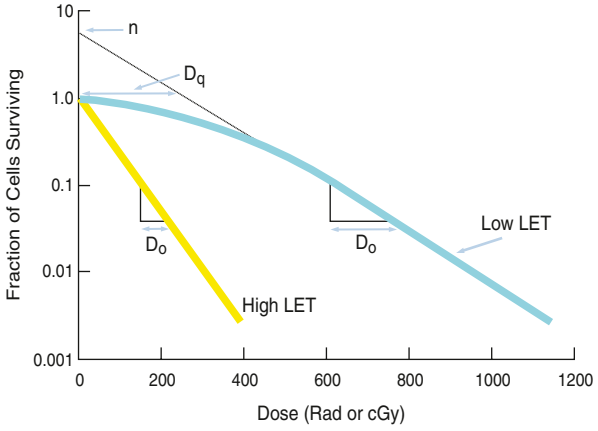

FIG. 15.11. Typical cell survival *curves*. The cell survival curve for low linear energy transfer (*LET*) radiations shows a shoulder of width D_q, which is called the quasithreshold dose. After D_q, the plot becomes linear on a semilog scale, indicating an exponential dose–response relationship. The extrapolation number n is obtained by extrapolating the linear portion of the curve back to the ordinate. D_0 is the dose obtained from the slope of the linear portion of the curve, at which 37 % of the cells survive. The survival curve for high-*LET* radiations shows no or little shoulder, indicating D_q to be zero and n to be unity.

The extrapolation number n is obtained by extrapolating the straight line portion of the survival curve back to the Y-axis. Its value depends on the width of the shoulder of the survival curve, that is, the quasithreshold value, D_q. Its value for mammalian cells varies between 1 and 10.

Although Eq. (15.1) has some merit in expressing cell killing by radiation, the *linear-quadratic model* provides a more accurate description of the radiation-induced cell killing. This model is mathematically expressed as

$$S = e^{-\alpha D - \beta D^2} \tag{15.2}$$

where S is the survival fraction of the cells irradiated with dose D and α and β are constants. For low-LET radiations, βD^2 is negligible at low doses, and the cell survival is proportional to the dose only, making the survival curve linear (Fig. 15.12). At higher doses, the cell survival is proportional to the square of the dose, and the curve tends to bend becoming concave downward (Fig. 15.12). For high-LET radiations, β is zero, and so the survival curve becomes linear.

Factors Affecting Radiosensitivity

As already mentioned, various factors affect the radiation damage in the cell and hence the survival curve. The dose rate, the LET of the radiation, the presence of chemical molecules and the stage of the cell cycle all affect the survival curve.

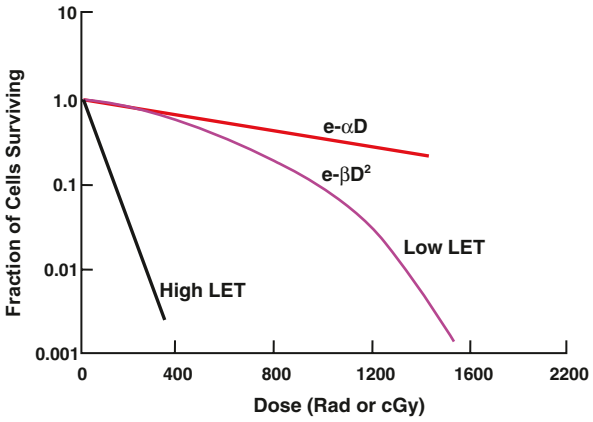

FIG. 15.12. Cell survival *curves* based on linear-quadratic model. The initial slope of the linear-logarithmic plot gives cell killing proportional to $e^{-\alpha D}$ and the latter part to $e^{-\beta D^2}$ which bends at higher doses. With high-LET radiations, β is zero, and the curve is exponentially expressed simply by $e^{-\alpha D}$.

Dose Rate

The dose rate, that is, the delivery of dose per unit time, is an important factor in cellular damage. The higher the rate of dose delivery, the greater will be the cell damage. At low-dose rates, only single-strand breaks of DNA molecules occur, and so cells have time to repair, whereas at high-dose rates double-strand breaks occur, and so repair is less likely to occur because of the shorter time available to the cells between ionizing events. Figure 15.13 illustrates the effects of two dose rates on the cell survival curve. The dose-rate effect is very important in radiation therapy, because unless an appropriate dose rate is prescribed, intended therapeutic effect may not be achieved. When a total dose is given to a patient in fractions over a period of time, it should be kept in mind that the interval between fractional doses should be short enough to keep repair of damage to abnormal cells to a minimum.

Linear Energy Transfer

High-LET radiations (e.g. α-particles, neutrons) do not exhibit a dose-rate effect on the survival curve. Also at high-dose rates (above 100 rad/min) of low- and moderate-LET radiations, no dose-rate effects are observed on the survival curve in contrast to low-dose rates. Thus, high-LET radiations exhibit no shoulder (i.e., no D_q) on the survival curve resulting in an extrapolation number of 1 (Fig. 15.12).

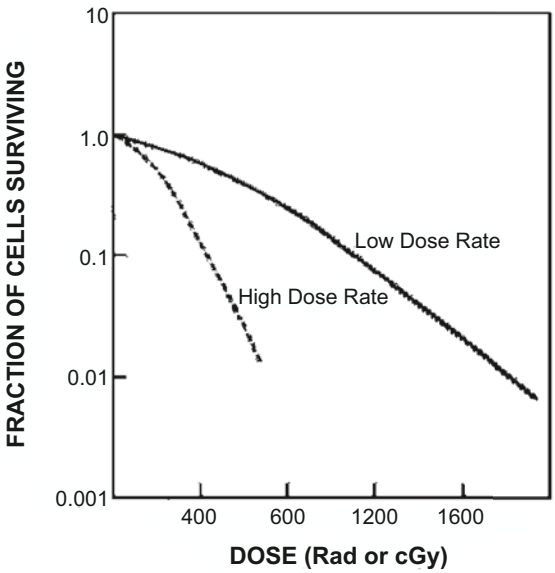

FIG. 15.13. The cell survival *curves* indicating the effect of dose rates. At high dose rates, the shoulder of the curve is reduced, with smaller values of D_q. The opposite is true at low dose rates.

High-LET radiations are densely ionizing radiations causing more double-strand breaks in the DNA molecules, and thus leading to more cell deaths than low-LET radiations, which are sparsely ionizing radiations (e.g. x-rays, γ-rays). Radiation damage by high-LET radiations is so severe that the chances of repair are minimal, and even if repair takes place, the cell is likely to be defective.

Chemicals

Several chemicals, if present during irradiation, have been found to augment or diminish the effects of radiation on cells. Agents that enhance the cell response to radiation are celled *radiosensitizers*, and those that protect cells from radiation-induced damage are called *radioprotectors*.

Radiosensitizers

Oxygen

Oxygen is the best-known sensitizer encountered in radiation biology. It has been found that hypoxic cells are resistant to radiation, whereas oxygenated cells are highly radiosensitive. Such radiosensitization by oxygen is called the *oxygen effect* and is measured by a quantity called the *oxygen enhancement ratio* (OER). The OER is given by the ratio of the dose required to produce a given radiation damage to cells in the absence of oxygen to that required to produce the same damage in the presence of oxygen. The oxygen effect occurs only when oxygen is administered simultaneously with radiation. It increases with O_2 tension up to 30 mm Hg, and remains constant at higher O_2 tension. For mammalian cells, the oxygen concentration required to produce a radiation response midway between hypoxic and aerobic conditions is approximately 0.5 %. The OER value reaches a maximum of 3.0 for x- and γ-radiations, whereas it is about unity for high-LET radiations such as α-particles.

Figure 15.14 illustrates the effects of oxygen on the survival curve. The presence of oxygen makes the curve much steeper, indicating the augmentation of cellular damage at smaller doses relative to the situation of no oxygen. The mechanism of the oxygen effect is not clearly understood but is most likely related to DNA strand breaks. It has been postulated, however, that oxygen combines with already formed free radicals, R•, to produce peroxidyl group $RO_2^{\bullet}$, which is more damaging to the DNA molecules. While normally R• could recombine with complementary molecular components to repair the cell, $RO_2^{\bullet}$ is an altered chemical entity and cannot help in cell repair. The oxygen effect is most predominant for γ- and x-rays, and is practically absent for high-LET radiations (e.g., α-particles).

It is known that hypoxic cells are present in tumors to different extents and exhibit resistance to radiation or chemical therapy of tumors. Tumor hypoxia is caused by imbalance between the O_2 supply and its consumption in the cell that results from inadequate blood supply due to structural change, difficulty in blood diffusion, or therapy-induced anemia. Hypoxia, in addition to reducing therapeutic efficacy, enhances malignant progression. The mean oxygen tension (pO_2) in hypoxic tumor

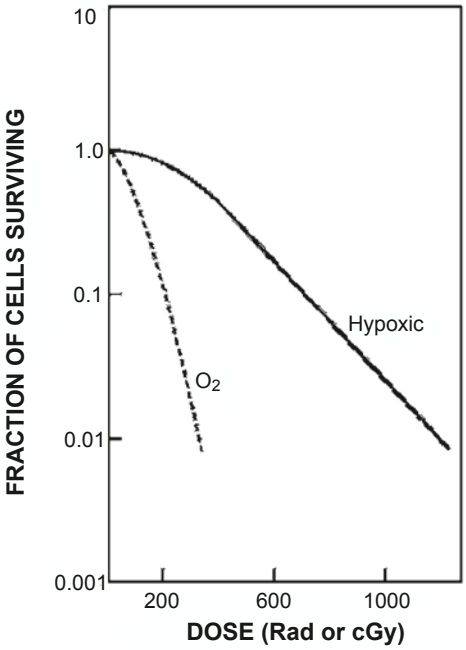

FIG. 15.14. The cell survival curve illustrating the effect of oxygen. In the presence of oxygen, the curve becomes steeper, indicating effective killing of the cells by radiation.

cells is substantially lower than in normal cells (~2 mm Hg for solid tumors versus ~50 mm Hg for normal tissues). To achieve greater efficacy in radiation treatment of tumors, it has been advocated to oxygenate the tumor cells and then to apply radiation to oxygenated cells. Oxygenation of patients has been carried out by having the patient breathe in a chamber filled with oxygen at 2–3 times the atmospheric pressure. Another method involves the administration of carbogen (a mixture of 95 % oxygen and 5 % CO_2) alone or in combination with nicotinamide. Treatment of oxygenated cells with radiation has resulted in only limited success.

It has been found experimentally that the proportion of hypoxic cells in a tumor remains the same before and after fractionated radiation therapy. Logically, radiotherapy should have killed more oxygenated cells and thus raised the proportion of hypoxic cells. Instead, it remains the same and has brought in the argument of reoxygenation of the tumor cells during fractional radiation therapy, provided sufficient time is allowed for this to happen. This phenomenon has an important implication in radiation therapy in that even though the proportion of hypoxic cells remains the same, the total number of hypoxic tumor cells will be killed by radiation over time, thus leading to a successful treatment. The degree of reoxygenation varies with tumor types. The mechanism of reoxygenation has been attributed to the fact that as the tumor shrinks in size, surviving cells that were previously deprived of oxygen diffusion due to distal location of the blood vessels find themselves closer to the blood supply and so reoxygenate.

Pyrimidines

Halogenated pyrimidines such as 5-chlorodeoxyuridine (ClUDR), 5-bromodeoxyuridine (BUDR), and 5-iododeoxyuridine (IUDR) are useful radiosensitizers. When cells are treated with these drugs for several days before irradiation with x- or γ-rays, cells become highly sensitive to radiation. Potentiation of radiosensitivity is due to the fact that these drugs are similar to the DNA precursor thymidine, and therefore are incorporated into the DNA molecule, making them more susceptible to damage by radiation. For optimal therapeutic gain in radiotherapy, patients should be treated for a period of time extending over several cell cycles to maximize drug incorporation into the cells.

Others

Radiosensitizers such as actinomycin D, puromycin, methotrexate, and 5-fluorouracil have been successfully used in combination with radiation to treat cancer. Whether these agents truly increase radiosensitivity or are simply toxic to the cells is still not clear.

Investigators have been trying to explore radiosensitizing chemicals to substitute for oxygen that requires the use of a high-pressure technique. Metronidazole (Flagyl), having a structure with high electron affnity, is a good radiosensitizer for hypoxic cells. Another useful radiosensitizer for hypoxic cells is misonidazole, which also has high electron affinity. Misonidazole is almost ten times more effective than metronidazole in sensitizing hypoxic cells. However, clinical trials with this agent provided only disappointing results. Another radiosensitizer of this kind is etanidazole, which is less toxic than misonidazole, and has great potential in radiotherapy. Most side effects of these products are related to neurotoxicity. These compounds are described as “oxygen mimics”.

Radioprotectors

The most common radioprotectors—substances that protect cells from radiation damage—include substances containing sulfhydryl groups (-SH), such as cysteine and cysteamine. These agents protect normal cells from radiation damage by combining with free radicals that are produced by radiation and would be toxic to normal cells. However, these compounds cause severe adverse reactions such as nausea and vomiting.

Less toxic compounds have been developed in which the -SH group is protected by a phosphate group. The phosphate group is hydrolyzed in vivo to release the -SH group for radioprotection. Two most effective compounds of this category are WR-638 and WR-2721 developed at Walter Reed Army Hospital, Washington, DC. Experimental evidence showed that these products concentrate more in normal cells and less in tumor cells. As a result, normal cells are protected better than tumor cells if these agents are administered immediately before the radiation dose is given. WR-2721, also called amifostine, is an aminothial and protects

bone marrow. Its most common toxic effects are hypotension and somnalence. Radioprotectors are most effective with low-LET radiations, because they cause minimal damage.

Stage of Cell Cycle

Radiation damage mostly occurs during the period of mitosis, the M phase, whereas least damage occurs during the DNA synthesis, the S phase. Thus, the stage of the cell cycle determines the extent of radiation damage. If mitotic death occurs in a cell after irradiation, the irradiated cell may go through one, two, or more mitotic phases trying to divide but ultimately dies. Exposure of cells to 100–1000 rad (100–1000 cGy) causes delay in the G_2 phase to M phase transition. An exposure of 1000 rad (1000 cGy) inhibits the progression of the S phase cells by 30 %, whereas the S phase to G_2 phase transition is not affected by such an exposure (Prasad 1995).

Apoptosis

While necrosis results from uncontrolled cell death due to cell lysis or inflammatory responses, *apoptosis* or programmed cell death occurs in a controlled fashion in that the cells play an important role in their own death. It is characterized by a sequence of stereotyped events that take place in discrete phases, following stress induced by a variety of external stimuli. Radiation is one of the stimuli that causes stress in the cell, whereby a group of proteins called caspases are activated. These proteins break down the key cellular components essential for normal cell function, ultimately resulting in the breakdown of the chromatin. Cells then condense to form membrane-enclosed horseshoe-like bodies, which are phagocytosed by nearby macrophages leading to apoptosis. Apoptosis typically occurs in all species.

Classification of Radiation Damage

Cell death is a measure of extreme radiation damage. Therefore, based on the degree of lethality induced by radiation, radiation damage can be classified into three categories: (1) lethal damage, which causes irreversible death; (2) sublethal damage (SLD), which normally repairs in hours, and thus avoids cellular death, unless followed by another sublethal damage; and (3) potentially lethal dose (PLD), which can potentially kill the cell but can be modified to repair under specific physicochemical conditions. All these damages are relevant in clinical radiation therapy as to the effectiveness of treatment. Lethal damage is a definite

end point in treatment, whereas SLD and PLD have variable effects in radiation therapy.

Sublethal damage occurs in mammalian cells, when a radiation dose is given in fractions at different time intervals rather than a single dose. There are four mechanisms, the so-called four R's that play a role in the SLD repair (SLDR) mechanism: repair, redistribution, regeneration, and reoxygenation. Repair involves the healing of the radiation-induced damage in the time interval between the two fractions of the dose. If the second dose is applied too soon after the first application, the damage does not have enough time to repair and the cell will die. In fractionated radiotherapy, normal tissues are spared by SLD because of its repair mechanism. In the redistribution process, the cells are desynchronized and sensitized to show increased damage. Following irradiation, the radiosensitive cells will die, and one would expect the proportion of radioresistant cells and hence the surviving fraction to increase. In fact, however, the surviving cells become sensitized and tend to die. This result depends on the fractionated dose and the time interval between the doses. Regeneration is a mechanism of response to depopulation of a cell cohort due to radiation damage, and depends on the types of tissue and their proliferating capacity. Protracting a fractionated dose should be beneficial to normal tissues and somewhat harmful to regenerating tumor cells. Reoxygenation discussed earlier is an effect that makes the hypoxic cells more radiosensitive in the presence of oxygen in fractionated radiotherapy.

Sublethal damage repair depends very much on the dose rate and in which stage of the cell cycles the cells are. At lower doses, more SLD can be repaired, and at higher doses, the chances of SLD repair diminish. The dose-rate effect varies with the types of tissue and species. For example, the testis of male rats is most radiosensitive, whereas the small intestine seems to be less affected by radiation. Also, SLD repair depends on the LET of radiations. The repair is significant with x-rays and γ-rays and almost nonexistent for neutrons and α-particles. SLD repair is very important in radiation therapy as it provides maximum survival of normal cells, while killing tumor cells.

Potentially lethal damage after a single dose of radiation can potentially kill the cell but it can be repaired (PLDR) under specific physicochemical conditions. For example, the survival of the HeLa cells increased after irradiation, when the cells were treated with excess thymidine or hydroxyurea for a period of 4 h post-irradiation. However, opposite results were obtained by other investigators. The importance of PLDR in radiotherapy is a matter of debate.

PLDR and SLDR are found with low-LET radiations (e.g., γ-rays and x-rays giving cell survival curves with a broad shoulder), while they are absent for high-LET radiations (neutrons and α-particles).

Sources of Radiation Exposure in the United States

The population at large receives radiation exposure from various sources such as ubiquitous natural background radioactivity, medical procedures, consumer products, activities related to industrial, security, medical, and educational research, and occupational sources. The estimates of various exposures are tabulated in Table 15.2. Annual total exposure for individuals in the US has significantly increased from ~360 mrem (3.6 mSv) in 1980–1982 to 625 mrem (6.25 msv) in 2006. Much of the increase is largely due to the prolific growth of medical procedures.

Ubiquitous background radiation comprises radon and thoron, cosmic rays, in vivo radionuclides, and terrestrial radiations. Radon (^{222}Rn) and thoron (^{220}Rn) exist in building materials and are prevalent in basement of the buildings. This exposure is an internal exposure due to inhalation of these gaseous products and amounts to 212 mrem (2.12 mSv) and 16 mrem (0.16 mSv), respectively, accounting for almost 37 % of the total exposure.

Cosmic rays originate in the solar system and the exposure varies with the altitude of places on earth. The average value is ~33 mrem (0.33 mSv) (5 %) with a range of 28 mrem (0.28 mSv) in Honolulu and 82 mrem (0.82 mSv) in Colorado Springs.

The in vivo radioactivity consists of natural ^{40}K, ^{232}Th and ^{238}U present in food and water, and are ingested internally by humans. This exposure amounts to 29 mrem (0.29 mSv) (4 %).

The terrestrial radiation exposure arises from radionuclides such as ^{40}K and the decay products of thorium and uranium in soil. Annually this adds about 21 mrem (0.21 mSv) (3 %).

Air travel at a height of 39,000 ft (12 Km) gives 0.5 mrem/h (5 μSv/h) resulting in an annual dose of 1 mrem (0.01 mSv) to those who fly.

Table 15.2. Annual effective dose per individual in the U.S. population from different sources for 2006.[a]

Sources	Average annual effective dose in mrem (mSv)
Natural sources	311 (3.11)
Radon & Thoron	228 (2.28)
External, space	33 (0.33)
External, terrestrial	21 (0.21)
Internal, ingestion	29 (0.29)
Medical procedures	300 (3.0)
CT	147 (1.47)
Nuclear medicine	77 (0.77)
Interventional radiology	43 (0.43)
Conventional radiography and fluoroscopy	33 (0.33)
Consumer products	13 (0.13)
Industrial, security, medical, education and research	0.3 (0.003)
Occupational	0.5 (0.005)
Total	~625 (6.25)

[a] Reprinted with permission of the National Council on Radiation Protection and Measurements, http://NCRPPublications.org. NCRP No 160: Table 1.1

Medical procedures contribute the highest exposure of all man-made radiation sources amounting to ~300 mrem (3.0 mSv). The breakdown of these exposures is as follows: CT (49 %); nuclear medicine (26 %); interventional radiology (14 %), and conventional radiography and fluoroscopy (11 %). Exposure from radiation therapy is relatively small.

Exposure due to industrial, security, medical education and research activities arise from the use of radioactivities in nuclear the fuel cycle, by the Departments of Energy and Homeland Security, by investigators in research, and radiactive waste disposal by medical facilities. The public is exposed to radiations from these sources in an annual average of 0.3 mrem (0.003 mSv).

Occupational exposure is received by the workers in reactor plants, coal mines, and other industries using radionuclides. This value is 0.5 mrem (0.005 mSv), which is quite small, because a great deal of precaution is taken to reduce exposure at work places.

Stochastic and Deterministic Effects

Two categories of radiation effects on biological systems are encountered: stochastic and deterministic. Stochastic effects are the biological effects that occur randomly, the probability of which increases with increasing dose without a threshold. Radiation-induced hereditary effects and cancer incidences are examples of stochastic effects. The assumption of no threshold is made on the belief that radiation damage to a few cells or a single cell could theoretically induce the genetic disorder or cancer, and the severity of the disease will be the same, if it ever occurs. It should be noted that the basic principle of ALARA (as low as reasonably achievable) in Nuclear Regulatory Commission (NRC) regulations is based on the assumption of risks linearly proportional to the dose without a threshold. Much debate has occurred regarding the assumption of the linear-no-threshold (LNT) theory (discussed below).

The deterministic or nonstochastic effects are induced by high radiation doses and the severity of the damages, rather than their probability of occurrence, increases with the dose. These effects have a threshold dose below which no damage is evident. Cataracts, skin erythema, sterility, and fibrosis are examples of deterministic effects induced by high radiation doses.

Acute Effects of Total Body Irradiation

Different tissues of the body respond differently to radiation, due to varying degrees of radiosensitivity. When an adult subject is irradiated over the entire body, various syndromes are manifested depending on the dose applied. The effects of radiation are characterized by the survival time of the species and various stages

of acute syndromes following the total-body irradiation. These effects are deterministic types and have a threshold dose.

Cell survival time varies with mammal species depending on the individual radiosensitivity. The radiosensitivity of a given species is commonly characterized by the lethal dose, $LD_{50/60}$, which is the dose that kills 50 % of the species in 60 days. The $LD_{50/60}$ for humans is 400–600 rad (400–600 cGy); for dogs, 300 rad (300 cGy); and for mice, 900 rad (900 cGy).

Acute radiation syndromes appear in four stages: prodromal, latent, manifest illness, and recovery or death. Each stage is dose dependent and can last for a few minutes to weeks. A minimum of 200–300 rad (200–300 cGy) is required for all four stages to be seen and can cause death.

In the prodromal stage, major symptoms are nausea, vomiting, and diarrhea and they occur in the early phase, lasting for only a short period of time depending on the dose. A dose of 50 rad (50 cGy) can induce nausea and vomiting. In the latent stage, biological damage slowly builds up without manifestation of any syndromes, again lasting for hours to weeks, depending on the dose. During the manifest illness stage, radiation syndromes appear as a result of the damage to the organs involved after the latent period, and the subject becomes ill. In the last stage, the subject either recovers or dies.

There are three categories of syndromes in the manifest illness stage depending on the dose: hemopoietic or bone marrow, gastrointestinal (GI), and cerebrovascular.

Hemopoietic Syndrome

Hemopoietic or bone marrow syndromes appear at a total body dose of 250–500 rad (250–500 cGy) following irradiation. At this dose, the precursors for RBCs and white blood cells (WBCs) are greatly affected, so much so that they lose the ability to reproduce. Also, the number of lymphocytes are greatly depressed, whereby the immune system of the body is suppressed. Loss of blood cell counts can be noticed at a dose as low as 10–15 rad (10–15 cGy). Thus, the body loses the defense against bacterial and viral infections and becomes susceptible to them. Immunosuppression by radiation occurs at doses as low as 100 rad (100 cGy) and 90–95 % of immunosuppression can take place in humans at doses of 200–400 rad (200–400 cGy).

At this dose level, the platelet count is drastically reduced, and therefore bleeding gradually progresses through various orifices owing to a lack of ability of the blood to coagulate. Fever, bleeding, and infection result, followed by ultimate death in 10–21 days. However, bone marrow transplantation at the appropriate time may prompt the recovery of the subject. Whereas at doses <100 rad (100 cGy) survival is almost certain, survival is virtually impossible at doses >500 rad (500 cGy).

Gastrointestinal Syndrome

Gastrointestinal (GI) syndromes are expressed at a total body dose of 500–1000 rad (500–1000 cGy) and include prodromal syndromes such as nausea,

vomiting, and diarrhea of more severity that appear within hours after exposure. The primary effect of radiation exposure in this range is that the intestinal crypt cells are destroyed and not replaced, and consequently the mucosal lining (villi) shrinks and hardens whereby the gut becomes nonfunctional. Because of the denudation of the gut, an intestinal ulcer may develop. These GI syndromes are also accompanied by drastic hemopoietic syndromes including immunosuppression, loss of white blood cells, and infection.

Thus, the loss of nutrients through ulcers, in combination with bacterial infection and excessive bleeding, results in GI death in 3–10 days after radiation exposure. Only aggressive medical treatment in the early stages of exposure may lead to recovery in cases at the lower end of the dose spectrum.

Cerebrovascular Syndrome

Cerebrovascular syndromes appear in a matter of minutes after radiation exposure at a total body dose of more than 10,000 rad (10,000 cGy). Because the nerve cells are radioresistant, such a large dose is required for cerebrovascular syndromes to appear. The symptoms include severe nausea, vomiting, and burning sensation of the skin that occurs within minutes of exposure, followed by the malfunction of the neuron motor pump giving rise to motor incoordination, intermittent stupor, coma, and ultimately death in two to three days. The cerebrovascular death sequence is so rapid that there is little time for significant changes to appear in other organs in the body. At this level of radiation dose, death is almost a certainty and medical help is of little use.

Long-Term Effects of Radiation

The long-term or late effects of radiation cause various syndromes long after the radiation exposure. These may appear after acute radiation syndromes subside following exposure to a single large dose or after exposure to many smaller doses over a period. The late effects may be somatic or genetic, depending on the respective cells involved. Somatic effects are seen in the form of carcinogenesis, life-shortening, cataractogenesis, and embryologic damage. On the other hand, genetic effects result in abnormalities in the offspring.

Somatic Effects

Carcinogenesis

Cancer develops in three stages: initiation, promotion, and progression. Initiation of cancer is caused by various agents such as chemicals, ultraviolet rays, radiation, and viruses. In the case of radiation, cancer is initiated by the action of radiation on the DNA molecule resulting in the mutation of the cell. Cancer pro-

moters are those agents that cannot initiate the cancer but simply promote it once it is started. Examples of tumor promoters are estrogen, phorbol ester, excessive fat, and radiation. Radiation acts as a promoter by inactivating tumor suppressive genes through the interaction of the free radicals produced in the cytoplasm by radiation. In these two stages, mutated cells proliferate at the site of cancer growth. One or more of these cells become aggressive and are likely to spread to other organs. This stage is called the progression or metastasis of the cancer.

At the cellular level, carcinogenesis is thought to be controlled by two types of genes: oncogenes and suppressor genes. There is evidence that oncogenes are responsible for the growth and proliferation of tumor cells, while suppressor genes inhibit the tumor cell growth. Most oncogenes have their counterpart, proto-oncogenes in normal cells, that are present throughout their eukaryotic evolution. Radiation or other carcinogens activate normal proto-oncogenes to several cancer-causing oncogenes and inactivate suppressor genes, resulting in cell proliferation to cause cancer. Chromosome aberrations (deletion or translocation) caused by radiation are responsible for oncogene activation. There are more than 300 oncogenes identified that are associated with various human cancers. For example, deletion of a part of the chromosome is responsible for the activation of N-*ras* oncogene associated with neuroblastoma. Similarly, a translocation between chromosomes 8 and 14 in humans activates the C-*myc* oncogene in B-cell lymphoma.

Suppressor genes exist in normal cells to control the cell growth and protect the genome against carcinogenic agents. After radiation damage, suppressor genes stop cell division and repair the damaged gene. Examples of suppressor genes include the p53 gene found in breast cancer, small cell lung cancer, and bladder cancer; the DCC gene in colon cancer; and the p105 Rb gene in retinoblastoma. Radiation can inactivate these suppressor genes and thus cause cell proliferation leading to malignancy.

Epidemiologic Evidence of Carcinogenesis

The latent period of malignancies varies with the type of malignancy and the absorbed dose. Leukemia has an average latent period of about 5–10 years, whereas solid tumors in the head, neck, pharynx, and thyroid have a minimum latent period of 10 years with an average of 20–30 years.

Malignancies have been observed in individuals who are exposed to radiation from medical treatment, radiation-related occupation (e.g., industrial exposure), and acts of war. Infants and children are more radiosensitive than adults, and the risk of cancer from radiation exposure in the former is greater than that in the latter, almost by a factor of 2.

In the early 1900s, radium-dial painters used to lick the brush bristle soaked with radium-containing paint to make a fine point for painting clock and watch dials. During the procedure, they ingested radium, which, as a chemical analog of calcium, localized in bone, causing bone tumors. In some cases, the quantity of radium ingested was large, and acute effects including death were observed.

Before the 1930s, the enlarged thymus gland of infants with acute respiratory distress syndromes was commonly treated with therapeutic doses of x-rays to reduce the enlargement. During irradiation, however, the thyroid glands also received a massive radiation dose. A statistically significant number of these infants developed thyroid cancer later in life (about 10 years later).

Radiologists who used x-rays in their profession were found to have a higher incidence of leukemia than other medical professionals. Dentists had higher incidence of finger lesions due to exposure to dental x-rays. These incidences occurred mostly before the 1950s, largely because of the lack of knowledge of radiation effects. Now, through better radiation protection practice, these incidences have been curtailed drastically.

From 1935 to 1944, approximately 15,000 patients with ankylosing spondilytis were irradiated with 100–2000 R over spine and pelvis. A 2-year follow-up showed an increased incidence of leukemia in this group of patients.

Increased incidences of leukemia, lung cancer, breast cancer, and thyroid cancer have been observed in the Japanese survivors of the atomic bomb attacks on Hiroshima and Nagasaki.

Uranium mine workers inhale a considerable amount of radioactive dust containing radon gas. The decay products of radon settle in the lungs, and radiations from them can cause lung cancer.

Dose–Response Relationship

A meaningful dose–response relationship for carcinogenesis should be based on data with both low and high radiation exposures. However, the low-dose data (below 10 rad or 10 cGy) that have been accumulated thus far are mostly inconclusive, because of the small sample size, lack of appropriate control, incomplete dosimetry, and other related factors. So risks at low doses are primarily estimated by extrapolation of the data from high-dose experiments. Several authoritative committees (international and national) are responsible for establishing the dose-response relationship, and they are the United Nations Scientific Committee of the Effects of Atomic Radiations (UNSCEAR), the Committee on the Biological Effects of Ionizing Radiations (BEIR), the International Commission on Radiological Protection (ICRP), and the National Council on Radiation Protection and Measurements (NCRP) in the United Sates. These committees base their analysis on the data of the Japanese survivors of the A-bomb attacks on Hiroshima and Nagasaki, data on human exposures mentioned above (see Epidemiologic Evidence of Carcinogenesis), and data from in vitro cell culture and animal studies.

The risk versus dose relationship has been controversial, particularly about the minimum level of radiation dose that induces cancer (Murphy 1991). Some experts propose that the dose–response relationship is linear, without a threshold dose, and that a very minimal dose can cause cancer (Fig. 15.15). A threshold dose is a dose below which no radiation damage occurs in an individual. The LNT dose–response relationship has been based on the extrapolation of high-dose data to low-dose data (below 10 rad or cGy) and has drawn a considerable debate as to

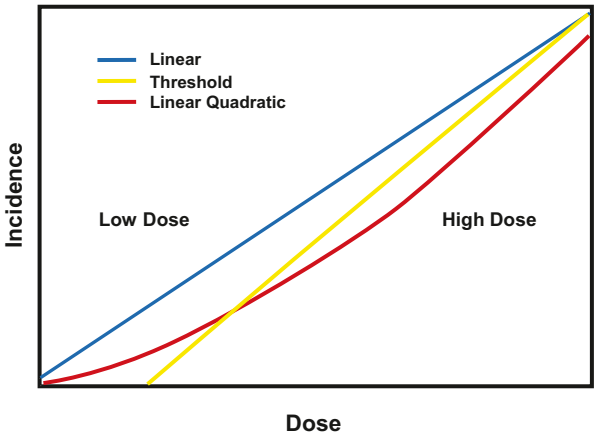

FIG. 15.15. Three general shapes of the dose–response curves permit prediction of different incidences of low-dose radiation effects when the *curves* are fitted to high-dose data. (Adapted from Murphy PH. Acceptable risk as a basis for regulation. *Radiographics* 1991;11:889–897.)

its validity. In one argument, the opponents of the theory question the validity of such extrapolation, because the mechanism of radiation damage may be quite different at doses that differ by orders of magnitude. Also, this group points out that the people living in high natural background radiation areas (e.g., Rocky Mountains) do not show to have any more apparent adverse health effects than those in low-dose areas (e.g., sea level). On the other hand, the proponents of the LNT theory suggest that a single hit by a radiation can cause the mutation of a cell, and consequently result in carcinogenesis in a later period, thus supporting the theory. The recent BEIR VII report strongly supports the LNT theory, suggesting that even the smallest dose can cause a small risk of cancer in humans.

All intermediate and high-energy data primarily obtained from the Japanese survivors of the A-bomb attacks are fitted by a linear quadratic curve (Fig. 15.15). The curve is linear at lower doses and becomes proportional to D^2 (quadratic) at higher doses. Yet, other experts believe that there is no risk of carcinogenesis up to a certain threshold dose, after which the curve becomes linear or quadratic (Fig. 15.15). While the linear response model is preferred for all solid tumors, the linear-quadratic model is more suitable for leukemia.

Risk Estimates of Excess Cancer

The BEIR VII Committee (2005) estimated the excess cancer risk based on the LNT theory and by extrapolation of high-dose incidences to the low-dose situations. It is estimated that 1 in 100 individuals is expected to develop solid tumor or leukemia from a radiation dose of 10 rem (0.1 Sv), whereas approximately 42 of these 100 persons are expected to develop these cancers from other causes.

Lower doses would produce proportionally lower risks. So, approximately 1 in 1000 individuals would expect to develop cancer from an exposure of 1 rem (0.01 Sv). Another estimate of cancer risk by BEIR VII is that 1 in 100 persons would likely develop cancer from a lifetime (70 year) exposure to low-LET natural background radiations excluding radon and high-LET radiations. For comparison, the ICRP estimate of cancer risk for the general population is 0.1 per Sv (0.1 % per rem) for high doses and dose rates, and 0.05 Sv (0.05 % per rem) for low doses and dose rates (ICRP 60, 1991).

Leukemia

Leukemia is one of the most common cancers induced by radiation in humans, accounting for one in five mortalities from radiocarcinogenesis. Risk of leukemia varies with age, with younger persons being more prone to radiocarcinogenesis than older persons. Based on a relative-risk linear quadratic dose response model, the BEIR V Committee (1990) predicts a risk of excess lifetime leukemia cancer mortality of 10 in 10,000 (0.1 %) with an exposure of 10 rad (10 cGy). The BEIR VII (2005) estimate of this value is 1–2.6 per 10,000 person years per Gy (1–2.6 per 100 person years per rad). Leukemia appears in as early as 2–3 years after the exposure, with an average latent period of 5–10 years.

Breast Cancer

The annual incidence of breast cancer in women in the United States is 1 in 11, with a high mortality rate. Several factors—age, estrogen level, heredity, demographics, race, number of children given birth to, and breastfeeding—all influence the risk of breast cancer. Women exposed to low-level radiation can develop breast cancer, and the risk is greater with younger ages than with older ages. According to the BEIR V (1990) report, the excess absolute risk of breast cancer in 25-, 35-, and 45-year-old women is 5, 4, and 2 in 10,000 per Gy (5, 4, and 2 in 100 per rad) respectively. The BEIR VII (2005) estimate of this value is 10 per 10,000 person years per Gy (10 per 100 person years per rad) at age 50. The risk of radiogenic breast cancer apparently is reduced if the dose is given in divided exposures.

While in the past, the breast cancer risk from mammography was of major concern, modern mammographic equipment is well designed and properly shielded, resulting in significant reduction in radiation exposure and hence a lower risk of breast cancer. According to the recommendations of the American College of Radiology, women over 40 should have annual mammography screening for breast cancer.

Other Cancers

Radiation-induced cancers in the thyroid, lungs, bone, skin, and other organs have been found in the general population and are influenced by a variety of etiologic factors such as heredity, occupation, age, sex, and hormonal level. For thyroid

cancer, the BEIR VII (2005) reports the excess absolute risk of 4.4 per 10,000 person years per Gy (4.4 per 100 person years per rad).

Radiation Damage to Skin

The skin is sensitive to radiation because of the presence of highly radiosensitive structures such as hair follicles and sebacious glands. The radiation effect on the skin is deterministic and has a threshold dose of about 100 rad (100 cGy). The primary skin reactions to radiation are erythema and dermatitis. Initial erythema appears in a few hours to a few days after radiation exposure, which is followed by dry desquamation characterized by atrophy of epidermal papillae and vascular changes. In the third or fourth week, erythema reappears with red, warm, edematous, and tender skin. Temporary hair loss (epilation) can occur at this stage. Severe erythema is followed by acute radiation dermatitis manifested by blister formation, dermal hypoplasia, edema, and permanent depilation. The normal skin reappears in 2–3 months.

The above effects depend on the dose, dose rate, LET of the radiation, and the duration of exposure, and vary from individual to individual and with the location in the same individual. Although sex is not a factor in skin reaction, age is an important factor, with the skin of younger people being more sensitive.

A low-level chronic exposure of radiation on the skin causes atrophy, hyperplasia, and hyperkeratosis. In addition, ulceration and deep fibrosis may result from such exposures. In rare instances, skin cancer, mainly squamous cell carcinoma, may develop.

Radiation Damage to Reproductive Organs

Extremely deleterious effects are expected from radiation exposure to the gonads, because of their high radiosensitivity. In males, spermatogonia are most radiosensitive, and spermatozoa and spermatids are radioresistant, whereas in females, the ovarian follicles are most radiosensitive. The radiation effects vary with the dose, dose rate, sex, and age.

Sterility is the important radiation effect that warrants special attention. In males, temporary sterility can be induced with a dose as low as 15 rad (15 cGy), whereas permanent sterility is reported with an acute dose of 500–600 rad (500–600 cGy) (Prasad 1995). Male sterility is evident by a reduced sperm count and low motility. In females, permanent sterility occurs with 320–625 rad (320–625 cGy), which is manifested by the damage to the ovarian follicles. If the dose is lower, then the follicles may recover in 5–6 months. Relatively larger doses are needed in younger women than in older women.

Nonspecific Life-Shortening

Studies have shown that exposure to ionizing radiations results in the shortening of the life span of mice (Rotblat and Lindop 1961). For acute total body exposure, the life span of mice, rats, and dogs is reduced by about 5 % per gray (UNSCEAR

1982). The irradiated group looks much older than the control group, and radiation effects are similar to those of normal aging, e.g., an increase in connective tissue and a decrease in parenchymal cells. During the period 1945–1955, American radiologists were found to have a shorter life-span than other medical professionals. But the issue of life-shortening by radiation is controversial, because in some cases it has been found that life span is rather lengthened by irradiation at low doses. Such observations have led to the concept of *hormesis*, which states that low doses of radiation are beneficial to health and prolong the life span. It is postulated that hormesis is secondary to an enhanced immune responsiveness due to radiation at low doses.

Cataractogenesis

The lens of the eye is sensitive to radiation and develops cataracts on irradiation with ionizing radiations. The incidence of radiation-induced cataracts is a deterministic effect and depends on the dose given. A dose of 10–30 rad (10–30 cGy) is required to produce cataracts in mice, whereas a threshold dose of about 200 rad (200 cGy) is needed to produce cataracts in humans in a single exposure. A larger dose is required if the dose is given in fractions, and high-LET radiations almost double the incidence of cataractogenesis. A minimum of 1 year is needed for the latent period of cataractogenesis.

Radiation Damage to Embryo and Fetus

The developing mammalian embryo is extremely sensitive to ionizing radiations, because many cells are differentiating at this stage. The degree of damage depends on the developmental stage of the embryo, the dose, and the dose rate. The entire fetal development is divided into three general stages: (1) *preimplantation*, a period of about 8–10 days between fertilization of the egg and its attachment to the uterine wall; (2) *major organogenesis*, a period of about 2–6 weeks, when major organs are developed; and (3) the *fetal stage*, the remainder of the pregnancy period, when the organs of the fetus grow further to enable the mammal to survive after birth.

The embryo in the preimplantation stage is most sensitive to ionizing radiations and mostly encounters prenatal embryonic death as a result of radiation exposure. In some species, a dose as low as 5–15 rad (5–15 cGy) is sufficient to cause deleterious effects on the embryo. At a dose of 200 rad (200 cGy) in the preimplantation stage, embryonic death is certain. Almost all embryos that survive the radiation exposure grow normally in utero and afterward, with the exception of a few that develop abnormalities later.

During the period of major organogenesis, embryos exposed to ionizing radiations develop abnormalities mostly related to the central nervous system (CNS) and bone. These abnormalities are too severe for the fetus to survive and ultimately result in neonatal death. At an exposure of 200 rad (200 cGy) to mouse embryos during this period, almost 70 % of the embryos later experienced neonatal death. Growth retardation also is noted at doses above 100 rad (100 cGy).

Often it is suggested that a therapeutic abortion should be considered if an embryo receives ~10 rad (10 cGy) during the first 6 weeks after conception.

During the fetal period, however, comparable doses do not cause any abnormality or neonatal death, because fetal cells are more radioresistant than embryonic cells. Relatively higher doses are needed to cause death in this period. A few cases of growth retardation have been noted. In utero irradiation with a dose of 1–2 rad (1–2 cGy) may increase the risk of childhood leukemia in the first 10–15 years by a factor of 1.5–2. Mental retardation in this period has been reported with doses as low as 10–20 rad (10–20 cGy), if given in the 8–15 weeks of gestation. Loss of IQ is estimated to be about 0.3 point per rad (0.003 point per Gy).

Because of these radiation effects, radiological procedures are contraindicated in pregnant women, and practitioners must exercise caution to determine the woman's status of pregnancy before these procedures. Before a procedure, it is a common practice to inquire of the patient if she is pregnant or when she had her last menstrual period, and thus unnecessary fetal exposure can be avoided. If the patient is pregnant and the procedure is essential, then the risk versus benefit to the patient from the procedure should be weighed by the practitioner with due consideration to the stage of pregnancy.

Genetic Effects

As mentioned above, ionizing radiations can cause changes in the DNA structure, which ultimately are expressed in gene mutations. Through the affected germ cells, these mutations propagate to future generations. Genetic effects are not expressed in the individual whose germ cells have been affected by radiation, but are expressed in future generations. Genetic effects appear as Down syndromes, achondroplasia, retinoblastoma, cystic fibrosis, sickle cell anemia, Tay-Sachs disease, and other chromosome disorders.

Spontaneous Mutations

In normal cells, genes occasionally undergo natural mutations even without radiation exposure. Such mutations are called *spontaneous mutations*, and their frequency is about 10^{-5} per gene per generation. This means that the chance of spontaneous mutation is 1 in 100,000. This frequency is increased by various mutagens such as chemicals and radiation.

In a given generation, radiation does not produce any new mutations and simply increases the frequency of spontaneous mutations. BEIR VII (2005) estimated the total risk for all classes of genetic diseases to be 3.0×10^{-5}–4.7×10^{-5} per rem (3.0×10^{-3}–4.7×10^{-3} per Sv) per generation. It indicates that the genetic risks are relatively small causes some genetic mutations. The dose-response relationship is linear without threshold, indicating that no dose is safe and any dose, however relatively small causes some genetic mutations. Furthermore, genetic damage is a function of the dose rate and the LET of ionizing radiations. High-LET radiations and high-dose rates cause more mutations. Genetic mutations may appear in future generations long after exposure has occurred.

Doubling Dose

The doubling dose is a measure of the increase in genetic mutations by radiation. It is the amount of radiation dose that doubles the spontaneous mutations in one generation in a species. It is calculated as a ratio of the average spontaneous and induced mutation rates in a set of genes. A small doubling dose indicates a large relative mutation risk and vice versa. In humans, it is considered to be of the order of 100 rad (100 cGy), but it depends on the dose rate, the gender, and the type of species (BEIR V 1990). Based on this doubling dose, the ICRP has given an estimate of the probability of induced hereditary disorders to be 0.6×10^{-2} per sievert (0.6×10^{-4} per rem) for the working population (ICRP 60, 1991).

Genetically Significant Dose

The genetically significant dose (GSD) is the dose that, if received by everyone of the entire population, would cause the same genetic damage as the gonadal dose now being received by a limited number of individuals of the population through medical procedures, natural radiations, TV viewing, flying at high altitudes, and so forth. The GSD is an index of the expected genetic damage on the whole population, and is calculated as an average value from the gonadal doses received from all exposures by the exposed personnel with proper weighting with respect to the chances of their having offspring. Thus, the GSD depends on the total number of individuals irradiated and the relative expectancy of their having children. The weighting factor is needed because older people have lesser probability of having offspring than younger people.

The contributions of various sources of radiation to GSD are given in Table 15.3. The GSD values from natural radiation sources are considered to be equal to the gonadal dose, because natural radiation exposes the entire population of all ages uniformly. Of all medical procedures, diagnostic x-rays contribute most to the GSD. It is, therefore, essential that strict protective measures are taken to avoid unnecessary gonadal exposure. Gonadal shields, appropriate collimation

Table 15.3. Annual genetically significant dose (GSD) in the U.S. population about 1980–1982[a].

Source	Contributions to GSD in mrems (mSv)
Natural sources	
Radon	10 (0.1)
Other	90 (0.9)
Medical	
Diagnostic x-rays	20–30 (0.2–0.3)
Nuclear medicine	2 (0.02)
Consumer products	5 (0.05)
Occupational	~0.6 (0.006)
Nuclear fuel cycle	<0.05 (0.0005)
Miscellaneous environmental sources	<0.1 (0.001)
Total	~132 (1.32)

[a] Adapted with permission from Table 8.2 in NCRP report No. 93, 1987.

of the x-ray beams, and limited and prudent application of repeat procedures definitely lead to a considerable reduction in GSD from medical procedures.

Genetic effects of radiation can be greatly reduced if a time interval is allowed between radiation exposure and conception. This is the consequence of some repair process after irradiation. It is, therefore, recommended for both men and women that conception should be deferred for about 6 months after a significant radiation exposure such as a radiation accident or radiation therapy involving high gonadal exposure. Such delay in conception is not needed for diagnostic procedures.

Risk Versus Benefit in Diagnostic Radiology and Nuclear Medicine

Millions of x-ray, dental x-ray, computed tomography (CT), and nuclear medicine procedures are performed in the United States for the diagnosis of diseases, and the number is increasing steadily over the years. Introduction of CT angiography and PET/CT in diagnostic procedures has added markedly to the radiation burden of patients. Practitioners and regulatory authorities are increasingly concerned of such high doses and are advocating for devising ways to minimize radiation exposure to the patient and the public.

Of all diagnostic radiological procedures, CT scans and fluoroscopic procedures give the highest effective doses, whereas dental and chest x-rays contribute only minimal effective doses. Gonadal doses are higher with fluoroscopic procedures than with head CT, chest x-ray, and dental procedures. This is primarily due to the fact that the gonads are out of the field of the latter procedures. It should be noted that the mammographic procedure contributes only a little to the total body dose compared to the breast. For obvious reasons, the highest gonadal dose comes from the procedures involving hips and pelvis. The GSD is about 9.8 mrad (98 μGy) for males compared to 20.9 mrad (209 μGy) for females (NCRP 100, 1989).

The doses to different organs from different nuclear medicine procedures are listed in Table 14.4 and the effective doses in Table 14.5 in Chapter 14. Radiation dose is always higher with long-lived and β-emitting radionuclides. The GSD values for females (1.9 mrad or 19 μGy) is almost twice those of males (1.1 mrad or 10.9 μGy) (NCRP 100, 1989).

Risks from diagnostic procedures include both somatic and genetic effects. Normally, these effects are minimal from diagnostic procedures for humans because doses from these procedures are considered low. Doses from nuclear medicine procedures are even lower than those from diagnostic x-ray procedures. However, based on the LNT model, there is no reason to believe that there is no risk from diagnostic exposures, no matter how small the doses are. There may not be acute effects, but long-term effects such as carcinogenesis, teratogenic effects from fetal exposure, and genetic effects in the future offspring can occur. The

probabilities of fatal cancers, nonfatal cancers, and hereditary effects have been estimated by the ICRP to be 4.0, 0.8, and 0.8 % per sievert, respectively, for adult radiation workers and 5.0, 1.0, and 1.3 % per sievert, respectively, for the whole population (ICRP 60 1991).

An important quantity in the assessment of risk from radiation exposures is the collective effective dose, which is defined as the sum of the products of the effective dose and the number of persons exposed for each diagnostic procedure. The total annual collective dose to the US population from all sources of radiation in 2006 is 187,000,000 person-rem (1,870,000 person–Sv) (NCRP 160 2009). The annual collective dose for radiation workers in healthcare is 55,000 person-rem (550 person-Sv) in 2006. Based on a collective dose of 55,000 person-rems (550 person-Sv), for medical radiation workers, the risk from 1 year of working as a radiation worker is 22 fatal cancers, 4 non-fatal cancers, and 4 serious heritable defects. These risks are quite low compared to the total radiation used annually.

The benefit from diagnostic procedures (both x-ray and nuclear medicine) is the immediate diagnosis of the disease that can lead to the appropriate treatment and its ultimate cure. Argument should prevail in favor of the benefit for the use of radiation for diagnosis over the risks that may appear in later years in the individual himself or the future offspring. However, a judicious use of these procedures is definitely warranted, and a procedure that is not needed should not be done. This argument for the prudent use of radiation also applies to different screening procedures using x-ray, such as mammography, chest x-rays, and dental x-rays. Many individuals are exposed for screening, but only a small number of people benefit from the early diagnosis, while most of the screened people turn out to be negative. For this reason, the American College of Radiology has recommended annual mammography only for women above 40 years of age, excluding younger women who are more radiosensitive, some of whom may likely develop breast cancer many years after mammography.

Risk to Pregnant Women

Since radiation can cause a devastating effect on the embryo and fetus in pregnant women, diagnostic radiological and nuclear medicine procedures are contraindicated in pregnant women, despite only a small risk involved with the individual exposed from these procedures. This is particularly important in nuclear medicine procedures, because radiopharmaceuticals reside in the body following a biological half-life and are likely to cross the placenta to cause the fetal damage. β-emitting radionuclides are more damaging than γ-emitting radionuclides. Radioiodine administered orally to pregnant women during the gestation period of 15–22 weeks can cross the placenta and localize in the fetal thyroid to the extent of 50–75 %. The fetal thyroid dose at 6 weeks of gestation is of the order of 2.1 Gy/MBq (7.8 rad/mCi) (Watson 1991).

In most cases, radiologic procedures are avoided in pregnant women by proper screening such as asking them prior to the procedure if they are pregnant or when they had their last menstrual period. However, at times, it is discovered after the procedure that the women is pregnant. In such situations, steps should be taken to estimate the dose received by the embryo or fetus based on the dosimetry parameters of the radiopharmaceutical. Depending on the period of pregnancy, the question of therapeutic abortion may be considered if the dose is excessive. Some experts believe that a dose of 10 cGy (10 rad) is a reasonable value above which therapeutic abortion should be considered. However, the decision to abort depends on a number of socio-personal factors.

In radionuclide therapy, pregnant women are absolutely excluded because of the anticipated excessive fetal dose. ^{131}I treatment of pregnant women is almost prohibited unless benefit outweighs the risk of the fetus from therapy. Besides the in utero effects, there is a small probability of thyroid cancer induced by the ^{131}I therapy of hyperthyroidism.

Questions

1. (a) What are the mechanisms of radiation damage?
   (b) Does the direct action or indirect action contribute more to radiation damage? Why?
   (c) Which are the free radicals that are most damaging to cells?
   (d) Does the presence of oxygen increase or decrease radiation damage?
2. (a) Why are erythroblasts more radiosensitive than red blood cells?
   (b) Which phase of the cell cycle is most radiosensitive?
   (c) Which molecule of the cell structure is most radiosensitive?
   (d) What are the different factors affecting radiation damage?
3. (a) Define D_0, D_q, and n as illustrated in the cell survival curve.
   (b) D_q is smaller for high-LET radiations than for low-LET radiations. True or false?
   (c) D_0 is smaller for high-LET radiations than for low-LET radiations. True or false?
   (d) What is the value of n for mammalian cells?
4. (a) The cell survival curve is steeper at high radiation doses than at low radiation doses. Explain why and its implication.
   (b) Does the shape of the cell survival curve vary with high-LET radiations and at very high-dose rates?
5. (a) Choose the dose in rad that has been suggested as a practical threshold for radiation-induced abortion: (i) 2; (ii) 5; (iii) 10; (iv) 20; (v) 50.
   (b) How many days after conception can prenatal death occur as a result of in utero irradiation?

(c) Which one of the following organs is most affected to be malformed by prenatal radiation exposure? (i) heart; (ii) stomach; (iii) head; (iv) gonads; (v) upper extremities.
(d) What is the period of pregnancy during which the incidence of abnormalities and malformations in human neonates is expected to be the highest?
(e) What are the effects of radiation on the fetus?
(f) The incidence of childhood leukemia after in utero irradiation with a few rad of diagnostic x-rays increases by a factor of (i) 1.5–2.0; (ii) 2.5–3.0; (iii) 3.5–6.0.

6. (a) What are the dose ranges and approximate time limits of death for hemopoietic, gastrointestinal, and cerebrovascular syndromes?
(b) What are the prodromal syndromes and when do they appear?
(c) What is the dose at which almost total immunosuppression occurs in humans?

7. (a) Define the oxygen enhancement ratio (OER).
(b) Why is the oxygen effect absent for high-LET radiations?
(c) What are radiosensitizers? Name some of them.
(d) What is the maximum OER for γ- and x-rays?
(e) Is misonidazole a radiosensitizer or radioprotector for hypoxic cells?
(f) What is the specific composition of radioprotectors and how do they function?

8. (a) What is the doubling dose and what is its value for humans?
(b) What are the doses at which permanent sterility can be induced in (a) males and (b) females?
(c) Define the genetically significant dose (GSD).
(d) What is the GSD for humans?
(e) Which one of all medical radiations contributes most to the GSD?
(f) What are the factors that influence the GSD?

9. (a) The mean latent period for radiation-induced leukemia is about (i) 5–10 years; (ii) 12–20 years; (iii) 21–30 years.
(b) The mean latent period for radiation-induced solid tumors is about (i) 5–10 years; (ii) 12–20 years; (iii) 21–30 years.
(c) Cataract can be induced in humans with (i) 10–30 rad (10–30 cGy); (ii) 100–110 rad (100–110 cGy); (iii) 200 rad (200 cGy).
(d) What is the risk of cancer in the general population from small doses of low-LET radiation exposure?

10. What are the two most common chromosome aberrations that are responsible for carcinogenesis?
11. In the linear quadratic model of the cell survival, what is the value of parameter β for high-LET doses?
12. Elucidate the mechanisms of sublethal damage repair and potentially lethal damage repair. Give an example of the latter.
13. What is the recent value of cancer deaths attributable to radiation exposure in Japanese survivors of the atomic bomb?

14. What are the different dose-response models preferred for solid tumors and leukemia?
15. What are the risk estimates of fatal cancer by the ICRP and the BEIR VII for the general population?
16. Describe apoptosis.

References and Suggested Readings

American Cancer Society. *Radiation Exposure and Cancer.* Atlanta, GA; 2003.

BEIR V Committee. *The Effects on Populations of Exposure to Low Levels of Ionizing Radiations.* Washington DC: National Academy of Sciences/National Research Council; 1990.

BEIR VII, Phase 2. *Health Risks from Exposure to Low Levels of Ionizing Radiations.* Washington, DC: National Academy of Sciences/National Research Council; 2005.

Hall EJ and Giaccia AJ. *Radiobiology for the Radiologist.* 7th ed. Philadelphia: JB Lippincott Williams & Wilkins; 2011.

ICRP report no. 26. *Recommendations of the International Commission on Radiological Protection.* New York: Pergamon; 1977.

ICRP report no. 60. 1990 *Recommendations of the International Commission on Radiological Protection.* New York: Pergamon, 1991.

Jaworowski Z. Radiation risk and ethies. *Physics Today.* 1999;52:24.

Mettler FA, Upton AC. *Medical Effects of Ionizing Radiations.* 3rd ed. Philadelphia: W.B. Saunders; 2008.

Murphy PH. Acceptable risk as a basis for regulation. *Radiographics.* 1991;11:889–897.

NCRP report no. 93. *Ionizing Radiation Exposure of the Population of the United States.* Bethesda, MD: NCRP; 1987.

NCRP report no. 100. *Exposure of the U.S. Population from Diagnostic Medical Radiation.* Bethesda, MD: NCRP; 1989.

NCRP report no. 160. *Ionizing Radiation Exposure of the Population of the United States.* Bethesda, MD: NCRP; 2009.

Nias AHW. *An Introduction to Radiobiology.* 2nd ed. Hoboken, NJ: Wiley; 1998.

Pizzarello DJ, Witcofski RL. *Medical Radiation Biology.* 2nd ed. Philadelphia: Lea & Febiger; 1982.

Prasad KN. *Handbook of Radiobiology.* 2nd ed. Boca Raton, FL: CRC Press; 1995.

Ring JP. Radiation risks and dirty bombs. *Health Phys.* 2004;86:S42–S47.

Rotblat J, Lindop P. Long-term effects of a single whole body exposure of mice to ionizing radiation, II. Causes of death. *Proc R Soc Lond* (*Biol*). 1961;154:350–368.

Travis EL. *Primer of Medical Radiobiology.* 2nd ed. Chicago: Year Book Medical Publishers; 1989.

United Nations Scientific Committee on the Effects of Atomic Radiation (UNSCEAR). Ionizing Radiations: *Sources and Biological Effects.* New York: United Nations, 1982.

United Nations Scientific Committee on the Effects of Atomic Radiation (UNSCEAR). Sources, Effects and Risks of Ionizing Radiation. New York, United Nations, 1988.

Watson EE. Radiation absorbed dose to the human fetal thyroid. In: 5th *International Radiopharmaceutical Dosimetry Symposium*. Oak Ridge, TN, May 7–10, 1991.

16
Radiation Regulations and Protection

Radiation hazards to humans are well documented. To minimize their risks, international and national organizations have been established to set guidelines for safe handling of radiations. As mentioned in Chapter 15, the ICRP and NCRP are two such organizations. They make recommendations and guidelines for radiation workers to follow in handling radiations. The Nuclear Regulatory Commission (NRC) and state agencies adopt many of these recommendations into regulations to implement radiation protection programs in the United States. The NRC regulations are published in the Federal Register in the form of the Code of Federal Regulations (CFR). The regulations pertinent to the practices of nuclear medicine are briefly described here.

Until 2005, the NRC regulated all reactor-produced by-product materials, while the individual State controlled the naturally-occurring and accelerator-produced radioactive materials (NARM). The Congress passed the Energy Policy Act in 2005, broadening the definition of by-product material to include NARM products and authorized the NRC to take control of all by-product materials. Over the years, the NRC developed regulatory policies to include NARM products and implemented them as of August 2009.

For convenience of operation, at present, 37 states have entered into agreement with the NRC (with Michigan intending to join at the time of this writing) to implement regulations concerning the use of radioactive materials (RAM) and thus to take control of regulatory management of RAM. These states are called the Agreement States. The rules and regulations implemented by the agreement states must be at least as strict as, if not stricter than, those of the NRC. They issue the license to use RAM and monitor their use and disposal.

License

Licenses are issued by the NRC or the Agreement State to various facilities, institutions, or individuals for the use of by-product materials and fall into several categories depending on the specific use as described below:

G. B. Saha, *Physics and Radiobiology of Nuclear Medicine,*
DOI 10.1007/978-1-4614-4012-3_16,

1. *General license*: A general license is given to any physician, veterinarian, clinical laboratory, or hospital to acquire, possess, transfer, or use of the following by-product materials in prepackaged units containing limited activities (given in parenthesis) for each specific use: ^{125}I (10 μCi or 370 kBq), ^{131}I (10 μCi or 370 kBq), ^{14}C (10 μCi or 370 kBq)), ^{3}H (50 μCi or 1.85 MBq)), ^{59}Fe (20 μCi or 740 kBq), ^{75}Se (10 μCi or 370 kBq), and ^{57}Co (10 μCi or 370 kBq). The licensee must be an authorized user according to 10CFR35 and can possess a maximum of 200 μCi (7.4 MBq) of the approved radionuclide at any one time and at any one location.
2. *Specific license of limited scope*: This license is granted to private or group practices and medical institutions for medical use of by-product materials in humans. The authorized users are specifically listed on the specific license of limited scope, but limited quantities of specific radionuclides for intended uses are granted. For patients requiring hospitalization under 10CFR35.75, only hospitals having inpatient facilities are authorized to treat such patients. The specific license of limited scope can also be issued to mobile services.
3. *Specific licenses of broad scope*: The specific licenses are given in two categories: one to manufacture or transfer for commercial distribution certain items containing by-product material (10CFR32) and the other to possess, use, and transfer by-product material in any chemical or physical form with the limitations of the maximum activity specified (10CFR33). The former types of specific licenses are typically given to commercial manufacturers. The latter type is called the specific license of broad scope or "broad license" and has three categories based on the maximum activity allowed for the receipt, acquisition, ownership, possession, use, and transfer of any chemical or physical form of by-product material (10CFR33.11). The Type A broad license allows specified quantities of activities usually in multicuries; the Type B broad license allows maximum activities of by-product material specified in 10CFR33.100, Schedule A, Column I; and the Type C license permits maximum activities of by-product material specified in 10CFR33.100, Schedule A, Column II, which are an order of magnitude less than those in the Type B license. In type B and Type C broad scope licenses, if two or more radionuclides are possessed at any time, then the possession limit of each is determined by calculating the ratio of the radionuclide in possession to the applicable quantity in part 33.100, schedule A, column I for Type B and those in column II for type C, and summing them up, which should not exceed 1.

In the Type A license, a radiation safety committee and a radiation safety officer are required to implement and monitor all aspects of radiation safety in the use and disposal of by-product material. Such licenses are mainly offered to large medical institutions with previous experience that are engaged in medical research, and in diagnostic and therapeutic uses of by-product material. Individual users are authorized by the radiation safety committee to conduct specific protocols using by-product materials.

The Type B specific license requires a radiation safety officer, but no radiation safety committee, to implement and monitor all radiation safety regulations. The Type C specific license requires neither the radiation safety officer nor the committee, but a definite statement that the by-product material will be used by the licensee or by persons under his direct supervision who has the training specified in 10CFR33.15.

In all cases of specific licenses, an application must be filed to the NRC using the NRC Form 313 with all information related to the possession, use, and disposal of by-product materials.

Radiation Protection

Rules and regulations pertaining to radiation protection set by the NRC are contained in 10CFR20. Because it is beyond the scope of this book to include the entire 10CFR20, only the relevant highlights are included.

Definition of Terms

Several terms related to absorbed dose as defined in the 10CFR20 are given here.

Committed dose equivalent ($H_{T,50}$) is the dose equivalent to organs or tissues of reference (T) that will be received from an intake of radioactive material by an individual during the 50-year period following the intake.

Committed effective dose equivalent ($H_{E,50}$) is the sum of the products of the weighting factors applicable to each of the body organs or tissues that are irradiated and the committed dose equivalent to these organs or tissues.

Controlled area means an area, beyond a restricted area but inside the site boundary, access to which is limited by the license for any reason.

Deep-dose equivalent (H_d), which applies to the external whole-body exposure, is the dose equivalent at a tissue depth of 1 cm (1000 mg/cm^2).

Shallow-dose equivalent (H_s), which applies to the external exposure of the skin or an extremity, is the dose equivalent at a tissue depth of 0.007 cm (7 mg/cm^2) averaged over an area of 1 cm^2.

Tissue weighting factor (W_T) for an organ or tissue is the proportion of the risk of stochastic effects resulting from irradiation of that organ or tissue to the total risk of stochastic effects when the total body is irradiated uniformly.

The values of W_T from the 10CFR20 are given in Table 14.5.

Effective dose equivalent (H_E) is the sum of the products of the committed dose equivalent to each of the body organs and tissues and the weighting factor of the corresponding organ or tissue ($H_E = \Sigma W_T \cdot H_{T,50}$). By later definition, this is called the effective dose.

Derived air concentration (DAC) is the concentration of a given radionuclide in air that, if breathed by the reference man for a working year of 2000 h under conditions of light work, results in an intake of ALI. DAC values are given in Table 1, column 3 of Appendix B in 10CFR20.

Annual limit on intake (ALI) is the derived limit on the amount of radioactive material allowed to be taken into the body of an adult worker by inhalation or ingestion in a year. These values are given in 10CFR20 (Table 1, Appendix B).

Total effective dose equivalent (TEDE) is the sum of the deep-dose equivalent (for external exposure) and the committed effective dose equivalent (for internal exposure).

Restricted area is an area where an individual could receive in excess of 5 mrem (0.05 mSv) per hour at 30 cm from a radiation source.

High-radiation area is an area where an individual could receive from a radiation source a dose equivalent in excess of 100 mrem (1 mSv) in 1 h at 30 cm from the source.

Very high-radiation area is an area where an individual could receive from radiation sources an absorbed dose in excess of 500 rad (5 Gy) in 1 h at 1 m from the source.

Unrestricted area is an area in which an individual could receive from an external source a dose of 2 mrem (20 μSv)/h and 50 mrem (0.5 mSv)/yr.

Caution Signs and Labels

The NRC requires that specific signs, symbols, and labels be used to warn people of possible danger from the presence of radiation. These signs use magenta, purple, or black color on yellow background; some typical signs are shown in Fig. 16.1.

Caution: Radiation Area. This sign must be posted in radiation areas.

Caution: High Radiation Area or *Danger: High-Radiation Area.* This sign must be posted in high-radiation areas.

Fig. 16.1. Various radiation caution signs and labels.

Caution: Radioactive Material or *Danger: Radioactive material*. This sign is posted in areas or rooms in which 10 times the quantity of any licensed material specified in Appendix C of 10CFR20 are used or stored. All containers with quantities of licensed materials exceeding those specified in Appendix C of 10CFR20 should be labeled with this sign. These labels must be removed or defaced before disposal of the container in the unrestricted areas.

Caution signs are not required in rooms storing the sealed sources, provided the radiation exposure at 1 foot (30 cm) from the surface of the source reads less than 5 mrem (50 μSv)/h. Caution signs are not needed in rooms where radioactive materials are handled for less than 8 h, during which time the materials are constantly attended.

Occupational Dose Limits

The annual limit of the occupational dose to an individual adult is the more limiting of (a) TEDE of 5 rem (0.05 Sv) or (b) the sum of the deep-dose equivalent and the committed dose equivalent to any individual organ or tissue other than the lens of the eye being equal to 50 rem (0.5 Sv). It should be noted that there is no lifetime cumulative dose limit in 10CFR20, although the NCRP recommends a lifetime cumulative dose of 1 rem (10 mSv) $\times$ age in years.

The annual limit on the occupational dose to the lens of the eye is 15 rem (0.15 Sv).

The annual limit of the occupational dose to the skin and other extremities is the shallow-dose equivalent of 50 rem (0.5 Sv).

Depending on the license conditions, both internal and external doses have to be summed to comply with the limits. A licensee may authorize under *planned special procedures* an adult worker to receive additional dose in excess of the prescribed annual limits, provided no alternative procedure is available. The total dose from all planned procedures plus all doses in excess of the limits must not exceed the dose limit (5 rem or 50 mSv) in a given year, nor must it exceed five times the annual dose limits in the individual's lifetime.

The annual occupational dose limits for minors is 10 % of the annual dose limits for adults. The dose limit to the fetus/embryo during the entire pregnancy (gestation period) due to occupational exposure of a declared pregnant woman is 0.5 rem (5 mSv), which amounts to approximately 50 m rem (0.5 mSv) per month assuming a 10 month pregnancy.

The total effective dose equivalent to individual members of the public is 0.1 rem (1 mSv) per year. However, this limit can be increased to 0.5 rem (5 mSv) provided the need for such a higher limit is demonstrated.

ALARA Program

The established dose limits are the upper limits for radiation exposure to individuals. The NRC has instituted the ALARA (as low as reasonably achievable) concept to reduce radiation exposure to individuals to a minimum. The ALARA concept calls for a reasonable effort to maintain individual and collective radia-

tion exposure as low as possible. Under this concept, techniques, equipment, and procedures are all critically evaluated. According to NRC Regulatory Guide, under the ALARA concept, when the exposure to a radiation worker exceeds 10 % of the occupational exposure limit in a quarter (Action Level I), an investigation is made by the RSO, and the report is reviewed by the RSC. When the exposure exceeds 30 % of the occupational exposure limit (Action Level II), corrective actions are taken or the licensee must justify a higher dose level for ALARA in that particular situation, but not to exceed annual occupational dose limit.

Principles of Radiation Protection

Of the various types of radiation, the α-particle is most damaging because of its charge and large mass, followed in order by the β-particle and the γ-ray. Heavier particles have shorter ranges and therefore deposit more energy per unit path length in the absorber, causing more damage. On the other hand, γ-rays and x-rays have no charge or mass and therefore have a longer range in matter and cause relatively less damage in tissue. Knowledge of the type and energy of radiations is essential in understanding the principles of radiation protection.

The cardinal principles of radiation protection from external sources are based on four factors: time, distance, shielding, and activity.

Time

The total radiation exposure to an individual is directly proportional to the time of exposure to the radiation source. The longer the exposure, the higher the radiation dose. Therefore, it is wise to spend no more time than necessary near radiation sources.

Distance

The intensity of a radiation source, and hence *the radiation exposure, varies inversely as the square of the distance from the source to the point of exposure*. It is recommended that an individual should keep as far away as practically possible from the radiation source. Procedures and radiation areas should be designed so that individuals conducting the procedures or staying in or near the radiation areas receive only minimum exposure.

The radiation exposure from γ-ray and x-ray emitting radionuclides can be estimated from the *exposure rate constant*, Γ, which is defined as the exposure from γ-rays and x-rays in R/h from 1 mCi (37 MBq) of a radionuclide at a distance of 1 cm. Each γ- and x-ray emitter has a specific value of Γ, which has the unit of $R \cdot cm^2/mCi \cdot h$ at 1 cm or, in System Internationale (SI) units, $\mu Gy \cdot m^2/GBq \cdot h$ at 1 m. The Γ values are derived from the number of γ-ray and x-ray emissions from the radionuclide, their energies, and their mass absorption coefficients in air.[1] Because γ-rays or x-rays below some 10 or 20 keV are absorbed by the container

[1] The Γ value of photon-emitting radionuclides can be calculated from the expression $\Gamma = 199\Sigma N_i E_i \mu_i$, where N_i is the fractional abundance of photons of energy E_i in MeV, and μ_i is the mass absorption coefficient (cm^2/g) of photons of energy E_i in air.

TABLE 16.1. Exposure rate constants of commonly used radionuclides.

Radionuclides	Γ_{20} (R · cm^2/mCi · h at 1 cm)	Γ_{20} (μGy · m^2/GBq · h at 1 m)[a]
^{137}Cs	3.26	88.11
^{99m}Tc	0.59	15.95
^{201}Tl	0.45	12.16
^{99}Mo	1.46	39.46
^{67}Ga	0.76	20.54
^{123}I	1.55	41.89
^{111}In	2.05	55.41
^{125}I	1.37	37.03
^{57}Co	0.56	15.16
^{131}I	2.17	58.65
^{18}F[b]	5.70	154.05

[a] R · cm^2 /mCi · h is equal to 27.027 μGy · m^2 /GBq · h.

[b] Personal communication with Dr. M. Stabin, Oak Ridge Associated Universities, Inc., Oak Ridge, Tennessee.

Adapted from Goodwin PN: Radiation safety for patients and personnel. In: Freeman LM, ed. *Freeman and Johnson's Clinical Radionuclide Imaging.* 3rd ed. Philadelphia: WB Saunders Co; 1984: 320.

and thus do not contribute significantly to radiation exposure, often γ-rays and x-rays above these energies only are included in the calculation of Γ. In these instances, they are denoted by Γ_{10} or Γ_{20}. The values of Γ_{20} for different radionuclides are given in Table 16.1.

The exposure rate X from an n-mCi radionuclide source at a distance d cm is given by

$$X = \frac{n\Gamma}{d^2} \tag{16.1}$$

where Γ is the exposure rate constant of the radionuclide.

Problem 16.1
Calculate the radiation exposure at 25 cm from a vial containing 30 mCi (1.11 GBq) of ^{201}Tl.

Answer
The exposure rate constant Γ_{20} of ^{201}Tl is 0.45 R · cm^2/mCi · h at 1 cm from Table 16.2. Therefore, using Eq. (16.1), at 25 cm

$$X = \frac{30 \times 0.45}{25^2} = 21.6 \text{ mR/h}$$

Because Γ_{20} of ^{201}Tl in SI units is 12.16 μGy · m^2/GBq · h at 1 m, X for 1.11 GBq of ^{201}Tl at 25 cm is

$$X = \frac{1.11 \times 12.16}{(0.25)^2}$$
$$= 215.96 \ \mu\text{Gy/h}$$

It should be pointed out that because the patient is not a point source, the exposure rate does not vary exactly as the inverse square of the distance.

Shielding

Various high atomic number (Z) materials that absorb radiations can be used to provide radiation protection. Because the ranges of α- and β-particles are short in matter, the containers themselves act as shields for these radiations. γ-Radiations, however, are highly penetrating. Therefore, highly absorbing material should be used for shielding of γ-emitting sources, although for economic reasons, lead is most commonly used for this purpose. The half-value layer (HVL) of absorbent material for different radiations is an important parameter in radiation protection and is related to linear attenuation coefficient of the photons in the absorbing material. This has been discussed in detail in Chapter 6.

Problem 16.2
Calculate the number of HVLs and the amount of lead necessary to reduce the exposure rate from 100 mCi (3.7 GBq) of ^{131}I to less than 10 mR/h at 10 cm from the source. (Γ = 2.17 R · cm^2/mCi · h at 1 cm and 1 HVL = 3 mm of lead).

Answer

$$\text{Exposure at 10 cm} = \frac{2170 \times 100}{10^2} = 2170 \text{ mR/h.}$$

A factor of 2170/10 = 217 or more would be needed to reduce the exposure to less than 10 mR/h. In terms of HVL, $2^8 = 256$, that is, 8 HVLs would be needed. Since 1 HVL = 3 mm of lead, 8 HVLs would be equal to 24 mm. Therefore, 8 HVLs or 24 mm of lead would be necessary.

Obviously, shielding is an important means of protection from radiation. Radionuclides should be stored in a shielded area. The radiopharmaceutical dosages for patients should be carried in shielded syringes. Radionuclides emitting β-particles should be stored in containers of low-Z material such as aluminum and plastic because in high-Z material, such as lead, they produce highly penetrating bremsstrahlung radiations. For example, ^{32}P is a β^- emitter and should be stored in plastic containers instead of lead containers.

Activity

It should be obvious that the radiation exposure increases with the intensity of the radioactive source. The greater the source strength, the more the radiation exposure. Therefore, one should not work unnecessarily with large quantities of radioactivity.

Personnel Monitoring

According to 10CFR20, personnel monitoring is required under the following conditions:

1. Occupational workers including minors and pregnant women likely to receive in 1 year a dose in excess of 10 % of the annual limit of exposure from the external radiation source
2. Individuals entering high or very high radiation areas

Monitoring for occupational intake of radioactive material is also required if the annual intake by an individual is likely to exceed 10 % of the ALIs in 10CFR20, Table 16.1, Appendix B, and if minors and pregnant women are likely to receive a committed effective dose equivalent in excess of 0.05 rem (0.5 mSv) in 1 year.

Three devices are used to measure the exposure of ionizing radiations received by an individual: the pocket dosimeter, the film badge, and the thermoluminescent dosimeter. The pocket dosimeter (Fig. 16.2) has been described in Chapter 7.

Film Badge

The film badge is most popular and cost-effective for personnel monitoring and gives reasonably accurate readings of exposures from β-, γ- and x-radiations. The film badge consists of a radiation-sensitive film held in a plastic holder (Fig. 16.2a, b). Filters of different metals (aluminum, copper, and cadmium) are attached to the holder in front of the film to differentiate exposure from radiations of different types and energies. Filters of metals of different densities stop different energy radiations, thus discriminating exposures from them. After exposure the optical density of the developed film is measured by a densitometer and compared with that of a calibrated film exposed to known radiation. Film badges are usually changed monthly for radiation workers in most institutions. Film badges provide an integral dose and a permanent record. The main disadvantage of the film badge

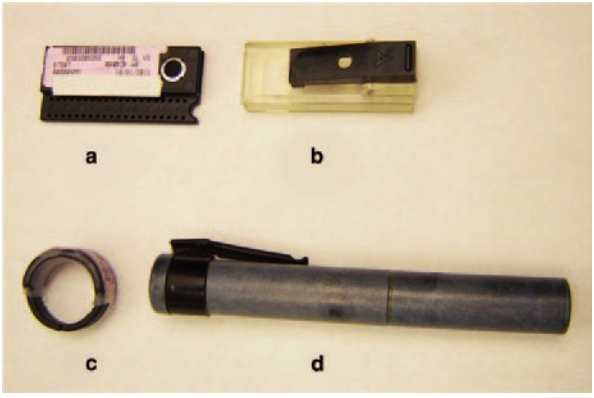

FIG. 16.2. **a** Film badge. **b** Film badge holder. **c** TLD ring badge. **d** Pocket dosimeter.

is the long waiting period (a month) before the exposed personnel know about their exposure. The film badge also tends to develop fog resulting from heat and humidity, particularly when in storage for a long time, and this may obscure the actual exposure reading. The film badges of all workers are normally sent to a commercial firm that develops and reads the density of the films and sends back the report of exposure to the institution. The commercial firm must be accredited by the National Voluntary Laboratory Accreditation Program (NVLAP) of the National Institute of Standards and Technology.

Thermoluminescent Dosimeter

A thermoluminescent dosimeter (TLD) consists of inorganic crystals (chips) such as lithium fluoride (LiF) and manganese-activated calcium fluoride (CaF_2:Mn) held in holders like the film badges and plastic rings (Fig. 16.2c). When these crystals are exposed to radiation, electrons from the valence band are excited and trapped by the impurities in the forbidden band. If the radiation-exposed crystal is heated to 300 to 400°C, the trapped electrons are raised to the conduction band; they then fall back into the valence band, emitting light. The amount of light emitted is proportional to the amount of radiation absorbed in the TLD. The amount of light is measured and read as the amount of radiation exposure by a TLD reader, a unit that heats the crystal and reads the exposure as well. The TLD gives an accurate exposure reading and can be reused after proper heating (annealing).

It should be noted that exposure resulting from medical procedures and background radiations are not included in occupational dose limits. Therefore, radiation workers should wear film badges or dosimeters only at work. These devices should be taken off during any medical procedures involving radiation such as radiographic procedures and dental examinations, and also when leaving after the day's work. Also radiation workers should not wear these badges for certain period of time after undergoing a diagnostic or therapeutic nuclear medicine procedure or radiation therapy permanent implant procedure.

Dos and Don'ts in Radiation Protection Practice

Do wear laboratory coats and gloves when working with radioactive materials.

Do work in a ventilated fume hood while working with volatile material.
Do cover the trays and workbench with absorbent paper.
Do store and transport radioactive material in lead containers.
Do wear a film badge while working in the radiation laboratory.
Do identify all radionuclides and dates of assay on the containers.
Do survey work areas for contamination as frequently as possible.
Do clean up spills promptly and survey the area after cleaning.
Do not eat, drink, or smoke in the radiation laboratory.
Do not pipette any radioactive material by mouth.

Do monitor hands and feet after the day's work.
Do notify the radiation safety officer (RSO) in the case of any major spill or other emergencies related to radiation.

Bioassay

NRC Regulatory Guide 8.20 gives the details of bioassay requirements for ^{131}I and ^{125}I radionuclides. Bioassays are required when the level of radioiodine activity handled (volatile or dispersible) exceeds the following values:
Open bench: 1 mCi (37 MBq)
Fume hood: 10 mCi (370 MBq)
Glove box: 100 mCi (3.7 GBq)

When the radioiodinated material is nonvolatile, the limits of activity are higher by a factor of 10. Stricter limits may be imposed in the license by the NRC.

For iodine radionuclides, bioassay is performed by the thyroid uptake test within 72 h and at 14 days after handling the radioactivity. Sometimes urine analysis may also be required soon after the exposure. Bioassays may be required for other radionuclides, depending on the amount and type of radionuclides.

Receiving and Monitoring of Radioactive Packages

Individual users or institutions are authorized to possess and use radioactive materials on issuance of a radioactive material license by the NRC or the Agreement State. The suppliers require documentation of licensing of the user as to the types and limits of quantities of radioactive material before shipping.

Monitoring of packages is required if the packages are labeled as containing radioactive material to check if the packages are damaged or leaking. A radioactive shipment must be monitored as soon as possible after receipt but no later than 3 h after delivery if the delivery takes place during normal hours, or not later than 3 h from the beginning of the next working day if it is received after working hours. Two types of monitoring are performed: survey for external exposure and wipe test for contamination on the surface of the package resulting from potential leakage of liquid. The survey reading of external exposure should not exceed 200 mrem/h (2 mSv/h) on the surface of the container or 10 mrem/h (100 μSv/h) at 1 m from the surface of the container. The wipe test is performed by swabbing an area of 300 cm^2 of the package and should show less than the limit of 6600 dpm or 110 Bq/300 cm^2. If the readings exceed these limits, the NRC and the final delivering carrier must be notified by telephone and telegram, mailgram, or facsimile. Advice should be sought from these authorities as to whether the shipment should be returned.

After all surveys are completed, the data must be entered into a receipt book. The information logged in includes the date of the receipt, the manufacturer, the lot number, name and quantity of the product, date and time of calibration, and survey data along with the name of the individual processing the receipt.

Radioactive Waste Disposal

Radioactive waste generated in nuclear medicine or pharmacy (e.g., syringes, needles, vials containing residual activities and contaminated papers, tissues, and liners) are disposed of by the following methods according to the guidelines set forth in 10CFR20 and 10CFR35.

1. Decay in storage
2. Release into a sewerage system
3. Transfer to authorized recipient (commercial land disposal facilities)
4. Other disposal methods approved by the NRC (e.g., incineration of solid waste and atmospheric release of radioactive gases)

The following is a brief description of different methods of radioactive waste disposal, but one should consult 10CFR20 and 10CFR35 for details.

Decay in Storage

Although 10CFR20 does not spell out the conditions of the decay-in-storage method, 10CFR35.92 describes this method in detail. Radionuclides with half-lives less than 120 days usually are disposed of by this method. These radionuclides are allowed to decay in storage and monitored before disposal. If the radioactivity reading of the waste is indistinguishable from background, it can be disposed of in the normal trash after removal or defacing of all radiation labels. This method is most appropriate for short-lived radionuclides such as ^{99m}Tc, ^{123}I, ^{201}Tl, ^{111}In, ^{67}Ga and ^{131}I commonly used in nuclear medicine. Radioactivities should be stored separately according to half-lives for convenience of timely disposal of each radionuclide.

Release into Sewerage System

The NRC permits radioactive waste disposal into the sewerage system provided the radioactive material is soluble or dispersible in water and the quantity disposed of monthly does not exceed the maximum permissible limits set in 10CFR20. Disposal depends on the total volume and flow rate of water used but is limited to 1 Ci (37 GBq) of ^{14}C, 5 Ci (185 GBq) of ^{3}H, and 1 Ci (37 GBq) of all other radionuclides annually. Excreta from humans undergoing medical diagnosis or treatment with radioactive material are exempted from these limitations. However, items contaminated with radioactive excreta (e.g., linen, diapers, etc., contaminated with urine or feces) are not exempted from these limitations. To adopt this method of radioactive disposal, one must determine the total volume and the flow of sewer water in the institution and the number of users of a specific radionuclide so that for each individual user, a limit can be set for sewer disposal of the radionuclide in question.

Transfer to Authorized Recipient

This method of transfer to an authorized recipient is adopted for long-lived radionuclides and usually involves transfer of radioactive wastes to authorized commercial firms that bury or incinerate at approved sites or facilities.

Although the columns of the ^{99}Mo–^{99m}Tc generators may be decayed to background for disposal to normal trash, a convenient method of disposing of this generator is to return them to the vendors, who let them decay and later dispose of them. Normally, the used generator is picked up by the authorized carrier when a new one is delivered.

Other Disposal Methods

A licensee may adopt methods of radioactive waste disposal different from those mentioned here, provided regulatory agency approval is obtained. Impact of such disposal methods on environment, nearby facilities, and population is heavily weighed before approval. Incineration of solid radioactive waste and carcasses of research animals containing radioactive materials is allowed by this method. Radioactive gases such as ^{133}Xe and ^{127}Xe are released by venting through the fumehood, provided their maximum permissible concentration at the effluent side of the exhaust to the atmosphere does not exceed the NRC limits. Radioactive waste containing 0.05 μCi (1.85 kBq) or less of ^{3}H or ^{14}C/g of medium used for liquid scintillation counting or animal tissue may be disposed of in the regular nonradioactive trash.

Records must be maintained as to the date of storage and the amount and kind of activity stored in a waste disposal log book. The stored packages must be labeled with pertinent information. The date of disposal and the amount of disposed activity must also be recorded in the log book, along with the initials of the individual disposing of the waste.

Radioactive Spill

Accidental spillage of radioactivity can cause unnecessary radiation exposure to personnel and must be treated cautiously and expeditiously. Appropriate procedures must be established for handling radioactive spills. There are two types of spills: major spill and minor spill. No definitive distinction exists between a minor and a major spill. A major spill usually occurs when the spilled activity cannot be contained in a normal way and can cause undue exposure to personnel. In the case of a major spill, the RSO should be notified immediately. In either case, the access to the area should be restricted. Areas, personnel, and equipment must be decontaminated, keeping in mind the principle of containment of radioactivity. Survey and wipe tests must be performed after decontamination. The RSO will investigate the accident and recommend corrective action if a major spill occurs.

Recordkeeping

Records must be maintained for the receipt, storage, and disposal of radioactive materials, as well as for various activities performed in the radiation laboratories. According to the NRC regulations, these records must contain specific information and must be kept for a certain period of time specified by the NRC.

Medical Uses of Radioactive Materials

The NRC and Agreement States regulate the medical uses of by-product materials by implementing 10CFR35. There are six categories of medical uses of radioactive materials according to 10CFR Part 35. They are: (1) radiopharmaceuticals for uptake, dilution, and excretion (10CFR35.100); (2) radiopharmaceuticals for imaging and localization including generators and kits (10CFR35.200); (3) radiopharmaceuticals for therapy (10CFR35.300); (4) sealed sources for brachytherapy (10CFR35.400); (5) sealed sources for diagnosis such as sources of ^{125}I and ^{153}Gd for bone mineral analysis (10CFR35.500); and (6) sealed sources for teletherapy such as sources of ^{60}Co and ^{137}Cs in teletherapy units or gamma stereotactic radiosurgery units (10CFR35.600).

The regulations for the medical use of all radioactive materials are given in 10CFR35, but radiopharmaceuticals under categories 1, 2, and 3 only are relevant in nuclear medicine. These radiopharmaceuticals must be approved for human clinical use by the FDA under an IND or NDA. The ^{99m}Tc activity is eluted from the ^{99}Mo-^{99m}Tc generator and reagent kits are used to prepare ^{99m}Tc-labeled radiopharmaceuticals according to instructions given by the manufacturer in the package inserts. Only reagent kits that are approved by the FDA under an IND or NDA may be used for radiopharmaceutical preparation. Many other radiopharmacenticals are prepared by the manufacturers using appropriate labeling methods. The following is a brief description of the pertinent rules of 10CFR35.

Applications, Amendments, and Notifications

As already mentioned, applications for a license and its renewals must be made by the licensee's management for the medical uses of by-product materials. Amendments to the license must be made by the licensee's management for the following:

(a) Appointment or discontinuation of an authorized user, radiation safety officer, authorized medical physicist, or authorized nuclear pharmacist
(b) Change of name or address of the licensee
(c) Change or addition of the use areas
(d) Use of excess or new by-product materials not permitted before in the license

Notification of the above must be made within 30 days of occurrence. Change or addition of areas of use for uptake and dilution (10CFR35.100) and for localiza-

tion and imaging (10CFR35.200) need not be amended. Licenses with Type A specific license of broad scope are exempt from these requirements.

Authority and Responsibilities of the Licensee

According to 10CFR35.24, the licensee's management is responsible for the overall implementation of the radiation protection program in the medical uses of by-product material. The licensee's management shall approve in writing all new authorized users, radiation safety officer, or nuclear pharmacist, and ministerial changes in the radiation safety program that do not require license amendment (10CFR35.26).

The licensee's management shall appoint a Radiation Safety Officer (RSO), who accepts in writing responsibilities to implement a radiation protection program. It may appoint one or more temporary RSOs for 60 days in a year, if all conditions of an RSO are met.

The licensee's management also must appoint a Radiation Safety Committee (RSC), if the licensee is authorized for two or more different types of uses of by-product material. Examples are the use of therapeutic quantities of unsealed by-product material (10CFR35.300) and manual brachytherapy (10CFR35.400), or manual brachytherapy and low-dose-rate therapy units (10CFR35.600), or teletherapy units (10CFR35.600) and gamma knife units (10CFR35.600). Use of by-product materials for both uptake and dilution (10CFR35.100) and imaging and localization (10CFR35.200) does not require an RSC. The RSC must include as a minimum an authorized user of each type of use permitted in the license, the RSO, a representative of the nursing service, and a representative of management, and in addition, other members, if appropriate. The NRC does not prescribe any definite frequencies of the RSC meetings nor record-keeping of the minutes.

Supervision

According to 10CFR35.27, a licensee that permits an individual to work under an authorized user or authorized nuclear pharmacist using by-product material must instruct the supervised individual to follow strictly all regulations and conditions of the license and all procedures involving by-product material. There is no requirement for periodic review of the supervised individual's work and records. The licensee is responsible for the acts and omissions of the supervised individuals.

Mobile Nuclear Medicine Service

According to 10CFR35.80, a licensee providing mobile nuclear medicine service to a client must

(a) Have a letter, or memorandum of understanding (MOU), signed by the licensee and the management of each client spelling out the details of the responsibility and authority of the client and the licensee,

(b) Calibrate and check the instruments for measuring dosages and surveying,
(c) Measure dosages and perform surveys of the area of uses at the client address, and
(d) The client must have a license for receiving and using by-product material.

Written Directives

According to 10CFR35.40, a written directive is required when a dosage greater than 30 μCi (1.11 MBq) of ^{131}I-NaI or a therapeutic dosage of an unsealed by-product material other than ^{131}I-NaI is administered to a patient or human research subject. The written directive must be dated and signed by an authorized user and must contain the patient's name, the dosage, the name of the drug, and route of administration. A revision of the written directive can be made, if necessary, provided it is signed and dated by the authorized user before administration. In case of an emergency, an oral revision to an existing written directive is acceptable, which must be followed by a written directive within 48 h.

According to 10CFR35.41, the licensee shall develop and maintain a copy of the written procedures for the written directive that include specific verifications of the identity of the patient before each administration, and that the administration is in accordance with the written directive. The identity of the patient may be verified by the name, driver's license, birthday, any hospital's I.D. number, and so on.

Measurement of Dosages

According to 10CFR35.63, all dosages for patient administration must be measured in an instrument (dose calibrator) that is calibrated with nationally recognized standards or the manufacturer's instructions (10CFR35.60). Although the methods of calibration are not specifically prescribed in 10CFR35, the constancy, accuracy, linearity, and geometry of the dose calibrator must be checked as described in Chapter 7.

For unit dosages, the activity can be determined by direct measurement or by the decay correction of the activity provided by the licensed manufacturer. For dosages other than unit dosages, the activity must be determined by direct measurement, a combination of measurement of radioactivity and mathematical calculations, or a combination of volumetric measurements and mathematical calculations based on the activity provided by the manufacturer.

Unless otherwise directed by the authorized user, the licensee may not use a dosage if it does not fall within the prescribed dosage range, or if it differs from the prescribed dosage by more than 20 %. The licensees who use only unit dosages calibrated and supplied by the manufacturer may not need to verify the dosage in a dose calibrator. If the injection time is different from the calibration time, the decay-corrected unit dosage can be used, if it is still within the prescription range.

Calibration, Transmission, and Reference Sources

The following sources of by-product material are permitted for check, calibration, transmission, and reference use (10CFR35.65):

(a) Sealed sources not exceeding 30 mCi (1.11 GBq) manufactured and supplied by a licensed manufacturer, or a licensee authorized to redistribute such sources
(b) Any by-product material with a half-life not longer than 120 days in individual amounts not exceeding 15 mCi (0.56 GBq)
(c) Any by-product material with a half-life longer than 120 days in individual amounts not to exceed the smaller of 200 μCi (7.4 MBq) or 1000 times the quantities in Appendix B of 10CFR30
(d) ^{99m}Tc in amounts as needed

A licensee may only use sealed sources for medical use, manufactured by a licensed manufacturer (10CFR49).

Requirement for Possession of Sealed Sources

According to 10CFR35.67, sealed sources of radionuclides with a half-life greater than 30 days, and containing more than 100 μCi (3.7 MBq) of γ- or β^--emitting material or more than 10 μCi (370 kBq) α-emitting material must be leak tested and inventoried semiannually. If a source shows a leak of 0.005 μCi (185 Bq) or more of removable contamination, it must be immediately removed from use and stored, disposed of, or repaired according to regulations, and a report must be filed with the NRC within five days of the leak test describing the source involved, the test results, and the action taken.

Labeling of Vials and Syringes

Each syringe and vial containing radioactivity must be labeled to identify the radioactive drug (10CFR35.69). Each syringe or vial shield also must be labeled, unless the label on the syringe or vial is visible through the shield. Although syringe shields are not required by the NRC regulations for administration of radiopharmaceuticals, they should be used to maintain ALARA exposures.

Surveys of Ambient Radiation Exposure Rate

According to 10CFR35.70, the NRC requires that the licensee shall survey all areas where unsealed byproduct material requiring a written directive is prepared for use or administered. However, the survey should be performed at the end of each day of use with a radiation detection instrument such as G-M counter. In addition, according to 10CFR20, weekly surveys must be conducted in areas of radiation use to maintain ALARA principles, e.g. areas where radiopharmaceuticals or waste is stored.

Area survey under 10CFR35.70 is not required in rooms where patients containing radioactivity are confined. Trigger levels must be established in each area by performing these tests under normal circumstances in the absence of any undue radioactive materials.

Weekly wipe tests of areas where radiopharmaceuticals are routinely prepared, administered, or stored must be done. The tests are performed by swabbing an area of 300 cm^2 with a wipe paper and counting the wipe in a well counter. Wipe test limits recommended by the NRC are: For ^{131}I, 200 dpm for unrestricted area and 2000 dpm for restricted area; for ^{99m}Tc, 2000 for unrestricted area and 20,000 for restricted area.

Calibration of Survey Instruments

According to 10CFR35.61, the survey meter must be calibrated before its first use, annually, and after repairs that affect calibration. Calibration must be made in all scales with readings up to 1000 mrem (10 mSv) per hour with a radiation source (e.g. ^{137}Cs) and two separated readings must be calibrated on each scale or decade (digital) that is used to show compliance. The date and the results of calibration must be noted on the instrument. The licensee may not use the survey instruments if the difference between the indicated exposure rate and the calculated exposure rate is more than 20 %.

Training and Experience Requirements for Medical Uses of By-Product Materials

Authorized users, radiation safety officers, and nuclear pharmacists are required to have appropriate training and experience for medical uses of by-product materials. Normally there are two methods of approval: (1) certification by a specific medical specialty board, and (2) training and work experience in radionuclide handling techniques applicable to specific medical use of by-product material. The names of the boards recognized by the NRC are posted on the NRC Web site. For recognition, each board must meet all requirements of the training and work experience in a specific category described below and be approved by the NRC.

The training part includes a specified period of didactic classroom and laboratory training in the areas of (a) radiation physics and instrumentation, (b) radiation protection, (c) mathematics pertinent to radioactivity, (d) chemistry of by-product material, and (e) radiation biology and radiation dosimetry (for radiation safety officer).

The work experience must be under an authorized user, radiation safety officer, or nuclear pharmacist depending on the specific authorization of by-product material requested and must include (a) ordering, receiving, and unpacking radioactive materials, and surveying; (b) calibration of dose calibrators and survey meters; (c) calculating, measuring, and preparing dosages for patients; (d) procedures for spill management; (e) safely administering dosages to patients (for

authorized users only); and (f) elution of radioactive generators (for localization and imaging studies).

In addition, approval by the training and experience method requires a written certification by a preceptor that the individual has acquired competence in the techniques to function independently for a specified use of by-product material.

The required hours of training and experience vary for different types of uses of radioactive material and are listed below.

Radiation Safety Officer (10CFR35.50)	200 h of classroom and laboratory training in radiation safety plus 1 year work experience under a radiation safety officer
Nuclear Pharmacist (10CFR35.55)	700 h of classroom and laboratory training and supervised work experience in nuclear pharmacy
Authorized User (10CFR35.190) (Uptake, dilution, and excretion)	60 h of training and work experience, including 8 h of classroom and laboratory training in radionuclide handling
Authorized User (10CFR25.290) (Localization and imaging)	700 h of training and experience including 80 h of classroom training in basic radionuclide handling
Authorized User (10CFR35.390) (Therapeutic use)	700 h of training and work experience, including 200 h of classroom training in basic radionuclide handling, plus 3 cases in each therapeutic use of by-product material
Authorized User (10CFR35.392) (Hyperthyroidism using less than 33 mCi (1.22 GBq) ^{131}I-NaI)	80 h of classroom and laboratory training in ^{131}I therapy procedures plus 3 cases of hyperthyroid treatments
Authorized User (10CFR35.394) (Thyroid cancer using greater than 33 mCi (1.22 GBq) ^{131}I-NaI)	80 h of classroom and laboratory training in ^{131}I therapy procedures plus 3 cases of thyroid cancer treatments

Report and Notification of a Medical Event

According to 10CFR35.3045, the term *medical event* has been substituted for "misadministration" and "recordable event"—terms commonly used in the past. A medical event occurs when a dose exceeds 5 rem (0.05 Sv) effective dose equivalent, or 50 rem (0.5 Sv) to an organ or tissue or skin from any of the following situations.

(a) The total dose delivered in therapy differs from the prescribed dose by 20 % or more,
(b) The total dosage delivered differs from the prescribed dosage by 20 % or more, or falls outside the prescribed dosage range,
(c) Administration of a wrong radioactive drug containing by-product material,
(d) Administration by a wrong route,
(e) Administration to a wrong individual.

The licensee must notify by telephone a medical event to the NRC Operation Center no later than 1 calendar day after discovery of the event, followed by a written report to the NRC Regional Office within 15 days. The report must in-

clude the licensee's name, prescribing physician's name, brief description of the event, cause of the event, effect of the event, if any, on the individual, corrective action taken, if any, and whether the affected individual or his or her relative or guardian has been notified. The individual's name or identification number shall not be included in the report.

The licensee shall notify the individual and the referring physician of the event no later than 24 h after the discovery, unless the referring physician personally takes the responsibility of informing or not informing the individual based on medical judgment. If a verbal notification is made, the licensee shall inform the individual of the availability of a written description of the event, which the licensee will provide upon request.

In addition, the licensee shall annotate a copy of the report filed with the NRC with the name and social security number or other identification number of the affected individual and provide a copy of the annotated report to the referring physician, if other than the licensee, within 15 days of occurrence of the event. Recordkeeping of medical events is not required because the reports are provided to the NRC.

Report and Notification of a Dose to an Embryo/Fetus or a Nursing Child

The licensee shall report to the NRC an event in which an embryo/fetus receives more than 5 rem (50 mSv) dose equivalent due to the administration of by-product material to a pregnant individual, unless such a dose was specifically approved in advance by the authorized user. Also, a report must be made to the NRC if the dose to a nursing child, from the administration of by-product material to a breast-feeding individual, exceeds 5 rem (50 mSv) total effective dose equivalent, or has resulted in unintended permanent functional damage to an organ or biological system of the child.

The conditions, timing, and descriptions of the report are identical to those of the medical events described above.

Release of Patients Administered with Radiopharmaceuticals

According to 10CFR35.75, a licensee can release a patient administered with a radiopharmaceutical or a permanent radioactive implant, provided the TEDE to any other individual from exposure to the released patient is not likely to exceed 500 mrem (5 mSv). Practically in nuclear medicine, patients treated with ^{131}I-NaI are commonly considered under these regulations. In these cases, when the activity in the patient is less than 33 mCi (1.2 GBq) or the measured exposure rate is less than 7 mrem/h (0.07 mSv/h) at 1 m, then the patient can be released. Based on administered activity, physical half-life, and assumption of other parameters, the maximum limits of activity and exposure from different radionuclides for release of patients has been calculated and given in Table 16.2 (U.S. NRC NUREG-1556, vol 9, 2002).

Table 16.2. Activities and dose rates for authorizing patient release.[a]

	Activity at or below which patients may be released		Dose rate at 1 m at or below which patients may be released	
Radionuclide	GBq	mCi	mSv/h	mrem/h
^{123}I	6.0	160	0.26	26
^{67}Ga	8.7	240	0.18	18
^{131}I	1.2	33	0.07	7
^{111}In	2.4	64	0.2	20
^{99m}Tc	28	760	0.58	58
^{201}Tl	16	430	0.19	19

[a] NRC NUREG 1556, vol. 9, 2002.

However, patients administered with higher ^{131}I-activities, as high as 200 mCi (7.4 GBq), may be released provided the dose calculations using patient-specific parameters show that the potential TEDE to any individual would be no greater than 0.5 rem (5 mSv) (NRC Regulatory Guide NUREG—1556, vol 9). The patient-specific calculations depend on the choice of the occupancy factor and the physical or effective half-life. An occupancy factor of 0.75 is chosen for $t_{1/2}$ of less than 1 day and a value of 0.25 for $t_{1/2}$ greater than 1 day. A value of 0.25 for the occupancy factor would be valid if the patient follows the instructions, such as, for the first 2 days, (1) maintain the distances from others, (2) sleep alone or, better yet, live alone, (3) do not travel by airplane or mass transportation, (4) do not travel in automobiles with others, (5) have the sole use of the bathroom, (6) drink plenty of water, and (7) limit visits by others. These instructions must be given in writing to the patients to follow after release.

The released patient must be given instructions, including written instructions, to maintain the dose as low as reasonably achievable if the TEDE to any other individual is likely to exceed 100 mrem (1 mSv). In the case of ^{131}I treatment, instructions must be given to the patient, when the activity in the patient is more than 7 mCi (259 MBq) or when the measured exposure rate exceeds 2 mrem/h (0.02 mSv/h) at 1 m. The limits of activity and exposure for different radionuclides used in nuclear medicine requiring instructions to be given to the patient for release are given in Table 16.3. If the dose to a breast-fed infant or child

Table 16.3 Activities and dose rates above which instructions should be given for patient release.[a]

	Activity above which instructions are required		Dose rate at 1 m above which instructions are required	
Radionuclide	GBq	mCi	mSv/h	mrem/h
^{123}I	1.2	33	0.05	5
^{67}Ga	1.7	47	0.04	4
^{131}I	0.24	7	0.02	2
^{111}In	0.47	13	0.04	4
^{99m}Tc	5.6	150	0.12	12
^{201}Tl	3.1	85	0.04	4

[a] NRC NUREG 1556, vol. 9, 2002.

Table 16.4. Limits of activities that require instructions to breast-feeding patients and recordkeeping.[a]

Radiopharmaceutical	Activity above which instructions are needed mCi (MBq)		Activity above which record is needed mCi (MBq)		Recommended duration of cessation of breast-feeding
^{131}I-NaI	0.0004	(0.01)	0.002	(0.07)	complete cessation
^{123}I-NaI	0.5	(20)	3	(100)	–
^{131}I-MIBG	2	(70)	10	(400)	12 h (4 mCi/150 MBq)
^{99m}Tc-DTPA	30	(1000)	150	(6000)	–
^{99m}Tc-MAA	1.3	(50)	6.5	(200)	12.6 h (4 mCi/150 MBq)
^{99m}Tc-Pertechnetate	3	(100)	15	(600)	12 h (12 mCi/440 MBq)
^{99m}Tc-DISIDA	30	(1000)	150	(6000)	–
^{99m}Tc-Glucoheptonate	30	(1000)	170	(6000)	–
^{99m}Tc-Sestamibi	30	(1000)	150	(6000)	–
^{99m}Tc-MDP	30	(1000)	150	(6000)	–
^{99m}Tc-PYP	25	(900)	120	(4000)	–
^{99m}Tc-RBC in vivo	10	(400)	50	(2000)	6 h (20 mCi/740 MBq)
^{99m}Tc-RBC in vitro	30	(1000)	150	(6000)	–
^{99m}Tc-Sulfur colloid	7	(300)	35	(1000)	6 h (12 mCi/440 MBq)
^{99m}Tc-MAG3	30	(1000)	150	(6000)	–
^{99m}Tc-WBC	4	(100)	15	(600)	12 h (12 mCi/440 MBq)
^{67}Ga-Citrate	0.04	(1)	0.2	(7)	1 wk (0.2 mCi/7 MBq)
^{111}In-WBC	0.2	(10)	1	(40)	1 wk (0.5 mCi/20 MBq)

[a] NRC regulatory Guide NUREG 1556, vol. 9, 2002.

could exceed 100 mrem (1 mSv) assuming continuous breast-feeding by a patient administered with radiopharmaceutical, then instructions on discontinuation of breast-feeding and consequences of failure to follow the guidance must also be given. Table 16.4 lists the activity limits for giving instructions to the breast-feeding patients and activity limits for cessation of breast-feeding. In 2008, the NRC issued a Regulatory Issue Summary (RIS) 2008–2011, "Precautions to Protect Children Who May Come in Contact with Patients Released after Therapeutic Administration of Iodine-131" as a supplement to the guidance for radioactive patient release. It recommends to have patients avoid direct or indirect contact with infants and young children for a specific period of time and have sufficient space (bedrooms, bathrooms, etc.) in the house for exclusive use by the patient only. Advice should be given to the patient as to the consequences, if any, from failure to follow the recommendations.

Records are not required if patients are released based on the activity in column 1 of Table 16.2. However, records of release of patients are required, if the TEDE is calculated by using the retained activity rather than the administered activity, using an occupancy factor less than 0.25 at 1 m, using a biological or effective $t_{1/2}$ or considering the shielding by tissue. Records are also required if instructions are given to a breast-feeding woman who may give a TEDE exceeding 500 mrem (5 mSv) to the infant from continuous breast-feeding (10CFR35.2075). Table 16.4 gives the activity limits that require record keeping in case of breast-feeding.

Recordkeeping

Records must be maintained for the receipt, storage, and disposal of radioactive materials, and also for various activities performed in the radiation laboratories. According to the NRC regulations, these records must contain specific information and be kept for a certain period of time. Table 16.5 lists different records that are required by the NRC and the period of time to be kept.

Dirty Bombs

A dirty bomb, also called a Radiological Dispersal Device (RDD), is a mix of explosive, such as dynamite, with radioactive materials. After the explosion, in addition to the immediate devastating effects of the explosive material causing injury and property damage, radioactive dust and smoke spread the radioactive contamination into the surrounding areas. Radioactive dust and smoke, if inhaled, can cause ill health effects. The use of dirty bombs by perpetrators is to spread radioactive contamination and create fear and panic, more than anything else. Subsequent decontamination could involve considerable time and cost.

A dirty bomb is not an atomic bomb and is primarily used to disrupt and not destroy the human life. Another type of RDD might involve a very high level of radioactive source hidden in a bus, train, or subway station, where people passing close to the source might get a significant dose of radiation. Prompt detection of these devices (bomb or radioactive source) is essential in order to take protective measures.

The sources of radioactive materials are the hospitals, research facilities, and industrial and construction sites where radioactivity is used for various purposes (diagnosis and treatment at hospitals, research work, sterilizing equipment, and check of welding). Some of the highly hazardous radioactive sources are cobolt-60, strontium-90, cesium-137, and iridium-192 used in industrial radiographic services. These radionuclides have long half-lives. Many of these sources are mostly in metallic capsule form and the likelihood of dispersion is minimal. However, they can be available in liquid and powder forms and potentially be used in dirty bombs, which can result in widespread contamination in the surrounding areas of explosion. Because one cannot see, taste, or feel radiations, excessive exposure can be received unknowingly by people in the vicinity of the area.

Types of Accidental Radiation Exposure

Radiation exposure from radiation accidents can be localized and/or whole-body type. The localized exposure may be caused by direct handling of or close proximity to highly radioactive sources. The local injury includes erythema, epilation, desquamation, ulceration, or blistering depending on the level of exposure. The

TABLE 16.5. Recordkeeping of various activities related to radioactive materials.

Type of operation	Information needed	Time to maintain the records
Written directives (10CFR35.2040)	Copy of the written directives	3 years
Procedures requiring written directives (10CFR35.2041)	Copy of the procedures	Duration of the license
Dosage of radiopharmaceuticals dispensed (10CFR35.2063)	Name, lot number, expiration date, patient's name or identification number, prescribed dosage and dispensed dosage, date and time of administration, and name of the individual	3 years
Calibration of dose calibrator (10CFR35.2060)	Model, serial number of the dose calibrator, date and results of test, and name of the individual	3 years
Calibration of survey meters (10CFR35.2061)	Model and serial number of the instrument, date and results of calibration, and name of the individual	3 years
Semiannual leak tests and inventory of sealed sources (10CFR35.2067)	Model and serial number of each source and its radionuclide, estimated activity, measured activity in μCi (Bq), date of test, location of source (inventory), and name of the individual	3 years
Moly breakthrough (10CFR35.2204)	μCi (kBq) of ^{99}Mo per mCi (MBq) of ^{99m}Tc, date and time of measurement, name of the individual	3 years
Thyroid bioassay and whole body counting (10CFR20.2106)	Name of the individual having the bioassay, date of reading, and the individual taking the measurement	Until the NRC terminates the license
Personnel exposure monitoring records (10CFR20.2106)	Must be on NRC-5 form according to items described in the form	Until the NRC terminates the license
Radioactive waste disposal by decay-in-storage (10CFR35.2092)	Date of disposal, instrument used, background reading, and surface reading of the waste container, and the name of the individual	3 years
Planned special procedures (10CFR20.2105)	Circumstances, name of authorizing individual, doses expected	Until the NRC terminates the license
Surveys (10CFR35.2070)	Date, area, trigger level (mR/h), survey data, instrument used, and name of the individual	3 years
Release of patients with unsealed by-product material (10CFR35.2075)	Basis of calculation to release the patient, such as retained activity, occupancy factor less than 0.25 at 1 meter, using T_p or T_e, or considering shielding by tissue	3 years
Instructions given to breast- feeding female (10CFR25.2075)	Instruction given if dose to the infant exceeds 0.5 rem (5 mSv)	3 years

treatment of choice for localized injuries is the use of antibiotic for infection and control of pain. In severe cases, amputation or plastic surgery is warranted.

The whole-body exposure causes various acute radiation syndromes that have been discussed earlier in this chapter. These syndromes include hemopoietic, gastrointestinal, and cerebrovascular syndromes depending on the absorbed doses. Although cerebrovascular syndromes occur with 10,000 rem (100 Sv), and result in death, the hemopoietic and gastrointestinal syndromes may be managed by bone marrow transplantation and other prophylactic treatment.

When a RDD explodes, radioactive material may be airborne and contaminate food and water. Internal contamination can occur from the ingestion of contaminated food and water, inhalation of the contaminated air, and diffusion through the skin or wounds. The principle of the treatment of internal contamination primarily involves dilution, displacement by nonradioactive material, complex formation, and blockage. In the case of internal contamination with radioiodine (e.g., incidences of fallout from a nuclear explosion or a nuclear reactor accident), both the NRC and FDA have approved the use of potassium iodide (KI) as a preventive measure. Such use of KI is intended to block the thyroid from trapping ^{131}I and it should be taken before the exposure or within several hours of exposure. The recommended daily dose is 130 mg of KI for adults, 65 mg for 3–18 year old, 32 mg for children 1 month to 3 year old, and 16 mg for infants less than 1 month old (Mettler and Voelz, 2002).

Outer garments such as clothing and shoes can be contaminated by radioactivity from the explosion of a dirty bomb. Such contamination does not constitute a medical emergency and most of it can be removed by taking off these garments. Minor skin contamination can be eliminated by thorough washing with water and detergent, and a shower, if appropriate. Skin should not be abraded by a heavy brush, as this may facilitate internal absorption. If an individual has a life-threatening condition in addition to the external contamination, the patient must be first managed for the condition before decontamination is carried out. Burns and wounds that are not contaminated should be first covered and then decontamination of the other affected areas carried out.

Protective Measures in Case of Explosion of a Dirty Bomb

According to the advisory of the NRC and the Center for Disease Control (available at www.nrc.gov and www.bt.cdc.gov), the following steps should be taken in case of a dirty bomb explosion.

1. If you are outside and close to the explosion of a dirty bomb, cover the nose and mouth with a mask or cloth to reduce the risk of breathing in radioactive dust or smoke. If possible, immediately go inside the building that is not affected by the explosion and remove the outer layer of clothing and shoes and seal them in a plastic bag, if available. Store the plastic bag in a safe place for decay of the radioactivity. Next, take a shower to remove any dust that remains on the body.

2. If you are inside and close to the incident that has occurred outside, close all the doors and windows and do not leave the building. Turn off heat and air conditioner to stop air circulation from outside.
3. Listen to the local news for further appropriate instructions.
4. Food and water are unlikely to be contaminated. If contaminated, do not consume these items. Local or federal authorities are likely to monitor the food and water in the area of explosion and inform the public of their suitability for consumption.
5. If it is definitely known that there is radioiodine contamination, KI should be orally administered within a short time according to the regimen described earlier.
6. Monitoring is essential and critical to estimate the level of contamination or decontamination using a GM counter and is performed by hospital personnel, police, and firefighters who are specially trained for this purpose.

Verification Card for Radioactive Patients

After the September 11, 2001 attack on the World Trade Center in New York, numerous security measures have been adopted by the U.S. Federal Government. Congress has passed laws to establish the Department of Homeland Security to implement and monitor different aspects of these security measures. Security checks of airline passengers, background scrutiny of many visitors and suspected terrorist groups, and implementation of the Patriot Act are some of the examples of these security actions that are currently in place. In view of the concerns over the use of dirty bombs by miscreants, the Homeland Security has established checkpoints at various strategic locations such as airports, tunnels, mass transit, bridges, border crossing points, historical monuments, landmarks, and the like, to monitor the transport of RDDs by using radiation detectors.

One pitfall of this measure is that patients who received radioactive materials for diagnostic and therapeutic purposes may trigger the monitors while passing through these checkpoints and undergo undue hassle with authorities to provide proof that the radioactivity was really from medical uses. These incidents have been reported all over the country. In 2003, the NRC issued a guidance "NRC Information Notice 2003–2022: Heightened Awareness for Patients Containing Detectable Amounts of Radiation from Medical Administration" to address this situation. In essence, according to this guidance, if a patient has detectable radioactivity due to a nuclear medicine test or a therapeutic implant, the licensee is asked to explain to the patient that during commuting, the internal activity may trigger the monitoring equipment installed in specific areas required by US Homeland Security Administration. It further recommends that the licensee considers providing a verification card with licensee's address, a contact phone number, and an assurance that the level of activity from the study poses no danger to the public and is allowed by NRC medical use regulations. Based on this, a verification card is designed containing information such as the name of the

patient, type of radionuclide administered, date of study, and a contact number. The patient is asked to carry the card as a proof of radioactive examination for a period of time (discussed below) till the activity is low enough not to trigger the monitoring equipment.

A question arises as to how long the patient who has undergone nuclear studies should carry the card. It depends on the half-life of the radionuclide, types of radiations the radionuclide emits, and the biological elimination of the radiotracer from the body. Zuckier et al. (2004) in a paper presented at The Radiological Society of North America annual meeting in Chicago suggested the following periods for different radionuclides for the patients to carry the card.

^{18}F	1 day
^{99m}Tc and ^{123}I	3 days
^{111}In	14–17 days
^{67}Ga and ^{201}Tl	30 days
^{131}I	95 days

Radiation Phobia

The public in general is unduly fearful of radiation because of several factors. One important factor is the graphic images of the devastating effects of the atomic bombs detonated in Hiroshima and Nagasaki in 1945, and to a lesser extent, the images of the Chernobyl reactor accident in 1986. The most noticeable effects of these incidents are death of living species and destruction of property at the site of the explosion and its immediate vicinity. Because of these images, many people associate radiation exposure with adverse health effects and death. These images are firmly embedded in the minds of the public causing perpetual fear of radiation. However, these incidents are very uncommon.

Another flashpoint in creating radiation phobia in the public's mind is the knowledge of assumption that any level of ionizing radiation is dangerous to health, alluding to the linear no-threshold (LNT) theory of the dose–response relationship. Psychological warfare with anecdotal rhetoric among the rival countries possessing nuclear weapons also creates fear of radiation among the public. Dreading effects of radiation on children and future offspring, and long-term damage to property are major concerns of the public. Furthermore, the media often play a role in exacerbating the problem of exposure from radiation accidents.

Is there a logical justification for this radiation phobia of the public? Definitely, nuclear detonation causes an instantaneous devastating effect on the population and property, and so can be a reason for fear and panic. But the long-term effects of low doses of radiations, even from the fallout of the atomic bombs in Japan and Chernobyl accident, have been shown to be relatively small. The average individual lifetime dose from the Chernobyl fallout is estimated to be 0.6–6 rem (6–60 mSv) (Jaworowski 1999). By comparison, the worldwide average annual dose an individual receives from natural radiation on earth is 220 mrem (2.2 mSv) and the lifetime dose of about 15 rem (150 mSv). In the United States, an individual receives an annual dose of about 311 mrem (3.1 mSv) from natural

sources including radon and a lifetime dose of 21 rem (210 mSv). These values are even ten times higher in some regions in India and Brazil, and yet incidence of excess cancer is not shown to be higher in these places.

People face risk of cancer, injuries, and even death from day-to-day living activities, such as driving, smoking cigarettes, drinking alcohol, eating food, and breathing air, in addition to hazardous job-related activities. Thirty-three percent of the population will contract cancer just from these activities without any radiation exposure, and 22 % will die from natural causes (American Cancer Society, 2003). If the population is exposed to 1 rem (10 mSv) of radiation exposure, the risk of cancer increases only by 0.1 % and half of them (0.05 %) will die, which is quite negligible (BEIR VII, 2005). Based on these arguments, it can be said that although nuclear explosions can be a cause for grave concern, low-dose radiations from medical facilities, natural background, and the like, are fairly safe relative to the hazards of different living activities, and the risk from such radiation exposure is small.

To allay the fears of radiation in the public's mind is essential and critical. It can be achieved through education of the public. People knowledgeable in radiation should talk to laymen explaining the relatively small risk of low-level radiations compared to many other day-to-day living activities. The media should play an important role in communicating this information to the public. Radiation experts should hold regular public seminars to explain the minimal risk of low-level radiation. Radiation-related professional organizations such as the Society of Nuclear Medicine, The Radiological Society of North America, Health Physics Society, and American Association of Physicists in Medicine should undertake appropriate approaches of communication with the public to shed their concern and fear of radiation.

Transportation of Radioactive Materials

The transportation of radioactive materials is governed by the U.S. Department of Transportation (DOT), which establishes the guidelines for packaging, types of packaging material, limits of radioactivity in a package, and exposure limits. Title 49 of the *Code of Federal Regulations* (49CFR) and 10CFR71 contain all these regulations related to packaging and transportation of radioactive materials.

There are two types of packaging:

Type A: This type of packaging is used primarily for most radiopharmaceuticals. Such packaging is sufficient to prevent loss of radioactive material with proper shielding to maintain the prescribed exposure during normal transportation. The limits of radioactivities of various radionuclides under this category are specified in 49CFR and 10CFR71.

Type B: When the radioactivity exceeds the limits specified in Type A, Type B packaging must be used. Such packaging is considerably more accident resistant and is required for very large quantities of radioactive material.

FIG. 16.3. The three types of U.S. Department of Transportation labels required for transportation of radioactive materials.

The packages must pass certain tests such as the drop test, corner drop test, compression test, and 30-min water spray test.

The radioactive packages must be labeled properly before transportation. There are three types of labels (Fig. 16.3) according to the exposure reading in mR/h at 1 m from the surface of the package (*transport index*). The criteria for the three labels are given in Table 16.6. The transport index (TI) must be indicated on the label and the sign "RADIOACTIVE" must be placed on the package. The maximum permissible TI value is 10, although it is limited to three for passenger-carrying aircrafts. For liquids, the label "THIS SIDE UP" must be placed on the package. Each package must be labeled on opposite sides with the appropriate warning label (one of the labels in Fig. 16.3). The label must identify the content and amount of radionuclide in curies or ecquerels. The package must contain shipping documents inside, bearing the identity, amount, and chemical form of the radioactive material and the TI.

Placards are necessary on the transport vehicles carrying yellow-III–labeled packages and must be put on four sides of the vehicle.

According to 49CFR173.421, radionuclides are exempted from the packaging and labeling requirements if only a limited quantity of these radionuclides is shipped. The surface exposure readings should not exceed 0.5 mR/h at all points of the package surface, and the wipe test indicates no removable contamination in

TABLE 16.6 Labeling categories for packages containing radioactive materials.

	Exposure (mR/h)	
Type of label	At surface	At 1 m
White-I	<0.5	–
Yellow-II	$>0.5 \leq 50$	<1
Yellow-III	$>50 \leq 200$	$>1 \leq 10$

No package shall exceed 200 mR/h at the surface of the package or 10 mR/h at 1 m. Transport index is the reading in mR/h at 1 m from the package surface (10CFR71).

TABLE 16.7. Limited quantities of several radionuclides that are exempt from shipping and labeling requirements, according to 49CFR I73.425.

	Quantity	
Radionuclides[a]	(mCi)	(MBq)
^{57}Co (s)	270	10,000
^{67}Ga (l)	8.1	300
^{123}I (l)	8.1	300
^{125}I (l)	8.1	300
^{131}I (l)	1.9	70
^{89}Sr (l)	1.6	60
^{111}In (l)	8.1	300
^{32}P (l)	1.4	50
^{99m}Tc (l)	11	400
^{201}Tl (l)	11	400
^{133}Xe (g)	270	10,000
^{18}F(l)	1.6	60

[a]*s* solid, *l* liquid, *g* gas.

excess of 6600 dpm/300 cm^2. The outside of the inner packaging or, if there is no inner packaging, the outside of the packaging itself bears the marking, "Radioactive". The outside of the package must be marked with UN2910. If the inner packaging materials read less than 0.5 mR/h for exposure and 6600 dpm/300 cm^2 for contamination, then the shipment is considered "Empty" and should be labeled "UN2908" on the outside. No shipping paper is required for both limited quantity or empty packages, if the material is not hazardous. The limited quantities for some important radionuclides are given in Table 16.7 based on 10^{-4} A_2 for liquids and 10^{-3} A_2 for solids and gases, as stated in 49CFR173.425. The values of A_2 are obtained from 49CFR173.435.

Employees who ship hazardous material including radioactive material must have hazmat training to be able to recognize and identify hazardous material, to conduct their specific function, and to enforce safety procedures to protect the public. The training must be given to a new employee within 90 days of employment and then repeated every three years. The training is provided by the hazmat employer or other public or private sources, and a record of training must be made.

European Regulations Governing Radiation

The European Union (EU) currently consists of 27 member countries in Europe, which adopts various rules and regulations that are uniformly applicable to all member states. There are several countries which have applied for joining the EU and others are considering joining. Regulations governing the use of ionizing radiations varied among member states until 1989 when the EU applied uniform

regulations for radiopharmaceuticals to be implemented by each member state. The European Regulatory Organizations of the EU has three main instruments: *Directives, Guidelines, and Regulations*. Directives are mandatory to be translated into national legislations and implemented in each member country. Guidelines are recommendations (not mandatory) for implementation of the Directives by each member country. Regulations are mandatory for all member countries without adoption into individual national legislation.

Use and control of radiation are regulated by Directives from the European Atomic Energy Community (EURATOM). Initial Directives 84/466 EURATOM, and 84/467 EURATOM were based on the recommendations of the ICRP, and mandate regulations for radiation protection for patients, radiation workers, and the public. Because the ICRP revised the basic standards for radiation protection in 1996, Directive 84/467 EURATOM was repealed and substituted with Directive 96/29/EURATOM. Upon further revision of the basic standards by the ICRP, the Directive 96/29/EURATOM has been amended by 97/43/EURATOM, and finally, Directive 84/466/EURATOM was repealed. These directives are similar to NRC 10CFR20 regulations in the US and address all aspects of radiation protection to individuals involved with radiation. They include exposure limits to workers, patients, minors, pregnant women, nursing mothers, and public members; monitoring of radiation areas and working personnel; designation of controlled and supervised (restricted) areas; optimization of radiation exposure (similar to ALARA in the US); survey of work areas; training and experience of the radiation workers and physicians; monitoring in the case of accidental or emergency exposure; record keeping; reporting of incidents; and so on. Table 16.8 shows the dose limits from radiation exposure to radiation workers and the public, which are somewhat different from those adopted by the US NRC 10CFR20. The disposal, recycling, or reuse of radioactive substances is required to have prior authorization, but may be exempted from these requirements if the clearance levels of radioactivity established by the member state comply with those of the EURATOM Directive. Directive 90/642 EURATOM provides regulations for monitoring exposure to outside workers. Interstate shipment of radioactive materials between member states is governed by Directive 1493/93 EURATOM. Personnel monitor-

TABLE 16.8. Dose limits from 96/29/EURATOM.

Limits	Exposed workers (aged over 18)	Apprentices and students	Public
Effective dose	100 mSv (10 rem) in a consecutive 5 year period, subject to a maximum of 50 mSv (5 rem) in a single year.	6 mSv (600 mrem)	1 mSv (100 mrem)
Equivalent dose for eye lens	150 mSv (15 rem)	50 mSv (5 rem)	15 mSv (1.5 rem)
Equivalent dose for the skin, hands, forearms, feet, ankle	500 mSv (50 rem)	150 mSv (15 rem)	50 mSv (5 rem)

ing is mandatory for all radiation workers by using specific monitoring devices. The use of radiation is approved by the issuance of a license to a qualified person with experience in handling radiation. All activities in the radiation area must be recorded. Similar to an RSO in the US, a radiation protection advisor (RPA) is an expert in radiation protection principles, who implements and supervises radiation safety regulations in radiation facilities. These individuals are known by different titles, namely, Radiation Protection Officers, Radiation Protection Advisors, or Radiation Protection Experts in different EU member states.

Although all EU regulations and Directives are equally applicable to all member states, the actual situation differs from country to country, because of the lack of effective implementation of the rules and regulations in many states. So in some member states, these Directives are effectively implemented, while in others they are leniently applied, and in some cases, there may be a breach of these community laws.

The detailed information of different Directives, Guidelines, and Regulations given above may be available from the EU website.

Questions

1. Define committed dose equivalent, deep-dose equivalent, total effective dose equivalent, radiation area, and high radiation area.
2. What are the annual dose limits for radiation workers for:
   (a) Whole body
   (b) Lens
   (c) Extremities
3. What is the dose limit in the unrestricted area and for the individual members of the public?
4. (a) Calculate the exposure rate at 10 inches from a 150-mCi (5.55 GBq)–^{131}I source (Γ_{20} of ^{131}I = 2.17 R · cm^2/mCi · h at 1 cm).
   (b) If the half-value layer (HVL) of lead for ^{131}I is 3 mm, how much lead is needed to reduce the exposure to 10 % of the calculated value at 10 inches?
5. Why is ^{32}P stored in plastic and not in lead containers?
6. What is the approximate amount of lead necessary to reduce the exposure rate from a 200-mCi–^{99m}Tc source to less than 5 mR/h at 20 cm from the source? (Γ_{20} of ^{99m}Tc = 0.59 R · cm^2/mCi · h at 1 cm = 15.95 μGy · m^2/GBq · h at 1 m; HVL of Pb for ^{99m}Tc = 0.3 mm).
7. If 1% of the primary beam exits through a patient with uniform attenuation, calculate the exposure at the midline of the patient.
8. (a) Who are required to wear personnel monitoring devices?
   (b) Film badges can discriminate different types of radiation. True or false?
   (c) Film badges can discriminate radiations of different energies. True or false?
   (d) Why are filters used in film badges?

(e) Filters convert radiation energies into visible light. True or false?
(f) Filters protect the individual from radiation exposure. True or false?
(g) Describe how thermoluminescent dosimeters work.

9. (a) What is the ALARA program?
(b) What is an Agreement State?
(c) How often should area surveys and wipe tests be performed in nuclear medicine?
(d) When does one take a bioassay?
(e) What are the NRC requirements for survey of the packages on receipt?
(f) Describe different methods of disposal of radioactive waste.
(g) What are the general principles of handling radioactive spillage?
(h) What is a transportation index (TI), and how is it used in the transportation of radioactive material?
10. What are the criteria for the release of patients administered with radiopharmaceutical?
11. What is a dirty bomb? How does it differ from an atomic bomb?
12. What are the common radionuclides used in the radiological dispersal device? What are the common sources of radioactive materials used in dirty bombs?
13. Describe the types of effects caused by radiation.
14. Describe the basic principles of decontamination of the contaminated individuals.
15. What are the recommended steps one should take in the case of the explosion of a dirty bomb?
16. The U.S. Homeland Security monitors radioactivity for dirty bombs at strategic points of commuting. The patients undergoing nuclear studies are given cards by the hospitals to carry as a proof of radioactive examinations. How long should the patient normally carry the card for ^{18}F, ^{99m}Tc, ^{123}I, ^{111}In, ^{67}Ga, ^{201}Tl, and ^{201}Tl?

References and Suggested Readings

Cox PH. European legislation and its effects on the production of radiopharmaceuticals. In: Sampson CB, ed. Textbook of Radiopharmacy 3rd ed. Amsterdam: Gordon and Brench Science Publishers; 1999.

Federal Register. Code of Federal Regulations. 10CFR20. Washington, DC: U.S. Government Printing Office; 1996.

Federal Register. Code of Federal Regulations. 10CFR31. Washington, DC: U.S. Government Printing Office; 1993.

Federal Register. Code of Federal Regulations. 10CFR33. Washington, DC: U.S. Government Printing Office; 1992.

Federal Register. Code of Federal Regulations. 10CFR35. Washington, DC: U.S. Government Printing Office; 2002.

Federal Register. Code of Federal Regulations. 10CFR71. Washington, DC: U.S. Government Printing Office; 1992.

Federal Registers. Code of Federal Regulations. 49CFR170 to 49CFR189. Washington, DC: U.S. Government Printing Office; 1989, 2004.

Jaworowski Z. Radiation risks and ethics, Physics Today. 1999; 52:24–290

Martin JE. *Physics of Radiation Protection.* Hoboken, NJ: Wiley Interscience; 2000.

Mettler FA, Voelz GI. Major radiation exposure—what to expect and how to respond. *New Eng J Med.* 2002; 346: 1554.

National Council on Radiation Protection and Measurements. *Basic Radiation Protection Criteria.* Bethesda, MD: NCRP Publication 39; 1971.

National Council on Radiation Protection and Measurements. *Nuclear Medicine–Factors Influencing the Choice and Use of Radionuclides Diagnosis and Therapy.* Bethesda, MD: NCRP Publication 70; 1982.

National Council on Radiation Protection and Measurements. *Ionizing Radiation Exposure of the Population of the United States.* Bethesda, MD: NCRP Publication 90; 1987.

National Council on Radiation Protection and Measurements. *Radiation Protection and Allied Health Personnel.* Bethesda, MD: NCRP Publication 105; 1989.

Shapiro J. *Radiation Protection.* 3rd ed. Cambridge, MA: Harvard University Press; 1990.

U.S. NRC NUREG-1556, vol 9. *Consolidated Guidance about Materials Licences,* U.S. Government Printing Office; 2002.

Zuckier L, Stabin M, Garetano G et al. Sensitivity of personal homeland security radiation detectors to medical radionuclides and implications for counseling of nuclear medicine patients. *RSNA Annual Meeting.* 2004; Abstract SSJ19-01.

Appendix A
Units and Constants

Energy

1 electron volt (eV)	$=1.602\times10^{-12}$ erg
1 kiloelectron volt (keV)	$=1.602\times10^{-9}$ erg
1 million electron volts (MeV)	$=1.602\times10^{-6}$ erg
1 joule (J)	$=10^{7}$ ergs
1 watt (W)	$=10^{7}$ ergs/s
	$=1$ J/s
1 rad	$=1\times10^{-2}$ J/kg $=100$ ergs/g
1 gray (Gy)	$=100$ rad
	$=1$ J/kg
1 sievert (Sv)	$=100$ rem
	$=1$ J/kg
1 horsepower (HP)	$=746$ W
1 calorie (cal)	$=4.184$ J

Charge

1 electronic charge	$=4.8\times10^{-10}$ electrostatic unit
	$=1.6\times10^{-19}$ C
1 coulomb (C)	$=6.28\times10^{18}$ charges
1 ampere (A)	$=1$ C/s

Mass and Energy

1 atomic mass unit (amu)	$=1.66\times10^{-24}$ g
	$=1/12$ the atomic weight of ^{12}C
	$=931$ MeV
1 electron rest mass	$=0.511$ MeV
1 proton rest mass	$=938.78$ MeV
1 neutron rest mass	$=939.07$ MeV
1 pound	$=453.6$ g

G. B. Saha, *Physics and Radiobiology of Nuclear Medicine,*
DOI 10.1007/978-1-4614-4012-3,

Length

1 micrometer, or micron (μm)	$=10^{-6}$ m
	$=10^{4}$ Å
1 nanometer (nm)	$=10^{-9}$ m
1 angstrom (Å)	$=10^{-8}$ cm
1 fermi (F)	$=10^{-13}$ cm
1 inch	$=2.54$ cm

Activity

1 curie (Ci)	$=3.7\times10^{10}$ disintegrations per second (dps)
	$=2.22\times10^{12}$ disintegrations per minute (dpm)
1 millicurie (mCi)	$=3.7\times10^{7}$ dps
	$=2.22\times10^{9}$ dpm
1 microcurie (μCi)	$=3.7\times10^{4}$ dps
	$=2.22\times10^{6}$ dpm
1 becquerel (Bq)	$=1$ dps
	$=2.703\times10^{-11}$ Ci
1 kilobecquerel (kBq)	$=10^{3}$ dps
	$=2.703\times10^{-8}$ Ci
1 megabecquerel (MBq)	$=10^{6}$ dps
	$=2.703\times10^{-5}$ Ci
1 gigabecquerel (GBq)	$=10^{9}$ dps
	$=2.703\times10^{-2}$ Ci
1 terabecquerel (TBq)	$=10^{12}$ dps
	$=27.03$ Ci

Constants

Avogadro's number	$=6.02\times10^{23}$ atoms/g · atom
	$=6.02\times10^{23}$ molecules/g · mole
Planck's constant (h)	$=6.625\times10^{-27}$ erg · s/cycle
Velocity of light	$=3\times10^{10}$ cm/sec
π	$=3.1416$
e	$=2.7183$

Appendix B
Terms Used in Text

Absorption A process by which the total energy of a radiation is removed by an absorber through which it passes.

Accelerator A machine to accelerate charged particles linearly or in circular paths by means of an electromagnetic field. The accelerated particles such as α-particles, protons, deuterons, and heavy ions possess high energies and can cause nuclear reactions in target atoms by irradiation.

Accuracy A term used to indicate how close a measurement of a quantity is to its true value.

Annihilation radiation γ-Radiations of 511 keV energy emitted at 180° after a β^+-particle is annihilated by combining with an electron in matter.

Apoptosis A process of cell death in which a programmed sequence of events leads to the elimination of cells making room for new cells.

Atomic mass unit (amu) By definition, one twelfth of the mass of ${}^{12}_{6}C$, equal to 1.66×10^{-24} g or 931 MeV.

Atomic number (Z) The number of protons in the nucleus of an atom.

Attenuation A process by which the intensity of radiation is reduced by absorption and/or scattering during its passage through matter.

Attenuation coefficient The fraction of γ-ray energy attenuated (absorbed plus scattered) per unit length of an absorber (linear attenuation coefficient, μ) or per gram of an absorber (mass attenuation coefficient, μ_m).

Auger electron An electron ejected from an energy shell, instead of a characteristic x-ray emission, carrying the energy equal to that of the x-ray minus its binding energy.

Average life (τ) *See* Mean life.

Avogadro's number The number of molecules in 1 g mole of any substance or the number of atoms in 1 g atom of any element. It is equal to 6.02×10^{23}.

Becquerel (Bq) A unit of radioactivity. One becquerel is equal to 1 disintegration per second.

Binding energy The energy to bind two entities together. In a nucleus, it is the energy needed to separate a nucleon completely from other nucleons in the nucleus. In a chemical bond, it is the energy necessary to separate two binding partners an infinite distance.

G. B. Saha, *Physics and Radiobiology of Nuclear Medicine,*
DOI 10.1007/978-1-4614-4012-3,

Biological half-life (T_b) The time by which one half of an administered dosage of a substance is eliminated by biological processes such as urinary and fecal excretions.

Bremsstrahlung γ-Ray photons produced by deceleration of charged particles near the nucleus of an absorber atom.

Carrier A stable element that is added in detectable quantities to a radionuclide of the same element, usually to facilitate chemical processing of the radionuclide.

Carrier-free A term used to indicate the absence of any stable atoms in a radionuclide sample.

Collimator A device to confine a beam of radiation within a specific field of view. Collimators may be converging, pinhole, diverging, and parallel-hole types.

Collimator efficiency The number of photons passing through the collimator for each unit of activity present in a source.

Collimator resolution A component of spatial resolution of an imaging system contributed by the collimator. It is also called *geometric resolution*.

Committed dose equivalent ($H_{T,50}$) The dose equivalent to organs or tissues of reference (T) that will be received from an intake of radioactive material by an individual during the 50-year period following intake.

Compton scattering In this process, a γ-ray transfers only a partial amount of energy to an outer orbital electron of an absorber, and the photon itself is deflected with less energy.

Conversion electron (e^-) *See* Internal conversion.

Critical organ *See* Organ, critical.

Cross section (σ) The probability of occurrence of a nuclear reaction or the formation of a radionuclide in a nuclear reaction. It is expressed in a unit termed *barn*; 1 barn = 10^{-24} cm^2.

Curie (Ci) A unit of activity. A curie is defined as 3.7×10^{10} disintegrations per second.

Dead time The period of time that a counter remains insensitive to count the next after an event.

Decay constant (λ) The fraction of atoms of a radioactive element decaying per unit time. It is expressed as $\lambda = 0.693/t_{1/2}$, where $t_{1/2}$ is the half-life of the radionuclide.

Deep-dose equivalent (H_d) Dose equivalent at a tissue depth of 1 cm (1000 mg/cm^2) resulting from external whole-body exposure.

Dose The energy of radiation absorbed by any matter.

Dosimeter An instrument to measure the cumulative dose of radiation received during a period of radiation exposure.

Dosimetry The calculation or measurement of radiation absorbed doses.

Effective dose The sum of the products of the committed dose equivalent to each of the body organs and tissues and the weighting factor of the corresponding organ or tissue. ($H_e = \Sigma W_T \times H_{T,50}$)

Effective half-life (T_e) Time required for an initial administered dose to be reduced to one half as a result of both physical decay and biological elimination of a radionuclide. It is given by $T_e = (T_p \times T_b)/(T_p + T_b)$, where T_e is the effective half-life, and T_p and T_b are the physical and biological half-lives, respectively.

Electron (e^-) A negatively charged particle rotating around the atomic nucleus. It has a charge of 4.8×10^{-10} electrostatic units and a mass of 9.1×10^{-28} g, equivalent to 0.511 MeV, or equal to 1/1836 of the mass of a proton.

Electron capture (EC) A mode of decay of a proton-rich radionuclide in which an orbital electron is captured by the nucleus, accompanied by emission of a neutrino and characteristic x-rays or Auger electrons.

Electron volt (eV) The kinetic energy gained by an electron when accelerated through a potential difference of 1 V.

Energy resolution Capability of a detecting system to separate two γ-ray peaks of different energies. It is given by the full width at half maximum (FWHM) of a given photopeak.

Erg The unit of energy or work done by a force of 1 dyne through a distance of 1 cm.

Fission (f) A nuclear process by which a nucleus divides into two nearly equal smaller nuclei, along with the emission of two to three neutrons.

Free radical A highly reactive chemical species that has one or more unpaired electrons.

Generator, radionuclide A device in which a short-lived daughter is separated chemically and periodically from a long-lived parent adsorbed on adsorbent material. For example, ^{99m}Tc is separated from ^{99}Mo from the Moly generator with saline.

Gray (Gy) The unit of absorbed radiation dose in SI units. One gray is equal to 100 rad.

Half-life ($t_{1/2}$) A unique characteristic of a radionuclide, defined by the time during which an initial activity of a radionuclide is reduced to one half. It is related to the decay constant λ by $t_{1/2} = 0.693/\lambda$.

Half-value layer (HVL) The thickness of an absorbing material required to reduce the intensity or exposure of a radiation beam to one half of the initial value when placed in the path of the beam.

Internal conversion An alternative mode to γ-ray decay in which nuclear excitation energy is transferred to an orbital electron, which is then ejected from the orbit.

Intrinsic efficiency The number of radiations detected divided by the number of radiations striking the detector.

Intrinsic resolution A component of the spatial resolution of an imaging system that is contributed by the detector and associated electronics and depends on the photon energy, detector thickness, and the number of PM tubes.

Ion An atom or group of atoms with a positive charge (cation) or a negative charge (anion).

Isobars Nuclides having the same mass number, that is, the same total number of neutrons and protons. Examples are $^{57}_{26}$Fe and $^{57}_{27}$Co.

Isomeric transition (IT) Decay of the excited state of an isomer of a nuclide to a lower excited state or the ground state.

Isomers Nuclides having the same atomic and mass numbers but differing in energy and spin of the nuclei. For example, ^{99}Tc and ^{99m}Tc are isomers.

Isotones Nuclides have the same number of neutrons in the nucleus. For example, $^{131}_{53}$I and $^{132}_{54}$Xe are isotones.

Isotopes Nuclides having the same atomic number, that is, the same number of protons in the nucleus. Examples are $^{14}_{6}$C and $^{12}_{6}$C.

$LD_{50/60}$ A quantity of a substance that, when administered or applied to a group of any living species, kills 50 % of the group in 60 days.

Linear energy transfer (LET) Energy deposited by radiation per unit length of the matter through which the radiation passes. Its usual unit is keV/μm.

Mass defect The difference between the mass of the nucleus and the combined masses of individual nucleons of the nucleus of a nuclide.

Mass number (A) The total number of protons and neutrons in a nucleus of a nuclide.

Mean life (τ) The average expected lifetime of a group of radionuclides before disintegration. It is related to the half-life and decay constant by $\tau = 1/\lambda = 1.44\ t_{1/2}$.

Metastable state (m) An excited state of a nuclide that decays to a lower excited or the ground state by isomeric transition with a measurable half-life.

Modulation transfer function A quantitative value of the spatial resolution of an imaging system.

Neutrino (v) A particle of no charge and mass emitted with variable energy during β^+, and electron capture decays of radionuclides. An antineutrino ($\bar{v}$) is emitted in β^- decay.

No carrier added (NCA) A term used to characterize the state of a radioactive material to which no stable isotope of the compound has been added purposely.

Nucleon A common term for neutrons or protons in the nucleus of a nuclide.

Organ, critical The organ that is functionally essential for the body and receives the highest radiation dose after administration of radioactivity.

Organ, target The organ intended to be imaged and expected to receive the greatest concentration of administered radioactivity.

Pair production γ-Rays with energy greater than 1.02 MeV interact with the nucleus of an absorber atom, and a positron and an electron are produced at the expense of the photon.

Photoelectric effect A process in which a γ-ray, while passing through an absorber, transfers all its energy to an orbital electron, primarily the K-shell electron of an absorber, and the photoelectron is ejected from the shell.

Photofraction The fraction of all detected γ-rays that contributes to the photopeak.

Physical half-life (T_p) *See* Half-life.

Precision A term used to indicate the reproducibility of the measurement of a quantity when measurements are made repeatedly.

Quality factor (*QF*) A factor dependent on linear energy transfer that is multiplied by absorbed doses to calculate the dose equivalents in rem. It is used in radiation protection to take into account the relative radiation damage caused by different radiations. It is 1 for x-, γ-, and β-rays and 10 for neutrons and protons.

Rad The unit of radiation-absorbed dose. One rad is equal to 100 ergs of radiation energy deposited per gram of any matter, or 10^{-2} J/kg of any matter.

Radiation weighting factor (W_r) A factor that depends on the types of radiation and is used to convert rad to rem in radiation protection. Rem = rad $\times$ W_r.

Range The straight line distance traversed by a charged particle in an absorber.

Relative biologic effectiveness (RBE) A factor used to calculate the dose equivalent in rem from rad. It is defined as the ratio of the amount of a standard radiation that causes certain biological damage to the amount of radiation in question that causes the same biological damage.

Roentgen The quantity of x- or γ-radiations that produces one electrostatic unit of positive or negative charge in 1 cm^3 of air at 0° C and 760-mm Hg pressure (standard temperature and pressure, STP). It is equal to 2.58×10^{-4} C/kg air.

Roentgen equivalent man (rem) A dose equivalent defined by the absorbed dose (rad) times the relative biological effectiveness or quality factor of the radiation in question.

Sensitivity The number of counts per unit time detected by an imaging device for each unit of activity present in a source. It is expressed in cps/μCi.

Shallow-dose equivalent (H_s) Dose equivalent at a tissue depth of 0.007 cm (7 mg/cm^2) averaged over an area of 1 cm^2 from external exposure to the skin.

Sievert (Sv) The SI unit of dose equivalent and equal to 100 rem.

Spatial resolution A measure of the ability of an imaging device to faithfully reproduce the image of an object. It is given by the modulation transfer function (MTF) and is determined by the Fourier transform of the line spread function.

Specific activity The amount of radioactivity per unit mass of a radionuclide or labeled compound.

Specific ionization The number of primary and secondary ion pairs produced by an incident radiation per unit path length in an absorber.

Thermal neutron Neutrons of thermal energy 0.025 eV.

Tissue weighting factor (W_T) The weighting factor of an organ or tissue is the proportion of risk of stochastic effects resulting from irradiation of that organ or tissue to the total risk of stochastic effects when the total body is irradiated uniformly.

Appendix C
Answers to Questions

Chapter 2

3. 81.3 %
7. 130 keV

Chapter 3

1. (a) 1.11×10^{15} atoms
   (b) 0.24 mg
2. (a) 4.75×10^{14} dpm
   (b) 216 Ci or 7.99×10^{12} Bq
3. 6.97 h
4. (a) 429 mCi (15.9 GBq)
   (b) 120.7 mCi (4.46 GBq)
5. 25.5 h
6. 4.03 days
7. 6.4 mCi (237 MBq)
9. 330 min
10. 63 %
11. 1.32 h
12. N/2
13. 143.6 mCi (5.3 GBq)
14. 11 h

Chapter 4

3. (a) 1707 ± 13.8 cpm
   (b) 1647 ± 14.9 cpm
4. 40,000 counts
5. 3 standard deviations
6. 1111 counts
7. 90 %

Chapter 5

8. 570.6 Ci (21.1 GBq)
9. 8.92 mCi (330 MBq)

Chapter 6

15. (a) 7.32 HVLs
    (b) 8 HVLs
17. 10 HVLs
18. 2.31 cm
19. 2 mm

Chapter 8

8. (a) 25 %
   (b) 50 %
14. 61.4 %

Chapter 9

5. (c) 1911 counts/cm^2

Chapter 10

6. (e) 0.35
10. (a) 1.2
    (b) 187
    (c) 224.5

Chapter 12

14. 0.84 cycles/cm

G. B. Saha, *Physics and Radiobiology of Nuclear Medicine,*
DOI 10.1007/978-1-4614-4012-3,

Chapter 14

1. 36,541 rad (365.4 Gy)
2. 350 rem (3.5 Sv)
7. 18,144 μCi · h
8. 1.06×10^{-2} rad/μCi · h
9. 1.2 rad (1.2 cGy)
11. 75.5 rem (0.76 Sv)

Chapter 16

4. (a) 0.5 R/h
   (b) 6.96 mm Pb
6. 1.77 mm Pb
7. 10 %

Index

G. B. Saha, *Physics and Radiobiology of Nuclear Medicine,*
DOI 10.1007/978-1-4614-4012-3,